January 2012

Innovative Desalination Systems Using Low-grade Heat

Chennan Li
University of South Florida, cli3@mail.usf.edu

Innovative Desalination Systems Using Low-grade Heat

by

Chennan Li

A dissertation submitted in partial fulfillment
of the requirements for the degree of
Doctor of Philosophy
Department of Chemical & Biomedical Engineering
College of Engineering
University of South Florida

Co-Major Professor: D. Yogi Goswami, Ph.D.
Co-Major Professor: Elias K. Stefanakos, Ph.D.
Norma Alcantar, Ph.D.
Babu Joseph, Ph.D.
Dale Johnson, Ph.D.
Daniel H. Yeh, Ph.D.

Date of Approval:
April 30, 2012

Keywords: Supercritical Organic Rankine Cycle, Heat Recovery, Efficiency, RO, MED, Ejector

DEDICATION

This work is dedicated to Dr. John Wolan, who was the graduate program advisor in Chemical and Biomedical Engineering, and a committee member for my Ph.D. proposal defense.

This work is also dedicated to all my experiences during the past 10 years.

ACKNOWLEDGEMENTS

Looking back, I am grateful for all I have received throughout these years. It is my pleasure to acknowledge those people who have made this work possible.

I want to thank my advisors, Drs. D. Yogi Goswami and Elias K. Stefanakos, for inspiring and encouraging me to be a researcher and engineer of innovative and critical thinking. Their knowledge, zeal and dedication towards research have influenced me so much through my graduate study at the University of South Florida. They have always been there to listen, support and give advice; they teach me not only technological knowledge, but also how to behave and react when I meet difficulties, troubles and unhappiness. Without their encouragement, mentoring and help, I would have never finished this PhD study.

My thanks also go out to my committee members for their valued suggestions and support in one way or another through my studies; the whole USF CERC crew who have made my life here so delightful and memorable; my friends from DICP, RICE, GAI, AECOM and GE who have given me support to finish my study.

My family to whom this dissertation is dedicated has been a constant source of love, concern, support and strength all these years and I would like to express my heart-felt gratitude to them.

TABLE OF CONTENTS

LIST OF TABLES

LIST OF FIGURES

ABSTRACT

Water and energy crises have forced researchers to seek alternative water and energy sources. Seawater desalination can contribute towards meeting the increasing demand for fresh water using alternative energy sources like low-grade heat. Industrial waste heat, geothermal, solar thermal, could help to ease the energy crisis. Unfortunately, the efficiency of the conventional power cycle becomes uneconomically low with low-grade heat sources, while, at the same time, seawater desalination requires more energy than a conventional water treatment process. However, heat discarded from low-grade heat power cycles could be used as part of desalination energy sources with seawater being used as coolant for the power cycles. Therefore a study of desalination using low-grade heat is of great significance.

This research has comprehensively reviewed the current literature and proposes two systems that use low-grade heat for desalination applications or even desalination/power cogeneration. The proposed two cogeneration systems are a supercritical Rankine cycle-type coupled with a reverse osmosis (RO) membrane desalination process, and a power cycle with an ejector coupled with a multi-effect distillation desalination system. The first configuration provides the advantages of making full use of heat sources and is suitable for hybrid systems. The second system has several advantages, such as handling highly concentrated brine without external electricity input as well as the potential of water/power cogeneration when it is not used to treat concentrated brine. Compared to different stand-alone power cycles, the

proposed systems could use seawater as coolant to reject low-grade heat from the power cycle to reduce thermal pollution.

CHAPTER 1 INTRODUCTION AND OBJECTIVES

1.1 Overview

Desalination has been practiced by ship-borne explorers since the early 1600s. The first commercial scale thermal desalination was used during World War II. Presently, 14,754 desalination facilities have been developed throughout the world. Historically, seawater desalination has been the most expensive way to produce drinking water at the commercial scale because of the high capital and energy costs [1–3]. However, desalination is increasingly recognized as a needed and viable option due to the rapid increase of the world population [4]. It is projected that close to 70% of the world population will face water shortage issues by 2025 [5–7]. Approximately 50% of the world's population lives within 200 km of a coast. Since the first commercial scale desalination plant was used during World War II, the world total contracted desalination capacity, as shown in Figure 1.1 based on data from ref. [8], has grown to 71.7 million m³ per day in 2010. From Figure 1.2 (based on data from ref. [8]) it can be seen that seawater desalination has undergone major market expansion since 2003. It is estimated that about 8.78 million tons of oil per year is required to produce 1 million m^3 per day of fresh water by desalination [9]. This indicates the importance of finding suitable alternative energy resources for desalination systems. Among all the alternative energy resources, low-grade heat sources such as solar energy have the highest potential to support future energy needs

[10][11]. In this context, developing technologies that efficiently make use of the efficient low-grade heat as energy sources for desalination is of great significance.

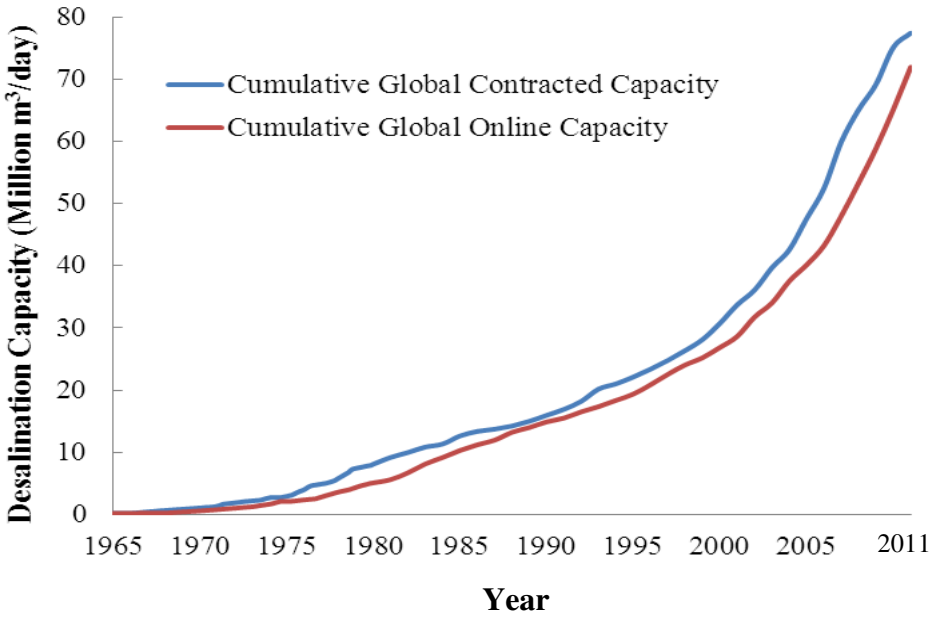

Figure 1.1 Total contracted commissioned desalination capacity, 1965 – 2010.

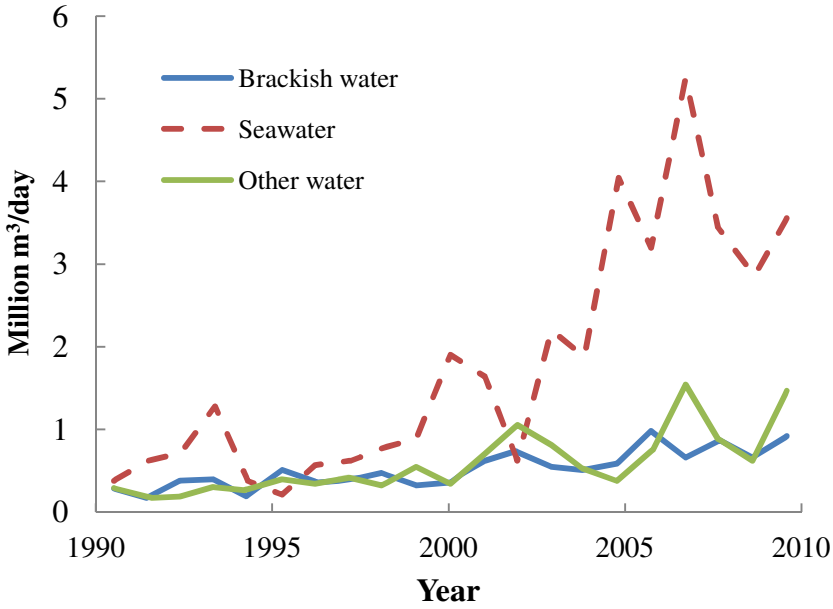

Figure 1.2 Annual new contracted desalination capacities by feed water, 1990 – 2010.

1.2 Objectives

This research focuses on suitable desalination systems that make use of low-grade heat sources. Current systems using low-grade heat have limitations that need to be improved. This research comprehensively summarizes the currently available systems and proposes two novel systems to better improve system integration. The results also clearly show the energy consumption of different desalination systems and the application areas of the proposed systems for different heat sources.

The first proposed system is the supercritical organic Rankine cycles (SORC) driven reverse osmosis (RO) system. The use of solar thermal energy for desalination by coupling an organic Rankine cycle (ORC) with the RO is one active research area. ORC is a promising technology for exploiting low-temperature heat sources including solar thermal, geothermal and waste heat. The advantage of coupling an ORC with a desalination system is that the seawater provides a heat sink for the ORC condenser, while at the same time it is preheated to increase the RO membrane permeability, leading to reduced power consumption. However, previous research mainly focused on ORC-RO systems for solar thermal applications suggesting that the same system could also be driven by geothermal energy, waste heat or biomass., Considering that the SORC is now getting more attention for power generation from low-grade heat sources (such as geothermal) due to their “smoother” heating process, SORC-driven RO using solar, geothermal and waste heat energy sources need to be analyzed.

The second system is a combination of a multi-effect distillation desalination (MED) system with a SORC and an ejector, which works like a combined heat, power and condensation system where ejector cooling is used to condense the final effect vapor of the MED system. A thermal process such as MED is robust, requires less pretreatment and could handle high concentration saltwater sources as compared to a

RO system. However, thermal desalination is regarded as energy intensive. Seawater desalination and frac flowback water desalination require more energy than conventional water treatment due to the higher salt concentration. Therefore, researchers have tried various methods to improve thermal energy utilization by combining different heat pumps. However, a system using heat pumps combined with MED requires heat as well as electricity. The proposed system could handle highly concentrated brine without additional electricity input.

CHAPTER 2 RESEARCH BACKGROUND

Historically, seawater desalination has been the most expensive way to produce drinking water at the commercial scale because of the high capital and energy costs [1–3]. However, it is projected that by 2050 about 1.7 billion people in 39 countries will face difficulties in meeting basic water needs [5–7]. Approximately 50% of the world's population lives within 200 km of the coast and many of the world's largest and fastest growing cities are near the coast. Therefore, in search of new sources of water supply, saltwater desalination is increasingly recognized as a viable option [4]. Since the first commercial scale desalination plant was used during World War II, the world total contracted desalination capacity has grown to 71.7 million m^3 per day in 2010 in accordance with the *International Desalination Association* (*IDA*) Worldwide Desalting Plant Inventory. The desalination market is and will keep on growing. In terms of oil consumption, it is estimated that about 203 million tons of oil per year is required to produce 22 million m^3 per day of desalinated water [9]. This indicates the importance of finding suitable alternative energy resources for the desalination systems.

Among all the alternative energy resources, solar energy is at the top of all the sources for its potential to provide for future energy needs. Apart from providing some useful data for comparison among the resources, Table 2.1 illustrates that the comparison is not always simple due to different calculation methods, standards, or assumptions in various studies in the literature. Many developing countries, which

Table 2.1 Worldwide technical potential energy, installed capacity, current economic potential and capacity factor [a]

Types of technology		Technical potential (TW)			Installed capacity (GW)	Installed capacity (GW)	Current economic potential (TW)	Worldwide capacity factor of technology in place
Solar	PV	342.26[b]	60 [c]	>50[d]	8.7[b]	5[c]	0.15-7.3[c]	0.1-0.2[b]
	CSP	0.89[b]			0.354[b]			0.13-0.25[b]
	Others	NA			NA			NA
Wind		46.77[b]	2[c]	20[d]	94.1[b]	6[c]	0.6[c]	0.205-0.42[b]
Geothermal		0.14[b]	11.6[c]	3.8[d]	9[b]	54[c]	0.6[c]	0.73[b]
Hydroelectric		1.88[b]	1.6[c]	1.6[d]	778[b]	650[c]	0.8[c]	0.416[b]
Wave		0.50[b]	NA	NA	0.00075[b]	NA	NA	0.21-0.25[b]
Tidal		0.02[b]	NA	NA	0.26[b]	NA	NA	0.2-0.35[b]
Nuclear		13.92[b]	NA	NA	371[b]	NA	NA	0.808[b]
Coal-ccs		1.25[b]	NA	NA	NA	NA	NA	0.65-0.85[b]
Biomass		NA	6-8[c]	9[d]	NA	1600[c]	NA	NA

(a) For comparison, the 2005 world electric power production was 2.08 W; the energy production for all purposes was 15.18 TW.
(b) Data from Reference [12];
(c) Data from Reference [11];
(d) Data from Reference [13].

normally could not afford to use desalinated water, are likely to have great need of water due to population growth. These countries, in general, have higher solar radiation also. For example, the average daily solar radiation in India is 4–7 kWh/m^2 [14] compared with the global average of 2.5 kWh/m^2. Therefore, solar energy driven/assisted desalination is becoming more viable despite its high capital cost.

Seawater desalination may be classified by the intended product as well as the process, as shown in Figure 2.1. The processes are further grouped as follows: a) those that allow water to pass through a membrane without phase change such as reverse osmosis (RO) and forward-osmosis (FO); b) processes that involve a phase change such as multi-stage flash (MSF); c) multi-effect distillation (MED); d) solar still (ST); e) humidification-dehumidification (HDH); f) passive vacuum desalination (PVD); g) membrane distillation (MD); and h) freezing-melting (FM). Process grouping also includes heat pump desalination applications such as a) thermal vapor compressor (TVC); b) mechanical vapor compressor (MVC); c) absorption heat pump desalination (ABHP); and d) adsorption heat pump desalination (ADHP). Processes for extracting salt such as electro-dialysis (ED), ion exchange (IE) and capacitive deionization (CDI) are normally used in brackish water desalination but not seawater desalination. Among all of the above mentioned desalination processes, MSF, MED, RO and ED account for about 95% of the global desalination capacity, as can be seen in Figure 2.2 [8].

2.1 Solar-assisted MSF

Multi-stage flash has the second largest installed desalination capacity after the RO systems. Most of the energy consumption of MSF is the thermal energy used to distill water, while some electricity is needed for pumping. As can be seen in Figure 2.3, MSF could be connected with a solar thermal heat source and the power

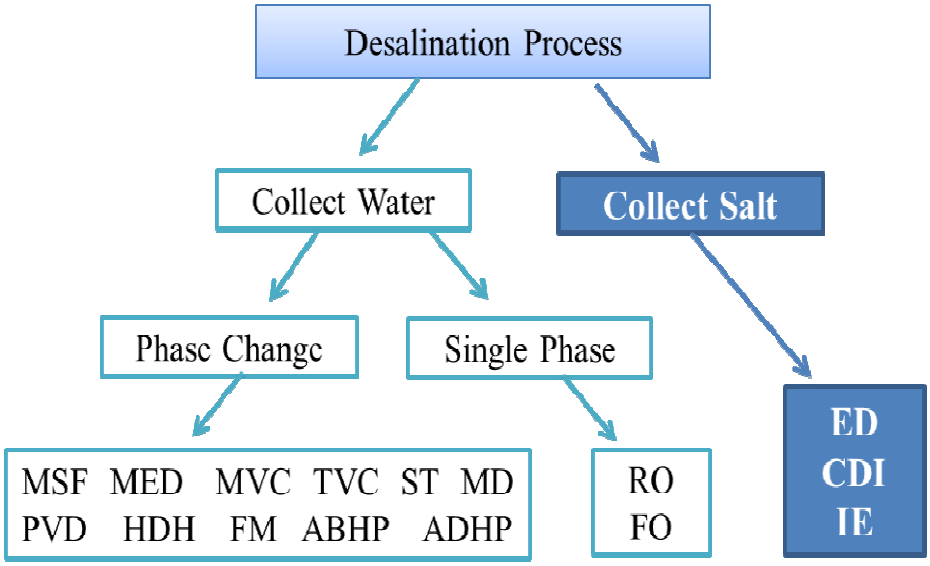

Figure 2.1 Desalination processes grouped based on which substance is extracted.

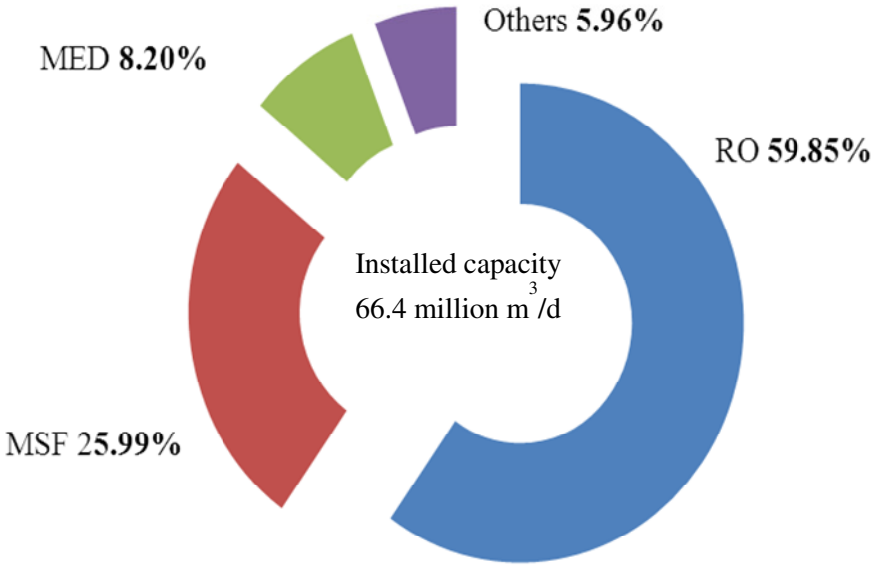

Figure 2.2 Total worldwide installed desalination capacities by technology, 2010.

grid at the same time, or it could be connected with a solar thermal system through a heat engine to provide heat and electricity at the same time. A solar pond type of solar thermal system may be especially applicable, since the produced salt could be used in the pond itself.

In an MSF process, seawater moves through a sequence of vacuumed reactors called stages that are held at successively lower pressures where seawater is preheated. External heat is supplied to heat the preheated seawater above its saturation temperature. Seawater is then successively passed from one stage to the next in which a small amount of water flashes to steam in each stage and the remaining brine flows to the next stage for further flashing. The flashed steam is condensed and collected as fresh water after removing the latent heat of condensation, to preheat the entering seawater at each stage. MSF is used in large-scale cogeneration power plants [15–19] because it can use low-quality steam rejected from power cycles as the heat source. Some researchers claim that MSF is not as thermally efficient as MED [20]. Others do not see any clear advantages in the thermodynamics between the MED and MSF processes, except that thermal losses are higher in the MSF than in the MED, due to its higher operating temperature [21].

2.1.1 Solar Pond-driven MSF

A solar pond (SP) is a stable pool of salt water in which the water salinity increases in the middle layer from its top to the bottom with a gradient that prevents convective mixing on absorbing solar radiation and the resulting increase in temperature, as shown in Figure 2.3. Water absorbs solar radiation going through it causing its temperature to rise. The shorter the wave length of sunlight, the deeper it can penetrate the water column as shown in Table 2.2 [22]. The amount of absorbed energy increases with depth producing a vertical temperature incline causing a density gradient decreasing with depth. Conversely, salinity increases with depth producing a vertical salinity incline causing a density gradient increasing with depth. Heat is passively collected and stored in the lower convective zone (LCZ) because the middle layer is a non-convective zone (NCZ).

Table 2.2 Spectral absorption of solar radiation in water

Wavelength (μm)	Layer depth				
	0	1 cm	10 cm	1 m	10 m
0.2–0.6	23.7	23.7	23.6	22.9	17.2
0.6–0.9	36.0	35.3	36.0	12.9	0.9
0.9–1.2	17.9	12.3	0.8	0.0	0.0
> 1.2	22.4	1.7	0.0	0.0	0.0
Total	100.0	73.0	54.9	35.8	18.1

Most commercial MSF units operate with a top brine temperature of 90-110°C [23] heated by steam while the solar pond operates in the range of 30-95 °C. Therefore, in solar pond-assisted MSF systems, the first stage of the MSF heat exchangers is changed to a liquid-liquid heat exchanger instead of steam-liquid heat exchanger [24]. Some selected solar pond-assisted MSF research studies are listed in Table 2.3.

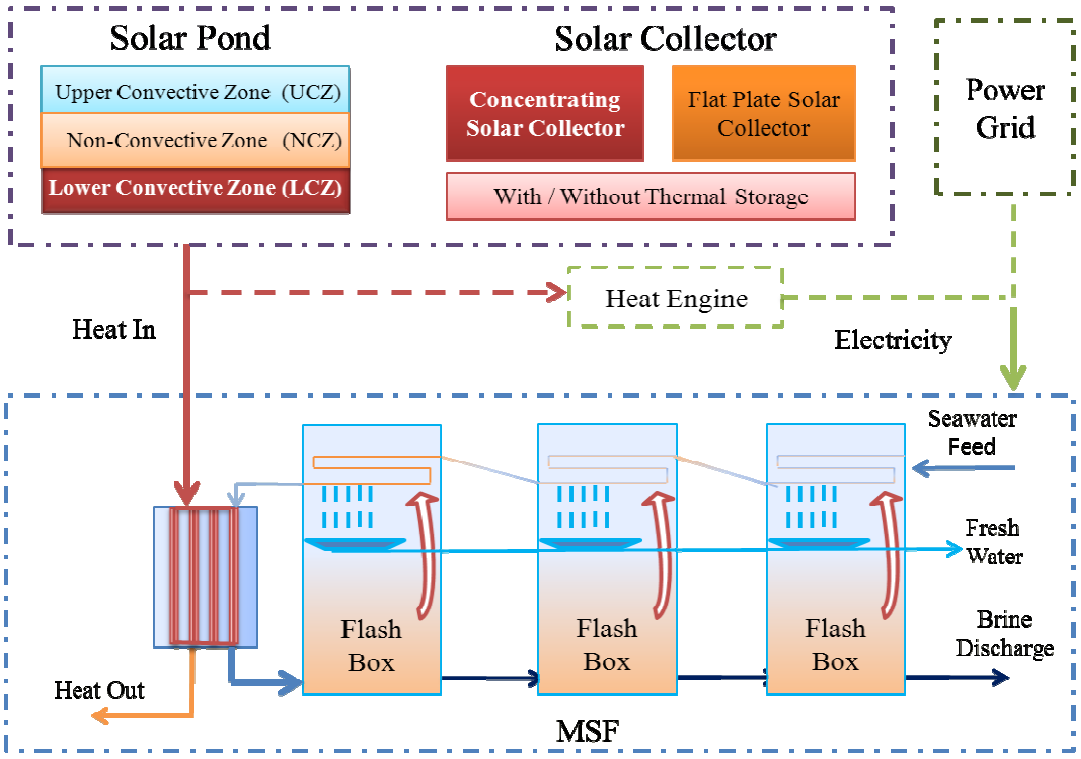

Figure 2.3 Schematic of solar-assisted multi-stage flash desalination process.

Table 2.3 Selected solar pond-assisted MSF research

Ref	Mod/exp.	Location /radiation	Pond size (m^2)	Top brine temp.(°C)	Capacity (m^3/d)	Cost ($/$m^3$)	GOR	N. of Stages	Desal cost perc.	SP cost perc.	Notes
[25]	Model	North Africa[(a)]	2500	<95	15	5.48	NA	12-14	0.728	0.272	(h)
			36000		300	2.39	NA		0.745	0.255	
[26]	Exp.	Qatar	1500	55-80	20	NA	NA	22	NA	NA	
	Model	5.5-6kWh/m^2/d	80000		1000	2.85	NA	NA	0.267[(b)]	0.18[(b)]	
			800000		10000	1.84	NA	NA	0.251[(b)]	0.174[(b)]	
[27]	Model	4.54 kWh/m^2/d[(m)]	7800	< 75, 95-120[(o)]	2040[(m)]	0.916[(p)]	9.2-12.5	NA	NA	NA	Hybrid
					12378[(n)]	0.827[(p)]	10.4-13.5				
[28]	Model	Tripoli, Libya [(e)]	70000	< 90[(d)]	1570[(g)]	1.8[(f)]	10 [(i)]	31 [(j)]	NA	NA	(k)
[29]	Mod/Exp.	El Paso, US	3000	57-77	1.6-9	NA	3.2-6.2	24	NA	NA	(l)
[24]	Model	246.3W/m^2	65361	88	550	3.71	6	20	0.343 [(c)]	0.590 [(c)]	(m)
			49441			3.42	8		0.431 [(c)]	0.502 [(c)]	
[30]	Model	Safat, Kuwait [(q)]	NA	< 78	1	1.785[(q)]	(r)	18	NA	NA	Hybrid
				< 78	1	2.835[(q)]					Solar

(a) Authors mentioned North Africa; use Tripoli, Libya, as the typical location, NASA data showed 5.11, 6.03 kWh/m^2/d for annual average global radiation and DNI average radiation.
(b) Interests, which are 7% for 15years, are not included.
(c) O&M cost is not considered.
(d) Solar pond temperature ranges 65-106 °C.
(e) Radiation is less than 350W/m^2 based on the paper; Using the same location, NASA shows monthly average horizontal radiation 5.11 kWh/m^2/d and DNI 6.03 kWh/m^2/d
(f) The minimum break even fuel cost was $209.261/ton, which occurred when the lower convective zone of the solar pond temperature was 90°C, a desalination process performance ratio of 8 with an interest rate of 6%. The cost varies $1.8-1.94/$m^3$ depending on the MSF GOR and pond T.
(g) Capacity varies 1238-1570 m^3/d based on solar pond temperature
(h) Auto Flash: A desalination unit which is capable of operating smoothly under variable input conditions. An inter-stage pressure regulation device was incorporated at each fluid passage (brine and distillate) to replace the conventional orifices between the stages.
(i) GOR 4-10 based on maximum solar pond temperature 90°C.
(j) The number of total stages varies from 14 to 31 based on solar pond T when GOR is 10. The relative MSF has 28 heat recovery stages and 3 heat rejection stages.
(k) About 73–185 m^2/m^3/day capacity depending on the storage zone temperature, peak clipping days and the performance ratio.
(l) Falling Film Spinflash unit.
(m) The main heat source is exhaust from a 30MW gas turbine at 550°C. Part of the heat is used to run a desalination plant and the rest is stored in a solar pond (depth 4m). Radiation data is the same with as (l).
(n) The main heat source is exhaust from a 120 MW gas turbine; the rest of the conditions are the same as (k). Based on the authors' proposed location, south of Tunisia, NASA data showed horizontal monthly annual average radiation at horizontal to be 4.54kWh/m^2/d and direct norm radiation 5.24kWh/m^2/d.

Table 2.3 (Continued)

(o) During peak time it is heated by a gas turbine, with seawater temperature at 95-120°C, while the rest of the time it is heated by a solar pond, at 75 °C

(p) The surface pond is covered by a transparent material to reduce heat losses and store solar energy. The price range is $09-0.1014/$m^3$ for a gas turbine and solar pond-driven separately. The average cost is $0.916/$m^3$; The price ranges from $0.821-0.862/$m^3$ for gas turbine and solar pond-driven separately, averaging $0.827/$m^3$.

(q) Converting to US dollar based on 1KD=$3.50 as the authors' mentioned, and based on author mentioned location, the NASA data showed 5.4 and 6.33 kWh/m^2 for monthly average horizontal and DNI radiation.

(r) The thermal energy input is 167 kJ/kg; and electricity energy input is, 25kJ/kg.

Due to the intermittence of solar radiation, conventional MSF with fixed orifices and weirs to control inter-stage pressures are not suited for these abrupt changes of pressure differences between stages. Atlantis "*Autoflash*" MSF [25] used a proprietary passive inter-stage pressure regulation system that could be self-regulating at each fluid passage between the stages. Since a solar pond is both a solar collector and stores energy in one, it overcomes the intermittent nature of solar energy. However, the solar pond has to be oversized for winter conditions, necessitating some of the surplus summer heat to be wasted [28]. On the other hand, waste heat from other sources (gas turbine, for example) may be used during periods of insufficient sunshine [31]. These kinds of hybrid solar pond systems could store extra waste heat, such as from gas turbine exhaust during peak times to lower the water production cost and the solar pond size [27]. Table 2.3 shows that a hybrid system using low-grade heat has a relatively lower water cost.

Solar ponds have many advantages over other solar desalination technologies [32], such as low cost per unit area of the collector, inherent storage capacity and capability of utilizing reject brine, which is often considered as a waste product for other processes [33]. In addition, the solar pond surface water could be used as cooling water because of its lower temperature during the summer months [29]. However, solar ponds need sunny conditions, and a large expanse of flat land. They might also have environmental impacts such as soil contamination by pond brine leakage [31], [34] In addition, the solar pond salinity profile needs to be carefully maintained, the saline water needs to be kept at low pH, the pond clarity needs to be monitored very carefully, and the wind factor needs to be considered before the construction.

2.1.2 Solar Collector-assisted MSF

Some researchers claim that it is better to use indirect solar desalination for large desalination projects [35], which means that a solar collector field is connected with a conventional distillation plant to provide thermal energy for the desalination process. Solar collectors can be classified as concentrating and non–concentrating types. Table 2.4 shows different thermal collectors and their operating temperatures [36]. Solar collectors are chosen based on the desired process temperature. Concentrating solar systems can be trough, dish or central receiver tower types. One of the main advantages of concentrating solar systems over most other renewable electricity technologies, is that they can operate in conjunction with large heat storage facilities (e.g. using molten salt or concrete), or in hybrid mode with fossil fuel or biomass, to compensate for the fluctuations in daily irradiance and to produce electricity beyond sunshine hours[37]. Table 2.5 shows the pictures of different solar technologies. Solar collectors are chosen based on the desired process temperature.

Some selected solar collector-assisted MSF seawater desalination systems are seen in Table 2.6. Hou [38] et al. used pinch analysis to optimize a solar MSF desalination process and concluded that in order to enhance the performance, a wide range of working temperatures of MSF is needed. Gained output ratio (GOR) is defined as the number of kilograms of desalinated water produced per kilogram of steam consumed. In order to gain higher GOR it is better to discharge the brine at the last stage. It was found that controlling the flash evaporation pressure is important, (i.e. by reducing the flash evaporation pressure from 0.014 MPa to 0.010 MPa), the desalination rate could increase almost five times in some direct solar thermal desalination systems [39].

Table 2.4 Solar collectors and their characteristics

Tracking	Collector type	Absorber	Concen. ratio	Operational range
Stationary	Flat plate (FPC)	Flat	1	30–80 °C
	Evacuated tube (ETC)	Flat	1	50–200 °C
	Compound parabolic (CPC)	Tubular	1–5	60–240 °C
Single–axis	Compound parabolic	Tubular	5–15	60–300 °C
	Linear Fresnel	Tubular	10–40	60–250 °C
	Parabolic trough (PTC)	Tubular	15–45	60–300 °C
	Cylindrical trough	Tubular	10–50	60–300 °C
Double–axis	Parabolic dish	Point	100–1000	100–500 °C
	Heliostat field	Point	100–1500	150–2000 °C

Table 2.5 Pictures of different solar technologies

Parabolic trough	Solar tower	Evacuated tube collector
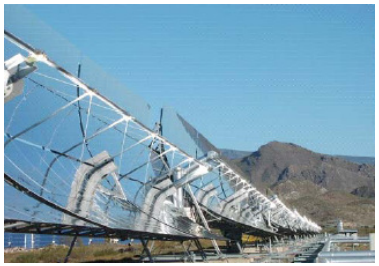		
Linear Fresnel	**Parabolic dish**	**Flat collector**
		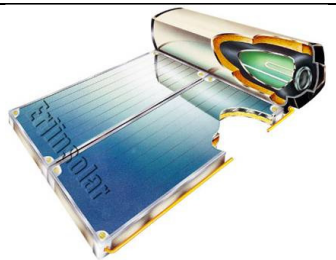
Solar pond	**Solar chimney**	**Photovoltaic**
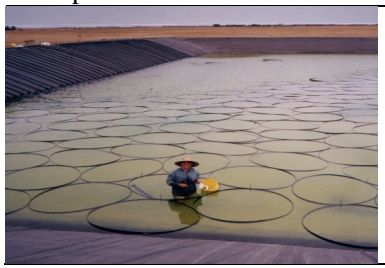	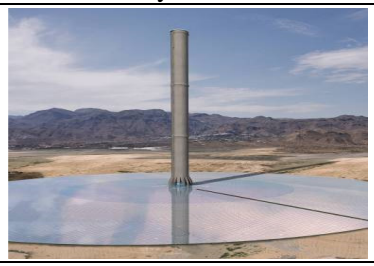	

Table 2.6 Some selected solar collector-assisted MSF seawater desalination systems

Ref	Mod/exp.	Location	Capacity (m^3/d)	Collector type	Collector size (m^2)	Cost ($/$m^3$)	N of stages	Top brine T (°C)	Global radiation (kWh/m^2/day) [a]	DNI (kWh/m^2/day) [a]
[40], [41]	Model	PSA, Spain [b]	1200-3000[b]	PTC[b]	41880[b]	2.5-4	24[b]	<105	4.65	5.6
[39]	Exp.	Tianjin, China	0.3	Flat	NA	4.67	1 [c]	78	4.36	5.58
			6	Flat	NA	3.9		78	4.36	5.58
[42]	Exp.	Gaza [d]	0.145	Flat	5.1	NA	3	NA	5.57	6.98
[43]	Model	Benghazi, Libya	8.3	Flat	1[e]	NA	NA	80	5.44	6.76
			13.2	CPC	1[e]	NA	NA	122		
[44]	Exp.	Tamilnadu, India[f]	0.0085[f]	Flat	2	9	1	NA	5.22	4.97
[45]	Mod/exp.	Suez, Egypt [g]	0.0025-0.0165	Flat	2.39	NA	1[g]	40-67	5.69	7.03

(a) Data based on locations author mentioned from NASA surface meteorology and solar energy. Global Solar Radiation (GSR) is defined as the amount of electromagnetic energy (solar radiation) incident on the surface of the earth; also referred to as total or global solar radiation. The average and percent difference minimum and maximum are given. Direct Normal Radiation (DNI) is defined as the amount of electromagnetic energy (solar radiation) at the Earth's surface on a flat surface perpendicular to the Sun's beam with surrounding sky radiation blocked.
(b) MSF GOR=10, capacity 100m^3/h; 10-16 m^3 water per m^2 collector; Location: Plataforma Solar de Almeria, Spain; PTC layout is horizontal north-south direction (Solar Kinetics T700A) with a distance of 7 m between homologous points into the solar field and row azimuth equal to 0 °. Synthetic thermal fluid (Santotherm 55) with inlet/outlet temperatures of 125 °C/205 °C or lower, but above 100 ° C; temperature change of the thermal oil in the solar field, about 80°C. The system has a thermocline vessel thermal storage.
(c)Seawater first flash evaporation then use generated vapor to distill brine
(d) Location: Al Azhar University at Gaza; Radiation range 2.83-8.19kWh/m^2/d, June–July
(e) Aperture area
(f) Maximum daily production is 8.5L/day, which is 3 times higher than a solar still at Tamilnadu, India with beam solar radiation range 400-900 W/m^2
(g)Performance ration 0.7-0.9, solar radiation ranges 2.79 - 5.12kWh/m^2/d

In general, MSF series-connected stages require precise pressure and temperature control and some transient time is needed to establish the normal running operation of the plant. Since the solar heat source is intermittent, an effective thermal storage system (i.e. a storage tank), can be used for thermal buffering [46]. MSF uses the seawater feed as the coolant which means that MSF uses sensible heat to recover the latent heat from the distilled water. Therefore MSF requires large amounts of seawater recirculating within the system and consumes more electricity than a MED process.

2.2 Solar-assisted Multiple Effect Distillation (MED)

Similar to the solar-assisted MSF process, the solar-assisted MED process also needs both thermal energy and mechanical energy. MED may be operated in three configurations: forward-feed, backward feed and parallel feed. Figure 2.4 shows the schematic of one solar-assisted parallel feed MED, in which seawater is delivered to a sequence of successively low pressure vessels, called effects. The external heat is supplied to the first effect and the generated vapor of the previous effect supplies its latent heat of condensation to the next effect.

Unlike MSF which recovers latent heat from the vapor by the sensible heating of the seawater, MED systems reuse latent heat to vaporize the seawater. The specific heat capacity of water is approximately 4 kJ/kg·K while the latent heat of vaporization is approximately 2300 kJ/kg, therefore MED systems normally have 2-14 effects while MSF systems have more than 20 stages. MED systems use falling film horizontal tube evaporator/condensers for high heat transfer efficiency [47], [48]; operate with a relatively low top brine temperature (usually lower than 75°C) to reduce scale formation and corrosion [49]; and can be combined with heat pumps to improve the overall efficiency [50–52]. The combination of economic costs and low

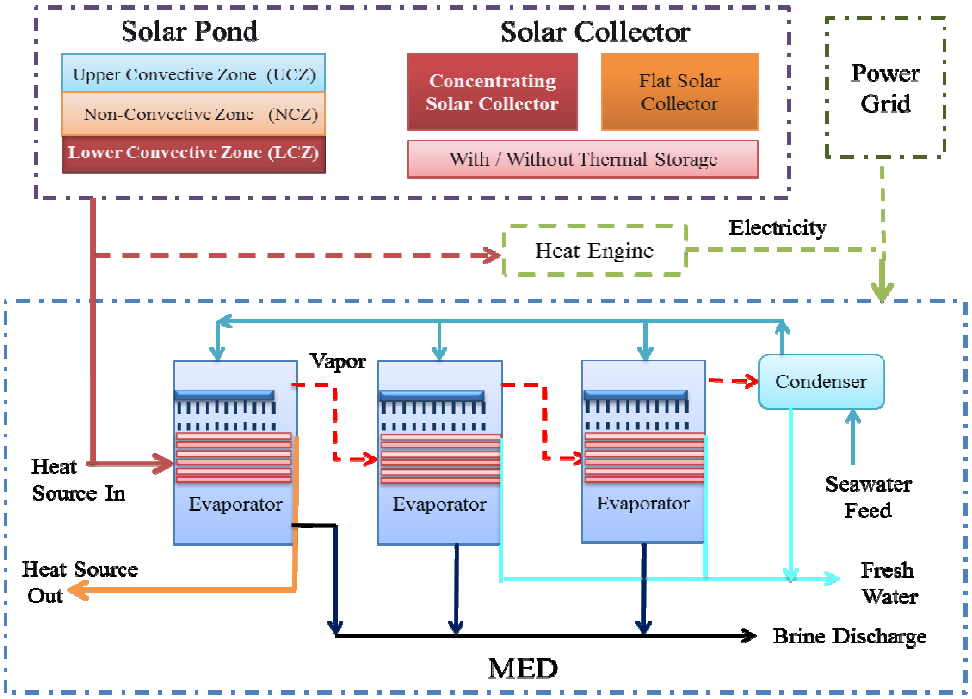

Figure 2.4 Schematic of solar-assisted multi-effect distillation desalination process.

energy consumption, together with the inherent durability of the low-temperature MED, avoid the necessity of comprehensive seawater pretreatment (such as with RO plants) and make the MED process one of the best candidates for safe and durable large capacity desalination [53]. Compared to MSF, MED has high overall efficiency, high heat transfer co-efficient, relative independent stages and less water recycling [54]. However, in order to lower the energy consumption, MED needs a large surface area of evaporators to reduce the temperature difference of adjacent stages., Some research has shown that when operating with high-pressure steam, MED consumed more energy than MSF [21].

2.2.1 Solar Pond-assisted MED

A solar pond-assisted MED system is similar to a solar pond-driven MSF system. However, the lower temperature need of MED makes the solar pond operation relatively easier. By mathematical modeling, Hawaj and Darwish [55] found that intermediate steam supply temperatures (80-90°C) are more efficient for

the operation of solar-assisted MEB systems because higher steam supply temperatures decrease the solar enhancement. A large ratio of solar pond surface area with MED heat transfer area leads to a continuous increase in pond temperature [55]. Garman and Muntasser [56] found that the optimum thicknesses for upper convective zone (UCZ), non-convective zone (NCZ) and lower convective zone (LCZ) were reported as 0.3m, 1.1m and 4m, respectively, for low-temperature MED systems. Some selected solar pond-assisted MED systems are listed in Table 2.7, which also includes a special multi-effect, multi-stage distillation system (MEMS) which is a combination of the MSF and MED systems [29], [57]. Table 2.7 also shows that hybrid systems, similar to the solar pond-assisted MSF plants, have lower unit water costs.

2.2.2 Solar Collector-assisted MED

Solar collector-assisted MED seawater desalination processes have been studied extensively. Table 2.8 shows some selected solar collector-assisted MED systems. Some solar MED systems were combined with heat pumps to improve their performance. Based on long-term tests, the technical feasibility and reliability of solar collector-assisted MED have been proved. Two long term experimental units are the Abu Dhabi solar desalination plant and the Solar Thermal Desalination (STD) Project at the Platforma Solar de Almeria (PSA), Spain.

The Abu Dhabi solar desalination plant, which operated from 1984 to 2002, used evacuated tube solar collectors (ETC) assisted MED systems [64]. Researchers developed a simulation program “SOLDES” [65] to predict the partial load performance [66], optimize the operating parameters so as to maximize the evaporator distillate production for every month of the year [67]. Some plant maintenance was needed, for example, dust deposition could cause the water production to drop to 40%

Table 2.7 Some selected solar pond-assisted MED seawater desalination systems

Ref	Model/exp.	Location/radiation	Pond size (m^2)	Top brine temp.(°C)	Desal cap. (m^3/d)	Cost ($/$m^3$)	N. of effects
[58]	Model [(a)]	Athens	30000	< 75	500	2	14
[59], [60]	Exp.	U. of Ancona (Italy).	625	< 65	30	3.66 [(d)]	4
[29], [57]	Model/ exp.	5.7 kWh/m^2/d [(f)]	3000	63-80	2.3 - 7.2 [(c)]	0.52 - 0.62 [(e)]	4 [(b)]
[61]	Experiment	Bundoora, Australia	720	< 85 [(g)]	0.9-2.3	18-22	3
	Model		11800		50-130	3.4-5.1	12
	Model		58900		260-650	1.7-3.4	12
[62]	Model	2000 kWh/m^2/y [(h)]	1200000	55	20000	0.89	(i)
			12000000		200000	0.71	(i)
			600000		20000	0.79	Hybrid [(j)]
			6000000		200000	0.65	Hybrid [(j)]
[63]	Model	2400 kWh/m^2/y	3300000-4200000	72	100000	0.67-1.44	12
[27]	Model	4.54 kWh/m^2/d[(k)]	7800	< 75, 95-120[(m)]	2348	0.618-0.64	30, hybrid
		4.54 kWh/m^2/d[(l)]			15044	0.465-0.471	

(a) It is assumed that the combined system begins operation in Spring at day N=100 when brine and soil are isothermal.
(b) Multi-effect, multi-stage flash distillation. The MEMS unit is a three effect, four stage system.
(c) This paper reported experimental tests showed that distilled water production rate is 450 to 2270 L/hour, 2.3-7.2 m^3/d;
(d) Reported data in 2.68 Euro, converting currency as 1 Euro U.S. dollar = $1.3656.
(e) Hybrid system estimated cost, assume system used brine from 1MGD-10MGD RO plant, solar pond liner cost is $4/$m^2$;
(f) The Location is EI Paso, and the annual average irradiation data is 5.7kWh/m^2/d.
(g) Solar pond supply temperature ranges between 50-85°C.
(h) Annual total insolation. Based on authors' mentioned location, NASA data shows annual radiation 5.72kWh/m^2/d horizontally, 7.43kWh/m^2/d direct beam radiation.
(i) MED operates with 6.5-7.5 kWhe/m^3 (including 1.5-20 kWhe/m^3 for pumping and other auxiliaries);
(j) MED followed by RO hybrid systems powered by a solar pond that are estimated to consume 5.5-6.5 kWhe/m^3.
(k) The main heat source is exhaust from a 30MW gas turbine at 550°C. Part of the heat is used directly to run a desalination plant and the rest is stored in a solar pond (depth 4m). Radiation data is the same with (l)
(l) Hybrid plants. Main heat source is exhaust from a 120 MW gas turbine, with the rest of the conditions the same as (k). Based on authors' proposed location, south of Tunisia, NASA data showed horizontal monthly annual average horizontal radiation is 4.54kWh/m^2/d and direct norm radiation is 5.24kWh/m^2/d.
(m) Peak time heated by gas turbine, the seawater temperature is 95-120°C while the rest of the time it is heated by a solar pond at 75 °C, and MED GOR is 21.5.

of the clean collector production [68]. The economic feasibility studies [69], [70] showed that it is not worth operating the desalination system solely on solar energy due to the high percentage of inactive time [71]. When electricity cost is above $0.071/kWh in Israel [72], the solar-MED plant is more economical than RO.

The Spain PSA site used a 14-stage forward-feed MED system with a capacity of 3 m^3/hour [78]. The project had two phases. Phase I studied the reliability and technical feasibility of a solar thermal technology application to seawater desalination which used PTC with 14-stage MED. Phase II used a double absorption heat pump to improve the system performance as shown in the next section.

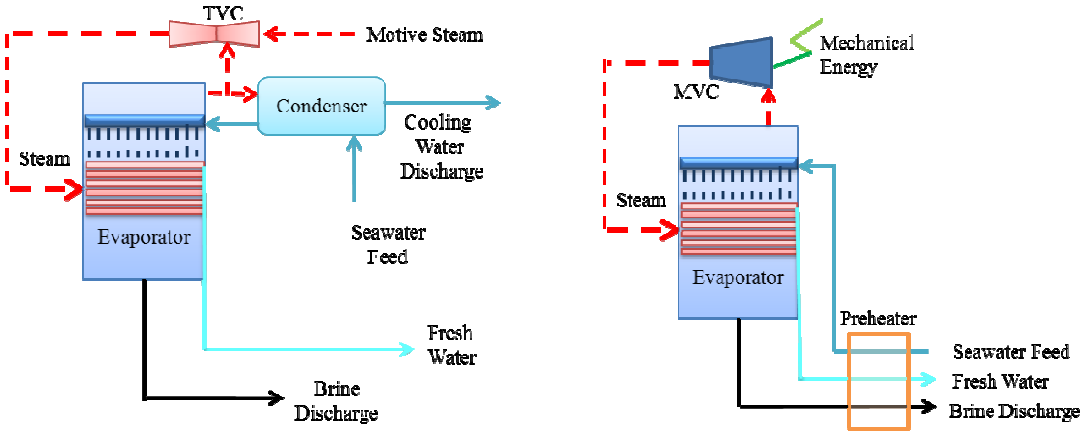

(a) Thermal vapor compression (TVC) (b) Mechanical vapor compression (MVC)

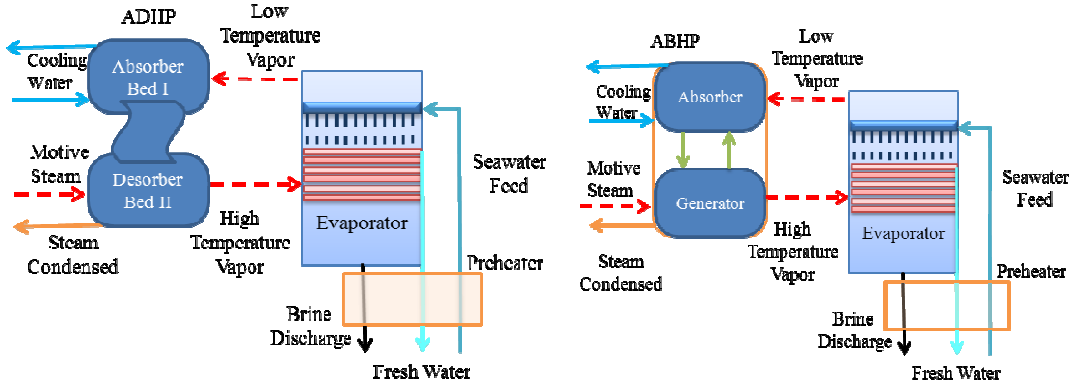

(c) Single effect adsorption heat pump (d) Single-effect absorption heat pump

Figure 2.5 Schematic of different heat pumps used in desalination.

Table 2.8 Selected solar-assisted MED systems

Ref	Mod/exp	Location/ radiation	Global radiation	DNI	Cost	Capacity	Collector	N of effects	Operation temperature	Collector area	Notes
[73]	Model	Richmond, California	4.57 [(j)]	5.54[(j)]	2.05-4.7	0.151	FPC/EPC	7-12	< 95	NA	
[72]	Model	Israel, Eilat [(i)]	5.65	6.91	0.92	10000	PTC	16	NA	NA	
		Zikim, Israel [(h)]	5.57	6.99	0.69	100000				750000-900000	Hybrid
[74]	Model	Southern Mediterranean	2000kWh/m²/y; peak radiation 1000W/m2		2	1000	ETC	NA	NA	NA	
[69]	Model	Abu Dhabi, UAE	5.61	6.41	8.6-9.9	100	ETC-PV	10-30	60-80	2500-12500	PV
					8.3-9.3	100	ETC				Diesel hybrid
					5-6.7	500					
					3.4-4.4	1000					
[75]	Exp.	Abu Dhabi, UAE	5.81 [(g)]	6.41	6.58-10 [(d)]	120	ETC	18 [(e)]	< 76.5	1862[(f)]	
[76]	Exp.	Sydney	4.98	5.93	4	100	FPC	NA	NA	NA	
					5.1		ETC				
[77]	Mod/exp	PSA, Spain [(k)]	4.65	5.6	NA	72[(l)]	PTC	14 [(l)]	<70	500	(l)

(a) \$1.1/m^3 for a hybrid plant using \$0.18/kg diesel oil when solar-steam is not available. Total land area is 14000m^2 for a solar-only 1000m^3/d plant; 1420000m^2 for 100000 m^3/d plant.

(b) A combination of a large number of effects of evaporation, together with high pressure saturated steam available for recycling, increased the calculated economic ratio (ER) from 7 to 16 -- a factor of 2.3, while the installation expenses grew by 60%.

(c) Utilization of solar energy is assumed to be about 2500 effective hours per year, which is about 30% of the storage capacity, or fossil fuel backup.

(d) When considering the contribution of capital amortization representing about 85% of the total cost and only 15% contributed by operation and maintenance expenses, and with water costing \$6.58, , the total cost of water ranges from about 7 \$/m^3 to 10 \$/m^3

(e) An 18 Stage MED system, with 17 preheaters, a performance ratio 12.4, and 3 tanks totaling 300m^3 as water heat accumulators.

(f) Collector total absorber area is 1862m^2, with each collector 1.75m^2.

(g) Authors' mentioned annual mean daily solar radiation at 5000 kcal/m^2 day.

(h) The author gave one case study at Zikim on the Southern end of Israel's Mediterranean shore.

(i) The author used Eilat as one typical place for an area close to Israel's Red Sea.

(j) Estimated from NASA data based on the author's location.

(k) Plataforma Solar de Almería, Spain. Phase I of the STD project considered the reliability and technical feasibility of the solar thermal technology application for seawater desalination.

(l) When Capacity is 3m^3/h, assume 24 hours operation which is 72m^3/day; a 14 effects MED has a performance ratio of 9.4-10.4; and vacuum is generated by hydro ejectors using 3 bar seawater.

2.3 Solar-assisted Heat Pump (HP) Desalination

HP units are generally used for small or medium scale [79], [80] applications and they are normally combined with other thermal processes [81–85]. There are four basic types of heat pump applications in desalination processes [50]. These include thermal vapor compressor (TVC) (Figure 2.5a), mechanical vapor compressor (MVC) (Figure 2.5b), absorption heat pump (ABHP) (Figure 2.5c) and adsorption heat pump (ADHP) (Figure 2.5d) [51].

TVC could be used with MED or MSF in different sizes of commercial desalination plants [86–89], in which the steam compression is carried out by an ejector and the vapor from the last effect of the MED process is carried by a motive stream back to the first effect. MVC is widely studied and used because of its simplicity and relatively low energy consumption [90–93]. The bottoming condenser is eliminated because the entire vapor formed in the last stage is routed to the mechanical vapor compressor, where it is compressed to the desired temperature and pressure in order to recover heat in the rejected brine and distillate product streams. ABHP [94–98] absorbs the last effect vapor through LiBr-water and discharges steam for use by the first effect; while ADHP [99], [100] uses zeolite-water or other pairs to recover vapor from the last effect MED and generate high-temperature steam through a desorber bed II. ABHP and ADHP are regarded to have higher potential for applications in desalination than TVC and MVC [51], [101], however, at the present time there are no commercial applications.

All heat pump-combined thermal desalination systems recover the low-temperature vapor from certain parts of the MED/MSF system and convert it to higher temperature vapor in order to improve the system efficiency. Furthermore, since low-temperature vapor could be recovered, the whole desalination system needs less

cooling water and consumes less electricity. The differences among various heat pump based systems are that (1) MVCs use electricity as energy source (Figure 2.8) and could be used as stand-alone desalination systems; (2) TVCs use higher temperature and pressure (>200kPa) steam; (3) ABHP and ADHP use either higher temperature steam or other heat sources in the absorption/adsorption cycles. Solar-assisted heat pumps combined with other desalination processes could be used as shown in Figure 2.8. MVC must be driven by mechanical energy therefore a photovoltaic (PV) system or a heat engine are used; TVC/ABHP/ADHPs use steam therefore they are connected between the solar thermal process and the thermal desalination process.

Photovoltaic (PV) cells can be made from common semiconductors like silicon or germanium or semiconductor compounds such as GaAs, CdTe, CuInGaSe, PV cells in their simplest form are large area electronic semiconductor diodes allowing current to flow in the reverse direction in the presence of light. PV cells can directly convert solar radiation into useful electricity, as shown in Figure 2.6 [22]. Cells are connected in series and/or parallel configurations to form a PV module or panel. Photovoltaic panels can be designed for specific voltage and current output when the sun rays strike the module normal to its surface with an intensity of 1,000 watts per square meter. Under these conditions the PV module power output is expressed in peak watts or peak kilowatts. Photovoltaic systems include an array of joined panels to produce the required electrical output. Figure 2.7 [22] shows a schematic of a PV system that includes storage (batteries) for a stand-alone operation. Since the PV systems generate a DC power output, an inverter is used to convert DC to AC. Photovoltaics can be employed independently or jointly with other sources to generate the electricity needed to power desalination systems.

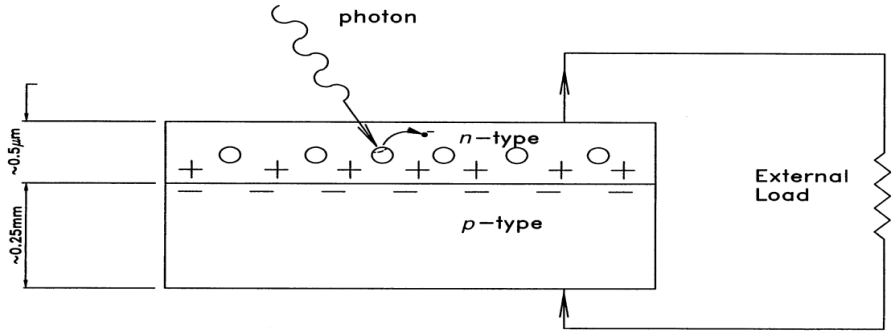

Figure 2.6 Photovoltaic cell schematic.

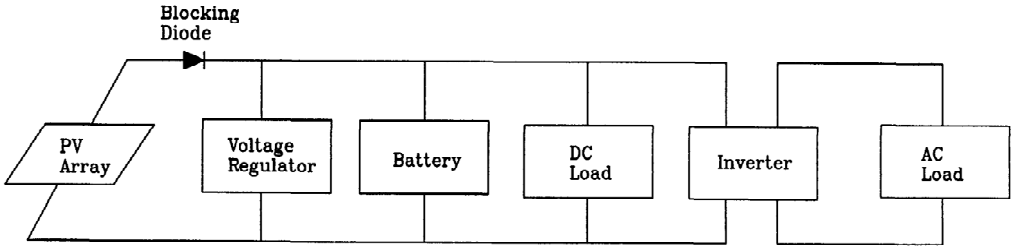

Figure 2.7 Schematic of a stand-alone photovoltaic system.

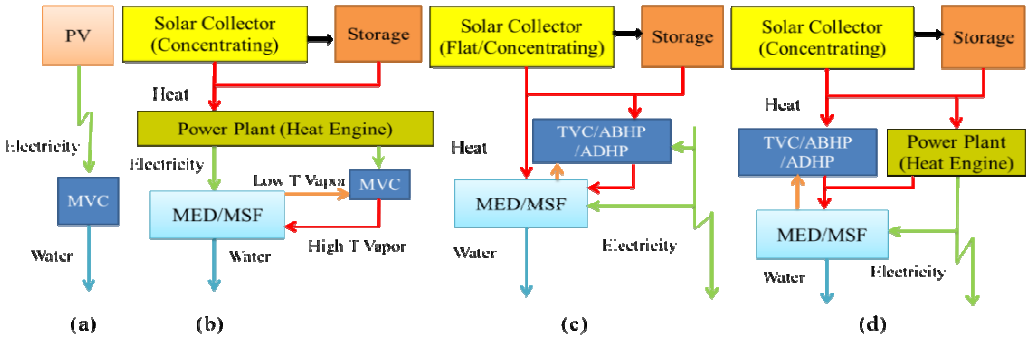

Figure 2.8 Possible configurations for the solar-assisted heat pumps and combinations.

Among all the research activities listed in Table 2.10, the project AQUASOL achieved the lowest experimental specific energy cost as listed in Table 2.9 [102]. The AQUASOL project is the continuation of the previous STD Project [41], [103–106] mentioned in section 2.2.2. It is composed of [107]: a) a 14-effect MED; b) a 500m^2 stationary CPC collector field; c) a 24 m^3 thermal storage system based on water; d) an advanced prototype of LiBr-H_2O double-effect absorption heat pump (DEAHP);

and e) a smoke tube gas boiler to guarantee 24 hr. operation. Researchers found that the connection between the absorption heat pump and the MED unit should not be direct by means of a closed water circuit that is heated by the heat pump and cooled by the MED unit, but rather, it should be indirect, by means of two auxiliary tanks [107].The cost could be lowered to about \$2 per m^3 of distillate for large plants [108], [109], which is comparable to conventional MED, but the optimization depends on the cost of fossil fuels and solar collectors [110].

2.4 Solar-assisted Reverse Osmosis (RO)

As illustrated in Figure 2.9, RO, which is the biggest desalination process internationally in terms of capacity, requires only electricity from PV or mechanical energy from a solar pond or collector through a heat engine such as a sterling engine or a Rankine engine, [111]. RO requires extensive water pretreatment but is energy

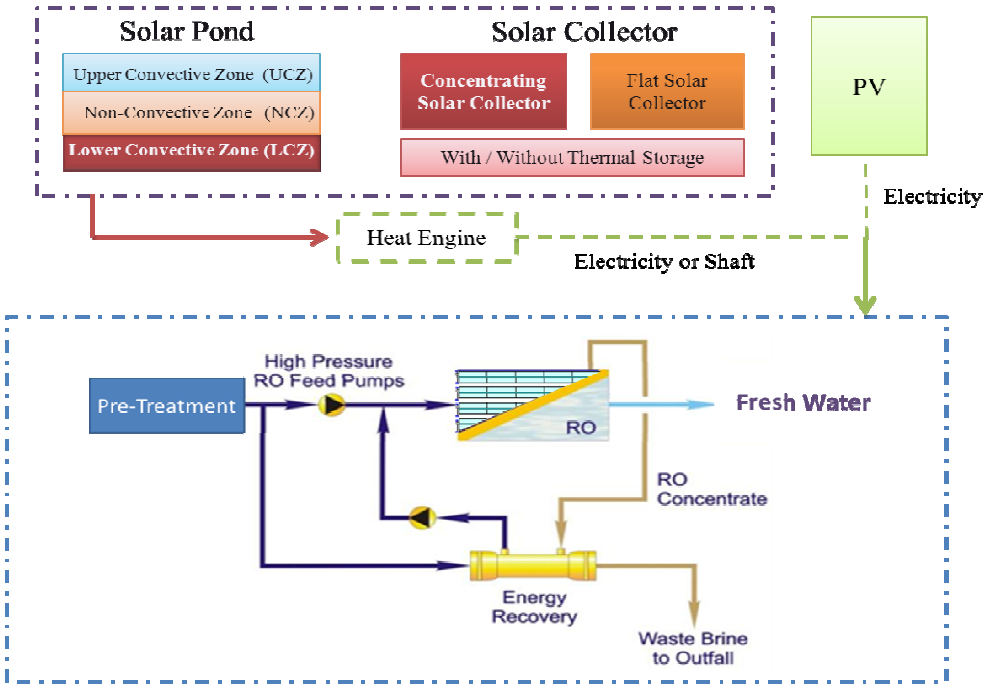

Figure 2.9 Schematic of solar-assisted RO process.

Table 2.9 Thermodynamic assessment of solar collector-MED desalination plants

Desalination system	Main energy consum. (kJ/kg)	Solar desalination system	Solar energy consum. [(a)] (kJ/kg)	Exergy performance of solar desalination system [(c)] (%)
DEAHP-MED	108 (at 180ºC)	PTC–DEAHP–MED	142	4.3
MED	240 (at 70ºC)	PTC–MED	315	2.0
MED	240 (at 70ºC)	LTC–MED	545–1600 333–369[(b)]	1.1–0.4 1.8–1.7

(a) Efficiency of solar collectors at solar irradiance of 800 W/m^2;
(b) If evacuated absorber tubes are used.
(c) Exergy of the distillated is 5.863 kJ/kg. Auxiliary energy consumption is not considered (PTC: parabolic trough collectors, LTC: low-temperature solar collectors).

Table 2.10 Summary of solar thermal desalination system using heat pumps

Authors'	Solar Systems	Heat Engines	Other Desal. Systems	Heat Pumps	Desal.Cap. (m^3/day)	Notes
Zejli[101]	PTC		MED	ADHP		Modeling a conceptual desalination plant using two adsorption reactors and a three-effect MED.
Palenzuela [112]	PTC	Steam Cycle	MED	TVC	48498	The PTC- MED-TVC system could compete with PTC+RO as the motive steam pressure is 2 bar,
Sharaf[113]	PTC		MED	TVC	4545	PTC-MED-TVC gives attractive results compared against PTC-MED-MVC technique.
		Toluene ORC	MED	MVC	4545	
Helal[114]	PV			MVC	120	Solar/Diesel Hybrid
Nguyen[115]	Flat		Evaporator	ABHP		Hybrid gas/solar-driven absorption heat pumps showed higher water yield than conventional solar stills.
Milow[108]	PTC		MED	DABHP (a)	72	Solar thermal desalination project (STP): Proves the technical feasibility of solar drive DABHP-MED system; cost \$2/m^3.
García-Rodríguez [109]	PTC		MED	DABHP	72-2400	STP Project: DEAPH-MED is more suitable for solar application than a MED only system due to the high energy cost required by solar field.
Alarcón-Padilla[102]	PTC		MED	TVC	72	Summarized STP project which tested PTC-driven MED, TVC-MED and DABHP-MED system. DABHP-MED is the most promising for a solar-driven desalination system which was further studied in AQUASOL project.
				DABHP		
Alarcón-Padilla[52], [107], [116], [117]	CPC(b)		MED	DABHP	72	AQUASOL project: Experimentally demonstrated the feasibility of the hybrid solar/gas desalination using DEAPH-MED. Reviewed past experience of DEAPH-MED and provided design suggestions.
Roca [118–120]	CPC		MED	DABHP	72	AQUASOL project: Described model control- feedback system.
Gomri[121]	Flat		Separation-Condense	AHT(c)		Developed one computer program for modeling AHT-Distillation system and provided energy and exergy analysis.

(a) DABHP: Double-effect absorption heat pump.
(b) CPC: compound parabolic concentrator.
(c) AHT: absorption heat transformer.

efficient compared to phase change thermal processes, and part of the consumed mechanical energy can be reclaimed from the rejected concentrated brine with a suitable energy recovery device such as a pressure exchanger. Osmosis is a natural phenomenon in which water passes through a membrane from the lower salt concentration side to the higher salt concentration side. To reverse the flow of water, a pressure larger than the osmotic pressure must be applied. Seawater pressure must be higher than the natural osmotic pressure, typically 2500 kPa, but is kept below the membrane tolerance pressure, typically between 6000 and 8000 kPa, forcing pure water molecules through the RO membrane pores to the fresh water side. Fresh water is collected while the concentrated brine is rejected. Among the reported solar-assisted RO seawater desalination research, PV driven RO and solar thermal heat engine driven RO are the most widely studied.

2.4.1 PV-assisted RO System

The PV powered RO system is very popular in demonstration plants [122–124] because both PV and RO are modular and easily scalable [125]. Considerable research has been carried out on whether to use: a) an energy recovery device [126]; b) a battery [127]; c) another power source, such as wind [128] or diesel [129], in a hybrid system; or d) another desalination method should be combined with RO to desalinate water [130]. A parametric study for economic analysis was conducted in [131] and optimization strategy was studied in [132]. Generally speaking, a PV-RO combination works like two independent units of PV and RO. Although there is still much room for improving the combination of both technologies, technical feasibilities normally are not the barriers as compared to the economic [133] and reliability considerations [134]. Table 2.11 lists a few selected seawater PV-RO and hybrid systems developed after the year 2000.

2.4.2 Solar Thermal Assisted RO System

Different from PV-RO plants which are almost commercially available in small-scale and compact plants, solar-thermal RO desalination plants, as illustrated in Table 2.12, are still far from commercialization. Some researchers [135], [136] have studied the application of solar thermal energy for desalination by coupling an ORC with the seawater reverse osmosis (ORC-RO). The advantage of coupling an ORC with a desalination system is that the seawater provides a heat sink for the ORC condenser while at the same time it is preheated to increase the RO membrane permeability, leading to reduced power consumption.

Table 2.11 Selected PV-assisted RO seawater plant

Systems (location)	Year	Additional power supply	Production (m^3/d)	Cost ($/$m^3$)	Battery	Energy recovery system	PV capacity (kW)	Source
Abu Dhabi, UAE	2008	Diesel	20	7.2	No	Yes	11.25	[137]
		No		7.3	No	Yes	22.49	
Agriculture University of Athens, Greece	2008	No	0.35	7.8	Yes	Yes	0.85	[126]
	2004	Wind	12	5.2	Yes	Yes	30.22	[128]
		No	12	6.64	Yes	Yes	13.2	
CRES, Laviro, Greece	2004	Wind	3.12	31.5	Yes	No	4	[138]
ITC-DESSOL, Gran Canaria, Spain	2003	No	10	13.16	Yes	No	4.8	[139]
CREST, Loughborough University, UK	2003	No	3.9	2	No	Yes	2.4	[140], [141]
CIEA-ITC, Canary Islands, Spain	2001	No	1.24	9.6	Yes	Yes	4.8	[142]
CRESTA, Curtin University of Technology, Australia	2007	Diesel	1	NA	Yes	No	1.2	[143]
GECOL at Ras Ejder, Libya	2005	Wind and grid	300	0.9	No	Yes	50	[144]

Table 2.12 Summary of solar ORC-driven seawater RO research

Author	Exp. or model	DNI(W/m^2) /location[a]	Cycle highest temp.	Cycle fluids	Cycle configuration	Pressure (bar)	RO pressure (bar)	Cycle efficiency	Collector area per kg fresh water (m^2/L/s)	Feed salinity (ppm)	Recovery rate [o]
Manolakos [148]	Model	Athens, Greece	75.8	134a	Single ORC	22	47.8	0.73-3.08	864[b]/648[m]	42710	0.18-0.2
Manolakos [146], [153]	Exp.	1000	75.8	134a	Single ORC	22	47.8	7	1056[C] /792[m]	42710	0.15
Kosmadakis [145], [147], [154]	Model	1000	137	245fa	Cascade upper cycle	26.6	56.2	11.8	432[d] /324[m]	42710	0.2
			75.8	134a	Cascade bottom Cycle	22					
Delgado-Torres[155]	Model	850	355.7[i]	Toluene	Cascade upper cycle	<41.26 [j]	55.3	21.29[i]	48.2[e],[f],[i]	35731	0.488
			129.8–130.3[i]	Isopetene	Cascade bottom Cycle	<33.78 [j]	55.3	10.59-13.06[i]			
			336.3[i]	MM[n]	Cascade upper cycle	<19.39 [j]	55.3	15.33[i]	65.2[e],[f],[i]		
			145[i]	Isopetene	Cascade bottom Cycle	<33.78[j]	55.3	10.93–13.44[i]			
Delgado-Torres [156]	Model	850	320-380[i]	Toluene	ORC with Recuperator	<41.26[j]	NA	29.48-31.78[i]	NA	NA	NA
			260-380[i]	MM	ORC with Recuperator	<19.39[j]	NA	23.87-25.93[i]	NA	NA	NA
Delgado-Torres [151]	Model	1000	145[l]	R245fa	ORC with Recuperator	20.866	52.4	15.46	73.7[e],[f]	35700	0.45
Bruno [157]	Model	800	87.3	R218	ORC with recuperator	<26.8[j]	64.8	7.81	1209.6[b],[g],[h]	36000	0.5
			120.9	R245	ORC with recuperator	<31.37[j]	64.8	13.24	603.1[b],[g],[h]	36000	0.5
			289.7	R601a	ORC with recuperator	<33.7[j]	64.8	27.61	336.0[b],[g],[h]	36000	0.5
			378.4	N-propyl benzene	ORC with recuperator	<32[j]	64.8	32.19	231.8[b],[g],[h]	36000	0.5
A.S.Nafey [k] [135]	Model	850	100	water	Rankine	0.576	67	10.17	449.4[d]	45000	0.3
		850	150	water	Rankine	2.755	67	13.34	402.5[d]	45000	0.3
		850	320	Toluene	Single ORC	32.78	67	26	166.3[d]	45000	0.3

Table 2.12 (Continued)

(a) DNI is direct normal radiation which is used for modeling design; the location is experimental or case study location and solar radiation data TM2 is used.
(b) Gross collector area is calculated by TMY2 data.
(c) Gross collector area from experimental data.
(d) Gross collector area calculated by design DNI data.
(e) Aperture area of collector calculated by design DNI data.
(f) Use 24 hours a day to convert from daily flow data.
(g) Use 7 hours a day to convert daily flow data.
(h) Case study results for location Barcelona.
(i) Data for LS3 collector using heat transfer fluids.
(j) Critical pressure of the fluids.
(k) Data selected from superheated condition.
(l) R245fa using heat transfer fluids with a recuperator effective factor of 0.8.
(m) Converted to aperture area.
(n) MM is Hexamethyldisiloxane.
(o) Recovery rate refers to the percentage of the feed seawater that is recovered as fresh water.

Kosmadakis et al. [136], [145–149] did the pioneering research on integrating ORC with RO and were the only ones who carried out both theoretical and experimental studies. The solar collectors they used could provide up to 150 ℃ for the ORC using R245fa as the working fluid in a topping cycle with R134a as the working fluid for the bottom cycle. The recovery of their RO system was less than 20% which is relatively low while most seawater desalination plants operate with recovery rates between at 35%-60% [150]. Delgado-Torres et al. [151] pointed out that a single ORC with R245fa as the working fluid would have a higher efficiency than the cascade system studied by Kosmadakis et al. when operating between the same two temperatures. Tchanche et al. [152] pointed out that the integration of different devices is not significantly rewarded with an efficiency gain; therefore, it is preferable to keep the configuration of the ORC simple when designing an ORC-RO system.

The solar collector could be a flat plate or evacuated tube collectors (ETC) to provide heat source temperatures less than 150℃ or concentrating collectors for higher temperatures. The relative organic Rankine cycle should use different organic fluids in order to match the solar collector and the heat source temperature. Some high-temperature (300-400℃ range) solar ORC-driven desalination system working fluids could be [151], [155], [156], [158–162]: toluene, octamethylcyclotetrasiloxane ($C_8H_{24}O_4Si_4$), decamethylcyclopentasiloxane ($C_{10}H_{30}O_5Si_5$), hexamethyldisiloxane ($C_6H_{18}OSi_2$) and tetradecamethylhexasiloxane ($C_{14}H_{42}O_5Si_6$). The later four compounds are usually referred to as D4, D5, MM and MD4M, respectively. Since RO needs only mechanical energy, which can be provided by a power cycle, the high-temperature ORC cycles with higher efficiency could provide more mechanical energy per unit collector area. However, which kind of collector is the best needs to

be analyzed case by case and will be affected by many factors such as the collector unit cost and location [157].

2.5 Solar-assisted Electrodialysis

Electrodialysis (ED), driven by electricity only, is a type of technology which arranges cationic and anionic ion-exchange membranes alternately in a direct current field (Figure 2.10), where the salt ions migrate from the dilute solution side to the concentrated solution side through ion-exchange membranes under the influence of an applied electric potential difference. ED processes are different from the MSF, MED and RO systems in that dissolved salts are moved away from the feed seawater rather than the reverse. They are not economically competitive for seawater applications because of the large quantities of salt, the high cost of electrodes, the expensive ion exchange membranes and relatively short life time of membranes when working in a high-density electric field [163], [164], therefore, most of the researchers used a PV driven ED process only for brackish water [165–168]. In a small-scale 10 m^3/d PV driven ED plant experiment, the seawater needs to recirculate a number of times before the desired water quality is obtained [169], [170]. So far, only a few studies have been carried out on solar-assisted ED seawater desalination [171], [172].

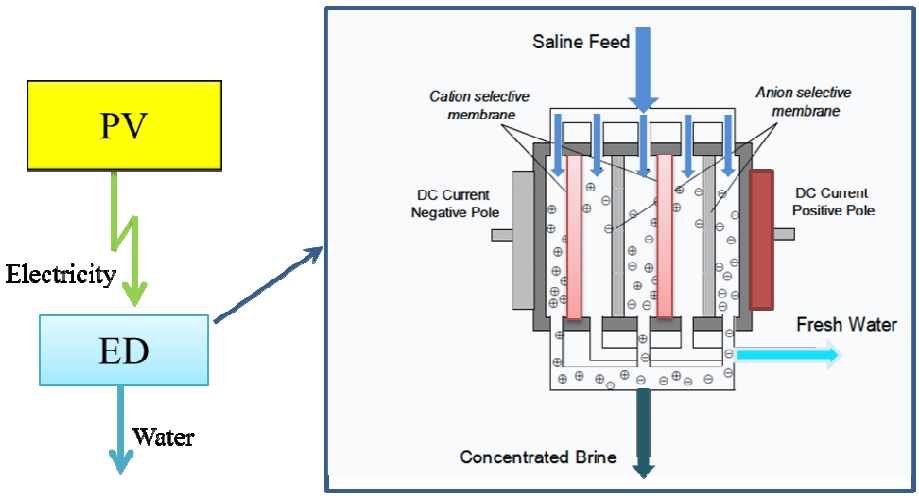

Figure 2.10 Schematic diagram of PV-assisted electrodialysis desalination process.

2.6 Solar-assisted Passive Vacuum Desalination (PVD)

The passive vacuum desalination (PVD) concept is to use a thermal system without using a steam ejector or vacuum pump in a small-scale thermal system application, as originally adopted by Goswami [173], [174] for desalination applications. The basic concept as seen in Figure 2.11 is that a thermal system is first filled with seawater to a height of more than 10 meters above the ground, then the water drains to create vacuum in the system. The vacuum is generated in the headspace left in a sealed tank taller than 10 meters when the standing column of water held by atmospheric pressure drops by gravity. Detailed description and analysis may be found in references [175–177] in which both theoretical modeling and experimental results are provided. Several researchers have used this idea as the basis and further developed different passive vacuum systems such as systems combined with sensible heat thermal energy storage (TES) [178], [179], combined with wind power [180], and combined with PV system [181] , as listed in Table 2.13.

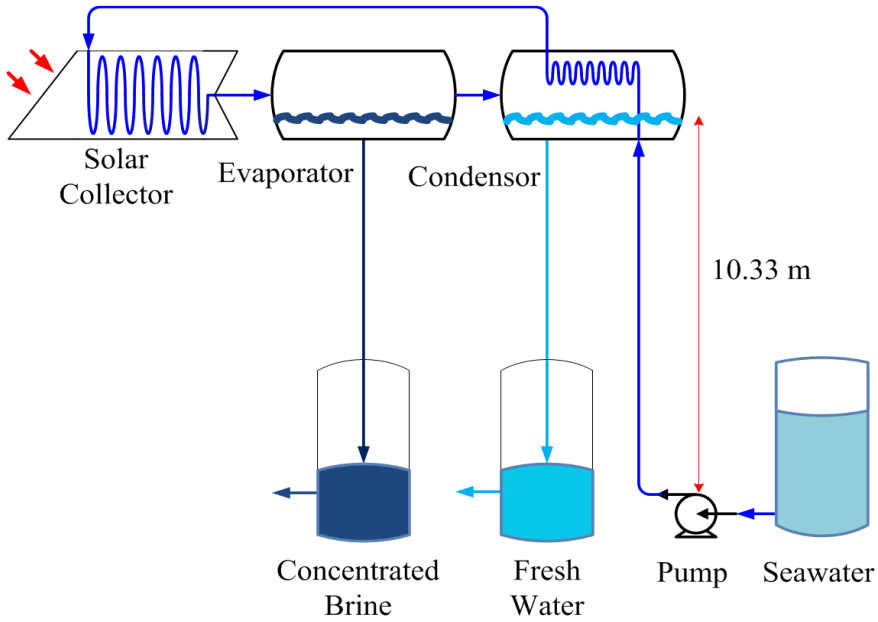

Figure 2.11 Single–stage passive vacuum flash desalination system.

Table 2.13 Research on passive vacuum desalination system

Authors	Year	Comments
Goswami [173], [174], [182]	2003 2004	Proposed and built evaporation-based PVD concept using a solar water heater. Experimental analysis confirmed theoretical modeling which showed that the effect of withdrawal rate and the depth of water in the evaporator were small, while the effect of heat source temperature is significant.
Nirmalakhandan[178], [179]	2008	PVD was combined with sensible thermal storage system and solar absorption air-conditioning system. Simulation showed energy consumption of less than 210kJ/kg freshwater produced.
Goswami [176], [177], [183]	2009 2010	Proposed and built flash system-based PVD system. Experimental results showed the process is feasible if operated at high temperatures and moderate flow rates. However non-condensable gas accumulation reduced water production rate.
Ayhan and Madani [180]	2010	PVD desalination system was combined with renewable energy such as wind and solar power giving a production cost of $1.00 per ton for a lifetime period of 20 years.
Nirmalakhandan [181]	2010	PVD combined with solar still and PV panel system. Experiments showed that the distillate system could produce twice as much freshwater as the simple solar still.

Though the passive vacuum method could generate vacuum by using natural gravity without using vacuum pumps, the non-condensable gases within the seawater can accumulate over time and affect the vacuum conditions in the evaporator. This lowers the overall heat transfer efficiency and reduces the fresh water production rate [174], [182], [183]. In summary, PVD is a simplified MSF/MED thermal system and could operate with less pretreatment compared to the RO. It is suitable for places like ships where the deck height is naturally more than 10 meters higher than the seawater level and where robust desalination systems are needed.

2.7 Solar Still

In a solar still, also called direct still system (Figure 2.12), the heat collection and distillation processes occur within the same system where solar energy is used directly for distillation by means of the greenhouse effect. Water vapor rises to the transparent cover by natural convection and condenses there. A solar still output might be affected by many factors including brine depth, vapor leakage, thermal insulation, cover slope, shape material, climate, et al. [184], [185]. The latent heat is normally wasted on the cover, therefore the system efficiency is relatively low with a daily production of about 3-4 l/m^2 [46].

Solar stills have been extensively studied [186], as listed in Table 2.14. A theoretical relationship of heat and mass transfer within the still was developed by Dunkle in 1961 [187]. Later, researchers developed different kinds of solar still systems, such as: solar stills coupled with solar collectors, as can be seen in Figure 2.12b [188–191]**;** solar stills with condensers (Figure 2.12c) [192], [193]; solar stills under low pressure [194], [195]; solar stills with heat recycling [196], [197]; multi-stage/multi-effect solar stills (Figure 2.12d) [198–200]; solar stills with heat storage [201–204]**;** and hybrid solar still/PV systems [205], [206].

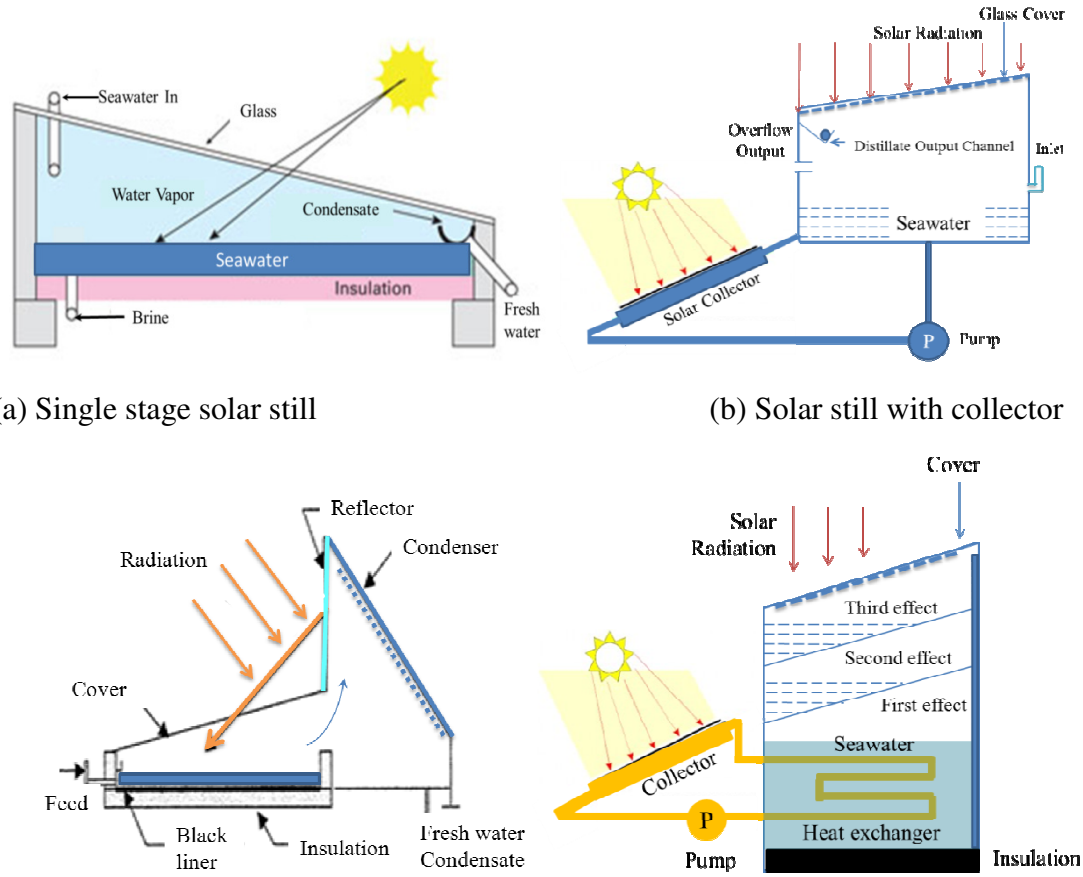

(a) Single stage solar still (b) Solar still with collector

(c) Solar still with condenser (d) Multi-stage solar still

Figure 2.12 Schematic of solar still.

2.8 Solar-assisted Humidification-Dehumidification (HDH)

The HDH process, which uses low-grade heat that could be supplied by solar collectors, is based on the fact that the saturation humidity roughly doubles for every 10°C increase in temperature. For example, air at 90^0C can hold five times more water than air at 70°C. When air comes in contact with salt water, it extracts some amount of vapor at the expense of sensible heat of salt water, causing cooling. On the other hand, the distilled water is recovered by maintaining humid air in contact with the cooling surface, releasing the latent heat of condensation from the vapor. HDH can be divided into two big groups: closed-air, open-water (CAOW) cycle and closed-water open-air (CWOA) cycle [207], [208]. More detailed system configurations, combinations and modeling could be found in reference [209]. Among all kinds of

Table 2.14 Selected solar still

Main feature	Author	Additional comments
W/collector	Kumar [188]	Water flow over the cover to increase the temperature difference.
	Lawrence [189]	System was operated under thermosiphon mode.
	Tiwari [190]	Thermal analysis showed that efficiency drop with increase of collector area.
	Yadav [191]	Numerical analysis agrees well with experimental results.
	Badran [192]	Coupled with flat collector and studied parameters (i.e. water depth, direction of still, radiation).
W/condenser	El-Bahi[192]	Output increased 70%.
	Fath [193]	Output increased 50%.
W/vacuum units	Tay[194]	Uses waste heat from steam turbine.
	Low [195]	Use turbine exhaust steam.
W/heat recovery	Mink [196]	Both latent heat and sensible heat to pretreat feed.
	Schwarzer[197]	Recover latent heat from the condensation process.
Multi-stage/ effect	Fernandez [198]	Each tray has a W-shape bottom that acts as a condenser for the pan below.
	Kumar [199]	Numerical model was developed and validated for a single effect still.
	Tanaka[200]	Vertical multiple-effect diffusion-type still with solar collector.
Heat storage	El-Sebaii [201]	Phase change material (PCM) was used for heat storage.
	Onyegegbu [202]	Still with thermal energy storage.
	Velmurugan[203], [204]	Solar stills integrated with a mini solar pond.
Hybrid system	Kumar[205]	Waste heat from PV system for water heating.
	Hidouri[206]	Solar still connected to a heat pump.

configurations, the multi-effect CAOW water-heated system is regarded as the most energy efficient [210]. The schematic of one solar-assisted multi-effect CAOW can be seen in Figure 2.13. The basic cycle has a solar collector as the heat source, an air humidifier and a dehumidifier. Seawater passes through the collector where the temperature rises and then through the humidifier where water vapor and heat are given up to the counter-current air stream which cools down the brine. Finally the air passes over the dehumidifier where fresh or seawater is used for cooling.

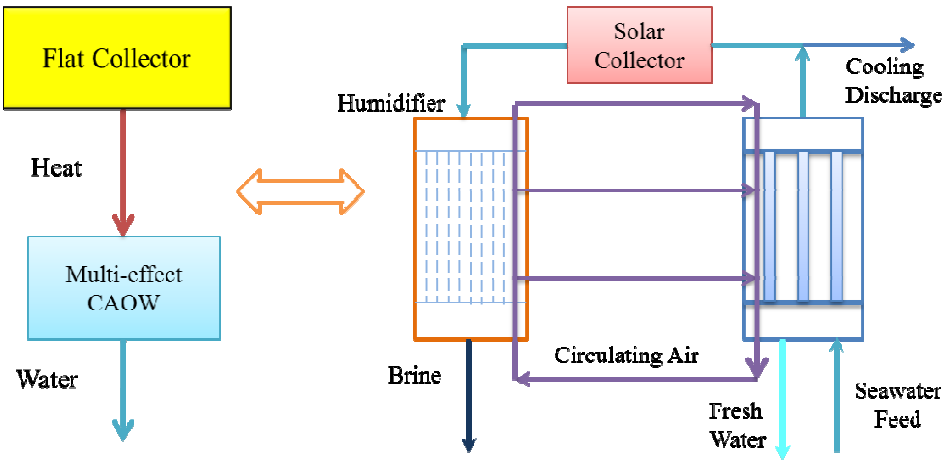

Figure 2.13 Schematic of solar-assisted multi-effect CAOW system.

The seawater greenhouse is another solar-assisted HDH application shown in Figure 2.14. A seawater greenhouse produces fresh water plus cools and humidifies the crop growing environment. It is suitable for arid regions because the plastic cover entraps long wave radiation and reduces transpiration; so, fresh water is produced and the environment is humidified. The seawater greenhouse is especially suitable for remote arid areas because it provides additional water supplies without relying on scarce groundwater; in essence, it makes agriculture immune to climatic variations.

The HDH process is still under research and development and there is still a lot of room to improve the process [211], [212]. Researchers have produced experimental results to verify the models [213–216], have tried different methods

including studying the ambient temperature effect [217], developing corrosion free HDH collectors [218], combining a cooling tower to improve water production [219], using pinch analysis to improve the system performance [220], [221], and adjusting the seawater/air flow ratio to maximize water production [222], [223].

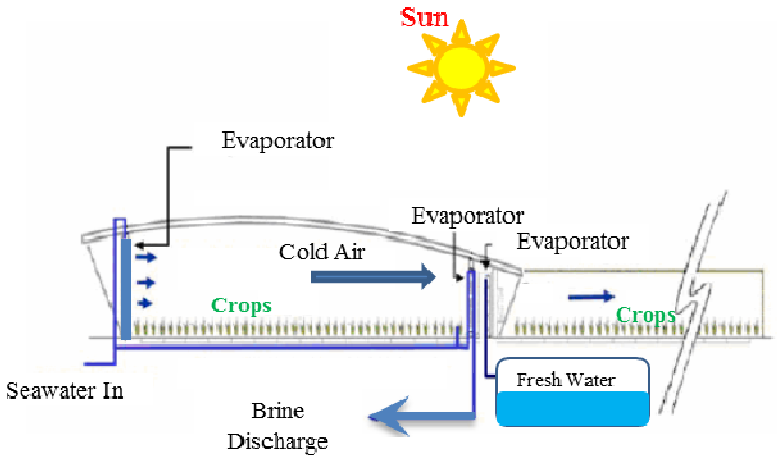

Figure 2.14 Solar-assisted seawater greenhouse.

It should be noted here that the predecessor of the single stage HDH cycle is a simple solar still whose energy cost is very high [224]. Therefore, theoretically, this system should be targeting small-scale applications [223] (from 5 to 100 m^3/day water production) for which the cost of water production is much higher than for large-scale systems. Several cost estimations and optimizations are given in references [225–227] with mixed results on whether or not HDH is more economical than small-scale RO as reported in references [76], [228].

2.9 Solar-assisted Membrane Distillation (MD)

Membrane distillation (MD) desalination requires both thermal energy and mechanical energy; therefore its combination with solar energy is similar to the solar-assisted MSF/MED process, as shown in Figure 2.15, which could use low-grade heat from solar collectors or a solar pond, electricity from a PV system or the power grid. MD is a separation process in which a hydrophobic, micro-porous membrane is used

with seawater on one side of the membrane and condensing vapor on the other side. The hydrophobic membrane prevents seawater from passing through the membrane pores and only allows the generated vapor to transfer to the other side. MD is a thermally driven process. The driving force is the partial pressure difference across the membrane. There are four kinds of configurations: a) direct contact membrane distillation (DCMD); b) air gap membrane distillation (AGMD); c) sweeping gas membrane distillation (SGMD); and d) vacuum membrane distillation (VMD). Detailed descriptions could be found in the reference [229].

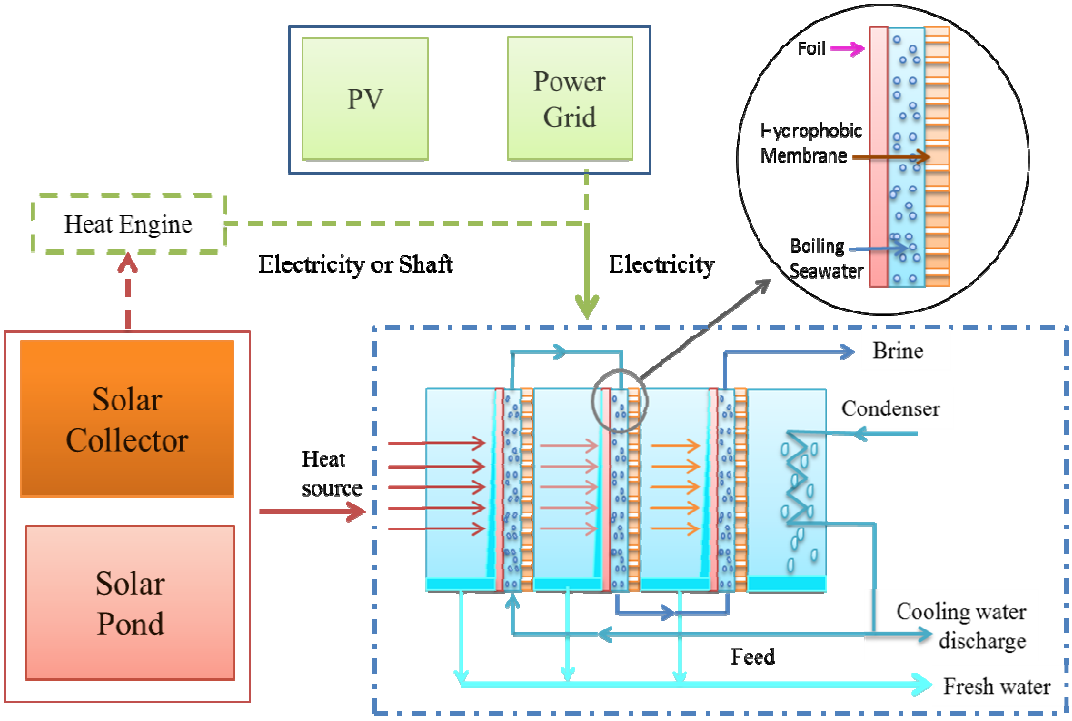

Figure 2.15 Schematic of solar-assisted membrane distillation.

As for the MD energy consumption and cost, there are some disagreements among the researchers. Some believe that [230] MD is unfavorable when compared with MED and MSF from an energy utilization point of view because of the additional resistance to mass transport and reduced thermal efficiency (due to heat conductivity losses) offered by the membrane. Others claim that the MD consumption

Table 2.15 Selected solar-assisted MD seawater desalination systems

Ref.	Mod/exp.	Project	MD type	Solar system	Cap.(m^3/d)	Notes
[33], [237]	Mod/exp.	El Paso	AGMD	Solar Pond	0.35	3000 m^2 solar pond, production 0.0016 $m^3/d/m^2$ of SGSP.
[235], [236], [238–241]	Exp.	MEMDIS, SMADES	DCMD	FPC-PV	0.1-0.5	Compact single loop MD systems using a 5.73-7m^2 FPC, 7-12 m^2 membrane area, GOR 3-6. Experiments carried out at Pozo Izquierdo (Grand Canary), Alexandria (Egypt), Irbid (Jordan), Morocco, Freiburg (Germany), and Tenerife (Spain)
					0.9	Two loop systems using a 72m^2 FPC, 1.44kWp PV, 3m^3 water tank, battery storage, 4 membrane modules, freed salinity at 55000ppm, RR 3-4.5%. Experiments at Aquba, Jordan
					1.6	Two loop systems using a 90m^2 FPC, 4m^3 water tank, 1.92kWp PV, no battery, 5 membrane module, PV for pumps, two loop systems, double glass collector with anti-reflective coating, feed water at 35000ppm, and RR 3.6%.
[234]	Model [c]	MEDINA	VMD	Solar pond	(d)	High fluxes of 140 L/h/m^2 could be reached for a vacuum pressure of 500 Pa and a membrane with a Knudsen permeability of 1.85×10^{-5} s $mol^{0.5}/m/kg^{0.5}$.
[242]	Exp.		NA	Solar still	NA	The effect of salt concentration on the membrane flux and the solar still was marginal. The contribution of the solar still in the distillate production was no more than 20% in the outdoor tests and less than 10% in the indoor tests.
[243]	Model/exp.	SMDDS	AGMD	FPC	0.64-0.71 [a]	Developed a model for SMDDS, with an FPC absorber area of 72m^2, membrane area of 10m^2, and a spiral wound AGMD structure. The use of a storage tank, an interior coil heat exchanger and a control system using conventional proportional/integral controllers could improve the system performance.
[244]	Model [c]	MEDESOL	AGMD [b]	CPC	0.5-50	Laboratory tests under defined testing conditions of all components will be performed in Spain and Mexico.

(a) Simulated results.
(b) Authors' mentioned that the experimental MD system will be AGMD modules while DCMD and VMD will also be theoretically analyzed.
(c) Experiments in progress.
(d) Model maximum fresh water production 617 L/h.

is comparable to that of MSF plants but the pumping power is less [231]. Nevertheless, by using novel materials and by optimizing the MD configuration, one could simultaneously reduce the temperature polarization and permeability obstructions of salt solutions in the DCMD [232], which might potentially reduce the cost. In addition, MD uses membranes that are robust and cheap, which means that MD could save on the chemical usage and seawater pretreatment costs compared with RO [233]. Some selected solar-assisted MD seawater desalination systems can be seen in Table 2.15, in which most solar-assisted MD systems operate at temperatures less than 80°C. MD driven by a solar pond has been shown to be feasible; however, modeling results have shown that combining solar collectors with the MD system could achieve a higher membrane permeation flux [234]. Though there are many cost estimations for MD desalination, there are only a few reports on solar MD seawater desalination costs. Banat et al. [235] estimated the water cost in the project "SMADES" as \$15/m^3 for a 100 L/day system using a 10m^2 membrane and 5.73m^2 flat panel collectors (FPC), and \$18/m^3 for a 500 L/day system FPC-PV driven MD using 40m^2 membranes and 72 m^2 FPC [236], and showed that by increasing the reliability and plant lifetime the cost could be further reduced.

Overall, solar-assisted MD is still under development. Reports on novel processes [245], experimentally confirmed modeling [246] and pilot demo plant evaluations [247] continue to appear in the literature. MD has the disadvantage compared to MED and MSF of additional resistance to mass transport by the membrane [230]. However because of the lower cost of MD materials, this disadvantage can be compensated for by using more area for heat and mass transfer. In addition, it could be used for high recovery or highly concentrated salt water

treatment, that RO could not handle, which normally requires high energy consumption.

CHAPTER 3 ENERGY ANALYSIS OF DESALINATION SYSTEMS

Chapter 2 analyzed different kinds of desalination systems combined with renewable energy sources such as solar energy. In order to select the best solar desalination-integrated system, it is important to understand its minimum energy requirements, energy recovery and major exergy destruction processes. Thermodynamic analysis and modeling of the desalination system is the key to understanding the integration of a desalination system with renewable energy sources.

3.1 System Integration Based on Energy Type

The total amount of water on Earth is $1.4*10^9$ km^3 with 97.5% as seawater and the remaining 2.5% as freshwater. A remarkable 80% of the freshwater is frozen in glaciers so that only 0.5% of the total amount available is found in lakes, rivers and aquifers. Freshwater differs substantially from seawater by the salt content. Based on the salt concentration, freshwater may have salinity up to 1,500 ppm. Saline water is classified as brackish water when the salt concentration is between 1,500 ppm and 10,000 ppm. Hard brackish water is when the salinity is 10,000 ppm to 35,000 ppm. Table 3.1 shows a very simple classification of natural water on the basis of its saline content. Typical seawater compositions (average salinity 35,000 ppm) are given in Table 3.2.

From Table 3.1, it is seen that the main difference between fresh water and seawater is the total content of dissolved solids consisting primarily of sodium (30%) and chlorine (55%). As a result, the physical properties of seawater, such as osmotic

pressure (which indicates the tendency of water to pass through semipermeable membranes), and Boiling Point Elevation (BPE) (which represents the increase in boiling temperature of a solution), are different from fresh water because both of them are strongly related to the concentration of salts in the solution. Osmotic pressure and BPE are fundamental properties in the design and operation of membrane and thermal desalination processes which will be discussed later. Table 3.3 shows the main thermodynamic properties of seawater.

Table 3.1 Water classification based on salinity content

Type	Total dissolved solids (TDS)	Note
Freshwater	<1,500	Variable chemical composition
Brackish water	1,500 – 10,000	Variable chemical composition
Salt water	> 10,000	Variable chemical composition
Seawater	10,000 - 45,000	Fixed chemical composition
Standard seawater	35,000	Fixed chemical composition

Table 3.2 Standard seawater composition

Chemical ion	Concentration [ppm]	Percentage of total salt content [%]
Chlorine Cl^-	19,345	55.0
Sodium Na^+	10,752	30.6
Sulfate SO_4^{2-}	2,701	7.6
Magnesium Mg^{2+}	1,295	3.7
Calcium Ca^{2+}	416	1.2
Potassium K^+	390	1.1
Bicarbonate HCO_3^-	145	0.4
Bromide Br^-	66	0.2
Borate BO_3^{3-}	27	0.08
Strontium Sr^{2+}	13	0.04
Fluoride F^-	1	0.003

Table 3.3 Thermodynamic properties of typical seawater

Density [kg/m^3]	1,024
Viscosity [kg/ms]	$1.074*10^{-3}$
Specific heat [kJ/kg ^oC]	3.998
Osmotic pressure [bar]	27
Boiling point elevation, at 20^oC [^oC]	0.32
Boiling point elevation, at 100 ^oC [^oC]	0.51

Figure 3.1 shows potential processes of solar technologies combined with seawater desalination technologies. Generally speaking, a solar-assisted desalination

system means that either solar energy is converted to electricity in order to power the RO/MVC process, or that solar radiation is collected by thermal collectors and this energy is used for the thermal desalination process. Solar methods which mainly produce electricity, such as photovoltaic (PV) [248], are suitable for combination with the membrane desalination process or a thermal process like MVC which only uses mechanical energy. Other solar technologies such as solar pond, solar collectors (including FPC, ETC, CPC, PTC), solar dish, Fresnel reflector, solar tower, could be used to generate electricity and heat at the same time. They could be combined with any kind of desalination technology based on the design. Since both solar and desalinations systems are developed independently and then coupled together, it is necessary to analyze them separately.

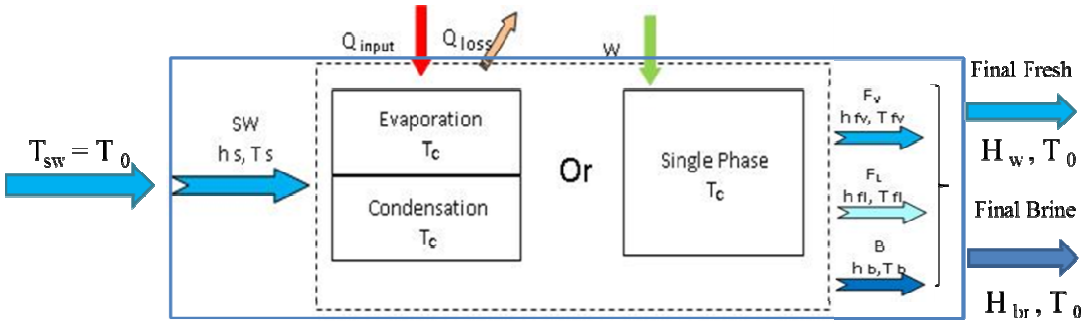

Figure 3.1 Black box model for the desalination minimum energy analysis.

3.2 Desalination System Considerations

In order to select the best solar desalination-integrated system, understanding of desalination minimum energy requirements, energy recovery and major exergy destruction processes is important. Reference [249] provides a specifically focus on energy issues of desalination.

3.2.1 Minimum Energy Requirement for Desalination

Minimum energy is required when the salt and water could be separated in a completely reversible process irrespective of the actual desalination processes [249],

[250]. Consider a desalination system as a black-box separator, with a separate control volume (within the blue boundary) surrounding it at some distance to make sure all inlet and outlet streams are at ambient temperature T_0 and pressure P_0. Product and reject streams may exit the desalination system at temperatures higher than the ambient temperature, T_0, which means the exergy associated with these streams could be used to produce some work. However, if the exergy associated with these streams is not harnessed but discarded to the environment, entropy S_{gen} is generated.

The general energy balance for a system is [251]

$$\sum_{i=1}^{\#inlet} \dot{m}_{in,i}\left(h_{in,i}+\frac{1}{2}\vec{v}_{in,t}{}^2+gz_{in,t}\right)+\sum_{i=1}^{heat\ terms}\dot{Q}_i+\sum_{i=1}^{work\ terms}\dot{W}_i = \sum_{i=1}^{\#outlet}\dot{m}_{put,i}\left(h_{out,i}+\frac{1}{2}\vec{v}_{out,t}{}^2+gz_{out,t}\right)+\sum_{i=1}^{heat\ terms}\dot{Q}_{out}+\sum_{i=1}^{work\ terms}\dot{W}_{out}+\frac{dU}{dt}+\frac{dKE}{dt}+\frac{dPE}{dt} \tag{3.1}$$

The general entropy balance for a system is

$$\sum_{i=1}^{\#inlet}\dot{m}_{in,i}\cdot s_{in,t}+\sum_{i=1}^{heat\ terms}\frac{\dot{Q}_i}{T_{b,i}}+\dot{S}_{gen}=\sum_{i=1}^{\#outlet}\dot{m}_{out,i}\cdot s_{out,t}+\frac{ds}{dt} \tag{3.2}$$

Simply based on Figure 3.1

$$W+Q_{input}-Q_{loss}+m_{sw}h_{sw}=m_bh_b+m_{fr}h_{fr} \tag{3.3}$$

$$\frac{Q}{T_0}+m_{sw}s_{sw}+S_{gen}=m_bs_b+m_{fr}s_{fr} \tag{3.4}$$

Using the specific Gibbs free energy as

$$g=h-TS \tag{3.5}$$

The energy balance becomes:

$$W+Q_{input}-Q_{loss}+m_{sw}g_{sw}=m_bg_b+m_{fr}g_{fr}+T_0S_{gen} \tag{3.6}$$

In a reversible process with no heat input and loss, T_0S_{gen} and $(Q_{input}-Q_{loss})$ are zero therefore the minimal work required for the separation of unit water from seawater is the difference in the Gibbs energy [86].

$$w_{min} = \frac{m_{br}g_{br} + m_w g_w - m_{sw}g_{sw}}{m_w} \quad (3.7)$$

where the subscripts *br*, *w* and *sw* represent rejected brine, produced fresh water and feed seawater (35,000ppm), and g is the specific Gibbs energy. The results can be seen in Figure 3.2 (a), (b), which shows that higher salt concentration and higher recovery rate require higher energy consumption. Based on the above equations, at 25ºC, standard seawater (35,000ppm) with 50% recovery, the reversible process requires 3.93kJ/kg. The current well designed seawater RO systems or controlled pilot scale plants energy consumption can be as low as ~7.92kJ/kg [252], which is two times the minimum required theoretical value. Considering pretreatment, post-treatment or other factors such as membrane fouling, pipe friction losses, pump efficiency, there is only about a 20% improvement possible [252].

3.2.2 Estimation of Energy Consumption

Assuming there is no heat loss to the environment, when a desalination process uses heat only, W is zero. When only electricity is used, Q_{input} is zero.

Energy balance

$$Q_{input} - Q_{loss} + m_{sw}h_{sw} = m_b h_b + m_{fl}h_{fl} + m_{fv}h_{fv} \quad (3.8)$$

$$h_{fv} = h_{fl} + \lambda \quad (3.9)$$

$$\text{Mass balance} \quad m_{sw} = m_b + m_{fl} + m_{fv} \quad (3.10)$$

$$m_{fr} = m_{fl} + m_{fv} \quad (3.11)$$

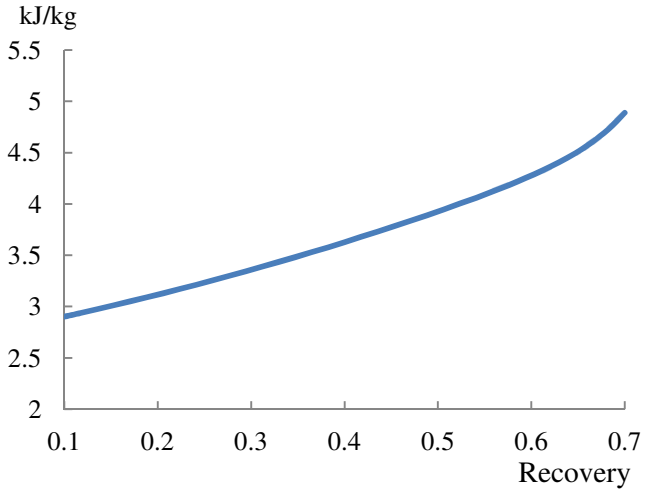

(a) Minimum energy required to desalinate seawater versus recovery rate (35g salt per kg seawater at 25℃).

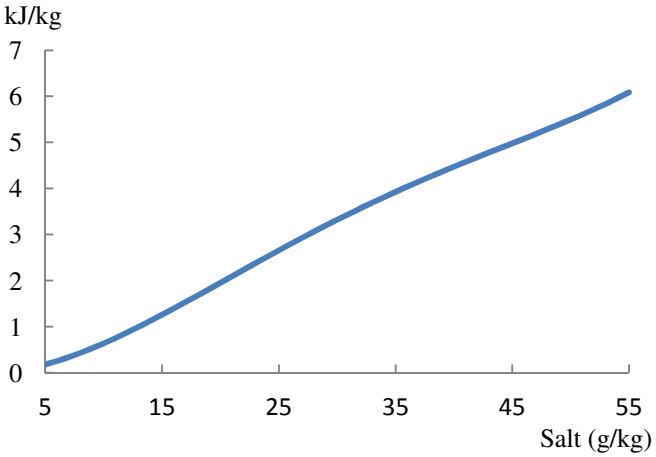

(b) Minimum energy required to desalinate water versus salt concentration at 25℃ .

Figure 3.2 Minimum energy required to desalinate seawater.

Based on mass and energy balance, the recovery rate could be expressed as

$$\alpha = \frac{m_f}{m_s} = \frac{\frac{(Q_{input}+W)-Q_{loss}}{m_s}+(h_s-h_b)}{(h_{fl}-h_b)+\frac{m_{fv}}{m_f}\lambda} \tag{3.12}$$

where h_{fl}, h_b, h_s are the specific enthalpy of fresh water vapor, concentrated brine and feed seawater respectively, α is the recovery rate, λ is the latent heat at the final product temperature; m_{fv} is the fresh water vapor mass, m_f is the sum of the mass of the final fresh water production which is the sum of vapor stream F_v and the final fresh water stream is F_L. If we define the specific energy consumption for a general

desalination process as $q_s = \frac{Q_{input}+W}{m_f}$; assume the feed seawater is at 25°C and the final products have the same temperature (including vapor, liquid fresh water and brine) without considering the temperature elevation caused by salt, Eq. (3.12) could be simplified as:

$$q_s = [(h_{fl} - h_b) - \frac{1}{\alpha}(h_s - h_b)] + \frac{m_{fv}}{m_f}\lambda \quad (3.13)$$

where $\frac{m_{fv}}{m_f}$ is vapor ratio which showed the vapor amount of the total final fresh water generated, and R is the recovery of the desalination process. Once the recovery, α, is fixed, the specific energy is directly related to the amount of vapor condensed by the cooling water which is discharged to the environment. Figure 3.4 shows the estimated specific energy consumption with vapor fraction of the total fresh water generated.

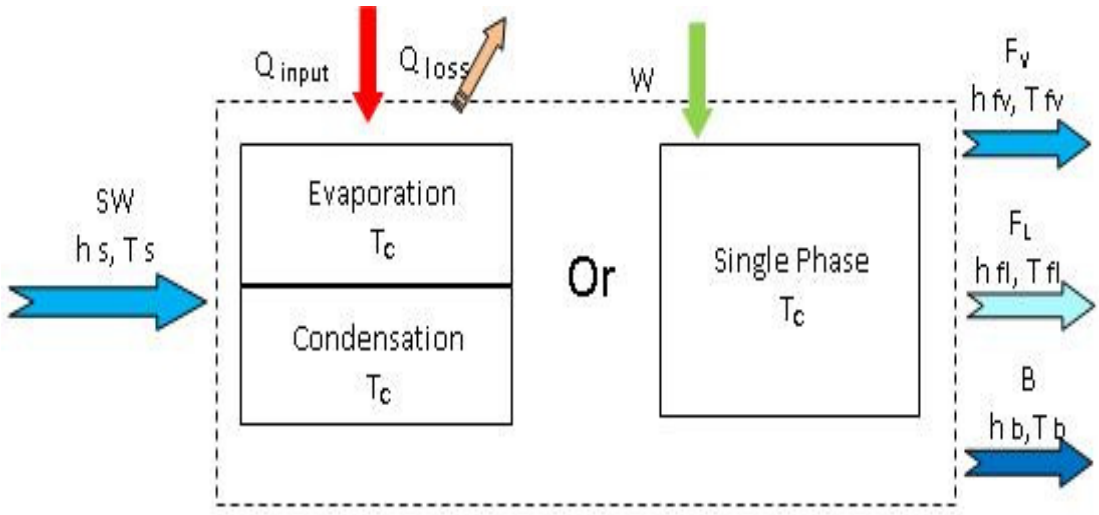

Figure 3.3 General overview of a desalination process

The lower the amount of vapor condensed by the discharged cooling water, the lower the energy it requires because less latent heat is wasted. This estimation shows that the RO process stands out among others because it uses almost ambient conditions to generate fresh water, no vapor needs to be condensed and no cooling

water is needed. Other processes, (i.e., MED, MSF, MVC, MD, HDH) could reduce energy consumption by recovering the latent heat from the generated vapor either by

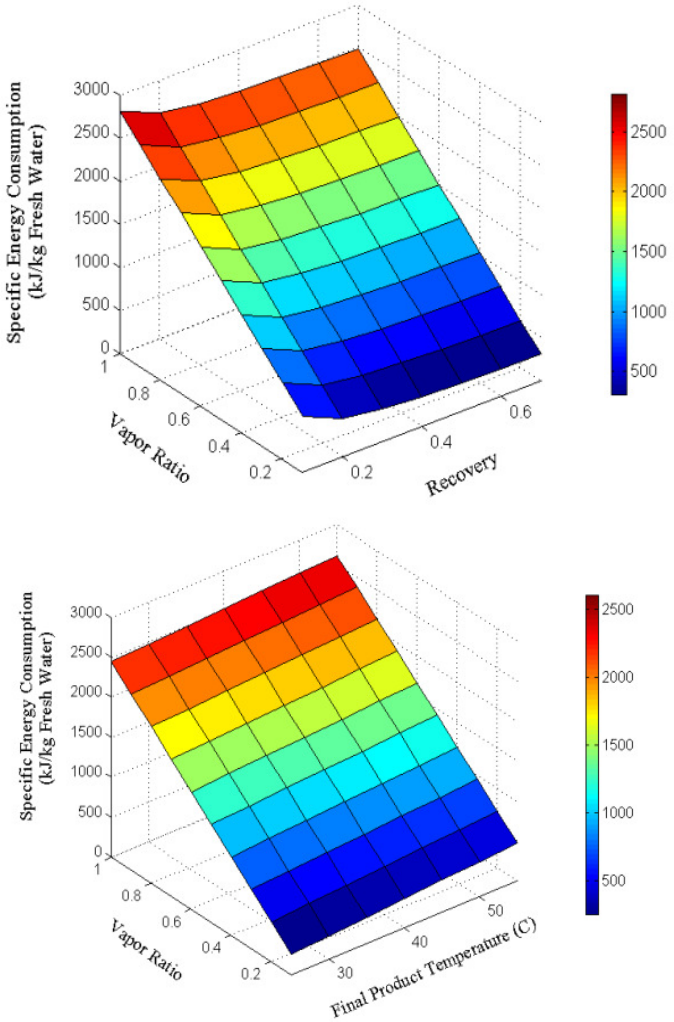

Figure 3.4 Specific energy consumption with vapor ratio and recovery when final product is at 35°C (upper); and final product temperature when recovery is 0.5 (lower).

preheating water or by reusing the latent heat so as to reduce the energy wasted in the cooling water. For single effect thermal processes, the vapor ratio is 1. Recently forward-osmosis has gained attention. Forward-osmosis makes use of the osmosis by extracting water from seawater using a concentrated extraction solution (also known as a draw solution), [253]. One of the draw solutions proposed is a mixture of NH_3, CO_2 and water which extracts fresh water from seawater by forward-osmosis. Fresh water is then gained from this solution by heating, decomposition, and the stripping

and recycling of ammonia and carbon dioxide gases [254]. They claimed that the energy savings of FO are projected to range from 72% to 85% compared to current technologies on an equivalent work basis [254]. However, the model and the equations used in the commercial software packages are not clearly stated. Regardless, this process also depends on phase change, although the latent heat of NH_3 is about 60% of the latent heat of water.

3.3 Energy Reduction in Desalination Processes

Although different desalination processes share the same minimum power requirements, independent of system configuration and technologies, it is not practical to operate systems reversibly to achieve the minimum energy consumption. Different driving forces for different desalination processes could cause different exergy destruction. A higher driving force leads to a higher water production rate with higher exergy destruction. This normally leads to smaller systems with higher energy consumption. The driving force of different desalination systems are: a) the excess pressure ΔP for RO; b) the excess voltage ΔE for ED; c) the additional temperature difference ΔT in excess of the boiling point elevation to allow for heat transfer for MVC and MED; and d) the additional temperature ΔT in excess of the boiling point elevation to allow for flashing for MSF [255]. The general form is given by [256]

$$\frac{dE_d}{dt} = -T_0 * \frac{d\Delta S}{dt} = -T_0 * (\Im * \Delta X) \tag{3.14}$$

where E_d is the exergy destruction, t is time, ΔS is the entropy change, $\Im$ is a flow rate, T_0 is the environmental temperature and ΔX is the generalized driving force conjugated to the flow $\Im$. For RO-based desalination processes, assume the excess pressure ΔP is 30 atm, temperature T is 25°C and the exergy destruction is

$$E_d = T_0 * S_{gen} = T_0 * \frac{\Delta P}{T} * \overline{V_w} * \frac{1}{18} = 3.04\ KJ/kg \tag{3.15}$$

where $\overline{V_w}$ is the molar volumn of pure water.

For an evaporation/flash based desalination process such as MED, MVC and MSF, the exergy destruction could be calculated as [256]:

$$E_d = T_0 * S_{gen} = T_0 * h_{fg} * \frac{\Delta T}{\bar{T}^2} * \frac{1}{18} \quad (3.16)$$

where h_{fg} is the latent heat of evaporation at average operation temperature which is $\bar{T} = \frac{T_v + T_c}{2}$, in which T_v is the temperature of vaporization and T_c is the temperature of condensation. ΔT is the temperature driving force of the heat exchanger, which has the minimum value of boiling point elevation (BPE) for reversible processes. Additional temperature difference in excess of the BPE is used for heat transfer. Assume the temperature driving force for MED, MVC and MSF are 1.5, 1.5 and 3°C, respectively; and assume the $\bar{T}$ for them are 50.75, 60.75 and 71.5 °C, respectively, the exergy destruction for the typical MED, MVC and MSF are 9.94, 10.16 and 17.52 KJ/kg fresh water, respectively.

3.4 A Fair Comparison of the Thermal Energy Requirement

Though the estimation in Section 3.2 and 3.3 shows that an RO process is energy efficient and has less exergy destruction than the thermal processes, one might claim that RO uses electricity while the thermal system uses thermal energy. A power cycle efficiency of η which reflected the real thermal energy consumption of an RO system is needed to fairly compare different desalination systems. Assume a seawater RO plant with an energy consumption of 13.32kJ/kg [252] - a MED system consumes 240kJ/kg [102]. If an RO consumes same amount of thermal energy as a MED system, the η only needs to be 5.55% while most power plant power cycle efficiency is more than 35%. For well-designed seawater RO systems or controlled pilot scale plants, the energy consumption can be as low as 7.92kJ/kg [252] while the currently reported lowest experimental energy consumption for MED coupled with a double absorption heat pump is 108kJ/kg. Using a heat source of 180℃ (from Table 2.9), the power

cycle efficiency η only needs to be 7.6% to make RO comparable with a MED-double absorption heat pump combination. With a 180℃ heat source, the power cycle efficiency could be higher than 7.6%.

There is another claim that increasing the number of stages of a thermal process or increasing the evaporator surface area could make the thermal process more energy efficient than an RO process. Assuming the plant and other conditions are equal, in order to reduce the exergy loss the driving force needs to be reduced requiring a larger "reaction" area. With larger capital cost however, the minimum temperature difference is BPE which is about 0.5-1°C. When the temperature difference between different stages are approaching BPE, the number of stages/effects increase, and the surface area of the evaporator also increase dramatically in order to generate the desired water production rate.

Theoretically, a thermal process like MED or HDH could contain more than 100 stages/effects [257], [258]. In reality, the size of the desalination system and the energy consumption must be balanced. Modern large-scale thermal desalination plants could have the temperature difference between adjacent stages as small as 2°C. Considering the seawater boiling point elevation (about 0.5-1°C) and saturation temperature drop (caused by pressure drop in the demister and tube), the net driving force of adjacent effects has approached 1°C already; as for the membrane process, the current seawater RO plants could use a pressure of only 10 to 20% higher than the osmotic pressure of the concentrate [252]. Therefore, reduction of the driving force in order to reduce the exergy destruction and the energy consumption is a necessary but challenging topic. Desalination is intensive in both energy consumption and capital investment. The water cost is a trade-off with the energy and equipment cost. By using large areas of membranes in RO/MD or more stages/effects in MSF/MED,

energy demands could be reduced but at a higher cost. If a low cost RO membrane and heat exchanger were available, energy consumption could be potentially reduced by using more material while maintaining the capital cost at a reasonable range. For example, even though the MD process uses a similar configuration as the MED or the MSF, it has the disadvantage of additional resistance to mass transport and reduced thermal efficiency (due to heat conductivity losses). However, it could exploit the advantages of a larger surface area to compensate for these disadvantages and still maintain a competitive capital investment [230]. Composite porous organic/inorganic membranes could have the potential to increase the heat conductivity and be used in a MD system. For the RO process, novel membranes results in better flux, and better rejection to salts and boron could also reduce the energy needed. The capital investment could also be reduced by using fewer membranes with higher flux and rejection abilities.

Therefore, in most cases, thermal system is more energy intensive than RO. Thermal process should be considered once the heat source is (<80 ℃) or conditions show that RO is not suitable for use as the desalination system. For example, when handling brackish water or even seawater, the RO process is energy efficient. However, it requires stringent pretreatment which increase the capital investment; besides, osmotic pressure increases dramatically with salt concentration, as shown in Figure 3.5, while the RO membrane could only sustain certain pressure due to the soft polymer materials. This limits the RO process application to high concentration feed water desalination applications. On the other hand, a thermal process such as MED is robust, requires less pretreatment and could handle highly concentrated salt water sources. Therefore thermal desalination is still important and needs to be further studied.

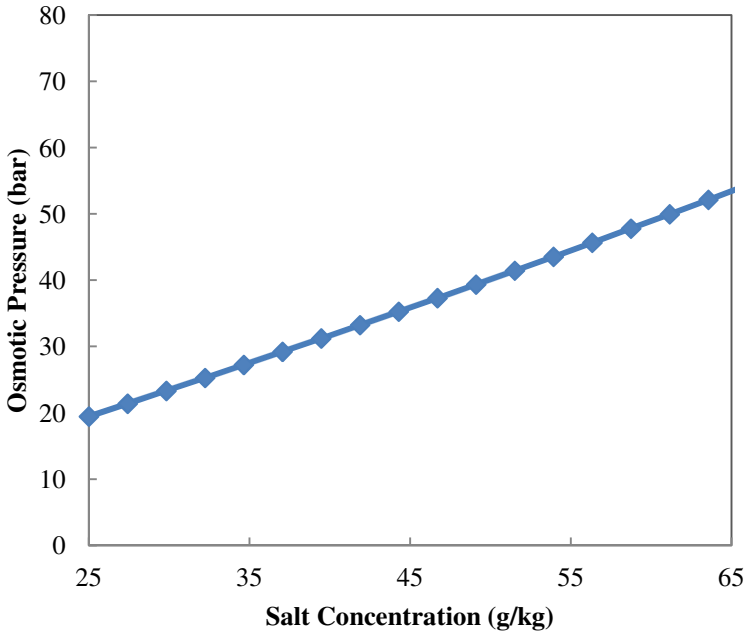

Figure 3.5 Osmotic pressure changes with salt concentration.

3.5 RO Model

3.5.1 Introduction of RO Membranes

Osmosis is a natural phenomenon in which a solvent (usually water) passes through a semi-permeable barrier from the side with lower solute concentration, to the higher solute concentration side (Figure 3.6 left). To reverse the flow of water, a pressure difference greater than the osmotic pressure difference is applied (Figure 3.6 right). As a result, separation of water from the solution occurs as pure water flows from the high concentration side to the low concentration side. This phenomenon is termed reverse osmosis.

In the RO process, seawater is initially treated to adjust its pH and to free it from particulates that negatively impact the membrane structure. It is then pumped to a network of semi–permeable membranes separating fresh water from concentrated brine. The seawater pressure is raised above its natural osmotic pressure, typically 25 bars, but is kept below the membrane tolerance pressure, typically between 60 and 80

bars, forcing pure water molecules through the membrane pores to the fresh water side. The separated water is then treated and collected as the fresh water product

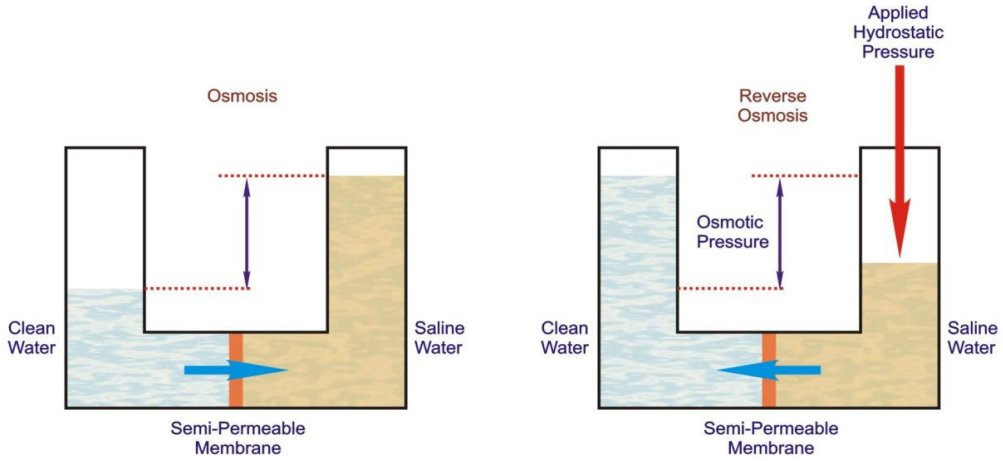

Figure 3.6 Schematic of osmosis and reverse osmosis phenomena.

while the concentrated brine is rejected. Reverse osmosis is very efficient because the mechanical compression energy can be reclaimed from the rejected concentrated brine with a suitable energy recovery device. The life of commercial membranes varies between 5-6 years which depends on the feed water quality, pretreatment conditions, and stability of operation. Major types of commercial reverse osmosis membranes include polyamide (PA) and cellulose acetate (CA). The composite polyamide membranes have two layers. One is a porous polysulfone support and the second is a semi-permeable layer of amine and carboxylic acid chloride functional groups. Two separate layers enables the independent optimization of the properties of the membrane support and salt rejecting skin, therefore PA membranes have higher specific water flux and lower salt passage than CA membranes. Typical CA membranes are made of a blend of cellulose triacetate and diacetate. The membranes are asymmetric with a dense surface layer about 0.1-0.2 micron which is used to remove salt. The remaining part of the membrane is spongy, porous and highly water

permeable. Water flux and salt rejection of a CA membrane are controlled by temperature annealing and duration.

PA composite membranes are more pH tolerant than CA membranes while sensitive to oxidative degradation such as free chlorine. On the contrary, CA membranes can tolerate limited levels of exposure to free chlorine. In addition, CA membranes have relatively smooth surfaces with little surface charge. Therefore CA membranes have a more stable performance than PA membranes in applications when the feed water has a high fouling potential due to their free chlorine tolerance and neutral surface.

3.5.2 RO Mathematical Model

RO mathematical models have been studied by many researchers [135]. Assuming steady state and a similar permeability coefficient for all salt ions, the net pressure difference across the membrane is:

$$\Delta P = \left(\frac{m_f}{3600 \times TCF \times FF \times A_e \times n_e \times n_v \times k_w}\right) + \Delta\Pi \tag{3.17}$$

where m_f is the produced fresh water mass rate, TCF is the temperature correction factor, FF is the membrane fouling factor, and A_e is the element area in m^2. k_w is the membrane water permeability, n_e is number of membrane elements, n_v is the number of pressure vessels, and$\Delta\Pi$ is the net osmotic pressure across the membrane which corresponds of the osmotic pressure difference between the concentrated brine with feed-in seawater. The exact number of these parameters (such as TCF, FF and k_w) depends on the membrane materials and manufacturing process therefore it is better to use the membrane manufacturers' provided system software to calculate the relative membranes provided by the company.

Large-scale RO systems normally have an energy recovery device (EDR) to reduce energy consumption. Low recovery consumes less energy in the separation

process but consumes more in pumping; therefore there is an optimized range for the seawater recovery. The work required for the RO process with an energy recovery device (EDR) may be estimated by:

$$W_{SWRO} = \frac{V_{fresh}}{\eta_{pump}} * \left(\frac{P_{sea}}{1-\alpha} + \Delta P\right) * [1 + \left(\frac{1}{\alpha} - 1\right) * (1 - \eta_{ERD}) \quad (3.18)$$

where α is the seawater desalination system recovery ratio, and ΔP is the overpressure above the osmotic pressure that drives the water flow through the membrane. P_{sea} is the osmotic pressure given by van't Hoff equation: $P_{sea} = cRT$, where c is the ionic molar concentration, R is the gas constant, and T is the absolute temperature. $\frac{P_{sea}}{1-\alpha}$ is the pressure used to overcome the concentrated brine osmotic pressure. The units of W, P, and V are kJ, kPa and m^3 (or m^3/s if using flow rate) respectively; η_{pump} is the high pressure pump efficiency, V_{fresh} is the fresh water volume, $\frac{V_{fresh}}{R}$ is the total seawater pumped by the pump, and η_{ERD} is the efficiency of ERD. The recovery rate ranges from 30% to 60% for RO, as can be seen in Figure 3.7. For thermal processes, the high recovery rate could reduce the energy consumed by the pumps but might cause potential scaling problems, therefore, a selection needs to be made for each individual case.

3.6 MED and the Combinations with Heat Pumps

The combination of economical specific MED plant costs with low energy cost, together with the inherent durability of a low-temperature MED avoiding the necessity of comprehensive seawater pretreatment (such as with RO plants) make the MED process one of the best candidates for safe and durable large capacity economical desalination options. MVC and TVC can be combined with the MED process to further improve the system performance.

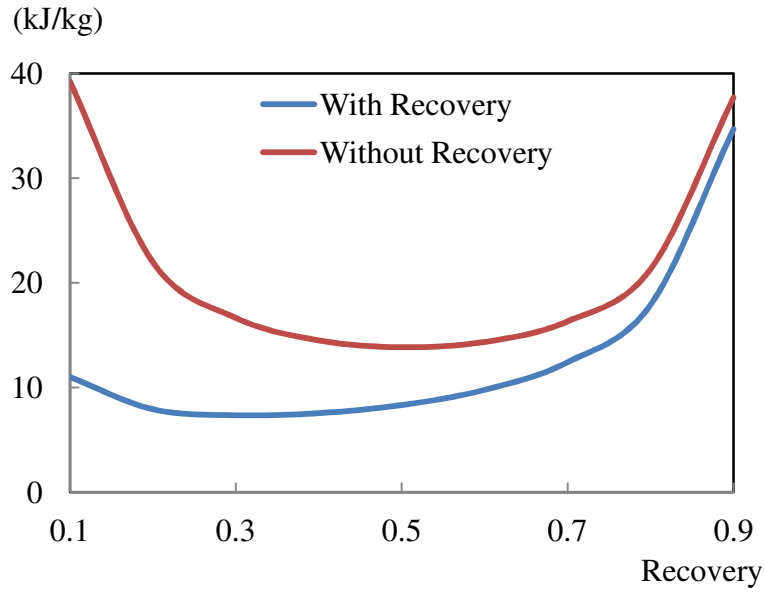

Figure 3.7 Specific energy consumption change with/without ERD (Pump efficiency 80%, ERD efficiency 80%).

3.6.1 MED Model and Analysis

A schematic diagram for the forward-feed Multiple Effect Distillation (MED) desalination process can be seen in the MED subsystem of Figure 3.8, in which seawater is delivered to a sequence of successively lower pressure vessels, called effects.

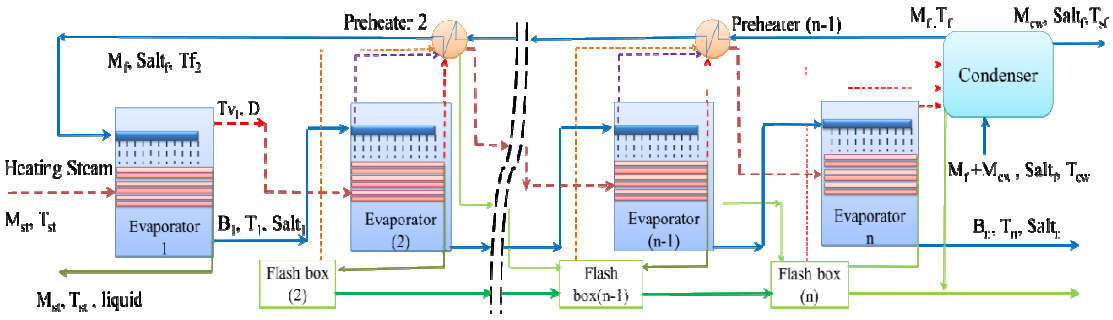

Figure 3.8 Schematic of a forward-feed multiple effect distillation.

There are n evaporators, n-2 feed water preheaters, n-1 flashing boxes and one condenser in the system. The seawater stream is heated from the intake T_{cw} to T_f. The function of the cooling seawater is to remove excess heat added to the system in

the first effect by the motive steam which has the mass rate M_{st} at the temperature of T_{st}. In the last effect, the heat load is equivalent to the latent heat of the vapor from the last effect of MED effect, which is the sum of the flashed-off vapors formed in the last effect and the associated water flash box. This amount of heat was delivered to the MED feed-in seawater with mass flow rate $(M_{cw} + M_f)$. The cooling seawater M_{cw} is rejected back to the sea while the rest M_f is sent to the 1st effect of MED after passing a series of preheater. In each forward-feed MED system, the 1st effect and the last effect (with condenser) are different from others; the 2nd effect to the (n-1)th effect are similar.

There are several assumptions made during the modeling process:

a) The vapor formed in the effects is salt free.
b) Energy losses from the effects to the surroundings are negligible.
c) The heat transfer efficiency in the exchange units, which include evaporators, condensers, and preheaters, is constant.
d) The physical properties of various streams are calculated at the temperature average of influent and effluent streams.
e) There are no pipe friction or vapor demister friction losses.

Each effect will have one boiling point elevation caused by the salt concentration and two different non-equilibrium allowances (NEA) due to the higher pressure and temperature from previous effects. The detailed mathematical model of these special parameters will be presented in Chapter 5. These effects caused by seawater properties could be calculated through EES (Engineering Equation Solver) library routines and equations written in related EES models for this research.

The detailed model from the 2nd effect to the (n-1)th effect is found in Chapter 5 for the proposed system. In this section, only the first effect and the last effect

condenser model will be described. However, the whole system modeling results of the forward-feed MED will be discussed.

The major energy and mass balance for the 1st effect are:

$$M_f = D_1 + B_1 \tag{3.19}$$

$$M_f * Salt_f = B_1 * Salt_1 \tag{3.20}$$

$$M_{st} * \lambda_{st} = M_f * Cp * (T_1 - Tf_2) + D_1 * \lambda_1 \tag{3.21}$$

The energy and mass balance for the final condenser are:

$$Q_{condenser} = (M_f + M_{cw}) * Cp_{condenser} * (T_f - T_{cw}) \tag{3.22}$$

where $Q_{condenser}$ is the heat load of the final condenser, λ_{st} is the latent heat of condensation of the motive steam M_{st}, λ_1 is the latent heat of vaporization at temperature Tv_1 at which temperature the vapor formed in the first effect, Cp is the mean specific heat capacity of water from feed-in temperature Tf_2 to the effect temperature T_1, $Cp_{condenser}$ is the mean specific heat capacity of the feed-in seawater temperature T_{cw} to the cooling water discharge temperature T_f, Tv_1 is less than the boiling temperature T_1 by the boiling point elevation BPE_1 caused by dissolved salt.

3.6.2 MED Model Results

A 14-effect forward-feed MED is modeled. Some fixed parameters are

a) The heating steam temperature is 65℃;
b) The vapor from the last effect is condensed at 35℃ ;
c) The recovery ratio α is 0.335;
d) Final condenser pinch is 2℃;
e) Ambient seawater temperature is 25 ℃;
f) Feed-in water salt concentration is 35g salt per kg seawater.

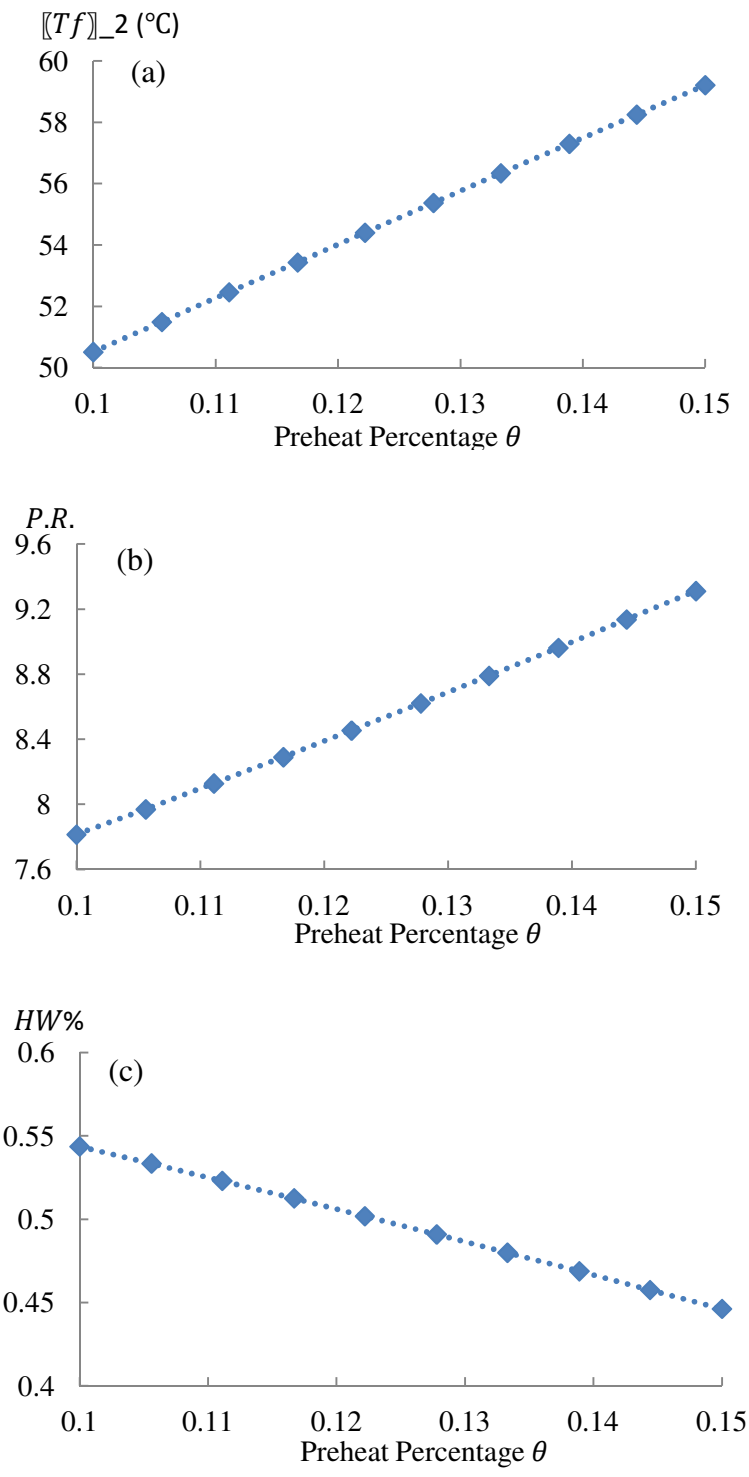

Figure 3.9 Preheat effect to: a) MED top brine temperature; b) Preheat effect to MED performance ratio; c) Preheat effect to wasted heat percentage.

In MED's ith effect, three vapor streams (vapor generated by evaporator, brine flash and condensate flash box associated with ith effect), flow into the preheater associated with this effect. A portion of the vapor θ_i is used for preheating the feed-in water and condensed in the next effect flash box. By adjusting the percentage of vapor used in the preheater, a few performance parameters of the MED will vary such as:

a) The performance ratio, $P.R.$, which is defined as the number of kg of distillate produced by a 2,300 KJ heat input.
b) The top brine temperature, Tf_2, which is the final seawater temperature before it is sprayed on the first effect evaporator.
c) The percentage of heat wasted, $HW\%$, which reflects the percentage of the heat load discharged to the sea by the cooling water based on the heat provided by the steam at the first effect.

The MED modeling results have shown it is desirable to preheat the feed-in seawater to higher temperatures, which means that using a greater percentage of vapor from previous stage to preheat the feed-in water could improve the MED energy efficiency. As can be seen in Figure 3.9, the more the vapor is condensed in the preheater, the higher the MED top brine temperature (Figure 3.9(a)), the higher the performance ratio of the MED system (Figure 3.9(b)) and the less the wasted heat discharged to the sea by the cooling water (Figure 3.9(c)).

By using the reported experimental data on the forward-feed MED system [259] ($P.R. = 9$, $\theta = 14.1\%$, $\alpha = 0.335$, $T_{st} = 65℃$ and the final fresh water production 0.83 kg/s), the detailed information of produced fresh water flow rate in each effect can be seen. Figure 3.11 shows that major fresh water production is from evaporation while water produced by flashing is only 10% of the water generated from the evaporators. The modeling results also show that as each effect's

temperature continues to drop (Figure 3.12), the brine concentration coming out of each effect continues to increase (Figure 3.10). The boiling point elevation in each effect as well as the non-equilibrium allowance in the brine flash and condensate flash will increase as the salt concentration increases, as can be seen in Figure 3.13.

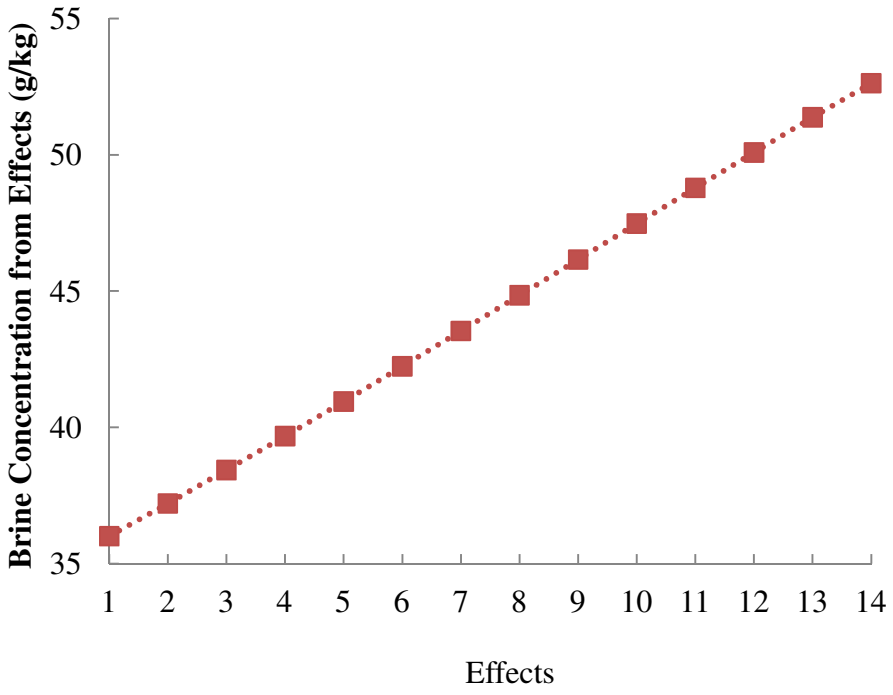

Figure 3.10 Brine concentration coming out of each effect.

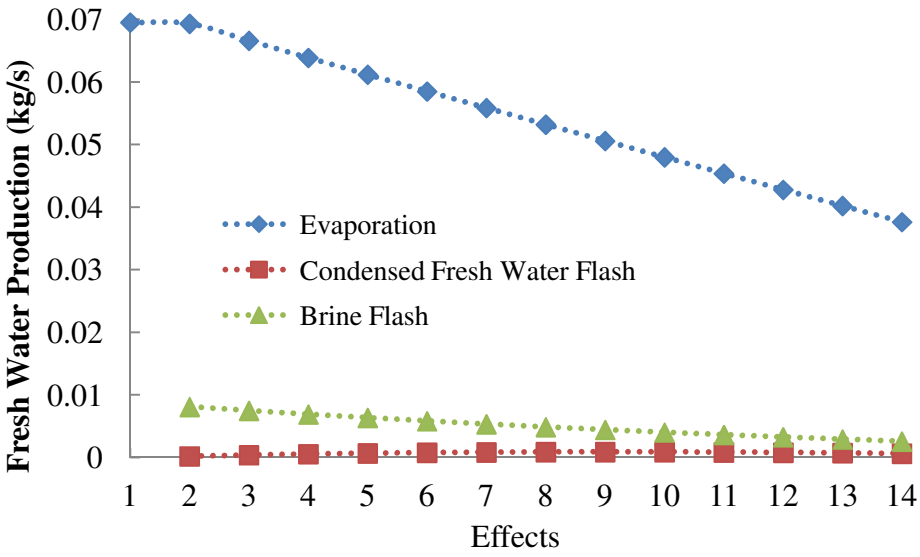

Figure 3.11 Fresh water production from evaporation, brine flash and condensate flash in each effect.

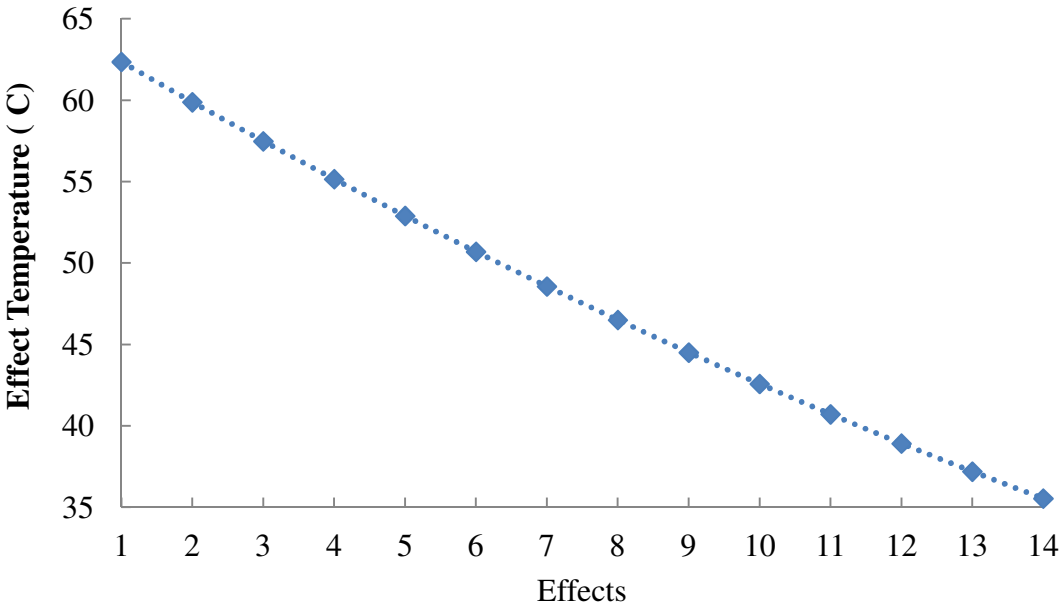

Figure 3.12 Temperature in each effect.

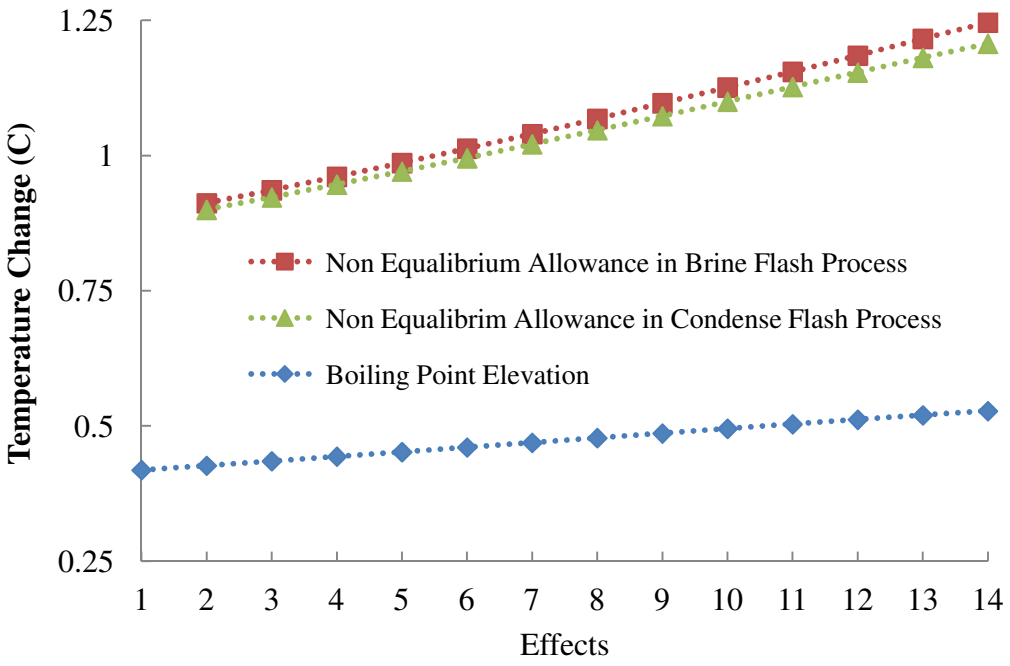

Figure 3.13 Temperature changes in the 14 effect forward flow MED (Boiling point elevation, NEA in condensate flash processes and NEA in brine flash processes).

3.6.3 MED Combined With Thermal Vapor Compressor (TVC)

As discussed in Section 2.2, MEDs are sometimes combined with a thermal vapor compressor (TVC) to recover the final effect low-temperature vapor in order to improve the system performance ratio, as can be seen in Figure 3.14. The MED modeling has been discussed before. The steam vapor compressor is modeled by the semi-empirical model developed by Al-Juwayhel [51]. The compression ratio (Cr) means the pressure ratio of the compressed and entrained vapors. The entrainment ratio (Er) is the flow rate ratio of the motive steam and the entrained vapor and is calculated by:

$$Er = 0.296 \times \frac{{P_{st}}^{1.19}}{{P_{ev}}^{1.04}} \times \left(\frac{P_m}{P_{ev}}\right)^{0.015} \times \left(\frac{3\times10^{-7}\times(P_m)^2-0.0009\times P_m+1.6101}{2\times10^{-8}\times(T_{ev})^2-0.0006\times T_{ev}+1.0047}\right) \quad (3.23)$$

P_m, P_{st} and P_{ev} in kPa are the pressures of the motive steam compressed vapor that will go to MED 1st effect and the entrained vapor, respectively; T_{ev} is in ℃. The equation is valid only when only the steam is the working fluid and is valid in the following ranges: $Er < 4$, $10\ ℃ < T_{ev} < 500\ ℃$, $100\ kPa < P_m < 3500\ kPa$, and $1.81 \leq \frac{P_{st}}{P_{ev}} = Cr \leq 6$.

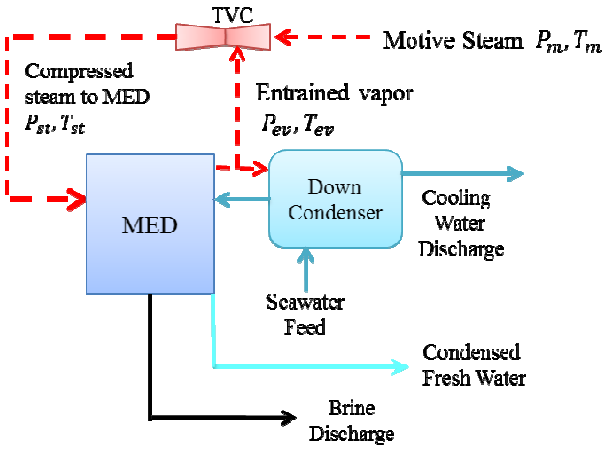

Figure 3.14 Schematic of MED-TVC.

The TVC could extract vapor from any effect in a MED system. The effect of extracting vapor from different effects of a 6-effect MED-TVC using 50-108℃ heating steam is shown in Figure 3.15, where a 6-effect MED is used as a reference. The specific area (sA) is defined as the ratio of the overall thermal desalination system heat exchanger surface area (m^2) to the fresh water production rate (kg/s). The specific heat consumption is the ratio of the total thermal input (kJ/s) to the fresh water production rate (kg/s). The feed-in seawater concentration is 35g/kg and the overall heat transfer coefficients for the evaporators, preheaters and condensers are from Ref. [260]. The data which do not meet the TVC model restrictions are removed. From the figure, it can be seen that the basic trends are similar while the energy consumption and the total MED system heat exchanger area are inversely proportional to each other. In reality, it is better to extract the vapor from the last effect so that all the evaporators have the same size. From the simulation, it can be seen that MED-TVC shows performance improvement, which can be expected (based on analysis of the estimation of energy consumption in Section 3.3) because the vapor from the last effect is partially recovered. However, the water saturated pressure is low at the MED last effect which is one of the reasons for the TVC low efficiency. Besides, the MED-TVC system requires an external electricity input to operate the pump. It is expected that a system could totally operate with just thermal energy.

3.7 Summary

In summary, the minimum energy required for all the desalination processes is the same irrespective of the actual desalination process. The RO process is naturally more energy efficient than a thermal process. However, the RO process could not be used to handle highly concentrated salt water such as fracture water generated from

natural gas production due to the exponential increase of osmotic pressure with salt concentration and the physical strength limitations of the RO membranes. Therefore

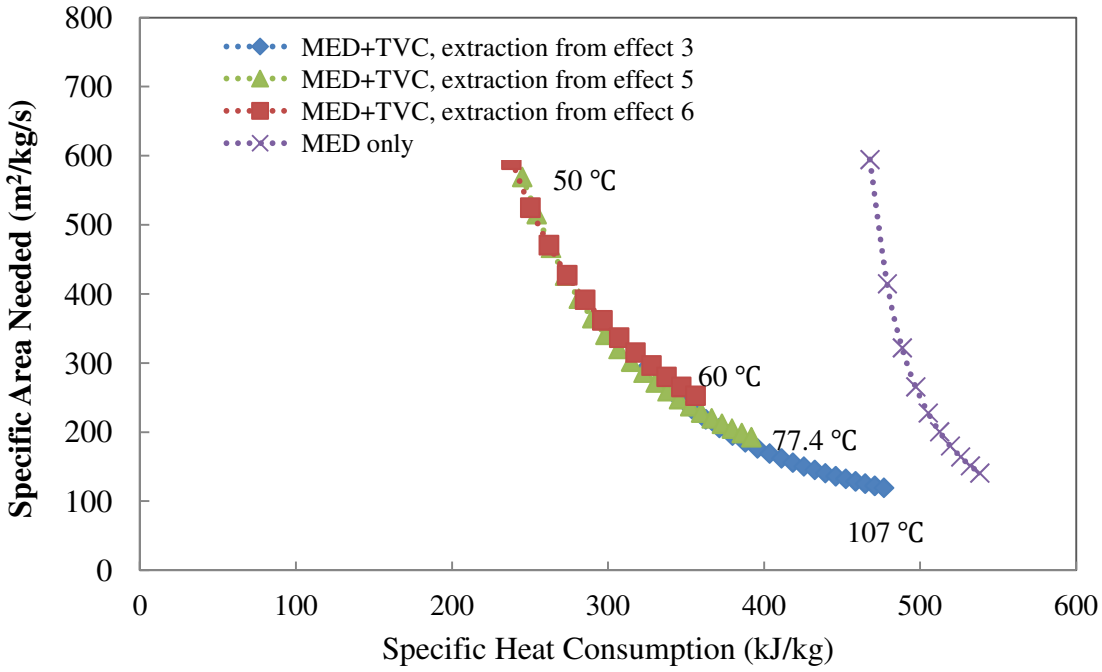

Figure 3.15 Effects of extracting vapor from different effect of a 6-effect MED system.

in some cases, such as availability of abundant low cost thermal energy, highly salty water or places requiring zero liquid discharge, thermal processes could be more appropriate. The previously discussed desalination system, no matter if it is RO or thermal process, requires external electricity input. Systems that rely only on low-grade heat sources to drive the RO desalination system are desirable. Furthermore, it is of great importance that desalination systems could operate without external electricity in order to improve the thermal system performance. The desalination cost could be further reduced by not only applying low cost energy sources but also low cost materials, which requires breakthroughs in materials development. Table 3.4 [261–263] summarizes a comparison of some of the major desalination processes.

Table 3.4 A comparison of different desalination processes

	MSF	MED	TVC	MVC	RO	ED
Operation temperature (°C)	35-120	35-100	>120	30-60	20-40	20-40
Pretreatment requirement	Low	Low	Low	Low	High	High
Scale problem	High	Medium	Medium	Medium	Low	Medium
Freshwater quality (ppm TDS)	<10	<10	<10	<10	350-500	350-500
Heat consumption (kJ/kg of product)	90-567	108-432	-	-	-	-
Electricity consumption (kJ/kg of product)	7.2-18	5.4-10	-	28-40	10-47	43
Prime energy consumption* (kJ/kg of product)	110-653	110-369	-	80-110	65-120	144
Energy recovery	Sensible to latent	Latent to latent	Recovery low-temperature vapor	Recovery low-temperature vapor	Pressure recovery	-
Sensible to feed-in seawater temperature	Yes	No	No	No	No	No
Others	Proven technology for large-scale plant.	Proven technology	Steam temperature >120°C, sacrifice power plant performance.	Limited to smaller size plants, need skillful operator.	Membrane replace every 5-7 years, cannot treat high salinity water.	Almost all brackish water application.

CHAPTER 4 REVERSE OSMOSIS DESALINATION DRIVEN BY LOW-TEMPERATURE SUPERCRITICAL ORGANIC RANKINE CYCLE

This chapter studies a novel idea of a supercritical organic Rankine cycle (SORC) driven seawater reverse osmosis (RO) system (SORC-RO). The system is suitable for using both recirculating heat sources (e.g. solar thermal) and once-through thermal energy resources (e.g. waste heat or geothermal). The SORC-RO system is analyzed using two types of low-grade heat sources with a maximum temperature of 150°C and compared with the conventional organic Rankine cycle driven seawater reverse osmosis system (ORC-RO). The results show that the SORC-RO system is able to make use of different heat sources and provide relatively stable performance. If the source is waste heat, the SORC-RO system could make full use of the heat source and reduce thermal pollution to the environment. A comprehensive list of working fluid candidates for the SORC-RO system using low-grade heat sources less than 150°C is proposed based on the critical pressure and temperature of the fluids.

4.1 The Proposed SORC-driven RO System

Figure 4.1 shows a schematic for both an ORC-driven RO and the proposed system which combines a RO with a SORC-driven by solar thermal, geothermal or industrial waste heat. The recuperator is circled by dotted line which will be used for an R245fa based ORC-driven RO system while for the proposed SORC-driven RO, no recuperator will be needed. The energy recovery device (ERD) recovers a part of the pressure head of the remaining brine to pre-pressurize the feed water, which would otherwise be wasted. In this system, the heat from the source generates

superheated vapor in the vapor generator. The vapor is led to the turbine to generate power for the OR system, and then condensed by the feed seawater which gets preheated. A pump driven by the turbine of the power cycle pressurizes the preheated seawater going into the RO unit.

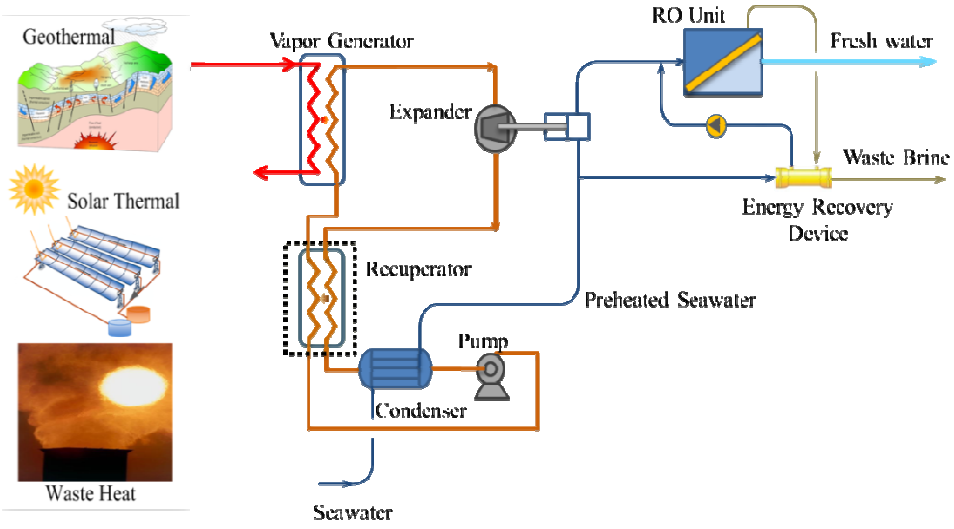

Figure 4.1 Schematic of ORC/SORC-RO system using low-grade heat.

Figure 4.2 (a) and (b) show the T-s diagrams of an ORC and a SORC, respectively. In both ORC and SORC, the working fluid is pressurized (1→2), heated (2→3), expanded (3→4), and condensed (4→1) to complete the cycle. The difference between them is that the working fluid of a SORC is pressurized above its critical pressure, resulting in its heating process bypassing the two-phase region. This "smoother" heating curve leads to a better thermal match with the heat source and less irreversibility. It is preferable to keep the configuration of the ORC/SORC simple when designing a small-scale ORC-RO system. However, when the cycle working fluid is a drying fluid such as R245fa, a heat recovery exchanger is needed to recover the heat from the superheated vapor coming out of the turbine [152]. As seen in Figure 4.2 (a), the vapor at point 4 is superheated which is used to heat the working fluid from point 2 to y while it gets cooled to point x.

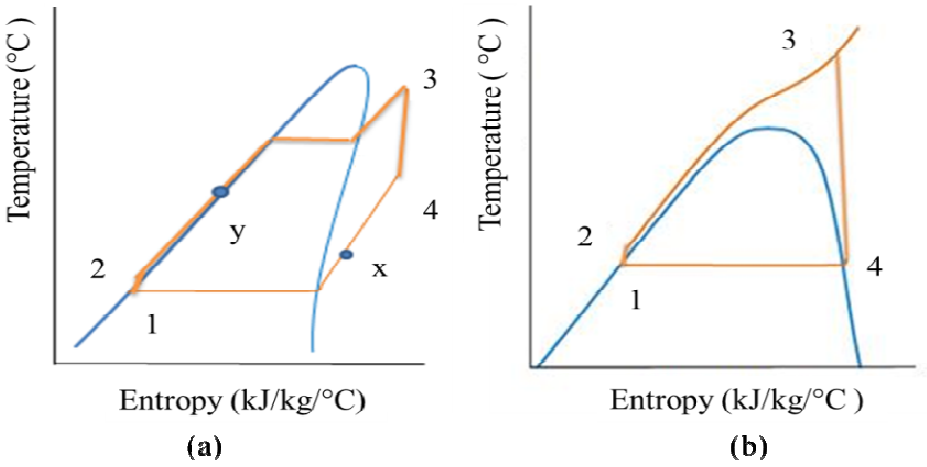

Figure 4.2 Process of (a) an organic Rankine cycle;
(b) a supercritical organic Rankine cycle.

The specific net work output of both SORC and ORC is:

$$w_{net} = (h_3 - h_4) - (h_2 - h_1) \tag{4.1}$$

The thermal efficiency of an ORC or a SORC with a heat recovery system is:

$$\eta_{th} = \frac{w_{net}}{Q_{in}} = \frac{(h_3 - h_4) - (h_2 - h_1)}{h_3 - h_y} \tag{4.2}$$

where h is the enthalpy of each point in the power cycle. x and y in Figure 4.2 are the points where hot and cold fluids come out of the recovery heat exchanger, separately. When there is no heat recovery exchanger, hy = h2 and the cycle is a simple cycle. In this study, the SORC cycle is a simple cycle while the ORC cycle has a heat recovery exchanger because the working fluid is a drying fluid.

4.2 System Simulation and Analysis

In this study, it is assumed that no preheated seawater is discharged without RO desalination treatment and all of the reheated seawater is desalinated with a 50% recovery rate, which implies that 50% seawater turns to potable water and the rest is rejected into the sea. Therefore, the power generated from the ORC/SORC cycles must provide enough energy for the 50% recovery rate of the RO system. As stated earlier, different working fluids in the ORC/SORC cycles would perform differently.

Here, only those working fluids that could meet the requirement of 50% recovery rate are considered. It is assumed that the working fluid of the power cycle is condensed at 37°C by the feed seawater which heats up from 25°C to 32°C, depending on the cooling load of the power cycle. Therefore, in this SORC-RO study, two criteria need to be met:

$$\mathrm{W_{cycle}} - \mathrm{W_{pump}} \geq \mathrm{W}_{SWRO} \tag{4.3}$$

$$\mathrm{Q_{condenser}} - \mathrm{W_{cycle}} = \mathrm{C_{p_{sw}}} \dot{\mathrm{m}}_{\mathrm{sw}} \Delta \mathrm{T_{sw}} \tag{4.4}$$

The analyses of the thermodynamic cycles are carried out assuming steady state operating conditions. Kinetic and potential energy variations in the system are assumed to be negligible and no heat and pressure losses are considered. All the work generated will be used for the RO system. The designed RO system is simulated with the Dow Chemical Reverse Osmosis System Analysis (ROSA72). The simulated system is a single stage RO system using 10 pressure vessels in each stage and 7 elements in each vessel. The feed seawater peak flow rate is 22.08 L/s and the Dow Chemical's FILMTEC™ SW30XHR-400i RO membrane is used. The membrane specifications and the proposed RO system parameters are shown in Table 4.1. When the feed seawater temperature rises, the permeated total dissolved solids (TDS) of the RO increase. In this study, effluents with a TDS level higher than that of US average tap water TDS (approximately 350 mg/L) were not considered. The temperature correction factor (TCF) for the membrane is obtained from reference [264] and is:

$$\mathrm{TCF} = \mathrm{EXP}\left[2640 * \left(\frac{1}{298} - \frac{1}{\mathrm{T}+273.15}\right); \text{when } \mathrm{T} \geq 25°\mathrm{C}\right. \tag{4.5}$$

$$\mathrm{TCF} = \mathrm{EXP}\left[3020 * \left(\frac{1}{298} - \frac{1}{\mathrm{T}+273.15}\right); \text{when } \mathrm{T} \leq 25°\mathrm{C}\right. \tag{4.6}$$

The SORCs and ORCs are simulated using ChemCAD, and the REFPROP database from the National Institute of Standards and Technology (NIST) is used for

thermophysical properties of the fluids. Table 4.2 lists all the assumptions made for this simulation.

Table 4.1 Preliminary design parameters of the RO unit

Seawater total dissolved solids (TDS)	35240 mg/L
Water classification	Seawater (Well/MF) SDI < 3
RO feedwater temperature	32°C
Seawater recovery	50.00 %
Element type	SW30XHR-440i
Maximum operating pressure	8.3 MPa
Stage	1
Pressure vessels per stage	10
Elements per pressure vessel	7
Average flux	0.23 L/m^2·min
Power consumption with ERD	92.356 KJ/s
Raw seawater flow to the system	22.08 L/s
Feed pressure	6.048 MPa
Total active area	2861 m^2
Concentrate pressure	5.96 MPa
Concentrate TDS	70244.42 mg/l
High pressure efficiency	0.8
Energy recovery device efficiency	0.9

Table 4.2 Values of fixed parameters for the proposed systems

	ORC-RO	SORC-RO
Condensation temperature, T_{cond}	37°C	37°C
Cycle pump efficiency, η_{pump}	0.85	0.85
Turbine efficiency, η_T	0.85	0.85
Boiler pinch	10°C	10°C
Recovery heat exchanger pinch	10°C	No recovery heat exchanger
Heat source temperature	150°C	150°C
Feed seawater temperature, $T_{sw,in}$	25°C	25°C
Mass of cooling seawater	22.08 L/s	22.08 L/s
Solar irradiance, G	1000W/m^2	1000W/m^2

4.3 Results and Discussion

4.3.1 Desalination System Results

The energy consumption of the proposed RO with respect to the seawater temperature is shown in Figure 4.3 (a). The required RO pressure and effluent water quality are shown in Figure 4.3 (b). It can be seen that both the RO pressure and the

energy consumption decrease when the seawater temperature increases, which is due to the increased flux through the membranes at higher temperatures. With the increased flux, the effluent water quality decreases, nevertheless, the effluent TDS still meets the average US tap water quality. The changes in RO pressure and energy consumption are more dramatic at lower seawater temperatures, indicating the necessity of seawater preheating at low-temperatures. Heated from 5°C to 32°C, the energy consumption is reduced by as much as 26.23%; while heated from 25°C to 32°C, the reduction is only 2.02%. Note that with seawater preheated to 32°C, the proposed RO system's pressure requirement is 6.048MPa, the energy consumption is 8.365 kJ per liter fresh water generated, and the effluent TDS is 238mg/L. Both the RO fresh water and discharged brine are at 0.137MPa.

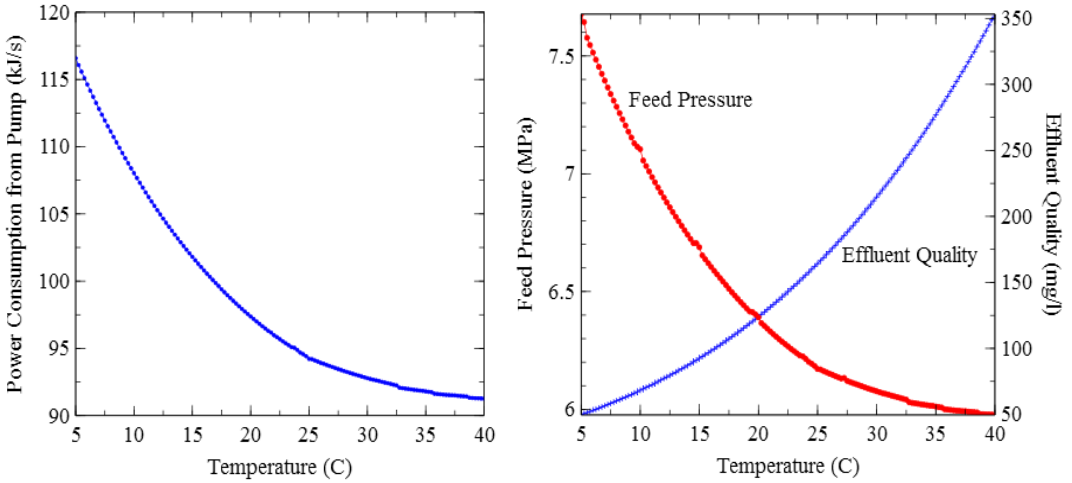

Figure 4.3 (a) Power consumption of the designed RO versus seawater temperature (left);
(b) RO system pressure and effluent TDS versus seawater temperature (right).

The proposed RO system is assumed to treat all the preheated seawater, which is 22.08L/s, from the power cycle condenser with a 50% recovery rate. The power generated from the power cycle is sufficient to meet the RO requirement. If the break-even thermal efficiency of the power cycle is η^*, below which the power generated is not adequate to process all the preheated seawater, then the power generated is:

$$W_{cycle} = Q_{in} \times \eta^* \tag{4.7}$$

The heat rejected from the condenser for seawater preheating is:

$$Q_{in} - W_{cycle} = C_{p_{sw}} * \dot{m}_{sw} * \Delta T_{sw} \tag{4.8}$$

where $C_{p_{sw}}$ is the heat capacity of the seawater in kJ/kg·K calculated from [260], ΔT_{sw} is the temperature rise of the seawater in °C. Combining Equations (4.7) and (4.8) we obtain:

$$W_{cycle} * \left(\frac{1}{\eta^*} - 1\right) = C_{p_{sw}} * \dot{m}_{sw} * \Delta T_{sw} \tag{4.9}$$

The break-even cycle efficiency η^* could be calculated based on Equation (4.9). The break-even cycle efficiency η^* and the energy needed for the proposed 22.08L/s raw seawater RO system are shown in Table 4.3. It can be seen that the bigger the ΔT_{sw}, the lower the η^* needed. For this case study, the ΔT_{sw} is limited to approximately 7°C, and the break-even cycle efficiency η^* is 12.71%. It has to been mentioned that the break-even efficiency tabulated below does not take into consideration the conversion loss between the mechanical energy and electrical energy. If a conversation efficiency of 98% is assumed, the actual break-even efficiency η^* needs to be 13.23%.

Table 4.3 Break-even cycle efficiency η^* and specific heat needed at different ΔT_{sw}

ΔT_{sw}	K	5	7	10	15
η^*	%	17.01	12.71	9.20	6.29
W_{cycle}	KJ/s	92.79	92.30	91.80	91.26

4.3.2 Desalination System Results

As mentioned earlier, a solar thermal source is treated as a recirculating source, while waste heat sources, such as exhausts from diesel engines and geothermal sources are considered as once-through. In this study, a recirculating fluid is assumed to be between 130°C-150°C, which is typical for evacuated tube solar

collectors (ETC) as discussed in [136], [145–149]. A once-through heat source is assumed to decrease from 150°C to 88°C, which is normal for geothermal plants.

For the SORC and ORC, the properties of the working fluids play a key role in the performance of the thermodynamic cycle. The fluid selection affects the system efficiency, operating conditions and economics. Chen et al. [265] did a comprehensive review on the selection of supercritical fluids and pointed out that isentropic and drying fluids are preferred in order to avoid two phase expansion in the turbine. In any case, the vapor quality at the turbine exhaust is considered higher than 90% to avoid any liquid droplet impingent on the turbine blades. Additional fluid selection criteria include the ozone depletion potential (ODP), global warming potential (GWP), the auto-ignition temperature and the ASHRAE safety classification. Based on these criteria propane (R290), Difluoromethane (R32), 1,1-Difluoroethane (R152a), and 1,1,1,3,3-pentafluoropropane (R245fa) were selected and studied further. Among these fluids, R245fa has been studied by several researchers [149] for conventional ORCs and was selected for comparison with the SORC fluids R290, R152a, and R32. These fluids have critical temperatures lower than the proposed power cycle's high temperature, which is 10°C lower than the heat source of 150°C, and therefore, they are examined in the SORCs. The properties of the selected working fluids are listed in Table 4.4.

The thermal efficiencies of the four working fluids with respect to the cycle high pressures are shown in Figure 4.4. Since the heat extracted from the heat source is partly converted into power to drive the RO system, while the rest is used to preheat the feed seawater without thermal discharge, the SORC or ORC cycle efficiency has to be sufficient to process all the preheated seawater. The dotted lines are the break-even thermal efficiencies for the systems. Below this line, the work generated from

Table 4.4 Critical parameters of the working fluid candidates

Working fluid	R290	R152a	R32	R245fa
T_c (°C)	96.74	113.26	78.105	154.01
P_c (MPa)	4.2512	4.5168	5.782	3.651
T_{NBP} (°C)	-42.11	-24.02	-51.65	15.14
MW (g/mol)	44.096	66.051	52.024	134.05
Max. pressure (MPa)	1000	60	70	200
Autoignition temp. (°C)	177[266]	455[267]	648 [266]	412 [266]
GWP 100 years	<10	124 [268]	<10	1030[269]

Note:T_c is critical temperature; p_c is critical pressure; T_{NBP} is normal boiling point temperature; *MW is* molecular weight; GWP is global warming potential.

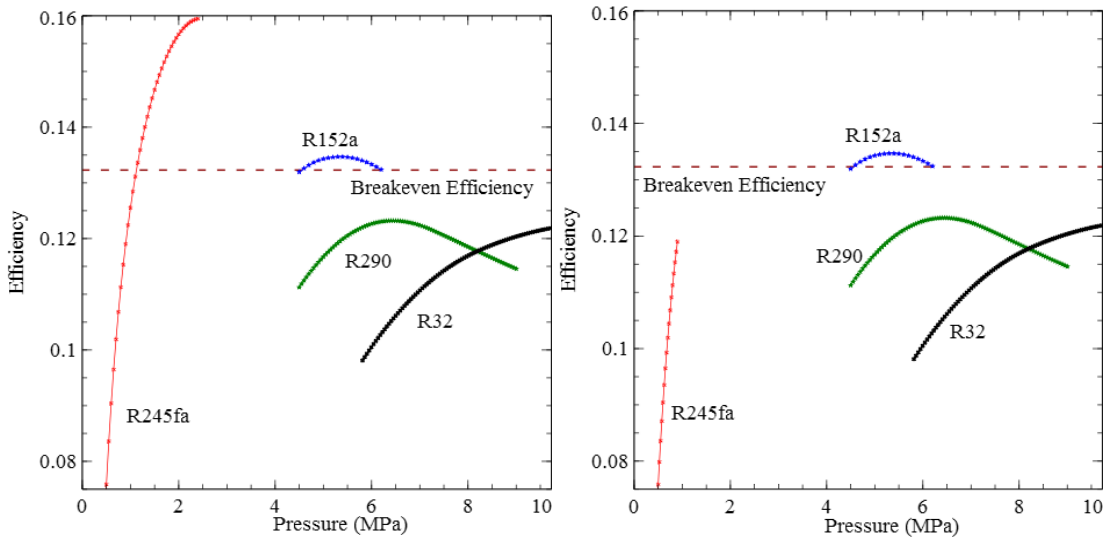

Figure 4.4 Fluids thermal efficiencies VS high pressure in the cycle.
(a) Recirculation heat source 150 – 130 °C
(b) Once-through heat source 150-88°C

the power cycle is not enough to treat all the preheated seawater without thermal discharge. Therefore, R290 and R32 are screened out due to their relatively low efficiencies. Since R245fa is a drying fluid with a significant amount of superheating at the turbine exit, an R245fa-based ORC has one recovery heat exchanger. Since R152a is an isentropic fluid, no recovery heat exchanger is required for the proposed SORC system. Figure 4.4 clearly shows that the R245fa-based ORC with recovery heat exchanger has a higher efficiency than others when using recirculating heat transfer fluids. However, it drops dramatically when the heat is a once-through type.

However, R152a could operate at 4-6.2 MPa with steady efficiency above the break-even efficiency no matter what kind of heat source is used.

It is evident that the type of heat source makes a significant difference for the performance of ORCs. This is due to the thermal profile of the heat source and its match with the ORC or SORC cycle. Figure 4.5 shows the two types of heat sources and their thermal matches with the ORC and SORC cycles in a T-ΔH diagram. The boilers are simulated with a pinch of 10 °C and heat load of 1000 kJ/sec. The temperature profile of the recirculating heat source is "flatter" due to the consideration of limiting the temperature difference between the inlet and outlet of the recirculating flow. The flatter temperature profile has a better thermal match with the R245fa-based ORC. In contrast, one would extract the maximum heat in a single cycle from the once though heat source. Therefore, its temperature profile is "steeper". The steeper temperature profile matches better with the R152a-based SORC. A steeper temperature profile also indicates a smaller mass flow needed with the same amount of heat transferred. Furthermore, in order to achieve a steeper temperature profile, the R245fa-based ORC boiler pressure needs to be lowered to satisfy the boiler pinch. As can be seen from Figure 4.5 (b), the R245fa pressure has to be dropped from 2.4MPa down to lower than 1MPa in order to meet the boiler pinch requirement. The pressures shown in Figure 4.5 (b) may not be optimum but clearly show the benefits of using a supercritical Rankine cycle for once-through heat sources.

4.3.3 Solar Collector Calculations

Instead of using the same efficiency for all the solar collectors based on the inlet and outlet temperatures of the entire solar field, the individual collector efficiency is calculated separately to reflect a different mean temperature of each collector. Matlab is used to calculate the total collector usage for the proposed

seawater RO plant handling 22.08 L/sec seawater with a 50% recovery. The following is the calculation of the solar collectors needed for different fluids and cycles. The

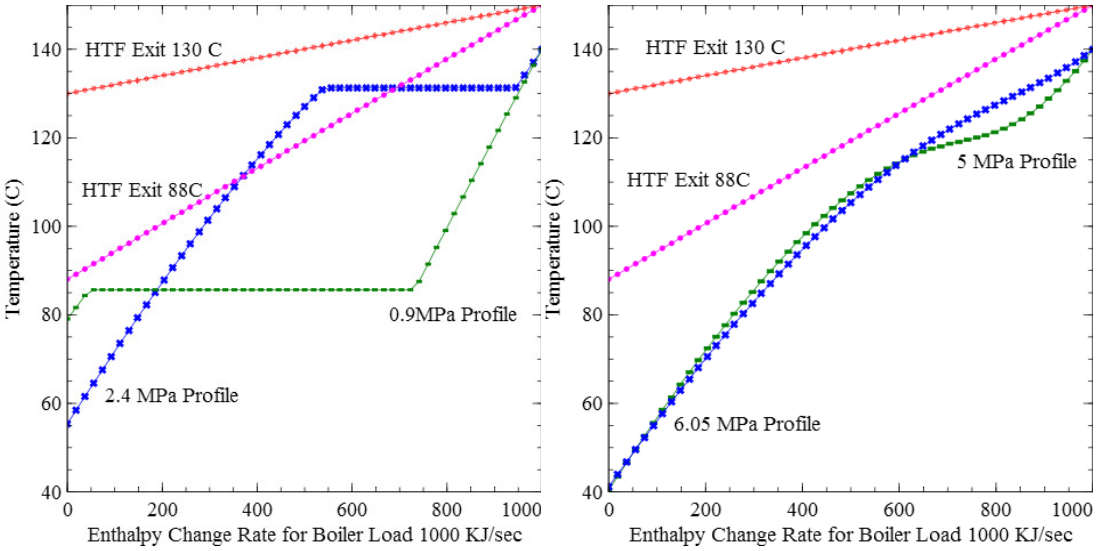

Figure 4.5 Thermal matches between the heat sources (a) with ORC cycle (left) and (b) with SORC cycle (right).

total solar collector aperture area (A) for each system is a function of the local solar irradiation, the power required for seawater desalination and the efficiencies of the solar and power cycles. The collector efficiency (η_{solar}) was calculated for a typical solar collector based on Equation (4.10) provided by the Solar Key Collector Database [270].

$$\eta_{solar} = \eta_{0a} - a_{1a} * \frac{(T_{mean} - T_{amb})}{G} - a_{2a} * \frac{(T_{mean} - T_{amb})^2}{G} \quad (4.10)$$

where η_{0a} is the optical efficiency at normal incidence of direct solar radiation, α_{1a} and α_{2a} are the co-efficients of the temperature-dependent heat loss coefficient, 0.751, 1.24 W/m^2·K and 0.0063W/m^2·K^2, respectively, which may vary based for different collectors; T_f is the mean temperature of each collector and T_{amb} is the ambient temperature, 25°C. G is the normal beam solar radiation (W/m^2). The working fluid for the proposed ETC collector is assumed to be 47% propylene glycol and 53% water by volume.

The heat needed for the power cycle is Q_{cycle} and the mass of the heat transfer fluid calculated from the power cycle is $\dot{m_{HTF}}$. At the solar field, $\dot{m_{HTF}}$ was split into n_l loops, each having a mass flow rate of $\frac{\dot{m_{HTF}}}{n}$, which is limited by the collector maximum allowable flow rate. The number of collectors n_{c_l} in each loop is calculated based on the temperature difference of the HTF in and out. The heat needed for the power cycle is given by Equation (4.11), as:

$$Q_{cycle} = n_{loop} * [c_{p_1} * \frac{\dot{m_{HTF}}}{n_{loop}} * \Delta T_1 + c_{p_2} * \frac{\dot{m_{HTF}}}{n_{loop}} * \Delta T_2 + \cdots + c_{p_{n_{c\_l}}} * \frac{\dot{m_{HTF}}}{n_{loop}} * \Delta T_{n_{c\_l}} \quad (4.11)$$

where C_p is the specific heat of the HTF which is a function of temperature as shown in Equation (4.12):

$$C_p = -3 * (10^{-5} * {T_{mean}}^3 + 0.0384 * {T_{mean}}^2 - 12.49 * T_{mean} + 4491.9) \quad (4.12)$$

The final collector area is given by Equation (4.13), as

$$A = n_{loop} * n_{c\_l} * \mathrm{A_a} \quad (4.13)$$

where $\mathrm{A_a}$ is the single collector aperture area, which, in this study, is 3.23m$^{2.}$

Figure 4.6 shows the solar collector areas needed for the R245fa-based ORC and R152a-based SORC with a cycle high-temperature of 140°C. The results show that the R245fa-based ORC with recovery heat exchangers needs a collector area of 1020 m^2 to 1260 m^2 under different cycle pressures and solar collector inlet temperatures. The lowest collector inlet temperature is about 100.5°C. If the collector inlet temperature is lower than 100.5°C, the power cycle would not meet the break-even efficiency due to the boiler 10°C pinch. When the heat transfer fluid's inlet and outlet temperatures are 124.5°C and 150°C, respectively, the solar collector area is the smallest, 1020m^2. Under this condition, the optimal power cycle pressure is 2.2 MPa.

Compared to the R245fa-based ORC, the R152a-based SORC-RO system needs a larger solar field of 1065m^2 to 1240m^2. However, it can be seen that the

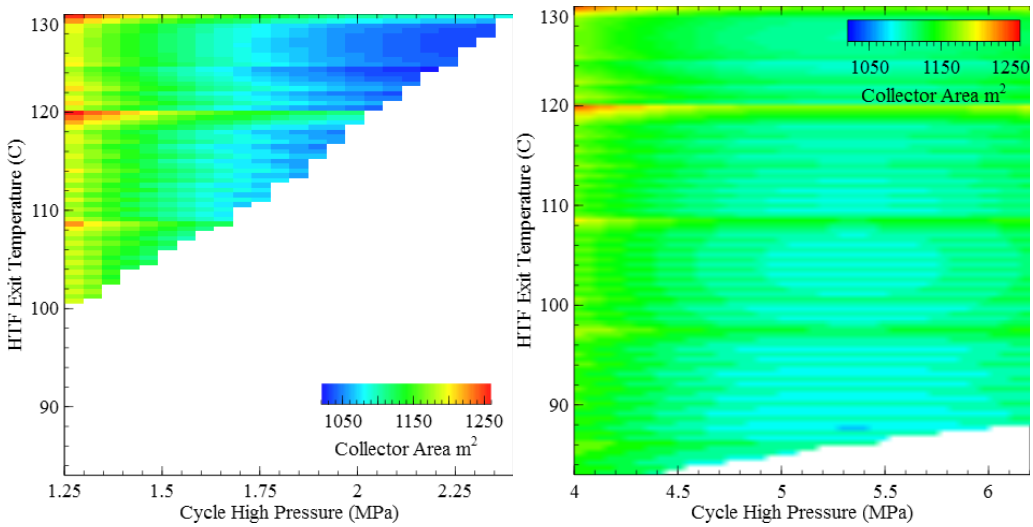

(a) R245fa-based ORC (b) R152a-based SORC

Figure 4.6 Solar collectors' areas using different heat sources with highest temperature of 150°C

temperature for the R152a-based SORC HTF exit, which is also the solar field inlet temperature, can be lower than 83°C. Also, the solar collector areas needed for different conditions are very close. The lowest collector area is achieved when the power cycle operates at 5.2MPa and the solar field inlet temperature is 84°C. Compared with Figure 4.4, the smallest collector area for the ORC-RO system is only about 4% less than that of optimized SORC-RO system, while the highest efficiency of the R245fa-based ORC is approximately 18% higher than that of the SORC system. This is due to the collector efficiency change with operating temperature, as shown in Figure 4.7. Solar collectors have higher efficiencies when operating at lower temperatures. Though the cycle's high temperature for both the SORC and ORC are 150°C, the mean solar field temperature for the SORC system is much lower due to the low solar field inlet temperature. The above calculation will vary with different solar collectors and, in this study, only a typical ETC solar collector is considered.

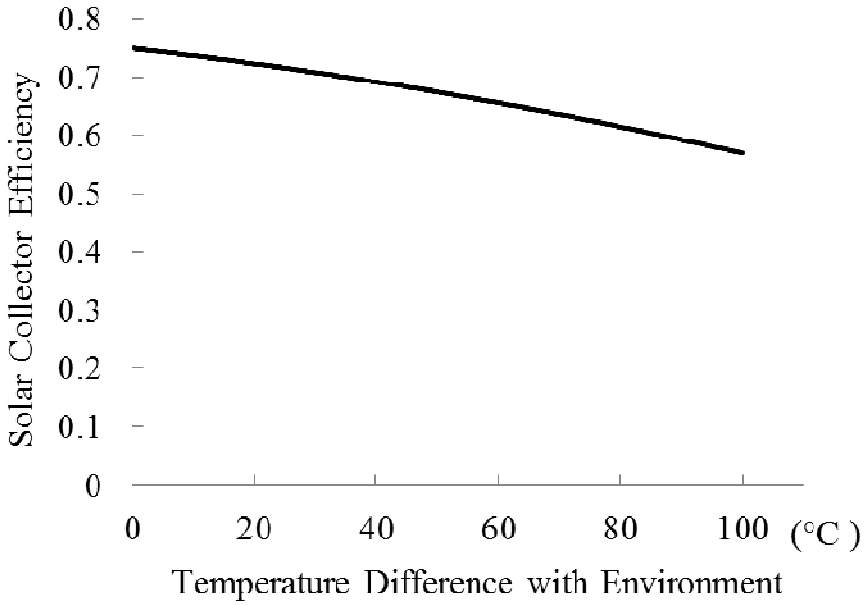

Figure 4.7 Solar collector efficiency curve.

Table 4.5 Cost comparison of solar ORC-RO systems

Ref.	Cycle high T (C)	Cycle fluids	Cycle configuration	Cost percentages			
				ORC	RO	Solar field	Others
[146], [153], [148]	75.8	134a	Single ORC	15	32	40	13
[145], [147], [154]	137	245fa	Upper cycle	25.36	23.36	40.83	10.45
	75.8	134a	Bottom cycle				
[157] (a)	87.344	R218	Single ORC with heat recovery exchanger	19.5	8.8	71.7(a)	0
	120.94	R245		16.1	7.2	76.7(a)	0
	289.73	R601a		27.9	12.5	59.6(a)	0
	378.44	(b)		32.9	18.5	48.5(a)	0.1

(a) Case study results for location Barcelona seawater RO; (b) N-propyl benzene.

Table 4.5 shows a cost comparison of the solar ORC-RO systems described in the literature. It is clear that the solar collector field represents a major cost fraction of the whole system. Therefore, from a system economics point of view, minimizing the solar collector area is the first priority. Based on the above discussion, if the only heat source is a recirculating type, an ORC-based system has a less than a 5% advantage.

4.3.4 Heat Transfer Fluid Discussions

For once-through heat sources like geothermal and industrial waste heat, one needs to extract the maximum possible amount of energy in one cycle. The heat transfer fluid is still assumed to be 47% propylene glycol and 53% water by volume, which is the working fluid for the ETC collector. If geothermal or waste heat sources are used, other heat transfer fluids can be used but the basic calculations and conclusions would be similar. Figure 4.8 shows the heat transfer fluid flow rate needed to power the proposed RO system in order to meet the system break-even efficiency. It is clear that the SORC-based system is able to use less heat transfer fluid, the minimum being about 2.75kg/s. However, the minimum HTF needed for the R245fa-based ORC system is 3.95kg/s. If the heat source is a geothermal fluid, the SORC-based system could potentially produce 40% more water using the same amount of geothermal fluid. When the heat source is waste heat, the SORC-based system would not only produce more water with the same heat source but also lower the waste heat to below 83°C and dramatically reduce thermal pollution.

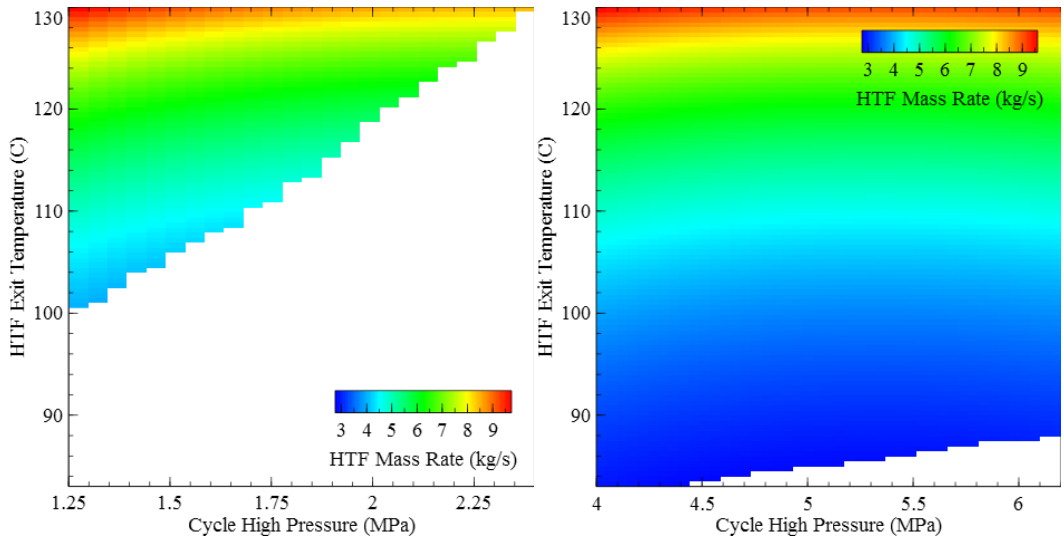

Figure 4.8 HTF usage comparison for the proposed ORC-RO and SORC-RO system:
(a) HTF use for R245fa-based ORC-RO system (left);
(b) HTF use for R152a-based SORC-RO system (right).

4.3.5 SORC-RO System Exergy Destruction Analysis

Inefficiency is caused by exergy destruction within the system and exergy losses to the environment. An exergetic analysis is conducted in this section to identify the exergy destructions and losses in each process of the ORC- or SORC-driven seawater energy recovery (SWRO) system so as to identify the potential of improvements. The exergy destruction and losses of each element of the system are expressed as follows. Refer to Figure 4.1 for the system configuration and the components. Dead state temperature is 25 °C.

For the pump, exergy destruction is:

$$E_{d_{Pump}} = W_p - \left(E_p^{out} - E_p^{in}\right) = W_p - \left[\left(H_p^{out} - H_p^{in}\right) - T_0\left(S_p^{out} - S_p^{in}\right)\right] \quad (4.14)$$

where W_p denotes the power of the pump, E_p^{in} and E_p^{out} are the exergy inlet and outlet of the pump, respectively; H and S are the enthalpy and entropy, respectively. T_0 is the dead state temperature.

For the turbine, exergy destruction:

$$E_{d_{Turbine}} = \left(E_t^{in} - E_t^{out}\right) - W_t = \left[\left(H_t^{in} - H_t^{out}\right) - T_0\left(S_t^{in} - S_t^{out}\right)\right] - W_t \quad (4.15)$$

where W_t denotes the power output of the turbine, E_p^{in} and E_p^{out} are the exergy inlet and outlet of the turbine, respectively; H and S are the enthalpy and entropy, respectively.

For the boiler, exergy destruction:

$$E_{d_{Boiler}} = \left(E_{HTF}^{in} - E_{HTF}^{out}\right) - \left(E_{SORC_F}^{out} - E_{SORC_F}^{in}\right) = \left[\left(H_{HTF}^{in} - H_{HTF}^{out}\right) - T_0\left(S_{HTF}^{in} - S_{HTF}^{out}\right)\right] - \left[\left(H_{SORC_F}^{out} - H_{SORC_F}^{in}\right) - T_0\left(S_{SORC_F}^{out} - S_{SORC_F}^{in}\right)\right] \quad (4.16)$$

$$\varepsilon_{boiler} = \frac{E_{SORC_F}^{out} - E_{SORC_F}^{in}}{E_{HTF}^{in} - E_{HTF}^{out}} \quad (4.17)$$

where E_{HTF}^{in} and E_{HTF}^{out} are the exergy inlet and outlet of the heat transfer fluids (HTF), $E_{SORC_F}^{in}$ and $E_{SORC_F}^{out}$ are the exergy inlet and outlet of the SORC or ORC working

fluids, and $\varepsilon_{\text{boiler}}$ is called boiler exergy efficiency. H and S are the enthalpy and entropy, respectively.

For the SORC or ORC power system, the exergy efficiency is determined by:

$$\varepsilon_{SORC} = \frac{W_t - W_p}{E_{HTF}^{in} - E_{HTF}^{out}} \tag{4.18}$$

For the condenser, exergy destruction:

$$E_{d_{condenser}} = (E_c^{in} - E_c^{out}) - (E_{sw}^{out} - E_{sw}^{in}) \tag{4.19}$$

$$\varepsilon_{condenser} = \frac{E_{sw}^{out} - E_{sw}^{in}}{E_c^{in} - E_c^{out}} \tag{4.20}$$

where E_c^{in} and E_c^{out} are the exergy inlet and outlet of the working fluids in the condenser, E_{sw}^{in} and E_{sw}^{out} are the exergy inlet and outlet of the seawater, and $\varepsilon_{\text{condenser}}$ is called condenser exergy efficiency.

For the SWRO, exergy destruction:

$$E_{d_{SWRO}} = 0.95W_{net} + E_{sw}^{out} - E_{brine}^{out} - E_{fresh}^{out} \tag{4.21}$$

where $0.95W_{net}$ means 5% loss during mechanical conversion, E_{sw}^{out} is the exergy of the preheated seawater for SWRO system; E_{brine}^{out} is the exergy of the concentrated brine discharge and E_{fresh}^{out} is the exergy of the fresh water generated.

For the whole system, the exergy gained from the heat source plus the exergy from the feed seawater is equal to the summation of all the exergy destruction of each component, plus the exergy in brine and fresh water finally generated. Therefore the whole system's exergy balance could be written as:

$$\left(E_{HTF}^{in} - E_{HTF}^{out}\right) + E_{sw}^{in} = E_{d_{SWRO}} + E_{d_{condenser}} + E_{d_{converstion}} + E_{d_{Boiler}} + E_{d_{Turbine}} + E_{d_{Pump}} + E_{brine}^{out} + E_{fresh}^{out} \tag{4.22}$$

Exergetic analyses of the system are conducted at the heat source temperature of 150°C. The system pressure is fixed at 6.048MPa which is determined by the designed SWRO system for feed seawater with 35240 ppm salinity and 50% recovery

at 32°C. Each component of the SORC-SWRO system's exergy destruction percentage could be seen from Figure 4.9. We see that except for the "useful" SWRO consumption, almost 50% of exergy is wasted, and among the exergy destruction, the boiler is the main irreversibility sector. Therefore selecting a suitable working fluid is the key to reduce the system's exergy destruction.

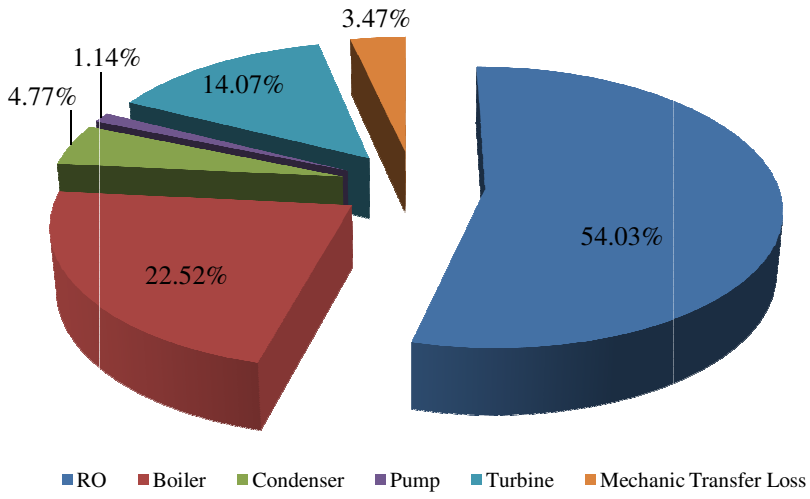

Figure 4.9 Exergy results of R152a SORC-SWRO.

4.3.6 Flexible Operation and Possible Working Fluids

The previous discussions show that the R152a-based SORC-RO system could operate with both a circulating type of heat source and once-through heat source. When using solar collectors to provide the heat, the total collector area is close to an ORC-RO-based system, with the collector area not varying much (1065m^2 to 1240m^2). Kosmadakis et al. [136] showed that using waste heat is more economical than a solar-driven desalination system at the current stage, and matches other hybrid desalination systems, listed in Table 4.6. If a conventional fossil fuel or waste heat is used, other desalination systems using hybrid power sources were more cost competitive. Therefore, it is expected that once-through heat sources or hybrid heat sources to drive SORC-RO systems, could potentially be more economical than a

Table 4.6 Solar desalination using hybrid system

Ref.	Solar system	Desal. system	Desal.cap. (m^3/d)	Cost ($/$m^3$)	Notes
[30]	Solar pond	MSF	1	1.785[(c)]	Hybrid system, 18 stages MSF system.
			1	2.835[(c)]	Solar only, 18 stages MSF system.
[27]	Solar pond	MSF	2040[(a)]	0.9-1.014[(d)]	Hybrid system, heat source from gas turbine exhaust at 550°C. Part of the heat is used to run a desalination plant and the rest is stored in a 4m deep 7800 m^2 solar pond. Peak time heated by gas turbine while rest of the time by solar pond.
			12378[(b)]	0.82-0.86[(d)]	
		MED	2348[(a)]	0.62-0.64	
			15044[(b)]	0.465-0.471	
[72]	PTC	MED	10000	0.92	Solar only, 16 stages MED.
			100000	0.69	Hybrid, 16 stages MED.
[69]	ETC-PV	MED	100	8.6-9.9	Solar only. Solar thermal with PV.
	ETC		100	8.3-9.3	Hybrid system, solar/diesel hybrid.
	ETC		500	5-6.7	Hybrid system, solar/diesel hybrid.
	ETC		1000	3.4-4.4	Hybrid system, solar/diesel hybrid.
[115]	FPC	Evaporator /heat pump	NA	NA	Hybrid gas/solar-driven absorption heat pumps showed higher water yield than solar stills.
[114]	PV	MVC	120	NA	Solar/diesel hybrid

(a) Main heat source is exhaust gas from a 30 MW gas turbine 550°C.
(b) Main heat source is exhaust gas from a 120 MW gas turbine.
(c) Convert to US dollar based on 1KD=3.5 dollar as authors' mentioned.
(d) The surface pond is covered by a transparent material to reduce heat losses and store solar energy.

solar-only RO desalination system. In addition, SORC-RO systems are more suitable for use with different heat sources.

They could operate in a wider range of temperatures without affecting the system performance. If conventional power waste heat is used at night (i.e. waste heat from a diesel engine) while solar energy is used during the day, the proposed SORC-RO system could provide consistent power and water, which are crucial for many remote areas. Table 4.7 lists the optimized conditions for an ORC-RO system and the proposed SORC-RO system. The "Heat to Water" performance is calculated from the heat input to the power cycle divided by the fresh water production. The "Solar Radiation to Water" is calculated by the total solar radiation on the collectors divided by the fresh water production, which is bigger than the "Heat to Water" value because there are solar collector efficiencies involved. As a comparison, Ref. [102] reports experimental data for a 14-Effect forward-feed MED system combined with a double-effect absorption heat pump using 180°C steam. According to Ref. [102] this is the most energy efficiency thermal desalination system in which the heat to water consumption is 108kJ/kg and solar energy to water consumption is 142 kJ/kg. Therefore, the proposed system is theoretically more efficient than a MED system.

Table 4.7 Comparison of the optimized conditions for ORC-RO and SORC-RO systems using low-grade heat sources

	R245fa	R152a
Heat to water (kJ/kg)	53.11	62.11
Solar collector area (m^2)	1020	1065
Solar radiation to water (kJ/kg)	92.39	96.47
HTF flow rate (kg/s)	6.651	2.903
HTF temperature range (°C)	124.5-150	87-150
Fresh water production (kg/s)	11.04	11.04
Cycle efficiency	15.86%	13.47%
Operation pressure (MPa)	2.2	5.3
Recuperator	Yes	No

There may be additional working fluids that can be explored for the SORC-driven RO desalination. Figure 4.10 shows working fluids with critical pressures in the range that may be useful for the RO pressure requirements. All of these fluids have zero ozone depletion potential. The R152a selected for this study is only an example to illustrate the SORC-RO system. Given other RO system requirements and heat sources, other fluids could potentially be better and the selection could be different based on the RO system design and heat source characteristics.

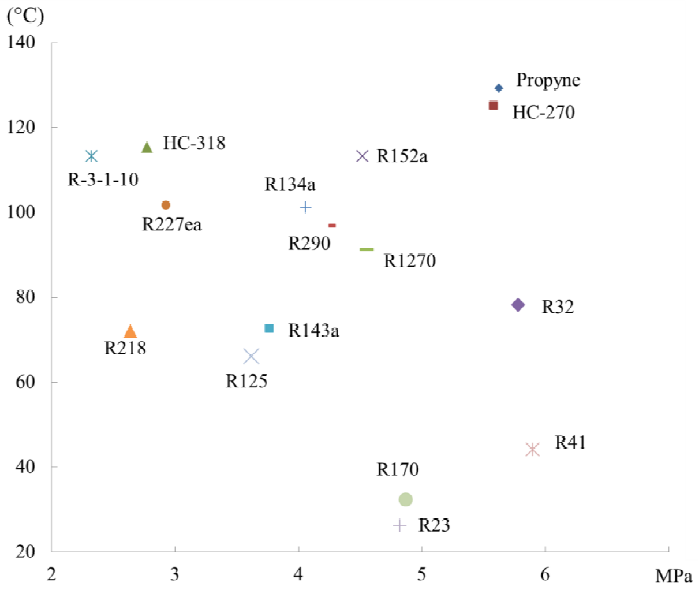

Figure 4.10 Potential fluids of SORC-RO application for low-temperature heat sources (<150°C).

4.4 Concluding Remarks

Supercritical organic Rankine cycles for seawater desalination applications using low-grade heat sources have been studied in this chapter. Two types of heat sources with the same maximum outlet temperature were considered. When the heat source is of the heat transfer fluid recirculating type (i.e. solar collectors), a conventional organic Rankine cycle using R245fa has limited advantages. However, when the heat sources are once-through type (i.e. waste heat or geothermal heat), a conventional ORC does not have enough pressure to meet the RO needs. Under such

conditions, a supercritical cycle shows better performance with higher efficiency and wider operation range. The final part of this chapter provided some potential fluids that could be used for the SORC-RO system when the heat source temperature is lower than 150°C (low-grade heat sources).

CHAPTER 5 POWER CYCLE, EJECTOR COMBINED WITH MULTI EFFECT DISTILLATION FOR CONCENTRATED BRINE TREATMENT

Thermal desalination processes such as multi-effect distillation (MED), multi–stage flash (MSF) and membrane desalination such as reverse osmosis (RO), are the dominant desalination processes with RO having the largest installed capacity (see Figure 1.1) [8]. When handling brackish water or even seawater, the RO process is energy efficient. However, it requires stringent pretreatment and osmotic pressure increases dramatically with salt concentration, as shown in Figure 5.1. This limits the RO process application to high concentration feed water desalination applications.

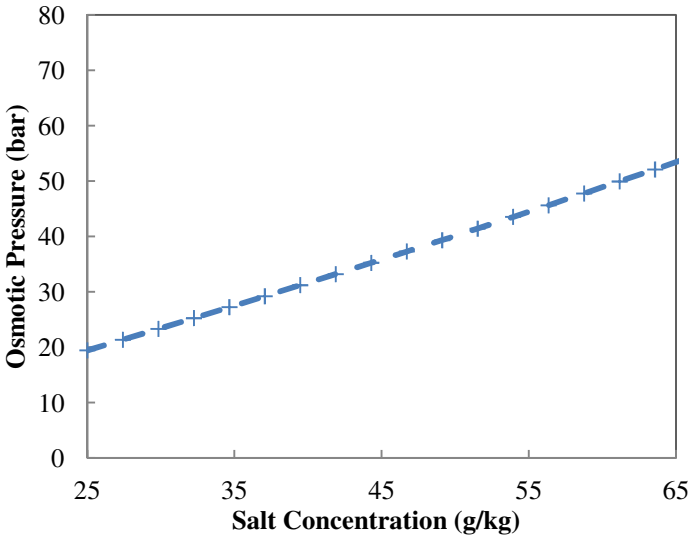

Figure 5.1 Osmotic pressure changes with salt concentration.

On the other hand, a thermal process such as MED is robust, requires less pretreatment and could handle highly concentrated brine. Therefore thermal

desalination is still important and needs to be further studied. However, thermal desalination is regarded as energy intensive. Seawater desalination and frac flowback water desalination require more energy as compared to conventional water treatment processes due to the higher salt concentration [1–3]. Therefore, it is necessary to use alternative energy resources for desalination processes to minimize environmental concerns [130], [180], [243], [271–274]. It is also important to improve the thermal desalination system's energy utilization.

The system studied in the chapter combines a MED desalination system with a Rankine cycle and an ejector. It works like a combined heat, power and condensation system where the ejector cooling is used to condense the final effect vapor of the MED system. Ejector cooling has been studied by many researchers [275], [276] and has some advantages such as fewer moving parts and low operating, installation and maintenance costs. In addition, the ejector cycle can use a wide range of refrigerants and many different heat sources [277]. The SORC power cycle provides power for the desalination system and therefore eliminates the need for additional electricity input.

5.1 System Description

The proposed SORC-Ejector-MED desalination system is composed of three subsystems: a Rankine cycle, a MED system, and an ejector loop schematically shown in Figure 5.2. The heat source, stream (3), heats the working fluid of the SORC in the boiler. The high pressure and temperature vapor (1) is expanded through a scroll expander to generate mechanical energy. The working fluid, stream (2), coming out of the expander enters the ejector as the primary steam. The very high velocity vapor at the exit of the nozzle produces a high vacuum and entrains the secondary flow [278], [279], stream (14), into the ejector to form the mixed steam (5). This condenses by first rejecting heat to the MED and then forming the liquid stream (6).

Stream (6) is split into two parts: one part, stream (7), is used as the working fluid of the SORC system and is pumped to the boiler to again be vaporized. The second part, stream (12), passes through a throttle valve and flows to the MED at low pressure and temperature where it is vaporized to stream (14) by absorbing the latent heat of condensation of the vapor from the last MED effect. The last MED effect vapor, stream (16), is condensed by both stream (14) from the ejector cycle and the feed brine stream (9). The application of the ejector under supercritical conditions has been reported in Ref. [280].

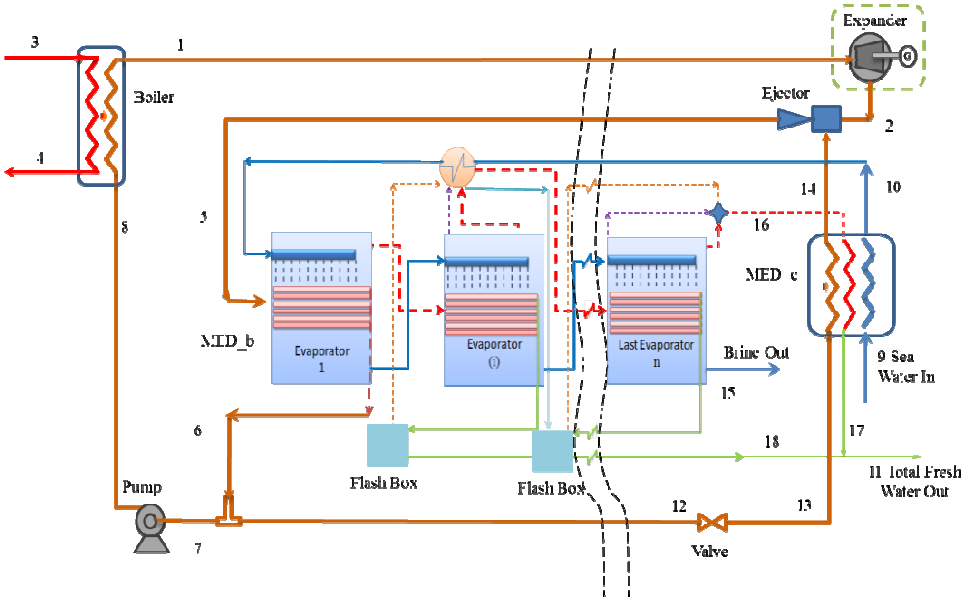

Figure 5.2 Schematic of the proposed SORC-Ejector-MED system.

The conventional ejector is simple with no moving parts, but typically suffers from low efficiencies. In recent years, researchers have developed high efficiency ejectors and have evaluated them both theoretically and experimentally [281], [282]. Some ejectors may have efficiencies of 90% under specific conditions [283]. In this study, the pressure exchange ejector, as illustrated in Figure 5.3 [285], is selected and modeled. More detailed modeling and experimental validation information about the pressure exchange ejector may be found in Ref. [284–287].

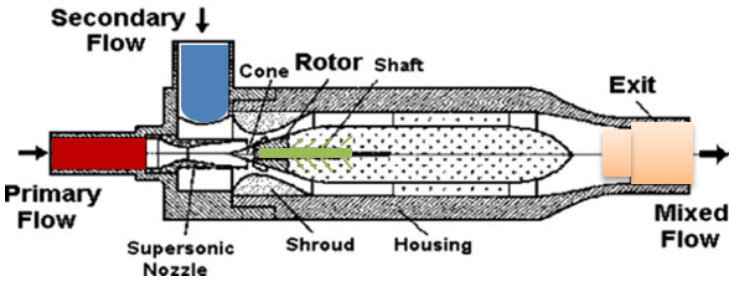

Figure 5.3 Schematic of pressure-exchange ejector.

Assuming the working fluid is an ideal gas, and both primary and secondary flows discharge at the same pressure and mix completely before discharging at point 4 without kinetic energy (Figure 5.4 (a)) [288], [289], then the pressure-exchange ejector can be represented by the turbomachinery analog, as shown in Figure 5.4 (b), [289], [290]. It also shows the H-S diagram of the process. The primary flow passes through the "turbine" which provides the energy to compress and thermally energize the secondary flow passing through the "compressor". The energy provided by the "turbine" is equal to the energy consumed by the "compressor".

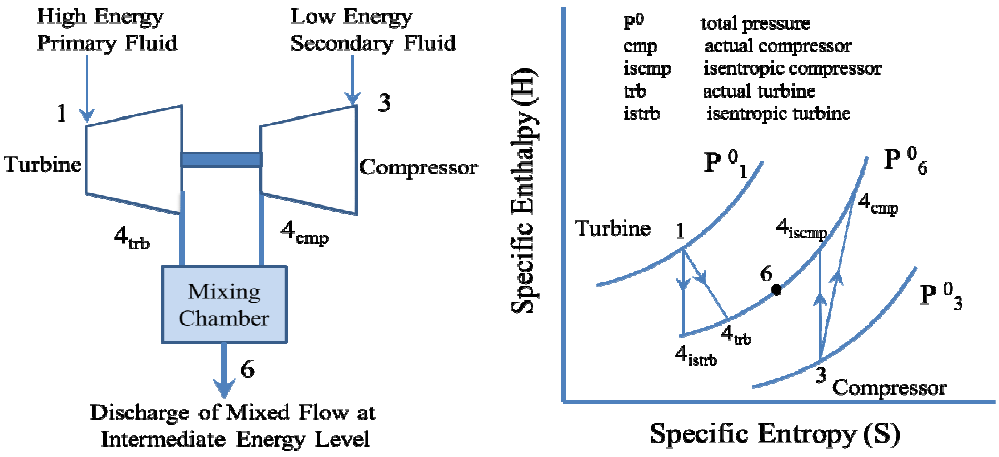

Figure 5.4 (a) Turbomachinery correlation diagram of the ejector and (b) the H-S diagram of the turbomachinery analog analysis for the ejector.

5.2 Mathematical Modeling

It is assumed that the system operates in steady state and the heat losses through the system components are negligible. The refrigerant is organic (i.e. R152a)

and it does not distill water directly. The principles of mass and energy conservation as well as the 2nd law of thermodynamics are employed to build the mathematical model. Brine properties are calculated based on Ref. [291] using Engineering Equation Solver (EES).

5.2.1 SORC-EJECTOR Subsystem Model

The major components of the SORC-Ejector subsystem are: boiler, turbine, evaporator, heater, regenerator, condenser, ejector, pumps and throttle valve. The mass balance equations for the SORC-Ejector are shown below:

$$m_1 = m_2 = m_7 = m_8 \tag{5.1}$$

$$m_{12} = m_{13} = m_{14} = m_2 * Er \tag{5.2}$$

$$m_5 = m_6 = m_2 + m_{14} \tag{5.3}$$

Energy balance equations for the system components are:

Boiler: $$Q_{Boiler} = m_1(h_1 - h_8) = m_3(h_3 - h_4) \tag{5.4}$$

Expander: $$W_{Expander} = m_1(h_1 - h_2) = m_1\eta_{expander}(h_1 - h_{2,s}) \tag{5.5}$$

Ejector: $$m_2h_2 + m_{14}h_{14} = m_5h_5 \tag{5.6}$$

Valve: $$h_{12} = h_{13} \tag{5.7}$$

Pump: $$W_{Pump} = m_7(h_8 - h_7) \approx \frac{m_7(p_8 - p_7)}{\rho\eta_{pump}} \tag{5.8}$$

MED_b: $$Q_{MED\_heating} = m_5(h_5 - h_6) \tag{5.9}$$

MED_c: $$Q_{MED\_condensing} = m_{16}(h_{16} - h_{17}) = m_{13}(h_{14} - h_{13}) + m_9(h_{10} - h_9) \tag{5.10}$$

where Q_{Boiler} is the thermal energy input to the SORC-Ejector subsystem, which is also the thermal energy input to the whole SORC-Ejector-MED system. The SORC-Ejector subsystem has two useful outputs: MED heating input, $Q_{MED\_heating}$, from the condensing stream 5 in MED_b and a part of the MED cooling input,

$Q_{MED\_condensing}$, from the evaporating refrigerant stream 13 in the MED_c part. The whole SORC-Ejector subsystem energy balance is:

$$Q_{Boiler} + m_{14}h_{14} + m_9h_9 = Q_{MED\_heating} + m_{14}h_{17} + m_9h_{10} \quad (5.11)$$

5.2.2 Mathematical Model for the MED Subsystem

A schematic diagram for the forward-feed Multiple Effect Distillation (MED) desalination process can be seen in the MED subsystem of Figure 5.2, in which feed brine is delivered to a sequence of successively lower pressure vessels, called "effects". The external heat is supplied to the first effect and the generated vapor supplies its latent heat of condensation to the next effect. The detailed modeling and parameters such as heat transfer coefficients as well as non-equilibrium allowance for a foward-feed MED process may be found from Ref. [292]. The proposed system consists of n evaporators, n-2 feed water preheaters, n-1 flashing boxes. The last effect condenser, which is MED_c in Figure 5.2, provides heat to both ejector loop and feed brine.

The assumptions for the MED subsystems are:

a) Constant heat transfer areas in the evaporators and feed preheaters in all effects.
b) Non-condensable gas is removed by the pretreatment and the venting system
c) There is no thermal loss and vapor leak to the environment
d) The formed vapors are salt free.
e) The wire mesh demister friction, pipe friction and the condensation pressure drop are negligible

Common parameters used in the following process model are listed in the List of Symbols. Referring to Figure 5.2, feed brine M_f is first introduced into MED_c, where its' temperature increases from T_{cw} to T_f. In a regular MED system, a part of

the feed water is used as cooling water to condense the final effect vapor wasting a large amount of energy. In the proposed system, the heat discharged by the last effect vapor condensation is absorbed by the SORC-Ejector system. The energy analysis in the discussion shows the benefits of combining the SORC-Ejector system with a MED system.

The MED subsystem could be considered as three parts, the first effect (Figure 5.5), the last effect (Figure 5.7) and the effects from 2 to n-1 (Figure 5.6). In these figures the green lines are fresh water produced during the desalination process (light green is condensed water from the preheater, dark green is condensed water from the evaporator, and normal green is produced fresh water from the flash box). The blue lines are the feed water or concentrated brine, and the dashed lines are the saturated vapors generated in the processes. The orange line is the vapor generated from condensed fresh water flash and the purple line is the brine flash vapor. The red line is from the evaporation process and dark red is the remaining vapor after preheater is sent to the next effect evaporator as the heat source.

The feed water passes condenser MED_c and a series preheater until the temperature increased from Tf to Tf_2 at the entrance of the first effect. The heat for the feed water is supplied by condensing a portion of the vapor formed in each effect. The feed water Mf is sprayed into the first effect, where it is heated to the boiling temperature T_1 before a small portion of the vapor D_1 is formed. The heat required to preheat the feed and for evaporating D_1 is released by stream 5 in the SORC-Ejector subsystem, as can be seen in Figure 5.5.

Energy and mass balance for the 1st effect:

$$M_f = D_1 + B_1 \tag{5.12}$$

$$M_f * Salt_f = B_1 * Salt_1 \tag{5.13}$$

$$Q_{MED\_heating} = m_5(h_5 - h_6) = M_f * Cp * (T_1 - Tf_2) + D_1 * \lambda_1 \quad (5.14)$$

where λ_1 is the latent heat of vaporization at temperature Tv_1 at which temperature the vapor formed in the first effect. Cp is the mean specific heat capacity of water from feed-in temperature Tf_2 to the effect temperature T_1. Tv_1 is less than the boiling temperature T_1 by the boiling point elevation BPE_1 caused by dissolved salt.

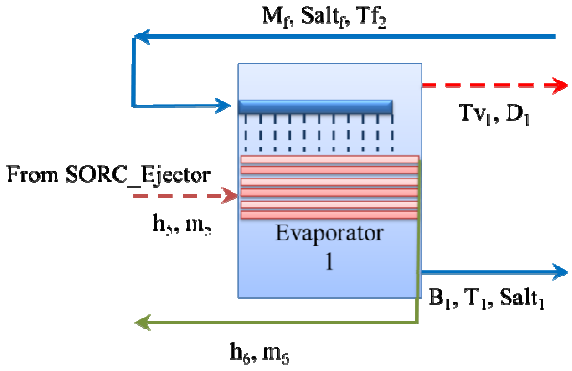

Figure 5.5 First effect of MED subsystem.

Effects 2 to n-1 have the same configurations, each with one evaporator, one preheater and one flash box, as shown in Figure 5.6. However, since the first effect has no preheater, the vapor generated from the first effect is all transferred to the 2nd effect, which makes it a little different than effects 3rd to n-1. Vapor d^*_i is formed by flashing the brine B_{i-1} due to its temperature being higher than the boiling temperature in effect i by the non-equilibrium allowance [292].

$$T^*_i = NEA^*_i + T_i = \frac{32*(T_{i-1}-T_i)^{0.55}}{Tv_i} + T_i = \frac{32*(T_{i-1}-T_i)^{0.55}}{T_i - BPE_i} + T_i \quad (5.15)$$

A small amount of vapor $\bar{d}_i$ is generated in the flash box due to the flashing of distillate condensed from previous effect. The temperature relationship is

$$\bar{T}_i = \overline{NEA}_i + Tv_i \quad (5.16)$$

Three vapor streams, d^*_i, $\bar{d}_i$ and D_i flow into the preheater of the effect. A portion of the vapor, θ_i, is used for preheating the feed water. A part of it is

condensed which goes into the flash box, the rest going to the next effect as vapor. Since that first effect has no brine flash or condensate flash, the only heat source for effect two is D_1. Because a majority of the vapor is generated by the evaporator, when the three vapor streams are mixed, it is assumed that the mixture temperature is Tv_i and the mixture latent heat isλ_i. The temperature of effect *i* is:

$$T_i = BPE_i + Tv_i \tag{5.17}$$

The major mass and energy balance of the repeated units from effect 2 to n-1 are as followed:

$$B_{i-1} = D_i + B_i + d^*{}_i \tag{5.18}$$

$$B_{i-1} * Salt_{i-1} = B_i * Salt_i \tag{5.19}$$

$$Q_{evapor,i} = \left(\bar{\mathrm{d}}_{(i-1)} + d_{(i-1)}{}^* + D_{(i-1)}\right) * (1 - \theta_{(i-1)}) * \lambda_{(i-1)} = D_i * \lambda_i$$

$$= Ue_i * A_{e,i} * (Tv_{i-1} - T_i) \tag{5.20}$$

$$Q_{preheater,i} = \left(\bar{\mathrm{d}}_i + d_i{}^* + D_i\right) * \theta_i * \lambda_i = M_f * Cp_i * (Tf_i - Tf_{i+1})$$

$$= Uc_i * A_{p,i} * LMTD_{p,i} = Uc_i * A_{p,i} * \frac{(Tf_i - Tf_{i+1})}{\ln\frac{(Tv_i - Tf_{i+1})}{(Tv_i - Tf_i)}} \tag{5.21}$$

$$Q_{brine\ falsh,i} = d_i{}^* * \lambda_i{}^* = B_{i-1} * Cp^*{}_{i-1} * (T_{i-1} - T^*{}_i) \tag{5.22}$$

$$Q_{condensate\ flash,i} = \bar{\mathrm{d}}_i * \bar{\lambda}_i$$

$$\approx ((\bar{\mathrm{d}}_{(i-1)} + d_{(i-1)}{}^* + D_{(i-1)}) * (1 - \theta_{(i-1)})) * \overline{Cp}_i * (T_i - \bar{T}_i)$$

$$+ (\bar{\mathrm{d}}_{(i-1)} + d_{(i-1)}{}^* + D_{(i-1)}) * \theta_{(i-1)} * \overline{Cp}_i * (Tv_{i-1} - \bar{T}_i) + (\sum_1^{i-1} D$$

$$+ \sum_2^{i-2} d^* - \overline{d_{(i-1)}}) * \overline{Cp}_i * (Tv_{i-1} - \bar{T}_i)$$

$$\approx (\sum_1^{i} D + \sum_2^{i-1} d^*) * \overline{Cp}_i * (Tv_{i-1} - Tv_i)$$

(5.23)

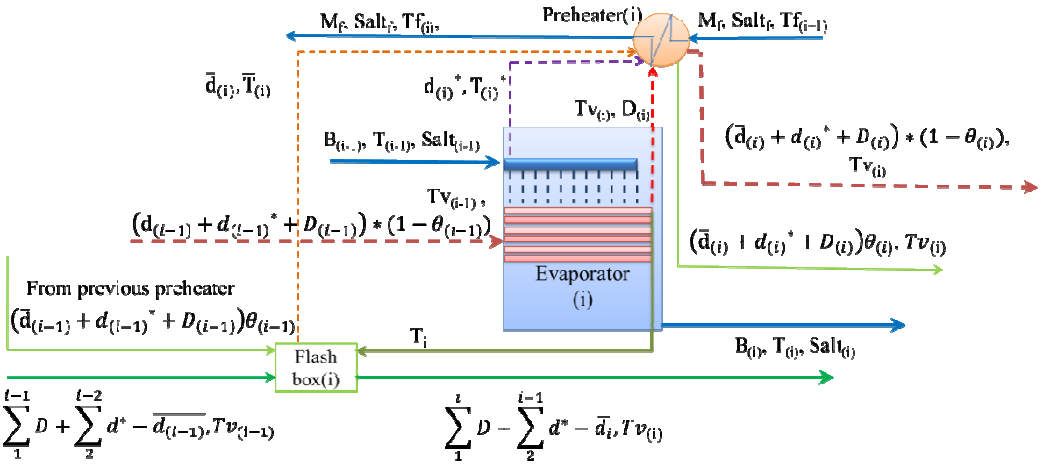

Figure 5.6 Effects 2 to n-1 of MED subsystem.

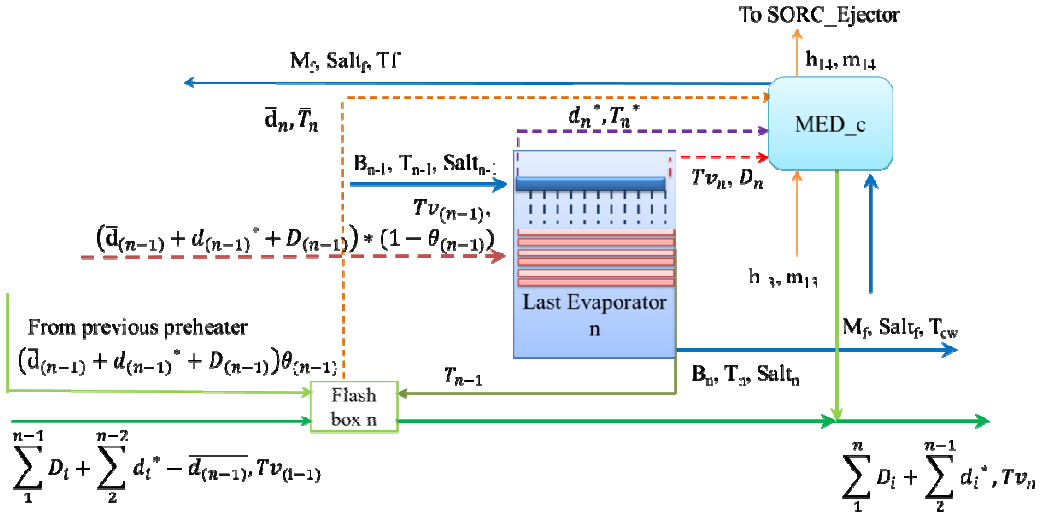

Figure 5.7 Last effect and connection with SORC-Ejector condenser.

The mass and energy balance for the final effect evaporator and flash box are the same as the previous, however, the last effect has no preheater and the vapor generated from the last effect flows into the condenser MED-c, as shown in Figure 5.7. The unevaporated brine flows by itself from effect to effect [292]. The additional equation for the final effect connected with MED-c is:

$$Q_{MED\_c} = \left(\bar{d}_n + d_n^{\,*} + D_n\right) * \lambda_n = m_{13}(h_{14} - h_{13}) + M_f * Cp_{MED\_c} * \left(T_f - T_{cw}\right) \tag{5.24}$$

where Cp_{MED_c} is the mean specific heat capacity of feed-in water temperature change from T_{cw} to T_f.

5.2.3 Exergy Destruction Analyses

Exergy analysis of a complex system can be performed by analyzing each component of the system separately. The exergy destruction, E_d, describes the irreversibility of the process and identifies the direction of potential improvements. For the MED subsystem, assuming the final fresh water product is salt free, the exergy destruction is calculated as:

$$E_{d,MED\_system} = m_5 e_5 + m_{10} e_{10} - m_6 e_6 - m_{16} e_{16} - m_{15} e_{15} - m_{18} e_{18} \quad (5.25)$$

where e is the specific exergy. For salt water streams 9, 10 and 15 the exergies are calculated based on Ref. [293] where the chemical potential of seawater needs to be considered:

$$e = (h - h^*) - T_0(s - s^*) + \sum_{i=1}^{n} w_i(\mu_i^* - \mu_i^0) \quad (5.26)$$

where T_0 is the ambient (or dead-state) temperature, and h, s, μ and w are the specific enthalpy, entropy, chemical potential and mass fraction, respectively. Properties with subscript "*" are at the same composition or concentration of the initial state but at the temperature and pressure of the environment (T_0, p_0). Here environmental temperature and pressure are at the restricted dead state, in which only the temperature and pressure are changed to the environmental values. However, the properties with "0" in the above equation (i.e.μ_i^0) are determined at the temperature, pressure and the brine concentration in the environment, which is called the global dead state. Detailed explanations may be found from Ref. [293]. For a pure fluid such as streams 5 and 6, the chemical exergy will vanish and the specific exergy of each stream is simplified as:

$$e = (h - h_0) - T_0(s - s_0) \quad (5.27)$$

For a steady state, steady-flow process, the exergy destruction of the components in the SORC-Ejector subsystems can be expressed as:

Boiler: $$E_{d,Boiler} = m_3e_3 + m_8e_8 - m_1e_1 - m_4e_4 \quad (5.28)$$

Expander: $$E_{d,Expander} = m_1e_1 - m_2e_2 - W_{Expander} \quad (5.29)$$

Ejector: $$E_{d,Ejector} = m_2e_2 + m_{14}e_{14} - m_5e_5 \quad (5.30)$$

Valve: $$E_{d,Valve} = m_{12}e_{12} - m_{13}e_{13} \quad (5.31)$$

Pump: $$E_{d,Pump} = m_7e_7 - m_8e_8 + W_{Pump} \quad (5.32)$$

MED_c: $$E_{d,MED\_c} = m_{16}e_{16} - m_{17}e_{17} + m_{13}e_{13} - m_{14}e_{14} + m_9e_9 - m_{10}e_{10} \quad (5.33)$$

5.2.4 System Parameters

A few performance evaluation parameters are:

a) Entrainment ratio (Er), which is defined as the ratio of the mass flow rates of the secondary and the primary flows. In this system it is:

$$Er = \frac{m_{14}}{m_2} \quad (5.34)$$

b) Compression ratio (Cr), which is defined as the ratio of the compressed fluid.

c) Pressure to the entrained fluid pressure. In this system it is:

$$Cr = \frac{P_5}{P_{14}} \quad (5.35)$$

d) Performance ratio (P.R.), which is defined as the number of kg of distillate per 2,300 KJ heat input. It is dimensionless and in this paper it can be expressed as:

$$P.R. = Distillate\ flow\ rate\ \left(\frac{kg}{s}\right) * \frac{2300(\frac{KJ}{kg})}{Power\ Input\ in\ MED\ first\ effect\ (\frac{KJ}{s})} \quad (5.36)$$

e) Power cycle efficiency, which is defined is as:

$$\eta_{th} = \frac{w_{net}}{Q_{in}} = \frac{W_{expander} - W_{pump}}{m_3(h_3 - h_4)} \quad (5.37)$$

f) Desalination minimum energy, w_{min} means the energy required to separate the fresh water from the brine in a completely reversible process. It is the difference in the Gibbs energy [86]:

$$w_{min} = \frac{m_{br}g_{br}+m_w g_w - m_{sw}g_{sw}}{m_w} = \frac{m_{15}g_{15}+m_{11}g_{11}-m_9 g_9}{m_{11}} \quad (5.38)$$

where subscripts br, w and sw represent rejected brine, produced fresh water and feed brine, and g is the specific Gibbs energy. Higher salt concentration and higher recovery rate result in higher minimum energy consumption.

g) Combined cycle exergy efficiency:

Conventional desalination plants exergy efficiency is defined as:

$$\eta_{exergy,desalination} = \frac{amount\ of\ water\ produced * w_{min}}{exergy\ input\ of\ the\ system} \quad (5.39)$$

Conventional exergy efficiency of a power plant is defined as:

$$\eta_{exergy,power\ cycle} = \frac{net\ work\ output}{exergy\ input\ of\ the\ system} \quad (5.40)$$

Since the proposed system has work and water as products, the combined cycle's exergy efficiency is defined as the sum of the net work generated with the minimum energy required to desalinate water, divided by the system exergy input:

$$\eta_{exergy} = \frac{W_{expander}-W_{pump}+m_{11}w_{min}}{m_3(exergy_3-exergy_4)} \quad (5.41)$$

5.3 Results and Discussion

5.3.1 MED System Discussion

5.3.1.1 Validation

The simulation was carried out using the Engineering Equation Solver (EES) software. The computerized models were validated based on reported experimental data on foward-feed MED systems [259]. The results in Table 5.1 indicate good agreement between the model predictions and the available experimental data. In the following simulation, the power cycle working fluid is condensed at 65°C and

discharges the heat to the desalination unit. This means that stream 6 is saturated liquid with a temperature of 65°C.

Table 5.1 Comparison of model predictions with the experimental data for MED unit[(a)]

Thermal input temperature (°C)	Performance ratio	Recovery rate		Thermal power input (kW)	
		Reference	Model	Reference	Model
57	8.9	0.2375	0.2375	137	135.6
60	9.1	0.275	0.275	153	153.5
63	9.3	0.3	0.3	166	163.9
65	9	0.3375	0.3375	191	190.5
68	10	0.3625	0.375	182	184.2
70	9.5	0.3625	0.3625	195	193.9
72	9.4	0.375	0.375	203	202.7
74	9.3	0.375	0.375	207	204.9

[(a)] MED final effect vapor temperature 35°C.

5.3.1.2 Salt Concentration Effect

An RO process is energy efficient for brackish water treatment, however, as Figure 5.8 (a) shows, the osmotic pressure more than doubles when feed water concentration doubles (from 35g/kg to 70g/kg). This makes it difficult for the RO process from being used for highly concentrated brine due to the physical strength limitations of RO polymer membranes. On the other hand, thermal desalination systems are not affected much by the feed water salt concentration. Using the earlier validated system model, the proposed MED subsystem was analyzed for thermal input temperature 65°C with a PR of 9 as in Table 5.1, and the final condenser approach temperature ΔT is 2°C. Figure 5.8 (b) showed that when performance is fixed, the MED subsystem surface area increased a little more than 40% when feed water salt concentration doubled. The specific area calculated from the model used heat transfer coefficients from Ref [292]. Therefore the proposed system is suitable for highly concentrated brine treatment.

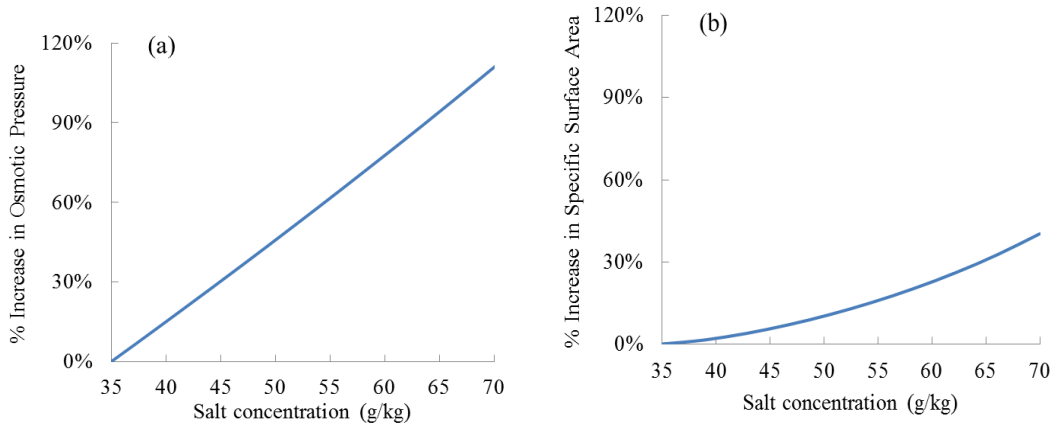

Figure 5.8 (a) Osmotic pressure change and specific area change compared to standard seawater 35g/kg salt concentration osmotic pressure; (b) Specific area increase percentage compared to seawater 35g/kg when the MED has constant PR=9 and condenser approach $\Delta T=2^0C$).

Figure 5.9 (a) shows the percentage of the final condenser cooling load divided by the MED first effect heat input. It clearly indicates that when the final condensing approach temperature is fixed and when the MED performance ratio is also fixed, a higher salt concentration brine needs more cooling water. This is because water with greater concentration has lower specific heat capacity, as shown in Figure 5.9 (b). Less vapor is needed to preheat the higher salty brine, as illustrated in Figure 5.8 (c), therefore more cooling water is needed to condense the final effect vapor which could cause environmental thermal pollution.

5.3.1.3 MED Energy Utilization Analysis

An estimation of energy consumption of a thermal desalination system has already been shown in Chapter 3; here only a summery will be provided. As Figure 5.10 shows, the thermal desalination process final products are brine, fresh water and vapor. The mass and energy balances may be written as:

Energy Balance $$Q_{input} - Q_{loss} + m_{sw}h_{sw} = m_b h_b + m_{fl}h_{fl} + m_{fv}h_{fv} \quad (5.42)$$

$$h_{fv} = h_{fl} + \lambda \quad (5.43)$$

Mass Balance $$m_{sw} = m_b + m_{fl} + m_{fv} \quad (5.44)$$

$$m_f = m_{fl} + m_{fv} \tag{5.45}$$

Assuming that there is no heat loss, the recovery rate R may be written from the 4 equations as:

$$R = \frac{m_f}{m_{sw}} = \frac{\frac{Q_{input}}{m_{sw}} + (h_{sw} - h_b)}{(h_{fl} - h_b) + \frac{m_{fv}}{m_f}\lambda} \tag{5.46}$$

where h_{fl}, h_b, h_{sw} are the specific enthalpy of fresh water vapor, brine and feed seawater respectively, and λ is the latent heat at the final product temperature. m_f is the sum of the mass of the final vapor stream m_{fv}, and the final fresh water liquid stream is m_{fl}.

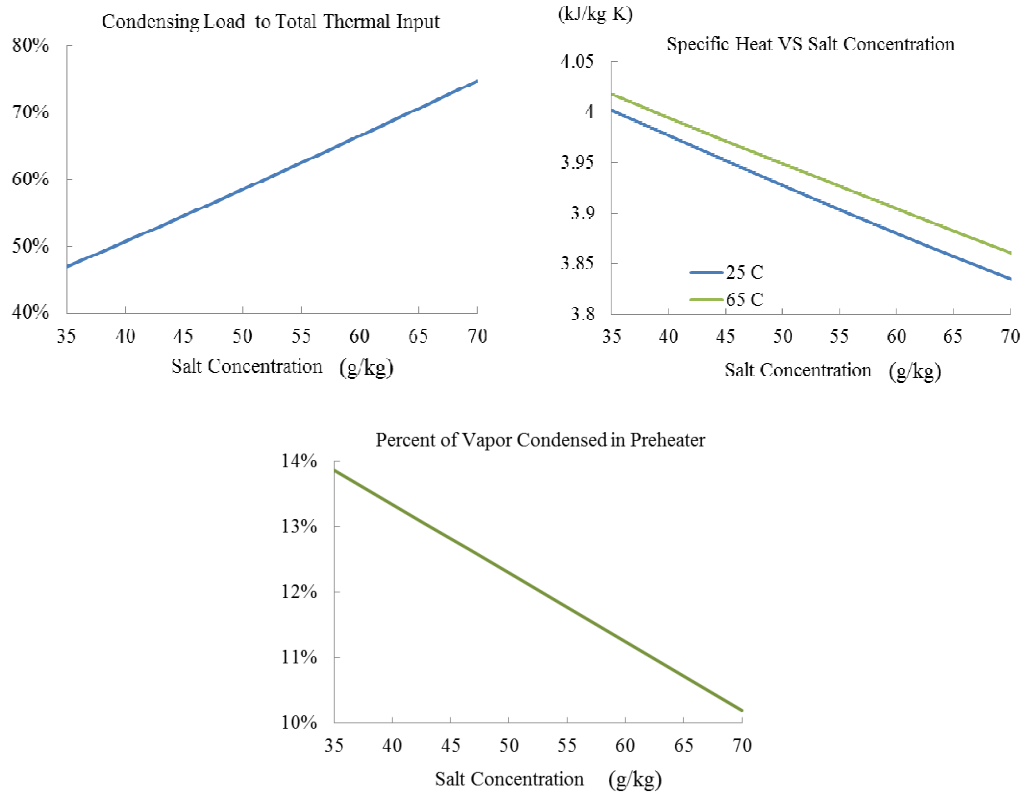

Figure 5.9 Effect of salt concentration on: (a) percent ratio of condensing load to heat input; (b) specific heat change; and (c) percent of vapor condensed in preheater (for PR=9, condenser approach ΔT=2°C).

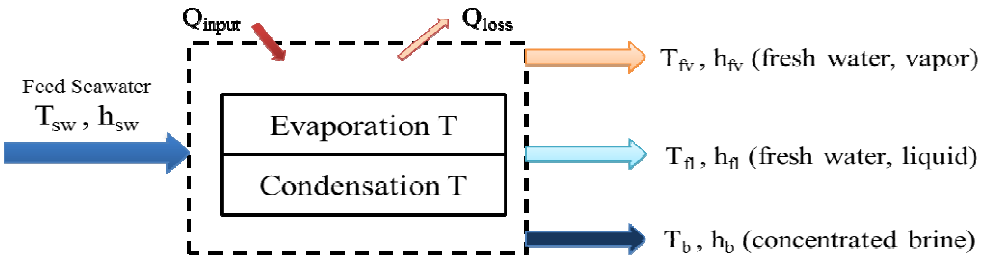

Figure 5.10 General overview of a thermal desalination process.

Assuming the feed seawater at 25°C and the final products including vapor, liquid fresh water and brine having the same temperature without considering the temperature elevation caused by salt, the specific energy consumption for a thermal desalination process, $q_s = \frac{Q_{input}}{m_f}$ may be written as:

$$q_s = [(h_{fl} - h_b) - \frac{1}{\text{Recovery}}(h_{sw} - h_b)] + \frac{m_{fv}}{m_f}\lambda \qquad (5.47)$$

Once the recovery rate is fixed, the specific energy is directly related to the amount of vapor condensed by the cooling water which is discharged to the environment. Figure 5.9 shows the estimated specific energy consumption with vapor fraction of the total fresh water generated for a recovery of 50%. The lower the amount of vapor condensed by the discharged cooling water, the lower the energy required because less latent heat is wasted.

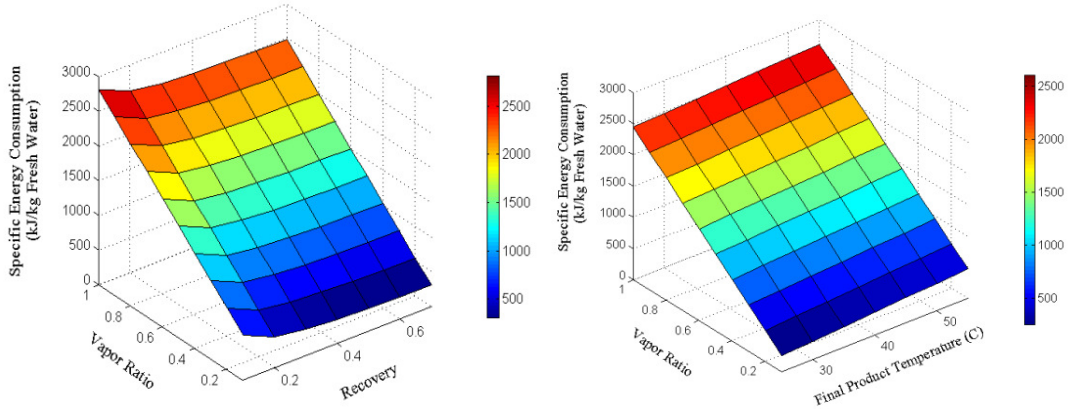

Figure 5.11 Variation of specific energy consumption with vapor fraction.
(a) and recovery when final product is at 35°C;
(b) and final product temperature when recovery is 50%.

5.3.1.4 MED System Summary

Based on the above analysis (Figure 5.9 and Figure 5.11) increased salt concentration will cause more vapor production in the last effect which means more cooling water is required. However, by recovering the latent energy in the last effect vapor that is wasted in a regular MED, the energy consumption could be reduced, while also reducing the thermal pollution. Increased salt concentration will not cause too much specific area change compared with the RO. Therefore the proposed thermal MED system is potentially suitable for highly concentrated brine treatment. By using an ejector to recover the latent heat of condensation from the last effect, cooling water is not needed which will make the desalination system more energy efficient.

5.3.2 SORC-EJECTOR Subsystem

In the proposed system, the heat source is assumed to be 150°C and after transferring heat to the system, the heat transfer fluid returns at 100°C. The ejector efficiency and its entrainment ratio, the system high pressure, the cooling temperature (stream 14 temperature), the MED performance ratio, and the feed water salt concentration all affect each other. Therefore sensitivity studies are carried out in order to find the key parameters for the system performance. In each case, the power cycle efficiency and system exergy efficiency changes will be studied first and the percentage of exergy destruction of each component will be shown last.

5.3.2.1 Power Cycle Pressure Effects

For this analysis, the feed water salt concentration is fixed at 35g/kg which is the standard seawater salt concentration. The MED performance ratio is fixed at nine which is the same as the reported experimental result using a 65°C heating source, final effect vapor is at 35^0C and the recovery of 0.3375 shown from Table 5.1. The power cycle's working fluid (stream 6) is condensed at 65°C to simulate the condition

listed in Table 5.1. The secondary flow of the ejector evaporates at 33°C which means the approach ΔT_{MED_c} is 2°C. The parameter conditions are listed in Table 5.2.

Table 5.2 Parameters for power cycle pressure effects sensitivity study

Fixed parameters	Independent parameters	Dependent parameters
(1) Brine conc.: 35g/kg (2) 14 effects MED PR.=9 (3) Ejector eff.= 47.5% (4) Cycle working fluid condensed at 65°C (5) ΔT_{MED_c} =2°C (6) MED condensed at 35°C (7) MED recovery=0.3375 (8) Pump eff.= 80% (9) Turbine eff.=85%	System high pressure which is stream 8 pressure.	(1) Entrainment ratio (Er) (2) System work output. (thermal efficiency). (3) Components exergy destruction compare. (4) System exergy efficiency.

When the pressure changes, the turbine pressure ratio will vary and cause the stream 2 pressure to change, which causes the ejector entrainment ratio to change due to the fixed ejector efficiency. Then the mixed stream 5 will also have a different temperature and mass flow rate. As a result, the mass flow rate of the power cycle will change and the net power output, the system exergy efficiency and the entrainment ratio will change accordingly. The results can be seen in Figure 5.12. It can be seen that the system exergy efficiency increases rapidly with pressure until the pressure is close to 5000 kPa, after which both the power cycle efficiency and system exergy efficiency start to stabilize. As the cycle's high pressure increases, the expander pressure ratio also increases, which causes the expander exit (stream 2) temperature to drop. In order to maintain the heat input to the MED system, the primary flow rate (which is the power cycle flow rate) needs to be increased which causes the entrainment ratio to drop since the secondary flow rate in the ejector cycle is constant.

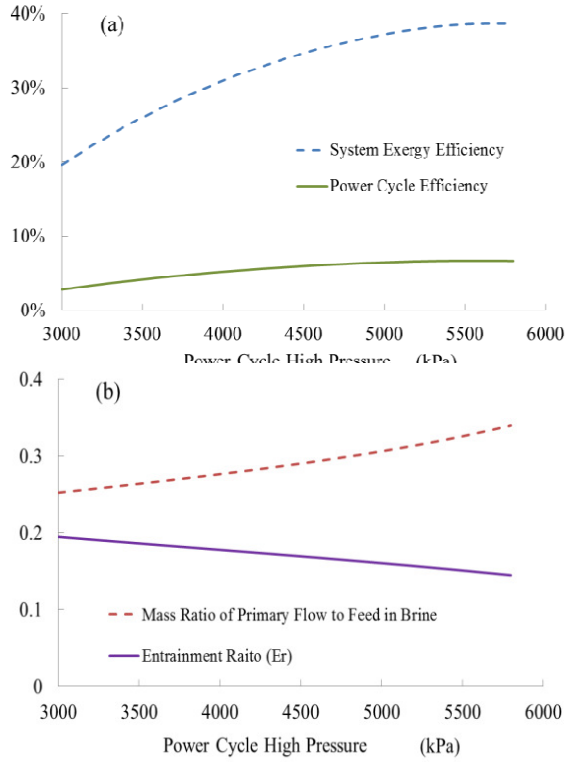

Figure 5.12 Effect of power cycle high pressure on system parameters.
(a) system exergy efficiency and power cycle efficiency; (b) entrainment ratio and mass ratio of primary flow to feed brine.

The exergy destruction of each component in the proposed system operating with 35g/kg feed-in brine and MED with P.R.=9 can be seen in Figure 5.13. It is clear that the main exergy destruction occurs in the MED system. MED is a series of heat exchangers and flash boxes, therefore, in order to improve the system performance, the surface area has to increase which will also increases capital costs. The second largest exergy destruction occurs at the boiler. The exergy destruction at the boiler side is affected by the thermal match between the working fluid and the heat source. The working fluid R152a used in this proposed system has a critical pressure of 4516.8 kPa and a critical temperature of 113.26 °C. When operating at supercritical conditions, the boiler has lower exergy destruction. Therefore the system pressure will be fixed at 4900kPa and a boiler pinch point of 8°C. The third largest exergy destruction is in the ejector which has an efficiency of 47.5%. The system exergy

efficiency increases from 19.6% to 38.6% with an increase in pressure from 3000 kPa to 5800 kPa. A detailed discussion of the ejector efficiency effects is presented in the following section.

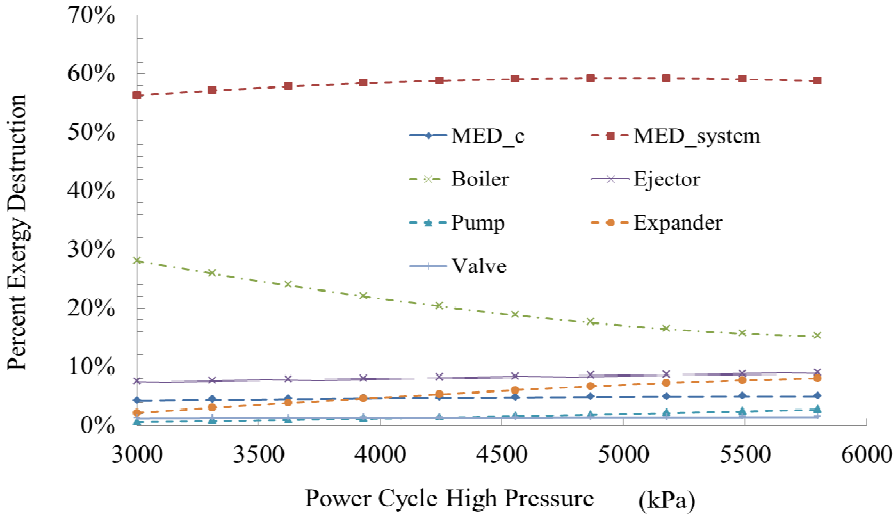

Figure 5.13 Effect of pressure on normalized exergy destruction in each component.

5.3.2.2 Effect of MED Performance Ratio

This section analyzes the effect of P.R. on other parameters. The rest conditions are the same as in section 4.2.1 with parameter conditions listed in Table 5.1. The water production is fixed at 2.7m^3/h of fresh water and the recovery rate is kept constant at 0.3375 while the performance ratio varies from 8.1 to 9.2. A change in the MED performance ratio in turn changes the ratio of the thermal loads of MED_c and MED_b, which further changes the system entrainment ratio and power cycle efficiency as well as the exergy efficiency. The parameters conditions are listed in Table 5.3.

Figure 5.14 shows the effect of performance ratio on the system parameters. It can be seen that the system exergy and power cycle efficiencies both increase with the MED performance ratio. The specific area (sA) starts to increase fast for P.R. larger than 9 and a recovery of 0.3375 in the MED system (Figure 5.14 (a)).; The ratio of the

thermal load at the first effect of MED to the final effect vapor condensation increases from 1.83 to 2.10, which means that more vapor is used to preheat the feed water and less vapor is discharged from the Effect 14. Therefore, less secondary flow is needed from the ejector cycle for cooling which reduces the entrainment ratio (Figure 5.14 (b)).

Table 5.3 Parameters for MED performance varies sensitivity study

Fixed parameters	Independent parameters	Dependent parameters
(1) Brine conc.: 35g/kg (2) System high pressure 4900kPa (3) Ejector eff.= 47.5% (4) Cycle working fluid condensed at 65°C (5) ΔT_{MED_c} =2°C (6) MED condensed at 35°C (7) MED recovery=0.3375 (8) Pump eff.=80% (9) Turbine eff.=85%	MED performance ratio (P.R.)	(1) Entrainment ratio (Er). (2) System work output (thermal efficiency). (3) Components exergy destruction compared. (4) System exergy efficiency.

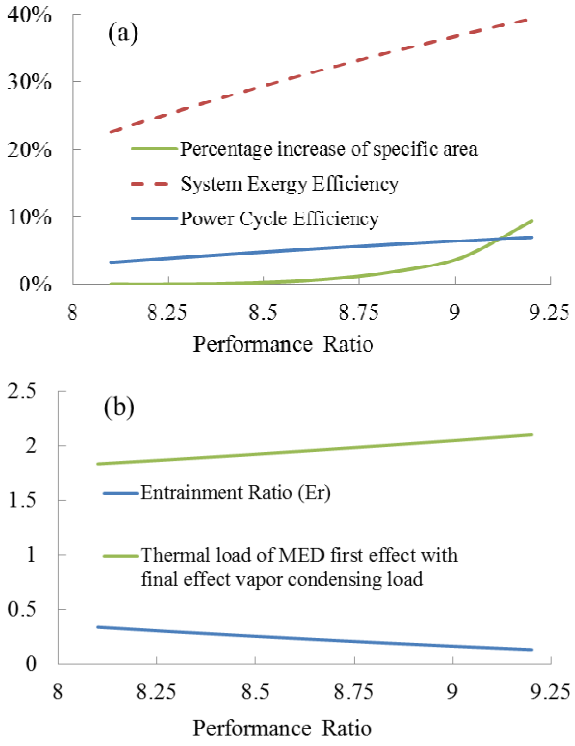

Figure 5.14 Effect of MED performance ratio on system parameters.
(a) System exergy efficiency, power cycle efficiency and specific area change; (b) entrainment ratio, ratio of the MED first effect thermal load to the final vapor condensation load, and the mass ratio between primary flow and feed-in brine mass rate.

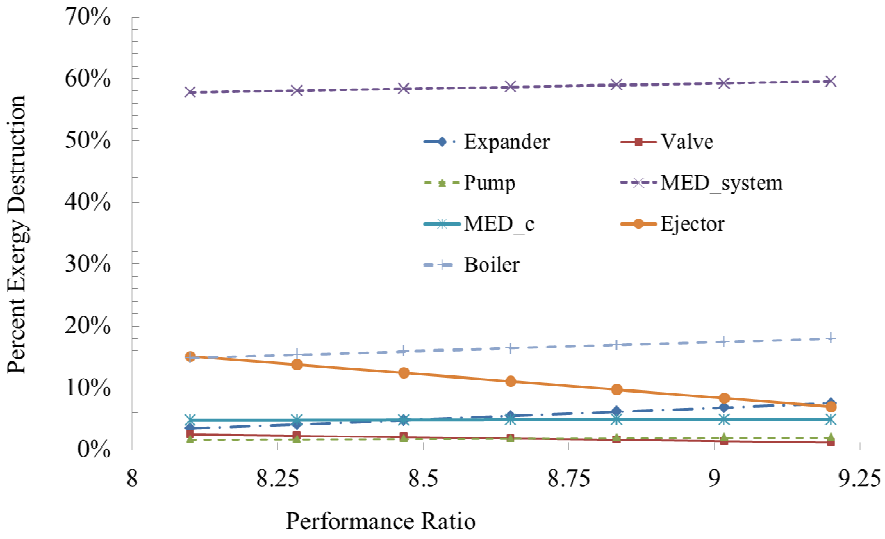

Figure 5.15 The normalized exergy destruction is compared with the MED P.R. change.

The exergy destruction of each component in the proposed system operating with 35g/kg feed-in brine and a system high operation pressure of 4900 kPa can be seen in Figure 5.13. It is clear that the main exergy destruction in the MED system is not affected by the performance ratio. Since the MED system is a series of heat exchangers, unless the heat exchangers' pinch is reduced, the system exergy destruction is hard to reduce. In order to reduce the heat exchanger pinch, the MED will require a larger surface area and less temperature difference between each effect.

One distinct difference between Figure 5.13 and Figure 5.15 is the exergy destruction in the ejector and the boiler. In Figure 5.13, the boiler exergy destruction is adjusted by the thermal match in the boiler which is affected by the system high pressure. While in Figure 5.15 the pressure is fixed at 4900 kPa therefore showing that the boiler exergy destruction is relatively stable. However, the ejector exergy destruction reduces as the P.R. increases, because more vapor is used to preheat the

feed water and less secondary flow is needed for the ejector as discussed before in Figure 5.14.

In summary, the higher P.R. of the MED system requires a larger surface area and more vapor is used to preheat the feed water, which allows the secondary flow of the ejector system to be reduced, and greater work being produced by the proposed system. The normalized exergy destruction analysis also showed that the system major exergy destruction was in the MED system, and the destruction percentage did not vary with the performance ratio of the MED system. The system exergy efficiency increased from 22.6% up to 39.4% as the performance ratio increased from 8.1 to 9.2.

5.3.2.3 Ejector Efficiency Effect

The reported ejector efficiencies vary from less than 10% to up to 90%, depending on the specific conditions [281], [276], [283], [289], [286]. The previous sensitivity study used a fixed 47.5% efficiency of the ejector. In this section the ejector efficiency is varied from 15% to 75% with Cr =2.244 in order to study the effect of the ejector efficiency on the whole system. The parameters are listed in Table 5.4.

Table 5.4 Parameters for ejector efficiency varies sensitivity study

Fixed parameters	Independent parameters	Dependent parameters
(1) Brine conc.: 35g/kg (2) System high pressure 4900kPa (3) 14 Effect MED P.R.=9 (4) Cycle working fluid condensed at 65°C (5) ΔT_{MED_c} =2°C (6) MED condensed at 35°C (7) MED recovery=0.3375 (8) Pump eff.=80% (9) Turbine eff.=85%	Ejector efficiency varies.	(1) Entrainment ratio (Er). (2) System work output (thermal efficiency). (3) Components exergy destruction compare. (4) System exergy efficienc.y

The parametric study results are shown in Figure 5.16. Figure 5.16 (a) shows a rapid increase in the system exergy and power cycle efficiencies with the efficiency of the ejector. When the ejector efficiency is close to 50%, the effects of ejector efficiency start to stabilize. Figure 5.16 (a) also shows that if the ejector is poorly designed, there could be no net work from the proposed system which means that external work needs to be provided to power the pump in the system. Figure 5.16 (b) shows that the entrainment ratio is relatively constant while the expander pressure ratio changes dramatically with the ejector efficiency. The low expander pressure ratio indicates that a scroll expander, which is economical though less efficient, may be used instead of an expensive turbine.

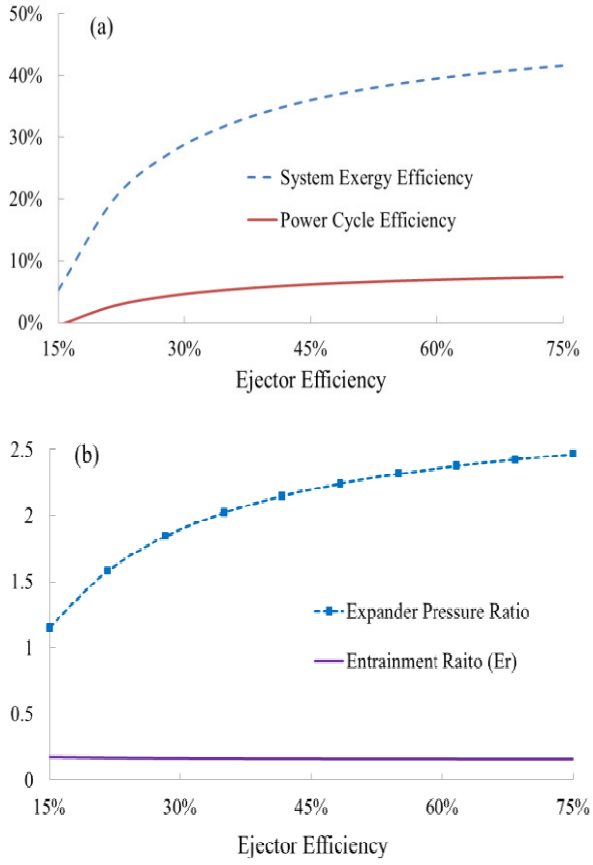

Figure 5.16 Effect of ejector efficiency on system parameters.
(a) system exergy efficiency and power cycle efficiency; (b) entrainment ratio and expander pressure ratio.

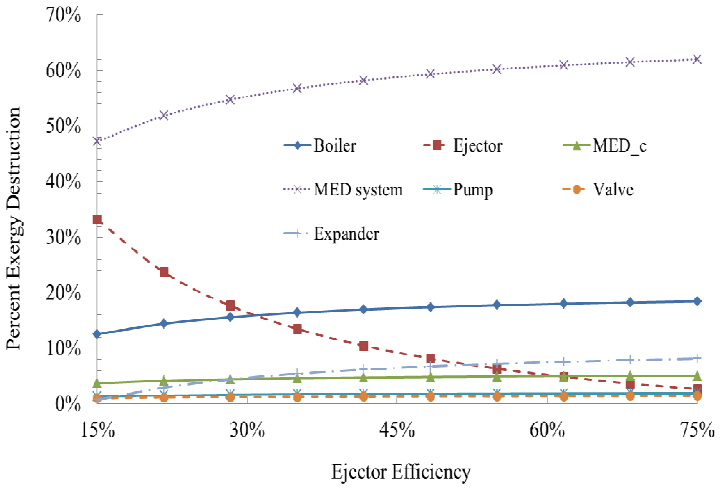

Figure 5.17 Normalized exergy destruction comparison with respective to ejector efficiency.

The exergy destruction of each component in the proposed system was operating with 35g/kg feed-in brine, the MED PR=9 and with the system's high operating pressure of 4900 kPa as can be seen in Figure 5.17. The main exergy destruction is still in the MED system and for ejector efficiency lower than 30%, the second largest exergy destruction occuring in the ejector. The overall system exergy efficiencies increase from 5.21% to 41.6% when the ejector efficiency increases from 15% to 75%, which clearly indicates the huge influence of the ejector efficiency on the entire system performance.

5.3.2.4 Salt Effect

Thermal desalination is not as energy efficient as the RO process when treating brackish water. However, it is suitable to handle highly concentrated brine which the RO system cannot handle. The required parameter conditions are listed in Table 5.5. Figure 5.18 shows that the proposed system performance decreases when the salt concentration increases. As previously discussed in Figure 5.9, when brine concentration increases, more vapor needs to be condensed when the performance ratio of the MED system is constant. Therefore the entrainment ratio needs to be

increased so as to accept more latent heat of condensation from the MED last effect vapor. In addition, the ejector destruction will be larger and account for a higher percentage of the whole system destruction.

Table 5.5 Parameters for salt concentration varies sensitivity study

Fixed parameters	Independent parameter	Dependent parameters
(1) Ejector efficiency=0.475 (2) System high pressure 4900kPa (3) 14 Effect MED P.R.=9 (4) Power cycle condensed at 65°C (5) ΔT_{MED_c} =2°C (6) MED condensed at 35°C (7) MED recovery=0.3375 (8) Pump eff.=80% (9) Turbine eff.=85%	Salt concentration change.	(1) Entrainment ratio (Er). (2) System work output (thermal efficiency). (3) Components exergy destruction compare. (4) System exergy efficiency.

One can observe that when the salt concentration is up to 55g/kg, there is no network from the system. For a system to be externally independent of electricity, an ejector with higher efficiency needs to be used. Table 5.6 indicates that when handling highly concentrated brine, only systems with high efficiency ejectors can be electricity independent.

Table 5.6 Impact of ejector efficiency and brine concentration on power cycle efficiency (with water production rate of 2.7m^3/h, high operation pressure 4900 kPa and MED P.R.=9)

Salt concentration (g/kg)	35	40	45	50	55	60
Ejector efficiency	Power cycle efficiency					
25%	3.60%	1.10%				
35%	5.30%	3.60%	1.60%	-0.80%		
45%	6.20%	4.90%	3.40%	1.60%	-0.40%	
55%	6.70%	5.70%	4.50%	3.10%	1.50%	-0.50%

5.4 System Performance When Treating Concentrated Brine

When the feed-in brine has a high salt concentration (55g/kg), the proposed system with P.R.=9 is as listed in Table 5.1. It shows that the system operates at a

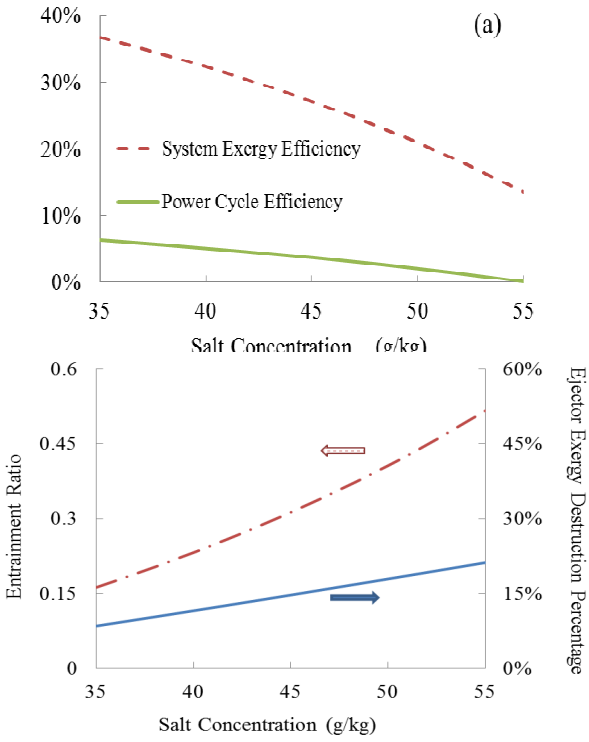

Figure 5.18 Effect of salt concentration on: (a) system exergy efficiency and power cycle efficiency; and (b) ejector entrainment ratio and ratio of the ejector destruction to system exergy destruction.

pressure of 4900 kPa with an ejector efficiency of 47.5% and no cooling water needed for the MED system. The system uses all its generated work. Table 5.7 lists the fixed parameters of the system. Table 5.8 showed the SORC-Ejector subsystem and Table 5.9 shows the results of MED system simulation.

Table 5.7 The condition of the fixed parameters

Environment temperature	25°C
Environment pressure	101325 Pa
Dead state brine salt concentration	35 g/kg
MED performance ratio	9
Pump isentropic efficiency (%)	80
Turbine isentropic efficiency (%)	85
Boiler pinch	8
Ejector efficiency	47.50%
MED fresh water production	0.748 kg/s (2.7 m^3/h)
Feed-in brine concentration	55 g/kg
Feed-in water	2.215 kg/s (8 m^3/h)
Final effect condensation temperature	35°C

Table 5.8 SORC-Ejector subsystem simulation results

State	t(°C)	P(Pa)	h(J/kg)	s(J/kg K)	m(kg/s)	e(kJ/kg)	Dryness
1	140	4900000	595279	2098	0.5097	128880	100
2	127.1	4006000	589871	2100	0.5097	122762	100
3	150	110000	204134	218.1	0.2208	34519	0
4	100	110000	118128	1.931	0.2208	12955	0
5	81.3	1687000	568529	2121	0.7729	95303	100
6	65	1687000	321308	1392	0.7729	65501	0
7	65	1687000	321308	1392	0.5097	65501	0
8	68.4	4900000	326391	1395	0.5097	69695	Supercritical
9	25	22012	96629	332.8	2.115	381.9	0
10	33	22012	127832	436.2	2.115	767.9	0
12	64.99	1687000	321292	1392	0.2632	17242	0
13	33	751840	321292	1405	0.2632	16168	0.2333
14	33	751840	527209	2078	0.2632	17586	1
15	35.9	5627	133337	441.1	1.468	2637	0
16	35	5627	2564000	8351	0.05106	4042	1
17	35	5627	146588	505	0.05106	35.17	0
18	35	5627	146588	505	0.6992	481.5	0

Table 5.9 MED system simulation results

Effect	$\boldsymbol{D}$(kg/s)	$\boldsymbol{Tv}$(°C)	$\boldsymbol{d}^{*}$(kg/s)	$\boldsymbol{T}^{*}$(°C)	$\overline{\boldsymbol{d}}$(kg/s)	$\overline{\boldsymbol{T}}$(°C)	$\boldsymbol{B}$(kg/s)	$\boldsymbol{Salt}$(g/kg)	$\boldsymbol{T}$(°C)	$\boldsymbol{Tf}$(°C)	$\boldsymbol{BPE}$(°C)
1	0.04941	62.16	-	-	-	-	2.166	56.25	62.85	-	0.6933
2	0.04931	60.15	0.00685	60.95	0.0001066	60.95	2.11	57.75	60.86	54.25	0.7049
3	0.04954	58.12	0.006646	58.96	0.0002254	58.95	2.054	59.33	58.84	52.45	0.7171
4	0.04967	56.07	0.00643	56.94	0.0003403	56.93	1.998	61	56.8	50.64	0.7301
5	0.04969	54	0.006204	54.91	0.0004501	54.9	1.942	62.75	54.75	48.83	0.7437
6	0.0496	51.92	0.005968	52.87	0.0005531	52.86	1.886	64.6	52.68	47.02	0.7582
7	0.04941	49.83	0.005723	50.82	0.0006476	50.8	1.831	66.55	50.6	45.21	0.7733
8	0.04911	47.72	0.005469	48.76	0.0007319	48.74	1.776	68.59	48.51	43.4	0.7893
9	0.0487	45.61	0.005207	46.69	0.0008041	46.67	1.722	70.74	46.41	41.62	0.8061
10	0.04817	43.49	0.004937	44.63	0.000862	44.6	1.669	72.99	44.31	39.84	0.8236
11	0.04751	41.36	0.004658	42.56	0.0009034	42.54	1.617	75.35	42.2	38.09	0.8419
12	0.04673	39.24	0.004371	40.5	0.0009259	40.47	1.566	77.8	40.1	36.36	0.861
13	0.0458	37.12	0.004076	38.45	0.0009267	38.41	1.516	80.36	38	34.66	0.8808
14	0.04473	35	0.003771	36.42	0.002562	36.37	1.468	83.02	35.9	-	0.9012

5.5 Concluding Remarks

In this chapter, a novel SORC-Ejector-MED system is proposed and simulated and a detailed sensitivity analysis is provided. The proposed system is based on thermal energy input at a temperature of 150°C, which could be from solar, geothermal or waste heat sources. The analysis shows that the proposed system can desalinate concentrated brine without external electricity input. The analysis also shows that major exergy destruction occurs in the MED subsystem, boiler and ejector. By selecting a suitable cycle operation pressure, the boiler exergy destruction could be reduced. The MED system is responsible for the largest exergy destruction in the system, but it is not easy to reduce the exergy destruction in this system without increasing the number of effects. By selecting high efficiency ejectors, the proposed system could handle highly concentrated brine without additional electricity input.

CHAPTER 6 SYSTEM INTEGRATION OF DESALINATION WITH LOW-GRADE HEAT

There are many kinds of desalination processes as well as many types of renewable energy sources. In this section solar energy is used as one typical renewable energy source to study its' integration with a desalination system. An interface is proposed to better estimate low-grade heat for a desalination application.

Selecting a suitable desalination process for seawater requires several design criteria including seawater quality, capital cost, operation and maintenance cost, energy efficiency, water quality requirements, environmental impact and other site-specific factors [294], [295]. Selecting a suitable solar system requires a number of considerations, such as location, energy storage method, operating temperature range, type of solar collector, working fluids, and plant configuration, [296]. When coupled together, though some systems require some minor changes for better integration, most of the reported solar desalination systems are not developed as a single system but are integrations of components developed independently [297].

6.1 System Integration Based on Energy Type

Figure 6.1 shows potential processes of solar technologies combined with seawater desalination technologies. Generally speaking, a solar-assisted desalination system means that either solar energy is converted to electricity in order to power the RO/MVC process, or that solar radiation is collected by thermal collectors and this energy is used for the thermal desalination process. Solar methods which mainly produce electricity (i.e., photovoltaic (PV) and solar chimney) [248], are suitable for

combination with the membrane desalination process or a thermal process like MVC which only uses mechanical energy. Other solar technologies such as solar pond, solar collectors (including FPC, ETC, CPC, PTC), solar dish, Fresnel reflector, and solar tower , which generate electricity and heat at the same time, could be combined with any kind of desalination technology based on the design. Since both solar and desalinations systems are developed independently and then coupled together, it is necessary to analyze them separately.

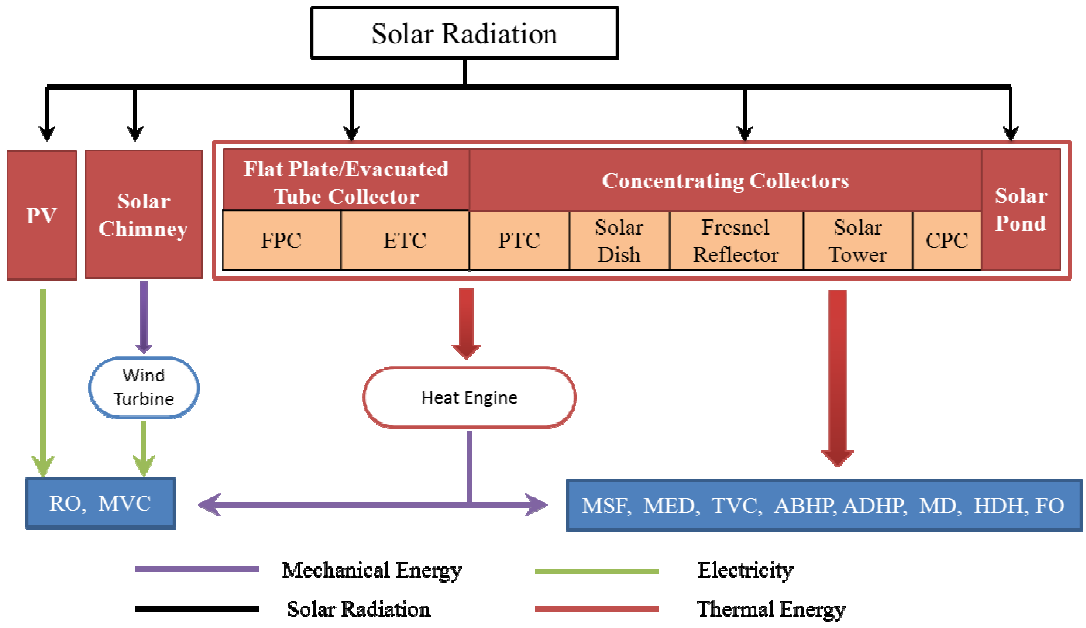

Figure 6.1 Potential process of solar desalination.

6.2 Solar System Considerations

The solar system costs could range from 17.4%-76.7% of the total system costs based on different system combinations, as can be seen in Table 6.1. With the exception of solar pond-driven desalination systems which do not need solar collectors, all other configurations have more than a 25% additional cost for the solar collectors. A solar pond requires a large surface area and the pond evaporation rate sometimes exceeds the water production rate, which makes it unsuitable for places with limited water resources [298]. As for the solar-assisted ORC-driven RO process,

the exergy analysis shows that for the ORC-RO system the exergy destruction in the power plant is almost 10 times greater than that in the RO subsystem [299]. This indicates that the overall efficiency depends more on the solar plant and less on the desalination system. The solar system is a very large part of the overall system cost and needs to be carefully selected. Location is one of the most important factors when selecting a solar system because the same solar desalination system will provide greater water production rate at locations with higher solar radiation thus lowering the overall water cost [238], [241].

6.2.1 Comparison of Solar Systems

In order to better select the processes, the advantages and disadvantages of solar systems used for indirect solar desalination are listed in Table 6.2. The extraterrestrial solar radiation passes through the atmosphere, as shown in Figure 6.2. The portion of the solar radiation that reaches the earth's surface with essentially no change in direction is the direct normal radiation (DNI). The scattered diffuse radiation reaching the surface from the sky is the sky diffuse radiation. Added together these are called global horizontal irradiation (GHI). Water vapor could absorb or scatter part of the solar radiation and, therefore, places with higher humidity (i.e. seaside) might have lower DNI as compared with places that are a certain distance away from the seaside. PV uses GHI while CSP uses DNI.

As for the direct solar desalination, a general rule of thumb for simple solar stills is 3–5 liters of water per day per m^2 [241]. For example, for a small family that consumes water at a rate of about $0.6m^3$/day [249], 120-$200m^2$ land area is needed if a simple solar still is used. The area might be doubled if one considers the spacing between the solar still systems, which implies that this may not be a realistic application because of the large area needed.

6.2.2 Concentrated Solar Power (CSP) vs. PV

CSP and PV are the two most studied solar technologies used for seawater desalination [74]. A CSP plant combined with an RO system is regarded as one of the best choices for solar desalination [160]. Comparing PV and CSP, CSP has the advantage by using a thermal storage system for longer hours of operation after sunset and the ability to use a backup fuel for unexpected conditions [300]. CSP is regarded as the appropriate solar power technology for multi-megawatt scale [301]. However, on a cloudy or foggy day, the DNI could be negligible and CSP plants would have little output. Therefore heat storage is a very important issue for CSP. New concepts on phase change materials tailored for CSP applications are presently under active research and development. In practice, DNI of 1900 kWh/m^2/year to 2100 kWh/m^2/ year is treated as the threshold for CSP [302]. Below that, other solar electric technologies which take advantage of both direct and diffuse irradiance (i.e.PV) may have some advantages [302]. Areas close to the sea could have higher humidity and therefore affect the DNI, as can be seen from Figure 6.3 which shows the locations suitable for CSP power plants. In addition, coastal areas normally have higher land value, tourist areas or high population density [303], while CSP requires large, flat land which could increase the cost of CSP-assisted desalination plants.

Table 6.1 Solar system costs as percentages of the total solar desalination system costs

Reference	System configuration	Desal. cost (%)	Solar system cost (%)	Others cost (%)	Notes
[146], [148], [153]	Collector+ORC+RO	32	40	27	Working fluids 134a, cycle high-temperature 75.8°C.
[145], [147], [154]		23.36	40.83	35.81	245fa top cycle fluids, 134a bottom cycle fluids, cycle high-temperature 137°C.
[135]		8.8[(a)]	71.7[(a)]	19.5	R218 as working fluids, cycle high-temperature 87.34°C.
		7.2[(a)]	76.7[(a)]	16.1	R245 as working fluids, cycle high-temperature 120.94°C.
		12.5[(a)]	59.6[(a)]	27.9	R601a as working fluids, cycle high-temperature 289.73°C.
		18.5[(a)]	48.5[(a)]	32.9	N-propyl benzene as working fluids, cycle high-temperature 378.44°C.
[25]	Solar pond + MSF	72.8	27.2	0	
		74.5	25.5	0	
[26]		26.7[(b)]	18[(b)]	55.3	
		25.1[(b)]	17.4[(b)]	57.5	
[24]		34.3 [(c)]	59 [(c)]	6.7	
		43.1 [(c)]	50.2 [(c)]	6.7	
[39]	Collector + MSF	27[(d)]	66.67	6.33	
		30[(d)]	60	10	
[75]	Collector + MED	20.09	73.78	6.1	
[128]	PV+RO	19	27	54	
[304]	PV+RO	69	31[(e)]	NA	
[145]	PV+RO	61	39[(f)]	NA	
[76]	Collector+HDH	NA	28	NA	

[(a)] Case study results for location Barcelona; [(b)] Interests, which are 7% for 15years, are not included; [(c)] O&M cost is not considered; [(d)] Only evaporator cost is considered, plant life=20 years. Annual operating 300 days and interest rate is 5%; [(e)] Without batteries; [(f)] With batteries.

Table 6.2 Comparison of different solar systems

	PV	Solar pond	Flat collector	Concentrating collector
Resource	GHI	GHI	GHI	DNI
Humidity	Tolerable	Tolerable	Tolerable	Not tolerable.
Dry areas	GHI: Less sensitive to dust.	GHI: less sensitive to dust.	GHI: Less sensitive to dust.	DNI: very sensitive to dust.
Land available	Easier to find.	More difficult.	Easier to find	More difficult.
Type of land	Light slopes tolerated.	Flat	Light slope tolerated.	Flat
Water	Not needed.	Needed	Needed	Needed
Connection to the grid	Low or medium voltage.	Low or medium voltage.	Low or medium voltage.	Medium or high voltage.
Complexity	Low number of different equipment.	Low number of different equipment.	Several different equipment.	Several different equipment.
Construction	Simple, quick and flexible.	Simple, quick.	Longer and complex.	Longer and complex.
Scalability	Small, medium, large-scale	Small-scale	Small and medium scale.	Large-scale
O&M	Simple, some staff at site.	Skillful operator needed.	Skillful operator needed.	Complex and skilled team.
Type of production	Distributed/central generation.	Distributed	Distributed	Central generation.
Storage	Battery	None	Battery or cheap thermal storage.	High-temperature thermal storage.
Output stability	Not stable, depends on irradiation.	Relatively stable.	Relatively stable with thermal storage.	Relatively stable with thermal storage.
Thermal plants integration	No	No	No	Yes
Developers	Many	NA	Many	Few

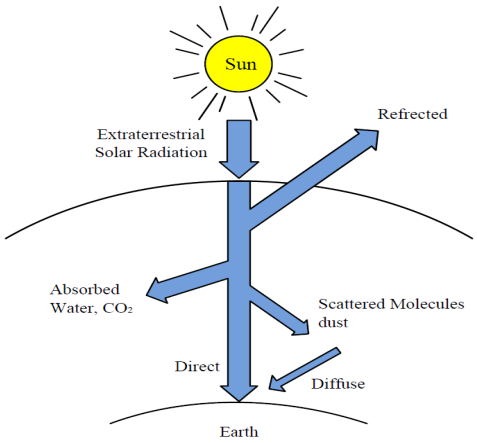

Figure 6.2 Attenuation of solar radiation.

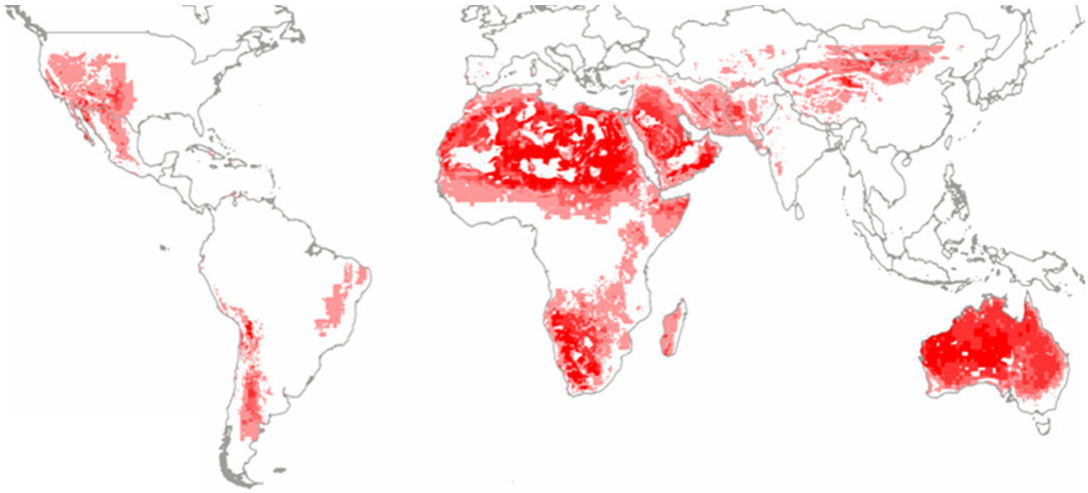

Figure 6.3 Locations suitable for CSP power plants [305].

6.2.3 PV-assisted Desalination

PV could be used to power an RO or MVC system which only use mechanical energy. The retail price for PV modules makes the solar sub-unit's cost a key factor in the economic feasibility of PV-RO desalination [306]. In recent years, PV prices have dropped dramatically. PVs' modular design makes scaling up a PV plant relatively easy allowing a project to be built in phases. PV operation does not need water at all, and the PV-RO combination are two systems developed independently. However, if the local community already has a small-scale de-centralized power generation system (i.e. diesel or natural gas) , PV alone could not make use of it,

unlike a CSP-based system which could be integrated with a fossil fuel-based power system. Furthermore, an RO desalination requires strigent pretreatment which normally needs skilled labor. Therefore in remote areas where it is hard to find skilled operators and where both energy and water are precious, the application of the PV-driven desalination system still needs to be carefully evaluated.

6.3 Desalination Capacity Effects

Reducing costs is the key driving force when considering solar desalination. Desalination costs are affected by many factors including solar system location, solar radiation, and desalination system energy efficiency, . In addition, the desalination system's capacity has a direct impact on the water cost, as illustrated in Figure 6.4, which lists the reported solar desalination systems with cost information. The source data for this figure is presented in the Appendix A.

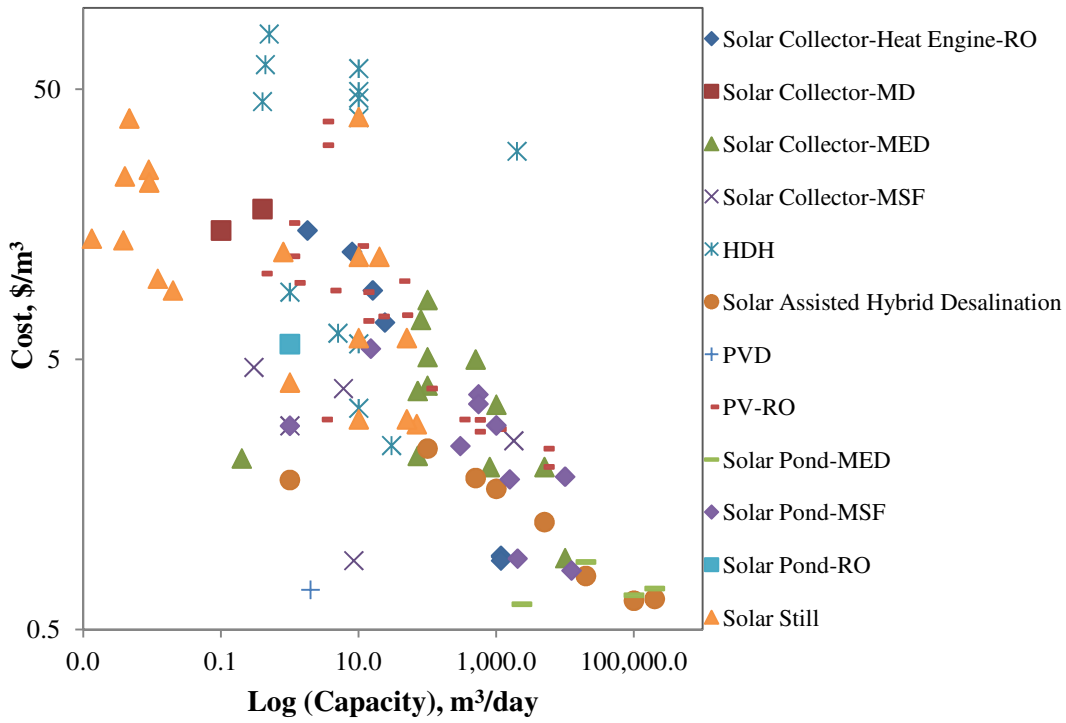

Figure 6.4 Solar desalination capacities vs. cost (the source data and the references for the points are shown in Appendix A).

From Figure 6.4, it is clear that larger capacity solar desalination plants will have lower water costs. Hybrid plants and solar pond-driven desalinaton plants generally have relatively lower unit water costs compared to other types of solar desalination systems when the capacities are similar. In addtion, most very small capacity (<0.1m^3/d) solar desalination systems with reported costs are solar still systems, while most large-scale (>1000m^3/d) solar desalination systems with reported unit water costs are either hybrid or solar-driven thermal processes. Information is available on only three PVD and solar MD solar-assisted seawater desalination systems and more studies are needed to arrive at meaningful cost conclusions. For small (0.1-100 m^3/d) and medium (100-1000m^3/d) capacities, there is no clear evidence on which combinations are better, which means the configuration selection must be made on a case-by-case basis, keeping in mind that optimization is a complex problem [307].

6.4 Environmental Impact

The brine discharged from desalination plants has a higher temperature and higher salinity than the seawater surrounding the plant. Many researchers have expressed concerns about the environmental and ecological impact caused by desalination plants, especially around older MSF plants discharging to the sea with little flushing [308]. Some ocean animals can not tolerate high salinity environments such as the oceanic posidonia, which can only tolerate a maximum salinity of 39 g/L NaCl while most discharge brine salinities are higher than 60 g/L NaCl. Therefore, high recovery or near zero liquid discharge technologies need to be further developed [309], [310]. Brauns studied the energy collected from salinity gradient power by reverse electro−dialysis combined with a seawater desalination unit [311], [312]. Similar ideas could be expanded by combining a solar-driven MED with a MVC

system during the day and operating just the MVC system at night. Temperature change is also a big concern for ocean animals since most desalination plants discharge brine at a temperature higher than 40℃. Many desalination plants mix untreated seawater with rejected brine in order to lower the discharge temperature. However, this involves more pumping power further increasing the desalination cost. Alarcón et al. incorporated an absorption heat pump ($LiBr–H_2O$) to partially recover heat rejected from the MED unit so that the heat discharged to the environment could be significantly reduced [102][313]. As for the potential environmental hazards caused by solar power systems, battery banks and heat transfer fluids are the main concerns. Implementing thermal energy storage systems can replace the need for batteries while including a properly sized HTF containment structure in the plant will help eliminate the hazard of an accidental HTF release.

6.5 Cogeneration and Process Using Low-grade Heat

Considerable research focuses on using solar desalination in remote, arid areas, which normally use small-scale desalination systems. Figure 6.4 shows that hybrid thermal systems generally have a relatively lower cost as compared with similar capacity solar only desalination systems, however, most of them have capacities larger than $100m^3$/day. For places far away from the power grid and water system, not only water is needed but also power is needed [314]. Small desalination systems using waste heat from decentralized diesel generators, decentralized small-scale natural gas engines or geothermal energy could achieve lower cost, especialy if solar is the only power supply [136]. Therefore, it is very important to study small-scale hybrid desalination systems. On the one hand, the hybrid system could reduce the fossil fuel energy consumption and save fuel transporation costs. On the other hand, hybrid systems could provide lower water costs and avoid the drawback of an

intermittent solar source while providing crucial water that is not weather or season dependent. However, not many studies have been reported on small-scale solar-assisted hybrid desalination systems. In addition, heat energy from solar collectors is not really the same as heat energy from waste heat. Waste heat sources are considered as "once-through" heat sources as opposed to the solar resource being a recirculating source. This difference could impact the choice of heat engines for the desalination system. Therefore, the two types of heat sources should be analyzed separately and it cannot be assumed that conclusions for solar thermal are valid for hybrid desalination or waste heat applications [265].

6.6 A Necessity to Develop a Design Tool

Section 6.1 only showed the possible combination of a solar-assisted desalination process, however, there are many kinds of combinations already. If other renewable energy sources (i.e., geothermal/industrial waste heat) are considered, the possible combinations will be overwhelming. Studies in Chapter 4 clearly showed that even when only thermal heat sources are considered, the choice of the connected system (power cycle) could be different. Studies in Chapter 5 showed that even when the system configuration is fixed, the variation of the water source salt concentration will definitely affect the selection of the components. All previous studies definitely showed the complication of using renewable energy sources (i.e., low-grade heat sources), for desalination. In order to make the selection process easier, a tool specially designed to assist the selection process in using low-grade heat sources for desalination is needed. However, to date there is no such user-friendly tools/interface available.

The research group at the University of South Florida's Clean Energy Research Center has started building user interfaces for two proposed novel systems,

discussed in previous chapters. These interfaces allow the user to: a) enter data about heat source temperature range, solar collector manufacture parameters (for CPC, ETC and FPC collectors) and specific heat capacity information of heat sources; b) enter desired power cycle operation pressure, maximum temperature and source water salt concentration; and c) select the organic working fluid to gain information about the power cycle efficiency, the solar collector area and whether a recuperator is needed, In addition, the interface could also allow the user to see whether there is some temperature crossover in the boiler so as to make certain the selected working fluid and temperature range are reasonable. The interface could enable users to review model details and obtain information for each effect of the thermal MED system. The expander/turbine could be a multi-stage turbine and the detailed work/pressure/enthalpy, information could also be listed. Some of the screen copies of the interface (Figure 6.5, Figure 6.6, Figure 6.7 and Figure 6.8) are displayed below.

Figure 6.5 Overall platform of the tool for using low-grade heat for desalination.

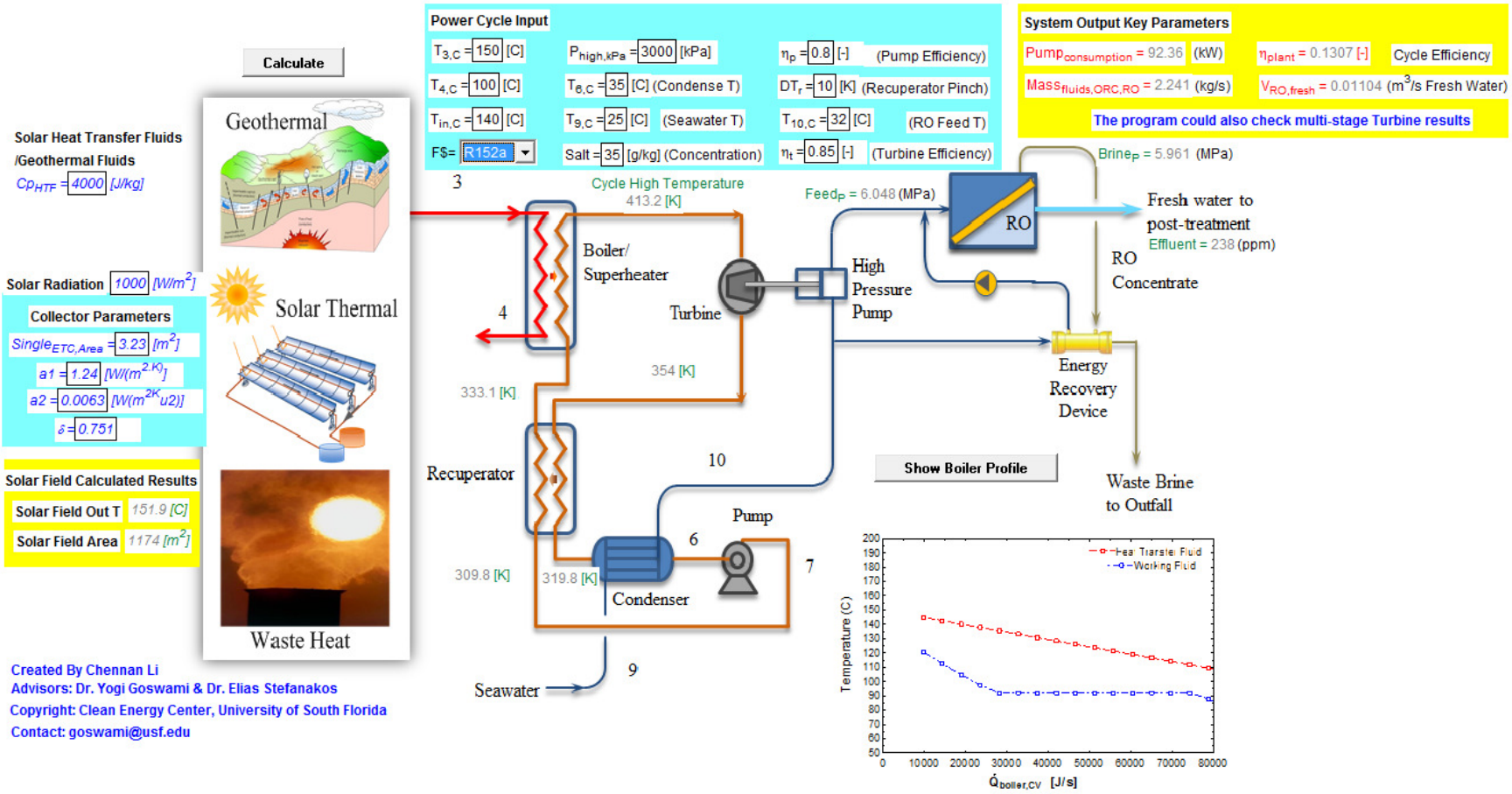

Figure 6.6 Interface for using low-grade heat for RO desalination.

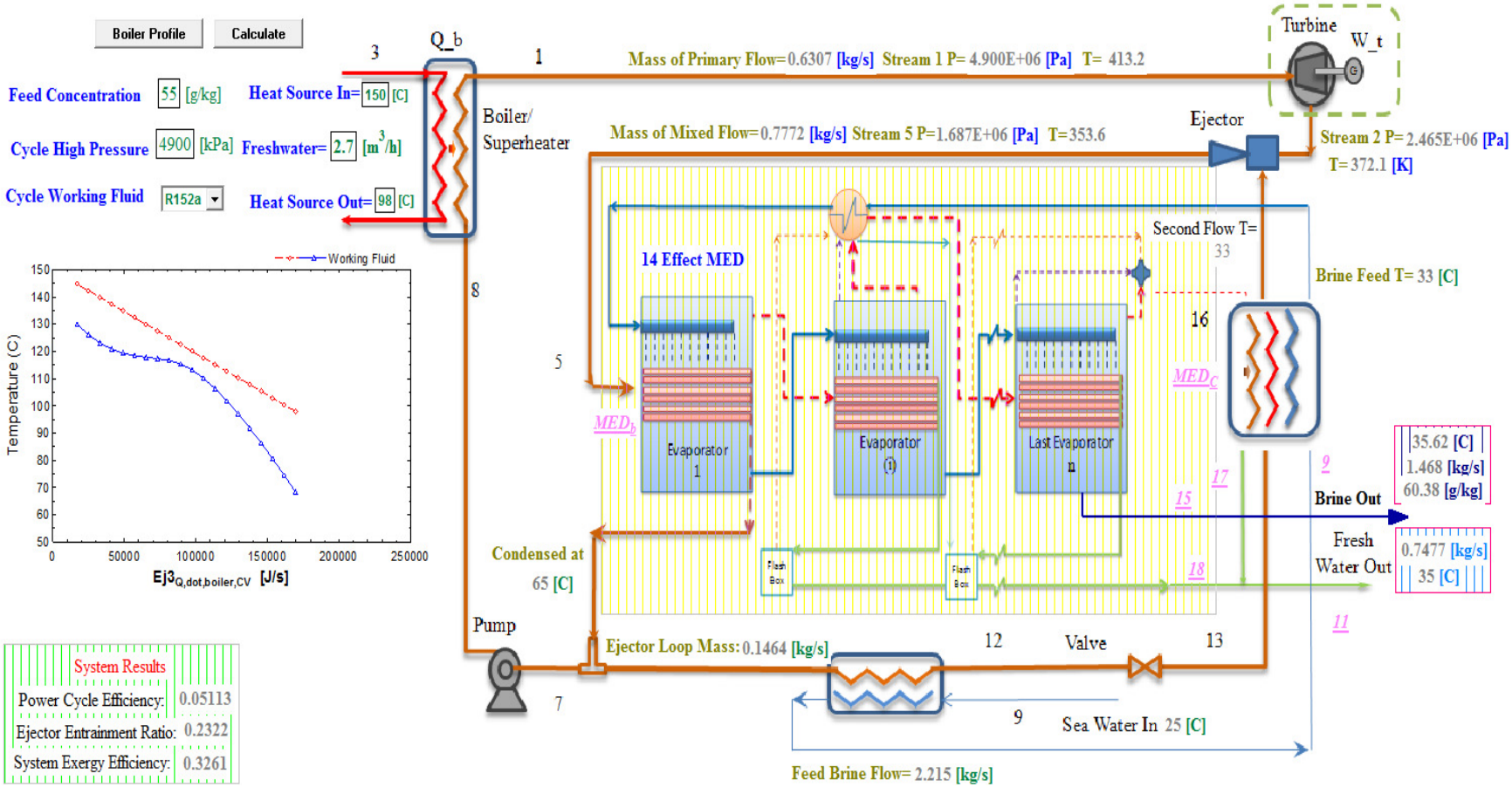

Figure 6.7 Interface for using low-grade heat for MED-Ejector desalination.

Exergy Destruction Percentage	
Boiler	0.1567
Ejector	0.1166
Valve	0.01931
Pump	0.01808
Expander	0.05435
MED System	0.5837
Final Condenser	0.05133

MED Detailed Information for Performance Ratio=9

Evaporator generated	Brine Flash generated	Condensate Flash generated
$D14_1 = 0.05929$ [kg/s]	$d14^*_2 = 0.007087$ [kg/s]	$\overline{d14}_2 = 0.0001545$ [kg/s]
$D14_2 = 0.05915$ [kg/s]	$d14^*_3 = 0.006636$ [kg/s]	$\overline{d14}_3 = 0.0003116$ [kg/s]
$D14_3 = 0.05739$ [kg/s]	$d14^*_4 = 0.006204$ [kg/s]	$\overline{d14}_4 = 0.0004467$ [kg/s]
$D14_4 = 0.05563$ [kg/s]	$d14^*_5 = 0.005788$ [kg/s]	$\overline{d14}_5 = 0.0005602$ [kg/s]
$D14_5 = 0.05384$ [kg/s]	$d14^*_6 = 0.00539$ [kg/s]	$\overline{d14}_6 = 0.0006524$ [kg/s]
$D14_6 = 0.05205$ [kg/s]	$d14^*_7 = 0.005006$ [kg/s]	$\overline{d14}_7 = 0.0007237$ [kg/s]
$D14_7 = 0.05023$ [kg/s]	$d14^*_8 = 0.004637$ [kg/s]	$\overline{d14}_8 = 0.0007743$ [kg/s]
$D14_8 = 0.04839$ [kg/s]	$d14^*_9 = 0.004282$ [kg/s]	$\overline{d14}_9 = 0.0008045$ [kg/s]
$D14_9 = 0.04653$ [kg/s]	$d14^*_{10} = 0.00394$ [kg/s]	$\overline{d14}_{10} = 0.0008146$ [kg/s]
$D14_{10} = 0.04464$ [kg/s]	$d14^*_{11} = 0.00361$ [kg/s]	$\overline{d14}_{11} = 0.0008048$ [kg/s]
$D14_{11} = 0.04272$ [kg/s]	$d14^*_{12} = 0.003291$ [kg/s]	$\overline{d14}_{12} = 0.0007755$ [kg/s]
$D14_{12} = 0.04077$ [kg/s]	$d14^*_{13} = 0.002983$ [kg/s]	$\overline{d14}_{13} = 0.000727$ [kg/s]
$D14_{13} = 0.03878$ [kg/s]	$d14^*_{14} = 0.002685$ [kg/s]	$\overline{d14}_{14} = 0.002199$ [kg/s]
$D14_{14} = 0.03675$ [kg/s]		

First Effect **Effect 2-13** **Last Effect**

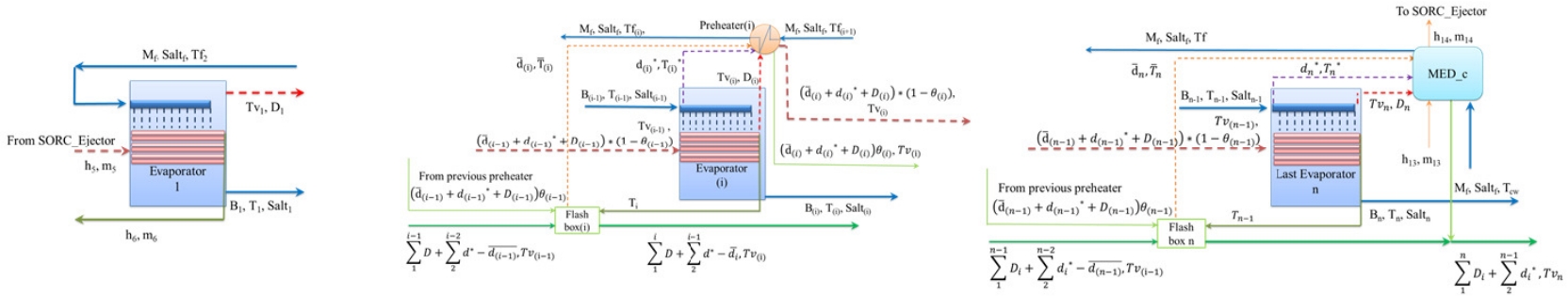

Figure 6.8 Results showing the detailed MED information in a MED-Ejector desalination system.

6.7 Concluding Remarks

Compared with conventional water treatment processes, desalination is an energy intensive process. Renewable energy sources such as low-grade heat sources are abundant and could be used for desalination applications, whose technical feasibility has already been proved. Most current solar desalination systems are two independent systems, renewable energy and desalination combined together, which are still relatively expensive and depend on location, weather and season. Current research shows that solar thermal/fossil/desalination hybrid systems are more economical and could overcome the intermittence of solar energy. Additional research is needed on solar/fossil fuel hybrid systems, especially waste heat from decentralized thermal power systems for water and power cogeneration because both are crucial in remote areas. In order to reduce fuel consumption and overcome the intermittence of the solar source, waste heat from decentralized systems could be used. However, any waste heat source or solar thermal heat source should be analyzed separately and it cannot be assumed that the conclusions for solar thermal are the same as for hybrid desalination or waste heat applications. With future cost reduction of solar systems and the development of novel solar technologies as well as accurate solar radiation data collection and modeling [315–317], solar thermal/low-grade heat desalination could be a valid option for future desalination plants.

CHAPTER 7 SUMMARY, PROSPECTS AND RECOMMENDATIONS

7.1 Summary

This work investigates the conversion of low-grade heat for desalination and power production. The motivation for this research was to select a suitable process for desalination using low-grade heat sources and improve the efficiency of the system energy conversion.

Compared with conventional water treatment processes, desalination is an energy intensive process, which highlights the need for finding suitable alternative energy resources for the desalination systems. A review of seawater desalination using solar energy is carried out in Chapter 2. Most current solar desalination systems consist of two independent systems (solar and desalination) combined together, which are still relatively expensive and depend on location, weather and season. Current research shows that solar/fossil/desalination hybrid systems and a system using waste heat from decentralized power systems are more economical and could overcome the intermittence of solar energy. Additional research is needed on solar/fossil fuel hybrid systems. This is especially true for waste heat from decentralized thermal power systems for water and power cogeneration, because these are crucial in remote areas. To reduce fuel consumption and overcome the intermittence of the solar source, waste heat from decentralized systems could be used. However, any waste heat source or solar thermal heat source should be analyzed separately and one cannot assume that the conclusions for solar thermal systems are the same as for hybrid desalination systems or waste heat usage applications.

In order to better select the most suitable process and system configuration for using low-grade heat to desalinate water, one can follow the analysis presented in Chapter 3. The theoretical minimum energy required for a desalination process and the exergy destruction of different desalination processes, could be used as criteria for the selection. RO/MED and MED combined with vapor compressors are studied and modeled to better understand and improve the two proposed novel systems.

Chapter 4 proposed a new system that used a supercritical organic Rankine cycle to directly drive a reverse osmosis desalination system. When treating regular seawater or brackish water, the RO process is more energy efficient. A power cycle making use of low-grade heat sources could be used to drive the RO system. The analysis of the heat source is of key importance. When the heat source is recirculating heat transfer fluid (i.e., solar collectors) a conventional organic Rankine cycle using R245fa has limited advantages. However, when the heat sources are the once-through type (i.e. waste heat or geothermal heat) a conventional ORC does not have enough pressure to meet the RO needs. Under such conditions, a supercritical cycle shows better performance with higher efficiency and wider operation range. For both conditions the selection of working fluids which better match the heat source profile are important to reduce the exergy destruction in the boiler. An investigation into potential working fluids suitable for low-grade heat sources (150°C) was carried out and suitable fluids were presented. This proposed SORC-RO system could make full use of both the recirculating and once-through type of heat sources. Therefore this could be applied to solar thermal/fossil hybrid systems to make use of the waste heat from the fossil fuel system and eliminate the intermittent behavior of a solar system, as well as reducing the solar desalination system cost.

In Chapter 5 a novel SORC-Ejector-MED system was proposed and analyzed. When water sources have higher salt concentration such as frac flow back, which is generated in natural gas mining processes, or concentrated brine from other desalination systems, a robust thermal desalination system has to be used. However, thermal desalination systems are energy intensive and require external electricity input. The proposed system could be energy independent to handle concentrated brine. In addition, the use of the ejector loop could improve the energy efficiency of the MED system. The analysis showed that the MED subsystem, boiler and ejector are three major exergy destruction parts. By selecting a suitable cycle operation pressure, the boiler destruction could be reduced. The MED system is the biggest exergy destruction part, but it is not easy to reduce the exergy destruction by improving performance without increasing the number of effects. By selecting high efficiency ejectors, the proposed system could handle highly concentrated brine without extra electricity input.

Chapter 7 summarized the possible configurations of solar desalination systems on the basis of the analyses of chapters 2, 4 and 5. Chapter 7 points out the complexity of using low-grade heat sources for desalination applications because water sources and energy sources could affect the system performance and the selections. Therefore a software tool which could easily be used for the design under different conditions should be developed. A platform and a few preliminary user-friendly interfaces were developed and presented.

7.2 Applications and Recommendations

The two novel systems proposed in this dissertation suggest great potential for the efficient and economical use of low-grade heat sources for desalination or

desalination/power cogeneration. This section offers prospects of the systems applications as well as recommendations for future research.

7.2.1 Application of Proposed Systems

Low-grade heat sources, below 150ºC are abundantly available as industrial waste heat, solar thermal, and geothermal, to name a few. Using low-grade heat sources for desalination could be useful in natural gas mining industries where large quantities of highly concentrated frac water are produced and plentiful waste heat is available onsite. The proposed systems could also be useful in the oil industry where a large amount of water is generated with the oil production process. Water at thousands of feet underground, is naturally at temperatures within the proposed system application temperature range. The proposed systems could also be useful in the iron and steel industry where many large plants are built close to the sea, and huge amounts of waste heat is wasted by using seawater to cool the process. For example, China has more than 50% of the iron and steel production capacity of the world and, in the next 10 years, the country plans to move almost all of the major iron and steel plants close to the sea to save transportation costs. The proposed systems can also be useful in geothermal applications where brines are extracted from underground. The proposed systems are obviously useful for solar desalination applications especially in remote islands where, during the day, solar thermal can be used to provide both power and water, while at night waste heat from diesel engines could be used. These systems are also suitable for some desert areas close to the sea such as the Sechura Desert of Peru which is close to the Pacific Ocean coast, and the Mediterranean Sea where water is scarce while abundant sunshine is available.

7.2.2 Recommendations for Future Research

The following are some recommendations for future work.

a) The platform/tool developed in Chapter 6 is still preliminary. The solar collector calculations are suitable for certain types of collectors. The solar collector models can be improved so that an accurate solar loss to the environment can be calculated.

b) In calculating the boiler profile in the platform, the once-through heat sources (i.e., geothermal or industrial waste heat) are assumed to have a constant specific heat capacity. In the future, a more accurate and less complicated expression that considers a non-constant specific heat capacity can be developed in order to accurately calculate the boiler pinch.

c) An economic analysis has not yet been developed for the current platform. Thus, an economic model could be developed that includes cost estimation.

d) Even though membrane distillation suffers from additional resistance to mass transport by the membrane as compared to MED, it has a lower cost of membrane materials and can use more area for heat and mass transfer. It could be used for high recovery or highly concentrated salt water treatment that RO could not handle, which normally requires high energy consumption. Therefore it is important to pursue the use of low-grade heat in the membrane distillation method without external electricity input.

e) It is important to study systems that can be continuously operated by incorporating a solar system (i.e. solar pond) and a diesel generation system, including the storage of waste heat and solar energy. These systems could also be very useful for applications in small or isolated islands and communities.

f) Finally, with the construction of the USF CERC solar thermal power plant, experiments that can simulate different types of heat sources and desalination systems can be carried out and compared to theoretical calculations.

REFERENCES

[1] R. F. Service, "Desalination Freshens Up," *Science*, vol. 313, no. 5790, pp. 1088 –1090, 2006.

[2] M. A. Shannon, P. W. Bohn, M. Elimelech, J. G. Georgiadis, B. J. Marinas, and A. M. Mayes, "Science and technology for water purification in the coming decades," *Nature*, vol. 452, no. 7185, pp. 301–310, Mar. 2008.

[3] Q. Schiermeier, "Water: Purification with a pinch of salt," *Nature*, vol. 452, pp. 260–261, Mar. 2008.

[4] Population Reference Bureau, World Population Highlights: Key Findings From Prb's 2010 World Population Data Sheet, Vol.65, No.2, July 2010.

[5] M. Mehanna, T. Saito, J. Yan, M. Hickner, X. Cao, X. Huang, and B. E. Logan, "Using microbial desalination cells to reduce water salinity prior to reverse osmosis," *Energy & Environmental Science*, vol. 3, p. 1114, 2010.

[6] A. Bajpayee, T. Luo, A. Muto, and G. Chen, "Very low temperature membrane-free desalination by directional solvent extraction," *Energy & Environmental Science*, vol. 4, p. 1672, 2011.

[7] A. R. Hoffman, "Water Security: A Growing Crisis and the Link to Energy," *AIP Conf. Proc.*, vol. 1044, no. 1, pp. 55–63, 2008.

[8] "The IDA Desalination Yearbook 2011-2012 | Water Desalination Report." [Online]. Available: http://waterdesalreport.com/knowledge/16. [Accessed: 21-Sep-2010].

[9] S. A. Kalogirou, "Seawater desalination using renewable energy sources," *Progress in Energy and Combustion Science*, vol. 31, no. 3, pp. 242–281, 2005.

[10] R. B. Swenson and F. de Winter, "The Production Peaks In Petroleum And Natural Gas: Information, Misinformation, Awareness, And Implications," presented at the In: Proceedings of the ISES 2005 solar world congress, 2005.

[11] J. Blanco, S. Malato, P. Fernández-Ibañez, D. Alarcón, W. Gernjak, and M. I. Maldonado, "Review of feasible solar energy applications to water processes," *Renewable and Sustainable Energy Reviews*, vol. 13, no. 6–7, pp. 1437–1445, Aug. 2009.

[12] M. Z. Jacobson, “Review of solutions to global warming, air pollution, and energy security,” *Energy & Environmental Science*, vol. 2, p. 148, 2009.

[13] A. Cho, “Energy’s Tricky Tradeoffs,” *Science*, vol. 329, no. 5993, pp. 786 – 787, 2010.

[14] T. V. Arjunan, H. S. Aybar, and N. Nedunchezhian, “Status of solar desalination in India,” *Renewable and Sustainable Energy Reviews*, vol. 13, no. 9, pp. 2408–2418, Dec. 2009.

[15] S. Mussati, P. Aguirre, and N. J. Scenna, “Optimal MSF plant design,” *Desalination*, vol. 138, no. 1–3, pp. 341–347, Sep. 2001.

[16] S. F. Mussati, P. A. Aguirre, and N. J. Scenna, “Improving the efficiency of the MSF once through (MSF-OT) and MSF-mixer (MSF-M) evaporators,” *Desalination*, vol. 166, pp. 141–151, Aug. 2004.

[17] E. Ali, “Understanding the operation of industrial MSF plants Part I: Stability and steady-state analysis,” *Desalination*, vol. 143, no. 1, pp. 53–72, May 2002.

[18] E. Ali, “Understanding the operation of industrial MSF plants Part II: Optimization and dynamic analysis,” *Desalination*, vol. 143, no. 1, pp. 73–91, May 2002.

[19] E. Cardona and A. Piacentino, “Optimal design of cogeneration plants for seawater desalination,” *Desalination*, vol. 166, pp. 411–426, Aug. 2004.

[20] J. de Gunzbourg and D. Larger, “Cogeneration applied to very high efficiency thermal seawater desalination plants,” *Desalination*, vol. 125, no. 1–3, pp. 203–208, Nov. 1999.

[21] M. A. Darwish and A. Alsairafi, “Technical comparison between TVC/MEB and MSF,” *Desalination*, vol. 170, no. 3, pp. 223–239, Nov. 2004.

[22] D. Y. Goswami, F. Kreith, and J. F. Kreider, *Principles of solar engineering*. Philadelphia, PA 19106: Taylor & Francis, 2000.

[23] G. Micale, L. Rizzuti, and A. Cipollina, *Seawater Desalination Conventional and Renewable Energy Processes*. SpringerLink, 2009.

[24] “Engineering Study Of Desalination Using Salt Gradient Solar Ponds,” Agency For International Development, 1981.

[25] T. Szacsvay, P. Hofer-Noser, and M. Posnansky, “Technical and economic aspects of small-scale solar-pond-powered seawater desalination systems,” *Desalination*, vol. 122, no. 2–3, pp. 185–193, Jul. 1999.

[26] M. Posnansky, “Technical and economical aspects of solar desalination with particular emphasis on solar pond powered distillation plants,” *Desalination*, vol. 67, pp. 81–95, Dec. 1987.

[27] M. J. Safi and A. Korchani, “Cogeneration applied to water desalination: Simulation of different technologies,” *Desalination*, vol. 125, no. 1–3, pp. 223–229, Nov. 1999.

[28] K. R. Agha, “The thermal characteristics and economic analysis of a solar pond coupled low temperature multi stage desalination plant,” *Solar Energy*, vol. 83, no. 4, pp. 501–510, Apr. 2009.

[29] H. Lu, J. C. Walton, and H. Hein, “Thermal Desalination using MEMS and Salinity-Gradient Solar Pond Technology,” U.S. Department of the Interior, Bureau of Reclamation, Desalination Research and Development Program Report No.80, Aug. 2002.

[30] R. K. Suri, A. M. R. Al-Marafie, A. A. Al-Homoud, and G. P. Maheshwari, “Cost-effectiveness of solar water production,” *Desalination*, vol. 71, no. 2, pp. 165–175, 1989.

[31] K. Tahri, “The prospects of fresh water supply for Tan Tan City from non-conventional water resources,” *Desalination*, vol. 135, no. 1–3, pp. 43–50, Apr. 2001.

[32] D. W. J. Hayes and J. A. L. Kipps, “Salt-gradient solar ponds from concentrated subsurface agricultural drainage waters of the San Joaquin Valley, California,” *Desalination*, vol. 88, no. 1–3, pp. 301–309, Oct. 1992.

[33] H. Lu, A. H. P. Swift, J. Hein, and J. C. Walton, “Advancements in Salinity Gradient Solar Pond Technology Based on Sixteen Years of Operational Experience,” *J. Sol. Energy Eng.*, vol. 126, no. 2, pp. 759–767, May 2004.

[34] V. Velmurugan and K. Srithar, “Prospects and scopes of solar pond: A detailed review,” *Renewable and Sustainable Energy Reviews*, vol. 12, no. 8, pp. 2253–2263, Oct. 2008.

[35] F. Trieb and H. Müller-Steinhagen, “Concentrating solar power for seawater desalination in the Middle East and North Africa,” *Desalination*, vol. 220, no. 1–3, pp. 165–183, Mar. 2008.

[36] S. Kalogirou, “The potential of solar industrial process heat applications,” *Applied Energy*, vol. 76, no. 4, pp. 337–361, Dec. 2003.

[37] I. L. García, J. L. Álvarez, and D. Blanco, “Performance model for parabolic trough solar thermal power plants with thermal storage: Comparison to operating plant data,” *Solar Energy*, vol. 85, no. 10, pp. 2443–2460, Oct. 2011.

[38] H. Shaobo, Z. Zhang, Z. Huang, and A. Xie, “Performance optimization of solar multi-stage flash desalination process using Pinch technology,” *Desalination*, vol. 220, no. 1–3, pp. 524–530, Mar. 2008.

[39] J. Jiang, H. Tian, M. Cui, and L. Liu, "Proof-of-concept study of an integrated solar desalination system," *Renewable Energy*, vol. 34, no. 12, pp. 2798–2802, Dec. 2009.

[40] L. García-Rodríguez and C. Gómez-Camacho, "Conditions for economical benefits of the use of solar energy in multi-stage flash distillation," *Desalination*, vol. 125, no. 1–3, pp. 133–138, Nov. 1999.

[41] L. García-Rodríguez and C. Gómez-Camacho, "Thermoeconomic analysis of a solar parabolic trough collector distillation plant," *Desalination*, vol. 122, no. 2–3, pp. 215–224, Jul. 1999.

[42] M. S. Abu-Jabal, I. Kamiya, and Y. Narasaki, "Proving test for a solar-powered desalination system in Gaza-Palestine," *Desalination*, vol. 137, no. 1–3, pp. 1–6, May 2001.

[43] M. A. Farwati, "Theoretical study of multi-stage flash distillation using solar energy," *Energy*, vol. 22, no. 1, pp. 1–5, Jan. 1997.

[44] J. Joseph, R. Saravanan, and S. Renganarayanan, "Studies on a single-stage solar desalination system for domestic applications," *Desalination*, vol. 173, no. 1, pp. 77–82, Mar. 2005.

[45] A. S. Nafey, M. A. Mohamad, S. O. El-Helaby, and M. A. Sharaf, "Theoretical and experimental study of a small unit for solar desalination using flashing process," *Energy Conversion and Management*, vol. 48, no. 2, pp. 528–538, Feb. 2007.

[46] S. Kalogirou, "Survey of solar desalination systems and system selection," *Energy*, vol. 22, no. 1, pp. 69–81, Jan. 1997.

[47] H. Raach and J. Mitrovic, "Simulation of heat and mass transfer in a multi-effect distillation plant for seawater desalination," *Desalination*, vol. 204, no. 1–3, pp. 416–422, Feb. 2007.

[48] V. N. Slesarenko, "Comparison of the efficiency of MSF and thin-film desalination plants," *Desalination*, vol. 158, no. 1–3, pp. 295–302, Aug. 2003.

[49] G. Kronenberg, "Cogeneration with the LT-MED desalination process," *Desalination*, vol. 108, no. 1–3, pp. 287–294, Feb. 1997.

[50] V. V. Slesarenko, "Heat pumps as a source of heat energy for desalination of seawater," *Desalination*, vol. 139, no. 1–3, pp. 405–410, Sep. 2001.

[51] F. Al-Juwayhel, H. El-Dessouky, and H. Ettouney, "Analysis of single-effect evaporator desalination systems combined with vapor compression heat pumps," *Desalination*, vol. 114, no. 3, pp. 253–275, Dec. 1997.

[52] D. C. Alarcón-Padilla, L. García-Rodríguez, and J. Blanco-Gálvez, "Experimental assessment of connection of an absorption heat pump to a multi-effect distillation unit," *Desalination*, vol. 250, no. 2, pp. 500–505, Jan. 2010.

[53] A. Ophir and F. Lokiec, "Advanced MED process for most economical seawater desalination," *Desalination*, vol. 182, no. 1–3, pp. 187–198, Nov. 2005.

[54] C. Sommarva, "Utilisation of power plant waste heat steams to enhance efficiency in thermal desalination," *Desalination*, vol. 222, no. 1–3, pp. 592–595, Mar. 2008.

[55] O. Al Hawaj and M. A. Darwish, "A solar pond assisted multi-effect desalting system," *Desalination*, vol. 99, no. 1, pp. 119–135, Nov. 1994.

[56] M. A. Garman and M. A. Muntasser, "Sizing and thermal study of salinity gradient solar ponds connecting with the MED desalination unit," *Desalination*, vol. 222, no. 1–3, pp. 689–695, Mar. 2008.

[57] H. Lu, J. C. Walton, and A. H.P. Swift, "Desalination coupled with salinity-gradient solar ponds," *Desalination*, vol. 136, no. 1–3, pp. 13–23, May 2001.

[58] P. T. Tsilingiris, "The analysis and performance of large-scale stand-alone solar desalination plants," *Desalination*, vol. 103, no. 3, pp. 249–255, Dec. 1995.

[59] G. Caruso and A. Naviglio, "A desalination plant using solar heat as a heat supply, not affecting the environment with chemicals," *Desalination*, vol. 122, no. 2–3, pp. 225–234, Jul. 1999.

[60] G. Caruso, A. Naviglio, P. Principi, and E. Ruffini, "High-energy efficiency desalination project using a full titanium desalination unit and a solar pond as the heat supply," *Desalination*, vol. 136, no. 1–3, pp. 199–212, May 2001.

[61] J. Leblanc, J. Andrews, and A. Akbarzadeh, "Low-temperature solar-thermal multi-effect evaporation desalination systems," *Int. J. Energy Res.*, vol. 34, no. 5, pp. 2151–2157, 2010.

[62] G. P., "Potential uses of solar energy for seawater desalination," *Desalination*, vol. 101, no. 1, pp. 11–20, Mar. 1995.

[63] H. Daniel, "The application of solar energy for large-scale seawater desalination," *Desalination*, vol. 89, no. 2, pp. 115–183, Dec. 1992.

[64] A. M. El-Nashar, "An optimal design of a solar desalination plant," *Desalination*, vol. 93, no. 1–3, pp. 597–614, Aug. 1993.

[65] A. M. El-Nashar, "Validating the performance simulation program 'SOLDES' using data from an operating solar desalination plant," *Desalination*, vol. 130, no. 3, pp. 235–253, Nov. 2000.

[66] A. M. El-Nashar, “Predicting part load performance of small MED evaporators - a simple simulation program and its experimental verification,” *Desalination*, vol. 130, no. 3, pp. 217–234, Nov. 2000.

[67] A. M. El-Nashar, “Optimizing the operating parameters of a solar desalination plant,” *Solar Energy*, vol. 48, no. 4, pp. 207–213, 1992.

[68] A. M. El-Nashar, “Seasonal effect of dust deposition on a field of evacuated tube collectors on the performance of a solar desalination plant,” *Desalination*, vol. 239, no. 1–3, pp. 66–81, Apr. 2009.

[69] A. M. El-Nashar, “The economic feasibility of small solar MED seawater desalination plants for remote arid areas,” *Desalination*, vol. 134, no. 1–3, pp. 173–186, Apr. 2001.

[70] A. M. El-Nashar, “Economics of small solar-assisted multiple-effect stack distillation plants,” *Desalination*, vol. 130, no. 3, pp. 201–215, Nov. 2000.

[71] S. Kalogirou, “Economic analysis of a solar assisted desalination system,” *Renewable Energy*, vol. 12, no. 4, pp. 351–367, Dec. 1997.

[72] D. Sagie, E. Feinerman, and E. Aharoni, “Potential of solar desalination in Israel and in its close vicinity,” *Desalination*, vol. 139, no. 1–3, pp. 21–33, Sep. 2001.

[73] T. Badawi W., “Optimal water cost from solar-powered multieffect distillation,” *Desalination*, vol. 44, no. 1–3, pp. 153–165, May 1983.

[74] M. T. Ali, H. E. S. Fath, and P. R. Armstrong, “A comprehensive techno-economical review of indirect solar desalination,” *Renewable and Sustainable Energy Reviews*, vol. 15, no. 8, pp. 4187–4199, 2011.

[75] A. M. El-Nashar and M. Samad, “The solar desalination plant in Abu Dhabi: 13 years of performance and operation history,” *Renewable Energy*, vol. 14, no. 1–4, pp. 263–274, May.

[76] S. Al-Hallaj, S. Parekh, M. M. Farid, and J. R. Selman, “Solar desalination with humidification-dehumidification cycle: Review of economics,” *Desalination*, vol. 195, no. 1–3, pp. 169–186, Aug. 2006.

[77] J. Blanco and D. AlarcóN, “The Psa Experience On Solar Desalination: Technology Development And Research Activities,” in *Solar Desalination for the 21st Century*, L. Rizzuti, H. M. Ettouney, and A. Cipollina, Eds. Dordrecht: Springer Netherlands, pp. 195–206.

[78] E. Zarza, J. Ajona, J. León, A. Gregorzewski, and K. Genthner, “Solar thermal desalination project at the Plataforma Solar de Almeria,” *Solar Energy Materials*, vol. 24, no. 1–4, pp. 608–622, Dec. 1991.

[79] N. H. Aly and A. K. El-Figi, “Mechanical vapor compression desalination systems -- A case study,” *Desalination*, vol. 158, no. 1–3, pp. 143–150, Aug. 2003.

[80] J. Siqueiros and F. A. Holland, “Water desalination using heat pumps,” *Energy*, vol. 25, no. 8, pp. 717–729, Aug. 2000.

[81] J. G. Ji, R. Z. Wang, L. X. Li, and H. Ni, “Simulation and Analysis of a Single-Effect Thermal Vapor-Compression Desalination System at Variable Operation Conditions,” *Chem. Eng. Technol.*, vol. 30, no. 12, pp. 1633–1641, Dec. 2007.

[82] A. S. Nafey, H. E. S. Fath, and A. A. Mabrouk, “Thermoeconomic design of a multi-effect evaporation mechanical vapor compression (MEE-MVC) desalination process,” *Desalination*, vol. 230, no. 1–3, pp. 1–15, Sep. 2008.

[83] Y. M. El-Sayed, “Thermoeconomics of some options of large mechanical vapor-compression units,” *Desalination*, vol. 125, no. 1–3, pp. 251–257, Nov. 1999.

[84] M. A. Darwish, “Thermal analysis of vapor compression desalination system,” *Desalination*, vol. 69, no. 3, pp. 275–295, 1988.

[85] A. O. B. Amer, “Development and optimization of ME-TVC desalination system,” *Desalination*, vol. 249, no. 3, pp. 1315–1331, Dec. 2009.

[86] Y. Wang and N. Lior, “Performance analysis of combined humidified gas turbine power generation and multi-effect thermal vapor compression desalination systems -- Part 1: The desalination unit and its combination with a steam-injected gas turbine power system,” *Desalination*, vol. 196, no. 1–3, pp. 84–104, Sep. 2006.

[87] Y. Wang and N. Lior, “Performance analysis of combined humidified gas turbine power generation and multi-effect thermal vapor compression desalination systems: Part 2: The evaporative gas turbine based system and some discussions,” *Desalination*, vol. 207, no. 1–3, pp. 243–256, Mar. 2007.

[88] K. Ansari, H. Sayyaadi, and M. Amidpour, “A comprehensive approach in optimization of a dual nuclear power and desalination system,” *Desalination*, vol. 269, no. 1–3, pp. 25–34, Mar. 2011.

[89] R. Kouhikamali and M. M., “Process investigation of different locations of thermo-compressor suction in MED-TVC plants,” *Desalination*, vol. In Press, Corrected Proof.

[90] Z. Zimerman, “Development of large capacity high efficiency mechanical vapor compression (MVC) units,” *Desalination*, vol. 96, no. 1–3, pp. 51–58, Jun. 1994.

[91] H. Ettouney, “Design of single-effect mechanical vapor compression,” *Desalination*, vol. 190, no. 1–3, pp. 1–15, Apr. 2006.

[92] M. Marcovecchio, P. Aguirre, N. Scenna, and S. Mussati, “Global Optimal Design of Mechanical Vapor Compression (MVC) Desalination Process,” in *20th European Symposium on Computer Aided Process Engineering*, vol. Volume 28, Elsevier, 2010, pp. 1261–1266.

[93] R. Bahar, M. N. A. Hawlader, and L. S. Woei, “Performance evaluation of a mechanical vapor compression desalination system,” *Desalination*, vol. 166, pp. 123–127, Aug. 2004.

[94] V. V. Slesarenko, “Desalination plant with absorption heat pump for power station,” *Desalination*, vol. 126, no. 1–3, pp. 281–285, Nov. 1999.

[95] Y. Wang and N. Lior, “Proposal and analysis of a high-efficiency combined desalination and refrigeration system based on the LiBr-H2O absorption cycle--Part 1: System configuration and mathematical model,” *Energy Conversion and Management*, vol. 52, no. 1, pp. 220–227, Jan. 2011.

[96] Y. Wang and N. Lior, “Proposal and analysis of a high-efficiency combined desalination and refrigeration system based on the LiBr-H2O absorption cycle--Part 2: Thermal performance analysis and discussions,” *Energy Conversion and Management*, vol. 52, no. 1, pp. 228–235, Jan. 2011.

[97] F. Mandani, H. Ettouney, and H. El-Dessouky, “LiBr---H2O absorption heat pump for single-effect evaporation desalination process,” *Desalination*, vol. 128, no. 2, pp. 161–176, Apr. 2000.

[98] R. Gomri, “Thermal seawater desalination: Possibilities of using single effect and double effect absorption heat transformer systems,” *Desalination*, vol. 253, no. 1–3, pp. 112–118, Apr. 2010.

[99] A. Al-Ansari, H. Ettouney, and H. El-Dessouky, “Water-zeolite adsorption heat pump combined with single effect evaporation desalination process,” *Renewable Energy*, vol. 24, no. 1, pp. 91–111, Sep. 2001.

[100] X. Wang and K. C. Ng, “Experimental investigation of an adsorption desalination plant using low-temperature waste heat,” *Applied Thermal Engineering*, vol. 25, no. 17–18, pp. 2780–2789, Dec. 2005.

[101] D. Zejli, R. Benchrifa, A. Bennouna, and O. K. Bouhelal, “A solar adsorption desalination device: first simulation results,” *Desalination*, vol. 168, pp. 127–135, Aug. 2004.

[102] D.-C. Alarcón-Padilla and L. García-Rodríguez, “Application of absorption heat pumps to multi-effect distillation: a case study of solar desalination,” *Desalination*, vol. 212, no. 1–3, pp. 294–302, Jun. 2007.

[103] L. García-Rodríguez and C. Gómez-Camacho, “Preliminary design and cost analysis of a solar distillation system,” *Desalination*, vol. 126, no. 1–3, pp. 109–114, Nov. 1999.

[104] L. García-Rodríguez and C. Gómez-Camacho, “Design parameter selection for a distillation system coupled to a solar parabolic trough collector,” *Desalination*, vol. 122, no. 2–3, pp. 195–204, Jul. 1999.

[105] L. García-Rodríguez and C. Gómez-Camacho, “Exergy analysis of the SOL-14 plant (Plataforma Solar de Almería, Spain),” *Desalination*, vol. 137, no. 1–3, pp. 251–258, May 2001.

[106] L. García-Rodríguez, A. I. Palmero-Marrero, and C. Gómez-Camacho, “Thermoeconomic optimization of the SOL-14 plant (plataforma solar de Almería, Spain),” *Desalination*, vol. 136, no. 1–3, pp. 219–223, May 2001.

[107] D. C. Alarcón-Padilla, L. García-Rodríguez, and J. Blanco-Gálvez, “Design recommendations for a multi-effect distillation plant connected to a double-effect absorption heat pump: A solar desalination case study,” *Desalination*, vol. 262, no. 1–3, pp. 11–14, Nov. 2010.

[108] B. Milow and E. Zarza, “Advanced MED solar desalination plants. Configurations, costs, future -- seven years of experience at the Plataforma Solar de Almeria (Spain),” *Desalination*, vol. 108, no. 1–3, pp. 51–58, Feb. 1997.

[109] L. García-Rodríguez and C. Gómez-Camacho, “Thermo-economic analysis of a solar multi-effect distillation plant installed at the Plataforma Solar de Almeria (Spain),” *Desalination*, vol. 122, no. 2–3, pp. 205–214, Jul. 1999.

[110] L. García-Rodríguez, A. I. Palmero-Marrero, and C. Gómez-Camacho, “Application of direct steam generation into a solar parabolic trough collector to multieffect distillation,” *Desalination*, vol. 125, no. 1–3, pp. 139–145, Nov. 1999.

[111] W. D. Childs, A. E. Dabiri, H. A. Al-Hinai, and H. A. Abdullah, “VARI-RO solar-powered desalting technology,” *Desalination*, vol. 125, no. 1–3, pp. 155–166, Nov. 1999.

[112] P. Palenzuela, G. Zaragoza, D. C. Alarcón-Padilla, E. Guillén, M. Ibarra, and J. Blanco, “Assessment of different configurations for combined parabolic-trough (PT) solar power and desalination plants in arid regions,” *Energy*, vol. 36, no. 8, pp. 4950–4958, Aug. 2011.

[113] M. A. Sharaf, A. S. Nafey, and L. García-Rodríguez, “Thermo-economic analysis of solar thermal power cycles assisted MED-VC (multi effect distillation-vapor compression) desalination processes,” *Energy*, vol. 36, no. 5, pp. 2753–2764, May 2011.

[114] A. M. Helal and S. A. Al-Malek, "Design of a solar-assisted mechanical vapor compression (MVC) desalination unit for remote areas in the UAE," *Desalination*, vol. 197, no. 1–3, pp. 273–300, Oct. 2006.

[115] M. Nguyen, S. B. Riffat, and D. Whitman, "Solar/gas-driven absorption heat-pump systems," *Applied Thermal Engineering*, vol. 16, no. 4, pp. 347–356, Apr. 1996.

[116] D.-C. Alarcón-Padilla, L. García-Rodríguez, and J. Blanco-Gálvez, "Assessment of an absorption heat pump coupled to a multi-effect distillation unit within AQUASOL project," *Desalination*, vol. 212, no. 1–3, pp. 303–310, Jun. 2007.

[117] D.-C. Alarcón-Padilla, J. Blanco-Gálvez, L. García-Rodríguezz, W. Gernjak, and S. Malato-Rodríguez, "First experimental results of a new hybrid solar/gas multi-effect distillation system: the AQUASOL project," *Desalination*, vol. 220, no. 1–3, pp. 619–625, Mar. 2008.

[118] L. Roca, M. Berenguel, L. Yebra, and D. C. Alarcón, "Preliminary modeling and control studies in AQUASOL project," *Desalination*, vol. 222, no. 1–3, pp. 466–473, Mar. 2008.

[119] L. Roca, J. L. Guzman, J. E. Normey-Rico, M. Berenguel, and L. Yebra, "Robust constrained predictive feedback linearization controller in a solar desalination plant collector field," *Control Engineering Practice*, vol. 17, no. 9, pp. 1076–1088, Sep. 2009.

[120] L. Roca, M. Berenguel, L. Yebra, and D. C. Alarcón-Padilla, "Solar field control for desalination plants," *Solar Energy*, vol. 82, no. 9, pp. 772–786, Sep. 2008.

[121] R. Gomri, "Energy and exergy analyses of seawater desalination system integrated in a solar heat transformer," *Desalination*, vol. 249, no. 1, pp. 188–196, Nov. 2009.

[122] S. M. Hasnain and S. A. Alajlan, "Coupling of PV-powered RO brackish water desalination plant with solar stills," *Desalination*, vol. 116, no. 1, pp. 57–64, Sep. 1998.

[123] S. Alawaji, M. S. Smiai, S. Rafique, and B. Stafford, "PV-powered water pumping and desalination plant for remote areas in Saudi Arabia," *Applied Energy*, vol. 52, no. 2–3, pp. 283–289, 1995.

[124] S. A. Alajlan and M. S. Smiai, "Performance and development of PV - plant for water pumping and desalination for remote area in Saudi Arabia," *Renewable Energy*, vol. 8, no. 1–4, pp. 441–446, May 1996.

[125] B. Parida, S. Iniyan, and R. Goic, "A review of solar photovoltaic technologies," *Renewable and Sustainable Energy Reviews*, vol. 15, no. 3, pp. 1625–1636, Apr. 2011.

[126] E. S. Mohamed, G. Papadakis, E. Mathioulakis, and V. Belessiotis, "A direct coupled photovoltaic seawater reverse osmosis desalination system toward battery based systems -- a technical and economical experimental comparative study," *Desalination*, vol. 221, no. 1–3, pp. 17–22, Mar. 2008.

[127] V. Amati, C. H. Zapater, E. Sciubba, and J. U. Marcuello, "Process Simulation of a Reverse Osmosis Desalination Plant Powered by Photovoltaic Panels for Kalymnos Island," *ASME Conf. Proc.*, vol. 2008, no. 48692, pp. 209–217, Jan. 2008.

[128] E. S. Mohamed and G. Papadakis, "Design, simulation and economic analysis of a stand-alone reverse osmosis desalination unit powered by wind turbines and photovoltaics," *Desalination*, vol. 164, no. 1, pp. 87–97, Mar. 2004.

[129] M. Kumaravel, K. Sulochana, R. Gopalaswami, and G. Saravanan, "Solar Photo Voltaics Powered Seawater Desalination Plants and their Techno-Economics," in *Proceedings of ISES World Congress 2007 (Vol. I – Vol. V)*, D. Y. Goswami and Y. Zhao, Eds. Springer Berlin Heidelberg, 2009, pp. 1402–1408.

[130] S. Bouguecha, B. Hamrouni, and M. Dhahbi, "Small scale desalination pilots powered by renewable energy sources: case studies," *Desalination*, vol. 183, no. 1–3, pp. 151–165, Nov. 2005.

[131] G. Fiorenza, V. K. Sharma, and G. Braccio, "Techno-economic evaluation of a solar powered water desalination plant," *Energy Conversion and Management*, vol. 44, no. 14, pp. 2217–2240, Aug. 2003.

[132] H. M. Laborde, K. B. França, H. Neff, and A. M. N. Lima, "Optimization strategy for a small-scale reverse osmosis water desalination system based on solar energy," *Desalination*, vol. 133, no. 1, pp. 1–12, Feb. 2001.

[133] E. Tzen, D. Theofilloyianakos, and Z. Kologios, "Autonomous reverse osmosis units driven by RE sources experiences and lessons learned," *Desalination*, vol. 221, no. 1–3, pp. 29–36, Mar. 2008.

[134] M. Thomson and D. Infield, "Laboratory demonstration of a photovoltaic-powered seawater reverse-osmosis system without batteries," *Desalination*, vol. 183, no. 1–3, pp. 105–111, Nov. 2005.

[135] A. S. Nafey and M. A. Sharaf, "Combined solar organic Rankine cycle with reverse osmosis desalination process: Energy, exergy, and cost evaluations," *Renewable Energy*, vol. 35, no. 11, pp. 2571–2580, Nov. 2010.

[136] G. Kosmadakis, D. Manolakos, S. Kyritsis, and G. Papadakis, "Design of a two stage Organic Rankine Cycle system for reverse osmosis desalination supplied from a steady thermal source," *Desalination*, vol. 250, no. 1, pp. 323–328, Jan. 2010.

[137] A. M. Helal, S. A. Al-Malek, and E. S. Al-Katheeri, "Economic feasibility of alternative designs of a PV-RO desalination unit for remote areas in the United Arab Emirates," *Desalination*, vol. 221, no. 1–3, pp. 1–16, Mar. 2008.

[138] E. Tzen, D. Theofilloyianakos, M. Sigalas, and K. Karamanis, "Design and development of a hybrid autonomous system for seawater desalination," *Desalination*, vol. 166, pp. 267–274, Aug. 2004.

[139] T. Espino, B. PeÃ±ate, G. Piernavieja, D. Herold, and A. Neskakis, "Optimised desalination of seawater by a PV powered reverse osmosis plant for a decentralised coastal water supply," *Desalination*, vol. 156, no. 1–3, pp. 349–350, Aug. 2003.

[140] M. Thomson and D. Infield, "A photovoltaic-powered seawater reverse-osmosis system without batteries," *Desalination*, vol. 153, no. 1–3, pp. 1–8, Feb. 2003.

[141] M. Thomson, M. S. Miranda, and D. Infield, "A small-scale seawater reverse-osmosis system with excellent energy efficiency over a wide operating range," *Desalination*, vol. 153, no. 1–3, pp. 229–236, Feb. 2003.

[142] D. Herold and A. Neskakis, "A small PV-driven reverse osmosis desalination plant on the island of Gran Canaria," *Desalination*, vol. 137, no. 1–3, pp. 285–292, May 2001.

[143] A. Al-Alawi, S. M Al-Alawi, and S. M Islam, "Predictive control of an integrated PV-diesel water and power supply system using an artificial neural network," *Renewable Energy*, vol. 32, no. 8, pp. 1426–1439, Jul. 2007.

[144] S. A. Kershman, J. Rheinländer, T. Neumann, and O. Goebel, "Hybrid wind/PV and conventional power for desalination in Libya—GECOL's facility for medium and small scale research at Ras Ejder," *Desalination*, vol. 183, no. 1–3, pp. 1–12, Nov. 2005.

[145] G. Kosmadakis, D. Manolakos, S. Kyritsis, and G. Papadakis, "Economic assessment of a two-stage solar organic Rankine cycle for reverse osmosis desalination," *Renewable Energy*, vol. 34, no. 6, pp. 1579–1586, 2009.

[146] D. Manolakos, G. Kosmadakis, S. Kyritsis, and G. Papadakis, "On site experimental evaluation of a low-temperature solar organic Rankine cycle system for RO desalination," *Solar Energy*, 2008.

[147] G. Kosmadakis, D. Manolakos, and G. Papadakis, "Parametric theoretical study of a two-stage solar organic Rankine cycle for RO desalination," *Renewable Energy*, vol. 35, no. 5, pp. 989–996, May 2010.

[148] D. Manolakos, G. Papadakis, E. S. Mohamed, S. Kyritsis, and K. Bouzianas, "Design of an autonomous low-temperature solar Rankine cycle system for reverse osmosis desalination," *Desalination*, vol. 183, no. 1–3, pp. 73–80, Nov. 2005.

[149] G. Kosmadakis, D. Manolakos, S. Kyritsis, and G. Papadakis, "Comparative thermodynamic study of refrigerants to select the best for use in the high-temperature stage of a two-stage organic Rankine cycle for RO desalination," *Desalination*, vol. 243, no. 1–3, pp. 74–94, Jul. 2009.

[150] C. Fritzmann, J. Löwenberg, T. Wintgens, and T. Melin, "State-of-the-art of reverse osmosis desalination," *Desalination*, vol. 216, no. 1–3, pp. 1–76, Oct. 2007.

[151] A. M. Delgado-Torres and L. García-Rodríguez, "Preliminary design of seawater and brackish water reverse osmosis desalination systems driven by low-temperature solar organic Rankine cycles (ORC)," *Energy Conversion and Management*, vol. 51, no. 12, pp. 2913–2920, Dec. 2010.

[152] B. F. Tchanche, G. Lambrinos, A. Frangoudakis, and G. Papadakis, "Exergy analysis of micro-organic Rankine power cycles for a small scale solar driven reverse osmosis desalination system," *Applied Energy*, vol. 87, no. 4, pp. 1295–1306, Apr. 2010.

[153] D. Manolakos, G. Papadakis, S. Kyritsis, and K. Bouzianas, "Experimental evaluation of an autonomous low-temperature solar Rankine cycle system for reverse osmosis desalination," *Desalination*, vol. 203, no. 1–3, pp. 366–374, Feb. 2007.

[154] G. Kosmadakis, D. Manolakos, S. Kyritsis, and G. Papadakis, "Simulation of an autonomous, two-stage solar organic Rankine cycle system for reverse osmosis desalination," *Desalination and Water Treatment*, vol. 1, pp. 114–127, 2009.

[155] A. M. Delgado-Torres and L. García-Rodríguez, "Double cascade organic Rankine cycle for solar-driven reverse osmosis desalination," *Desalination*, vol. 216, no. 1–3, pp. 306–313, Oct. 2007.

[156] A. M. Delgado-Torres and L. García-Rodríguez, "Comparison of solar technologies for driving a desalination system by means of an organic Rankine cycle," *Desalination*, vol. 216, no. 1–3, pp. 276–291, Oct. 2007.

[157] J. Bruno, J. Lopezvillada, E. Letelier, S. Romera, and A. Coronas, "Modelling and optimisation of solar organic rankine cycle engines for reverse osmosis desalination," *Applied Thermal Engineering*, vol. 28, no. 17–18, pp. 2212–2226, Dec. 2008.

[158] A. M. Delgado-Torres and L. García-Rodríguez, "Preliminary assessment of solar organic Rankine cycles for driving a desalination system," *Desalination*, vol. 216, no. 1–3, pp. 252–275, Oct. 2007.

[159] A. M. Delgado-Torres, L. García-Rodríguez, and V. J. Romero-Ternero, "Preliminary design of a solar thermal-powered seawater reverse osmosis system," *Desalination*, vol. 216, no. 1–3, pp. 292–305, Oct. 2007.

[160] L. García-Rodríguez and A. M. Delgado-Torres, "Solar-powered Rankine cycles for fresh water production," *Desalination*, vol. 212, no. 1–3, pp. 319–327, Jun. 2007.

[161] A. M. Delgado-Torres, "Solar thermal heat engines for water pumping: An update," *Renewable and Sustainable Energy Reviews*, vol. 13, no. 2, pp. 462–472, Feb. 2009.

[162] A. M. Delgado-Torres and L. García-Rodríguez, "Status of solar thermal-driven reverse osmosis desalination," *Desalination*, vol. 216, no. 1–3, pp. 242–251, Oct. 2007.

[163] "Review of water resources and desalination technologies. by Miller, James Edward, Sandia National Laboratories, Albuquerque, NM." 2003.

[164] T. Xu and C. Huang, "Electrodialysis-based separation technologies: A critical review," *AIChE J.*, vol. 54, no. 12, pp. 3147–3159, Dec. 2008.

[165] J. M. Ortiz, E. Expósito, F. Gallud, V. García-García, V. Montiel, and A. Aldaz, "Desalination of underground brackish waters using an electrodialysis system powered directly by photovoltaic energy," *Solar Energy Materials and Solar Cells*, vol. 92, no. 12, pp. 1677–1688, Dec. 2008.

[166] J. M. Ortiz, E. Expósito, F. Gallud, V. García-García, V. Montiel, and A. Aldaz, "Photovoltaic electrodialysis system for brackish water desalination: Modeling of global process," *Journal of Membrane Science*, vol. 274, no. 1–2, pp. 138–149, Apr. 2006.

[167] N. Ishimaru, "Solar photovoltaic desalination of brackish water in remote areas by electrodialysis," *Desalination*, vol. 98, no. 1–3, pp. 485–493, Sep. 1994.

[168] H. M. N. AlMadani, "Water desalination by solar powered electrodialysis process," *Renewable Energy*, vol. 28, no. 12, pp. 1915–1924, Oct. 2003.

[169] O. Kuroda, S. Takahashi, S. Kubota, K. Kikuchi, Y. Eguchi, Y. Ikenaga, N. Sohma, K. Nishinoiri, S. Wakamatsu, and S. Itoh, "An electrodialysis seawater desalination system powered by photovoltaic cells," *Desalination*, vol. 67, pp. 33–41, Dec. 1987.

[170] A. Al-Karaghouli, D. Renne, and L. L. Kazmerski, "Technical and economic assessment of photovoltaic-driven desalination systems," *Renewable Energy*, vol. 35, no. 2, pp. 323–328, Feb. 2010.

[171] M. Sadrzadeh and T. Mohammadi, "Treatment of seawater using electrodialysis: Current efficiency evaluation," *Desalination*, vol. 249, no. 1, pp. 279–285, Nov. 2009.

[172] M. Sadrzadeh and T. Mohammadi, "Seawater desalination using electrodialysis," *Desalination*, vol. 221, no. 1–3, pp. 440–447, Mar. 2008.

[173] S. Al-Kharabsheh and D. Y. Goswami, "Theoretical Analysis of a Water Desalination System Using Low Grade Solar Heat," *J. Sol. Energy Eng.*, vol. 126, no. 2, pp. 774–780, May 2004.

[174] S. Al-Kharabsheh and D. Y. Goswami, "Experimental study of an innovative solar water desalination system utilizing a passive vacuum technique," *Solar Energy*, vol. 75, no. 5, pp. 395–401, Nov. 2003.

[175] O. Miyatake, "Comparative study of flash evaporation rates," *Desalination*, vol. 96, no. 1–3, pp. 163–171, Jun. 1994.

[176] M. Abutayeh and D. Y. Goswami, "Passive vacuum solar flash desalination," *AIChE J.*, vol. 56, no. 5, pp. 1196–1203, 2009.

[177] M. Abutayeh and D. Y. Goswami, "Solar Flash Desalination Under Hydrostatically Sustained Vacuum," *J. Sol. Energy Eng.*, vol. 131, no. 3, pp. 031016–7, 2009.

[178] V. G. Gude and N. Nirmalakhandan, "Desalination Using Low-Grade Heat Sources," *J. Energy Engrg.*, vol. 134, no. 3, pp. 95–101, 2008.

[179] V. G. Gude and N. Nirmalakhandan, "Desalination at low temperatures and low pressures," *Desalination*, vol. 244, no. 1–3, pp. 239–247, Aug. 2009.

[180] T. Ayhan and H. Al Madani, "Feasibilty study of renewable energy powered seawater desalination technology using natural vacuum technique," *Renewable Energy*, vol. 35, no. 2, pp. 506–514, Feb. 2010.

[181] V. G. Gude and N. Nirmalakhandan, "Sustainable desalination using solar energy," *Energy Conversion and Management*, vol. 51, no. 11, pp. 2245–2251, Nov. 2010.

[182] S. Al-Kharabsheh and D. Yogi^Goswami, "Analysis of an innovative water desalination system using low-grade solar heat," *Desalination*, vol. 156, no. 1–3, pp. 323–332, Aug. 2003.

[183] M. Abutayeh and D. Y. Goswami, "Experimental Simulation of Solar Flash Desalination," *J. Sol. Energy Eng.*, vol. 132, no. 4, pp. 041015–7, Nov. 2010.

[184] R. Tripathi and G. N. Tiwari, "Effect of water depth on internal heat and mass transfer for active solar distillation," *Desalination*, vol. 173, no. 2, pp. 187–200, Mar. 2005.

[185] H. N. Singh and G. N. Tiwari, "Monthly performance of passive and active solar stills for different Indian climatic conditions," *Desalination*, vol. 168, pp. 145–150, Aug. 2004.

[186] K. Sampathkumar, T. V. Arjunan, P. Pitchandi, and P. Senthilkumar, "Active solar distillation--A detailed review," *Renewable and Sustainable Energy Reviews*, vol. 14, no. 6, pp. 1503–1526, Aug. 2010.

[187] R. V. Dunkle, CSIRO, and C. and W. International Heat Transfer Conference 1961-1962 : Boulder, *Solar water distillation : the roof type still and a multiple effect diffusion still*. [Melbourne :: C.S.I.R.O, 1961.

[188] S. Kumar and G. N. Tiwari, "Performance evaluation of an active solar distillation system," *Energy*, vol. 21, no. 9, pp. 805–808, Sep. 1996.

[189] S. A. Lawrence and G. N. Tiwari, "Theoretical evaluation of solar distillation under natural circulation with heat exchanger," *Energy Conversion and Management*, vol. 30, no. 3, pp. 205–213, 1990.

[190] G. N. Tiwari, S. Kumar, P. B. Sharma, and M. Emran Khan, "Instantaneous thermal efficiency of an active solar still," *Applied Thermal Engineering*, vol. 16, no. 2, pp. 189–192, Feb. 1996.

[191] Y. P. Yadav and A. S. Prasad, "Performance analysis of a high temperature solar distillation system," *Energy Conversion and Management*, vol. 36, no. 5, pp. 365–374, May 1995.

[192] O. O. Badran and H. A. Al-Tahaineh, "The effect of coupling a flat-plate collector on the solar still productivity," *Desalination*, vol. 183, no. 1–3, pp. 137–142, Nov. 2005.

[193] H. E. S. Fath and S. M. Elsherbiny, "Effect of adding a passive condenser on solar still performance," *Energy Conversion and Management*, vol. 34, no. 1, pp. 63–72, Jan. 1993.

[194] J. H. Tay, S. C. Low, and S. Jeyaseelan, "Vacuum desalination for water purification using waste heat," *Desalination*, vol. 106, no. 1–3, pp. 131–135, Aug. 1996.

[195] S. C. Low and P. J. H. Tay, "Vacuum desalination using waste heat from a steam turbine," *Desalination*, vol. 81, no. 1–3, pp. 321–331, Jul. 1991.

[196] G. Mink, M. M. Aboabboud, and É. Karmazsin, "Air-blown solar still with heat recycling," *Solar Energy*, vol. 62, no. 4, pp. 309–317, Apr. 1998.

[197] K. Schwarzer, E. Vieira da Silva, B. Hoffschmidt, and T. Schwarzer, "A new solar desalination system with heat recovery for decentralised drinking water production," *Desalination*, vol. 248, no. 1–3, pp. 204–211, Nov. 2009.

[198] J. Fernández and N. Chargoy, "Multi-stage, indirectly heated solar still," *Solar Energy*, vol. 44, no. 4, pp. 215–223, 1990.

[199] S. Kumar and G. N. Tiwari, "Optimization of design parameters for multi-effect active distillation systems using the Runge-Kutta method," *Desalination*, vol. 121, no. 1, pp. 87–96, Jan. 1999.

[200] H. Tanaka, Y. Nakatake, and M. Tanaka, "Indoor experiments of the vertical multiple-effect diffusion-type solar still coupled with a heat-pipe solar collector," *Desalination*, vol. 177, no. 1–3, pp. 291–302, Jun. 2005.

[201] A. A. El-Sebaii, A. A. Al-Ghamdi, F. S. Al-Hazmi, and A. S. Faidah, "Thermal performance of a single basin solar still with PCM as a storage medium," *Applied Energy*, vol. 86, no. 7–8, pp. 1187–1195, Jul. 2009.

[202] S. O. Onyegegbu, "Nocturnal distillation in basin-type solar stills," *Applied Energy*, vol. 24, no. 1, pp. 29–42, 1986.

[203] V. Velmurugan and K. Srithar, "Solar stills integrated with a mini solar pond -- analytical simulation and experimental validation," *Desalination*, vol. 216, no. 1–3, pp. 232–241, Oct. 2007.

[204] V. Velmurugan, J. Mandlin, B. Stalin, and K. Srithar, "Augmentation of saline streams in solar stills integrating with a mini solar pond," *Desalination*, vol. 249, no. 1, pp. 143–149, Nov. 2009.

[205] S. Kumar and A. Tiwari, "An experimental study of hybrid photovoltaic thermal (PV/T)-active solar still," *Int. J. Energy Res.*, vol. 32, no. 9, pp. 847–858, Jul. 2008.

[206] K. Hidouri, R. Ben Slama, and S. Gabsi, "Hybrid solar still by heat pump compression," *Desalination*, vol. 250, no. 1, pp. 444–449, Jan. 2010.

[207] S. Parekh, M. Farid, J. Selman, and S. Alhallaj, "Solar desalination with a humidification-dehumidification technique — a comprehensive technical review," *Desalination*, vol. 160, no. 2, pp. 167–186, Jan. 2004.

[208] G. P. Narayan, M. H. Sharqawy, E. K. Summers, J. H. Lienhard, S. M. Zubair, and M. A. Antar, "The potential of solar-driven humidification-dehumidification desalination for small-scale decentralized water production," *Renewable and Sustainable Energy Reviews*, vol. 14, no. 4, pp. 1187–1201, May 2010.

[209] E. Hisham, "Design and analysis of humidification dehumidification desalination process," *Desalination*, vol. 183, no. 1–3, pp. 341–352, Nov. 2005.

[210] H. Müller-Holst, M. Engelhardt, M. Herve, and W. Schölkopf, "Solar thermal seawater desalination systems for decentralised use," *Renewable Energy*, vol. 14, no. 1–4, pp. 311–318, May 1998.

[211] S. Hou and H. Zhang, "A hybrid solar desalination process of the multi-effect humidification dehumidification and basin-type unit," *Desalination*, vol. 220, no. 1–3, pp. 552–557, Mar. 2008.

[212] K. H. Mistry, J. H. Lienhard V, and S. M. Zubair, "Effect of entropy generation on the performance of humidification-dehumidification desalination cycles," *International Journal of Thermal Sciences*, vol. 49, no. 9, pp. 1837–1847, Sep. 2010.

[213] C. YamalI and I. Solmus, "A solar desalination system using humidification-dehumidification process: experimental study and comparison with the theoretical results," *Desalination*, vol. 220, no. 1–3, pp. 538–551, Mar. 2008.

[214] A. M. Abdel Dayem and M. Fatouh, "Experimental and numerical investigation of humidification/dehumidification solar water desalination systems," *Desalination*, vol. 247, no. 1–3, pp. 594–609, Oct. 2009.

[215] E. H. Amer, H. Kotb, G. H. Mostafa, and A. R. El-Ghalban, "Theoretical and experimental investigation of humidification-dehumidification desalination unit," *Desalination*, vol. 249, no. 3, pp. 949–959, Dec. 2009.

[216] S. M. Soufari, M. Zamen, and M. Amidpour, "Performance optimization of the humidification-dehumidification desalination process using mathematical programming," *Desalination*, vol. 237, no. 1–3, pp. 305–317, Feb. 2009.

[217] K. Zhani and H. Ben Bacha, "Experimental investigation of a new solar desalination prototype using the humidification dehumidification principle," *Renewable Energy*, vol. 35, no. 11, pp. 2610–2617, Nov. 2010.

[218] M. Rommel, "Solar thermally driven desalination systems with corrosion-free collectors," *Renewable Energy*, vol. 14, no. 1–4, pp. 275–280, May 1998.

[219] H. Marmouch, J. Orfi, and S. B. Nasrallah, "Effect of a cooling tower on a solar desalination system," *Desalination*, vol. 238, no. 1–3, pp. 281–289, Mar. 2009.

[220] S. Hou, S. Ye, and H. Zhang, "Performance optimization of solar humidification-dehumidification desalination process using Pinch technology," *Desalination*, vol. 183, no. 1–3, pp. 143–149, Nov. 2005.

[221] S. Hou, "Two-stage solar multi-effect humidification dehumidification desalination process plotted from pinch analysis," *Desalination*, vol. 222, no. 1–3, pp. 572–578, Mar. 2008.

[222] J. Orfi, M. Laplante, H. Marmouch, N. Galanis, B. Benhamou, S. B. Nasrallah, and C. T. Nguyen, "Experimental and theoretical study of a humidification-dehumidification water desalination system using solar energy," *Desalination*, vol. 168, pp. 151–159, Aug. 2004.

[223] J. Orfi, N. Galanis, and M. Laplante, "Air humidification-dehumidification for a water desalination system using solar energy," *Desalination*, vol. 203, no. 1–3, pp. 471–481, Feb. 2007.

[224] M. M. Alhazmy, “Minimum work requirement for water production in humidification--dehumidification desalination cycle,” *Desalination*, vol. 214, no. 1–3, pp. 102–111, Aug. 2007.

[225] A. Eslamimanesh and M. S. Hatamipour, “Economical study of a small-scale direct contact humidification-dehumidification desalination plant,” *Desalination*, vol. 250, no. 1, pp. 203–207, Jan. 2010.

[226] A. Eslamimanesh and M. S. Hatamipour, “Mathematical modeling of a direct contact humidification-dehumidification desalination process,” *Desalination*, vol. 237, no. 1–3, pp. 296–304, Feb. 2009.

[227] M. Zamen, M. Amidpour, and S. M. Soufari, “Cost optimization of a solar humidification-dehumidification desalination unit using mathematical programming,” *Desalination*, vol. 239, no. 1–3, pp. 92–99, Apr. 2009.

[228] H. E. S. Fath and A. Ghazy, “Solar desalination using humidification--dehumidification technology,” *Desalination*, vol. 142, no. 2, pp. 119–133, Feb. 2002.

[229] A. Cipollina and G. Micale, “Coupling sustainable energy with membrane distillation processes for seawater desalination,” in *Nuclear & Renewable Energy Conference (INREC), 2010 1st International*, 2010, pp. 1–6.

[230] S. Al-Obaidani, E. Curcio, F. Macedonio, G. Di Profio, H. Al-Hinai, and E. Drioli, “Potential of membrane distillation in seawater desalination: Thermal efficiency, sensitivity study and cost estimation,” *Journal of Membrane Science*, vol. 323, no. 1, pp. 85–98, Oct. 2008.

[231] A. M. Alklaibi and N. Lior, “Membrane-distillation desalination: Status and potential,” *Desalination*, vol. 171, no. 2, pp. 111–131, Jan. 2005.

[232] T. Y. Cath, V. D. Adams, and A. E. Childress, “Experimental study of desalination using direct contact membrane distillation: a new approach to flux enhancement,” *Journal of Membrane Science*, vol. 228, no. 1, pp. 5–16, Jan. 2004.

[233] G. W. Meindersma, C. M. Guijt, and A. B. de Haan, “Desalination and water recycling by air gap membrane distillation,” *Desalination*, vol. 187, no. 1–3, pp. 291–301, Feb. 2006.

[234] J.-P. Mericq, S. Laborie, and C. Cabassud, “Evaluation of systems coupling vacuum membrane distillation and solar energy for seawater desalination,” *Chemical Engineering Journal*, vol. 166, no. 2, pp. 596–606, Jan. 2011.

[235] F. Banat, N. Jwaied, M. Rommel, J. Koschikowski, and M. Wieghaus, “Performance evaluation of the ‘large SMADES’ autonomous desalination solar-driven membrane distillation plant in Aqaba, Jordan,” *Desalination*, vol. 217, no. 1–3, pp. 17–28, Nov. 2007.

[236] F. Banat and N. Jwaied, “Economic evaluation of desalination by small-scale autonomous solar-powered membrane distillation units,” *Desalination*, vol. 220, no. 1–3, pp. 566–573, Mar. 2008.

[237] J. Walton, L. Huanmin, C. Turner, S. Solis, and H. Hein, “Solar and Waste Heat Desalination by Membrane Distillation,” U.S. Department of the Interior Bureau of Reclamation, Desalination and Water Purification Research and Development Program Report 81, Apr. 2004.

[238] J. Koschikowski, M. Wieghaus, M. Rommel, V. S. Ortin, B. P. Suarez, and J. R. Betancort Rodríguez, “Experimental investigations on solar driven stand-alone membrane distillation systems for remote areas,” *Desalination*, vol. 248, no. 1–3, pp. 125–131, Nov. 2009.

[239] J. Koschikowski, M. Wieghaus, and M. Rommel, “Membrane Distillation for Solar Desalination,” in *Seawater Desalination*, G. Micale, L. Rizzuti, and A. Cipollina, Eds. Berlin, Heidelberg: Springer Berlin Heidelberg, 2009, pp. 165–187.

[240] F. Banat, N. Jwaied, M. Rommel, J. Koschikowski, and M. Wieghaus, “Desalination by a ‘compact SMADES’ autonomous solarpowered membrane distillation unit,” *Desalination*, vol. 217, no. 1–3, pp. 29–37, Nov. 2007.

[241] H. E. S. Fath, S. M. Elsherbiny, A. A. Hassan, M. Rommel, M. Wieghaus, J. Koschikowski, and M. Vatansever, “PV and thermally driven small-scale, stand-alone solar desalination systems with very low maintenance needs,” *Desalination*, vol. 225, no. 1–3, pp. 58–69, May 2008.

[242] F. Banat, R. Jumah, and M. Garaibeh, “Exploitation of solar energy collected by solar stills for desalination by membrane distillation,” *Renewable Energy*, vol. 25, no. 2, pp. 293–305, Feb. 2002.

[243] H. Chang, G.-B. Wang, Y.-H. Chen, C.-C. Li, and C.-L. Chang, “Modeling and optimization of a solar driven membrane distillation desalination system,” *Renewable Energy*, vol. 35, no. 12, pp. 2714–2722, Dec. 2010.

[244] J. Blanco Gálvez, L. García-Rodríguez, and I. Martín-Mateos, “Seawater desalination by an innovative solar-powered membrane distillation system: the MEDESOL project,” *Desalination*, vol. 246, no. 1–3, pp. 567–576, Sep. 2009.

[245] H. J. Zwijnenberg, G. H. Koops, and M. Wessling, “Solar driven membrane pervaporation for desalination processes,” *Journal of Membrane Science*, vol. 250, no. 1–2, pp. 235–246, Mar. 2005.

[246] T.-C. Chen and C.-D. Ho, “Immediate assisted solar direct contact membrane distillation in saline water desalination,” *Journal of Membrane Science*, vol. 358, no. 1–2, pp. 122–130, Aug. 2010.

[247] C. Dotremont, “Seawater desalination with memstill technology - a sustainable solution for the industry,” *Water Practice and Technology*, vol. 5, pp. 1–7, May 2010.

[248] X. Zhou, B. Xiao, W. Liu, X. Guo, J. Yang, and J. Fan, “Comparison of classical solar chimney power system and combined solar chimney system for power generation and seawater desalination,” *Desalination*, vol. 250, no. 1, pp. 249–256, Jan. 2010.

[249] R. Semiat, “Energy Issues in Desalination Processes,” *Environmental Science & Technology*, vol. 42, no. 22, pp. 8193–8201, Nov. 2008.

[250] Y. Cerci, “The minimum work requirement for distillation processes,” *Exergy, An International Journal*, vol. 2, no. 1, pp. 15–23, 2002.

[251] S. Klein and G. Nellis, *Thermodynamics*. Cambridge University Press, 2011.

[252] M. Elimelech and W. A. Phillip, “The Future of Seawater Desalination: Energy, Technology, and the Environment,” *Science*, vol. 333, no. 6043, pp. 712 –717, 2011.

[253] Z. Liu, H. Bai, J. Lee, and D. D. Sun, “A low-energy forward osmosis process to produce drinking water,” *Energy & Environmental Science*, vol. 4, p. 2582, 2011.

[254] R. L. McGinnis and M. Elimelech, “Energy requirements of ammonia–carbon dioxide forward osmosis desalination,” *Desalination*, vol. 207, no. 1–3, pp. 370–382, Mar. 2007.

[255] K. S. Spiegler and A. D. K. Laird, *Principles of Desalination*, 2nd ed. Academic Press Inc, 1980.

[256] K. S. Spiegler and Y. M. El-Sayed, “The energetics of desalination processes,” *Desalination*, vol. 134, no. 1–3, pp. 109–128, Apr. 2001.

[257] B. F. DODGE and A. M. ESHAYA, “Thermodynamics of Some Desalting Processes,” in *Saline Water Conversion,Chapter 3*, vol. Advances in Chemistry, Vol.27, American Chemical Society, 1960, pp. 7–20.

[258] G. P. Narayan, M. H. Sharqawy, J. H. Lienhard V, and S. M. Zubair, “Thermodynamic analysis of humidification–dehumidification desalination cycles,” *Desalination and Water Treatment*, vol. 16, no. 1–3, pp. 339–353, 2010.

[259] P. Fernández-Izquierdo, L. García-Rodríguez, D.-C. Alarcón-Padilla, P. Palenzuela, and I. Martín-Mateos, “Experimental analysis of a multi-effect distillation unit operated out of nominal conditions,” *Desalination*, vol. 284, no. 0, pp. 233–237, Jan. 2012.

[260] H. T. El-Dessouky and H. M. Ettouney, *Fundamentals of Salt Water Desalination*. Elsevier, 2002.

[261] N. M. Wade, "Technical and economic evaluation of distillation and reverse osmosis desalination processes," *Desalination*, vol. 93, no. 1–3, pp. 343–363, Aug. 1993.

[262] M. Abutayeh, "Theoretical and Experimental Simulation of Passive Vacuum Solar Flash Desalination," University of South Florida, [Tampa, Fla.], 2010.

[263] R. Deng, L. Xie, H. Lin, J. Liu, and W. Han, "Integration of thermal energy and seawater desalination," *Energy*, vol. 35, no. 11, pp. 4368–4374, Nov. 2010.

[264] "FILMTEC Membranes System Design: System Performance Projection." [Online]. Available: http://msdssearch.dow.com/PublishedLiteratureDOWCOM/dh_0036/0901b803800362e9.pdf?filepath=liquidseps/pdfs/noreg/609-02057.pdf&fromPage=GetDoc.

[265] H. Chen, D. Y. Goswami, and E. K. Stefanakos, "A review of thermodynamic cycles and working fluids for the conversion of low-grade heat," *Renewable and Sustainable Energy Reviews*, vol. 14, no. 9, pp. 3059–3067, Dec. 2010.

[266] "Programme on Safety and Health at Work and the Environment (SafeWork)," 28-Apr-2011. [Online]. Available: http://www.ilo.org/safework/lang--en/index.htm. [Accessed: 28-Apr-2011].

[267] "Safety Data Sheets." [Online]. Available: http://www.bocsds.com/uk/sds/.

[268] "Global Warming Potentials of ODS Substitutes | Ozone Layer Protection | US EPA." [Online]. Available: http://www.epa.gov/Ozone/geninfo/gwps.html. [Accessed: 15-May-2011].

[269] ESRL CSD Webmaster and N. US Department of Commerce, "Scientific Assessment of Ozone Depletion 2006 - Executive Summary." [Online]. Available: http://www.esrl.noaa.gov/csd/assessments/ozone/2006/executivesummary.html#B8. [Accessed: 15-May-2011].

[270] "The Solar Keymark Database." [Online]. Available: http://solarkey.dk/solarkeymarkdata/qCollectorCertificates/ShowQCollectorCertificatesTable.aspx.

[271] R. A. Abdelrassoul, "Potential for economic solar desalination in the Middle East," *Renewable Energy*, vol. 14, no. 1–4, pp. 345–349, May 1998.

[272] H. Al-Qahtani, "Feasibility of utilizing solar energy to power reverse osmosis domestic unit to desalinate water in the state of Bahrain," *Renewable Energy*, vol. 8, no. 1–4, pp. 500–504, May 1996.

[273] L. García-Rodríguez, "Seawater desalination driven by renewable energies: a review," *Desalination*, vol. 143, no. 2, pp. 103–113, May 2002.

[274] V. G. Gude, N. Nirmalakhandan, and S. Deng, "Renewable and sustainable approaches for desalination," *Renewable and Sustainable Energy Reviews*, vol. 14, no. 9, pp. 2641–2654, Dec. 2010.

[275] J. Wang, Y. Dai, L. Gao, and S. Ma, "A new combined cooling, heating and power system driven by solar energy," *Renewable Energy*, vol. 34, no. 12, pp. 2780–2788, 2009.

[276] Y. Dai, J. Wang, and L. Gao, "Exergy analysis, parametric analysis and optimization for a novel combined power and ejector refrigeration cycle," *Applied Thermal Engineering*, vol. 29, no. 10, pp. 1983–1990, 2009.

[277] K. Chunnanond and S. Aphornratana, "Ejectors: applications in refrigeration technology," *Renewable and Sustainable Energy Reviews*, vol. 8, no. 2, pp. 129–155, Apr. 2004.

[278] K. Pianthong, W. Seehanam, M. Behnia, T. Sriveerakul, and S. Aphornratana, "Investigation and improvement of ejector refrigeration system using computational fluid dynamics technique," *Energy Conversion and Management*, vol. 48, no. 9, pp. 2556–2564, Sep. 2007.

[279] Y. Rafet, "Experimental investigation of performance of vapor ejector refrigeration system using refrigerant R123," *Energy Conversion and Management*, vol. 49, no. 5, pp. 953–961, May 2008.

[280] D. Li and E. A. Groll, "Transcritical CO2 refrigeration cycle with ejector-expansion device," *International Journal of Refrigeration*, vol. 28, no. 5, pp. 766–773, Aug. 2005.

[281] B. J. Huang, J. M. Chang, C. P. Wang, and V. A. Petrenko, "A 1-D analysis of ejector performance," *International Journal of Refrigeration*, vol. 22, no. 5, pp. 354–364, Aug. 1999.

[282] K. Cizungu, A. Mani, and M. Groll, "Performance comparison of vapour jet refrigeration system with environment friendly working fluids," *Applied Thermal Engineering*, vol. 21, no. 5, pp. 585–598, Apr. 2001.

[283] W. Somsak, "Cfd Optimization Study Of High-Efficiency Jet Ejectors," Dissertation of Doctor Of Philosophy, Texas A&M University, 2010.

[284] C. Garris, W. J. Hong, C. Mavriplis, and J. Shipman, "A New Thermally Driven Refrigeration System with Environmental Benefits," presented at the 33rd Intersociety Engineering Conference on Energy Conversion, Colorado Springs, CO, 1998.

[285] W. J. Hong, K. Alhussan, H. Zhang, and C. A. Garris Jr., "A novel thermally driven rotor-vane/pressure-exchange ejector refrigeration system with environmental benefits and energy efficiency," *Energy*, vol. 29, no. 12–15, pp. 2331–2345, Dec. 2004.

[286] K. V. Bulusu and J. Garris, "The Influence of Shear Layer Turbulence on Stationary Pseudoblades in Supersonic Pressure Exchange Inducing Flow Fields," *J. Fluids Eng.*, vol. 133, no. 11, pp. 111102–13, Nov. 2011.

[287] C. A. Garris Jr., "Pressure Exchange Ejector," U.S. Patent US 7497666 B2Mar-2009.

[288] K. V. Bulusu, D. M. Gould, and J. Garris, "Evaluation of Efficiency in Compressible Flow Ejectors," *ASME Conf. Proc.*, vol. 2008, no. 48692, pp. 531–554, Jan. 2008.

[289] D. Gould, "Theoretical Analysis of the Steam Pressure Exchange Ejector for an Automotive Air Conditioning Application," Master of Science Thesis, George Washington University, Department of Mechanical and Aerospace Engineering, 2009.

[290] K. Martin, "An Investigation of the Effect of Variable Ejector Efficiency on the Performance Characteristics of a Steam Condenser in an Ejector Refrigeration System," Master of Science Thesis, The George Washington University., Washington, D.C., 2005.

[291] M. H. Sharqawy, J. H. Lienhard V, and S. M. Zubair, "Thermophysical properties of seawater: A review of existing correlations and data," *Desalination and Water Treatment*, vol. 16, pp. 354–380, Apr. 2010.

[292] H. El-Dessouky, I. Alatiqi, S. Bingulac, and H. Ettouney, "Steady-State Analysis of the Multiple Effect Evaporation Desalination Process," *Chemical Engineering & Technology*, vol. 21, no. 5, pp. 437–451, May 1998.

[293] M. H. Sharqawy, J. H. Lienhard V, and S. M. Zubair, "On exergy calculations of seawater with applications in desalination systems," *International Journal of Thermal Sciences*, vol. 50, no. 2, pp. 187–196, Feb. 2011.

[294] Minton, Paul E, "Handbook of Evaporation Technology," 1986. [Online]. Available: http://www.knovel.com/web/portal/browse/display?_EXT_KNOVEL_DISPLAY_bookid=264. [Accessed: 21-Sep-2010].

[295] A. Gastli, Y. Charabi, and S. Zekri, "GIS-based assessment of combined CSP electric power and seawater desalination plant for Duqum--Oman," *Renewable and Sustainable Energy Reviews*, vol. 14, no. 2, pp. 821–827, Feb. 2010.

[296] O. A. Hamed, E. I. Eisa, and W. E. Abdalla, "Overview of solar desalination," *Desalination*, vol. 93, no. 1–3, pp. 563–579, Aug. 1993.

[297] M. Papapetrou, M. Wieghaus, and C. Biercamp, *Roadmap for the development of desalination powered by renewable energy-Promotion for Renewable Energy for Water Production through Desalination*. Hrsg.: Fraunhofer ISE, Freiburg/Brsg.:, 2010.

[298] F. Suárez, S. W. Tyler, and A. E. Childress, "A theoretical study of a direct contact membrane distillation system coupled to a salt-gradient solar pond for terminal lakes reclamation," *Water Research*, vol. 44, no. 15, pp. 4601–4615, Aug. 2010.

[299] N. Bouzayani, N. Galanis, and J. Orfi, "Thermodynamic analysis of combined electric power generation and water desalination plants," *Applied Thermal Engineering*, vol. 29, no. 4, pp. 624–633, Mar. 2009.

[300] A. Sharma, V. V. Tyagi, C. R. Chen, and D. Buddhi, "Review on thermal energy storage with phase change materials and applications," *Renewable and Sustainable Energy Reviews*, vol. 13, no. 2, pp. 318–345, Feb. 2009.

[301] D. Mills, "Advances in solar thermal electricity technology," *Solar Energy*, vol. 76, no. 1–3, pp. 19–31, Jan. 2003.

[302] "Technology Roadmap - Concentrating Solar Power." International Energy Agency, 2010.

[303] "Center for International Earth Science Information Network (CIESIN)." [Online]. Available: www.ciesin.com.

[304] D. Manolakos, E. S. Mohamed, I. Karagiannis, and G. Papadakis, "Technical and economic comparison between PV-RO system and RO-Solar Rankine system. Case study: Thirasia island," *Desalination*, vol. 221, no. 1–3, pp. 37–46, Mar. 2008.

[305] "Desertec Foundation," Desertec Foundation. Available: http://www.desertec.org/.

[306] A. Hussain, D. A. Gobaisi, and A. M. El-Nashar, "Application of Solar Energy in Desalting Seawater," in *Proceedings of ISES World Congress 2007 (Vol. I – Vol. V)*, D. Y. Goswami and Y. Zhao, Eds. Berlin, Heidelberg: Springer Berlin Heidelberg, 2008, pp. 2799–2804.

[307] R. BaÃ±os, F. Manzano-Agugliaro, F. G. Montoya, C. Gil, A. Alcayde, and J. GÃ^{3}mez, "Optimization methods applied to renewable and sustainable energy: A review," *Renewable and Sustainable Energy Reviews*, vol. 15, no. 4, pp. 1753–1766, May 2011.

[308] D. A. Roberts, E. L. Johnston, and N. A. Knott, "Impacts of desalination plant discharges on the marine environment: A critical review of published studies," *Water Research*, vol. 44, no. 18, pp. 5117–5128, Oct. 2010.

[309] Y. Oren, E. Korngold, N. Daltrophe, R. Messalem, Y. Volkman, L. Aronov, M. Weismann, N. Bouriakov, P. Glueckstern, and J. Gilron, "Pilot studies on high recovery BWRO-EDR for near zero liquid discharge approach," *Desalination*, vol. 261, no. 3, pp. 321–330, Oct. 2010.

[310] C. R. Martinetti, A. E. Childress, and T. Y. Cath, "High recovery of concentrated RO brines using forward osmosis and membrane distillation," *Journal of Membrane Science*, vol. 331, no. 1–2, pp. 31–39, Apr. 2009.

[311] P. Dlugolecki, J. Dabrowska, K. Nijmeijer, and M. Wessling, "Ion conductive spacers for increased power generation in reverse electrodialysis," *Journal of Membrane Science*, vol. 347, no. 1–2, pp. 101–107, Feb. 2010.

[312] E. Brauns, "Salinity gradient power by reverse electrodialysis: effect of model parameters on electrical power output," *Desalination*, vol. 237, no. 1–3, pp. 378–391, Feb. 2009.

[313] L. Lourdes, Ed., "Assessment Of Most Promising Developments In Solar Desalination," in *Solar Desalination for the 21st Century*, Dordrecht: Springer Netherlands, 2007, pp. 355–369.

[314] A. Fernández-García, E. Zarza, L. Valenzuela, and M. Pérez, "Parabolic-trough solar collectors and their applications," *Renewable and Sustainable Energy Reviews*, vol. 14, no. 7, pp. 1695–1721, Sep. 2010.

[315] M. Roeb, M. Neises, N. Monnerie, C. Sattler, and R. Pitz-Paal, "Technologies and trends in solar power and fuels," *Energy & Environmental Science*, vol. 4, p. 2503, 2011.

[316] B. Müller, W. Arlt, and P. Wasserscheid, "A new concept for the global distribution of solar energy: energy carrying compounds," *Energy & Environmental Science*, 2011.

[317] F. J. Tapiador, "Assessment of renewable energy potential through satellite data and numerical models," *Energy & Environmental Science*, vol. 2, p. 1142, 2009.

[318] M. Papapetrou, E. S. Mohamed, D. Manolakos, G. Papadakis, V. J. Subiela, and B. Peñate, "Operating RE/Desalination Units," in *Seawater Desalination*, G. Micale, L. Rizzuti, and A. Cipollina, Eds. Berlin, Heidelberg: Springer Berlin Heidelberg, 2009, pp. 247–272.

[319] M. Khedr, "Techno-Economic investigation of an air humidification-dehumidification desalination process," *Chemical Engineering & Technology*, vol. 16, no. 4, pp. 270–274, Aug. 1993.

[320] I. Houcine, M. BenAmara, A. Guizani, and M. Maâlej, "Pilot plant testing of a new solar desalination process by a multiple-effect-humidification technique," *Desalination*, vol. 196, no. 1–3, pp. 105–124, Sep. 2006.

[321] M. T. Chaibi, M. J. Safi, and M. Hsairi, “Performance analysis of a solar desalting unit in south tunisia,” *Desalination*, vol. 82, no. 1–3, pp. 187–196, Aug. 1991.

[322] H. MüLler-Holst, “Solar Thermal Desalination Using The Multiple Effect Humidification (MEH)-Method,” in *Solar Desalination for the 21st Century*, L. Rizzuti, H. M. Ettouney, and A. Cipollina, Eds. Dordrecht: Springer Netherlands, pp. 215–225.

[323] P. C. M. de Carvalho, D. B. Riffel, C. Freire, and F. F. D. Montenegro, “The Brazilian experience with a photovoltaic powered reverse osmosis plant,” *Progress in Photovoltaics: Research and Applications*, vol. 12, no. 5, pp. 373–385, Aug. 2004.

[324] B. G. Keeper, R. D. Hembree, and F. C. Schrack, “Optimized matching of solar photovoltaic power with reverse osmosis desalination,” *Desalination*, vol. 54, pp. 89–103, 1985.

[325] D. Herold, V. Horstmann, A. Neskakis, J. Plettner-Marliani, G. Piernavieja, and R. Calero, “Small scale photovoltaic desalination for rural water supply - demonstration plant in Gran Canaria,” *Renewable Energy*, vol. 14, no. 1–4, pp. 293–298, 1998.

[326] E. Tzen, K. Perrakis, and P. Baltas, “Design of a stand alone PV - desalination system for rural areas,” *Desalination*, vol. 119, no. 1–3, pp. 327–333, Sep. 1998.

[327] A. A. Madani, “Economics of desalination for three plant sizes,” *Desalination*, vol. 78, no. 2, pp. 187–200, Aug. 1990.

[328] E. E. Delyannis and A. Delyannis, “Economics of solar stills,” *Desalination*, vol. 52, no. 2, pp. 167–176, 1985.

[329] A. E. Kabeel, A. M. Hamed, and S. A. El-Agouz, “Cost analysis of different solar still configurations,” *Energy*, vol. 35, no. 7, pp. 2901–2908, Jul. 2010.

APPENDICES

Appendix A. Review of Solar Energy Driven Desalination System Cost

Reported costs of solar energy driven desalination systems are reviewed here.

Ref.	Cost ($)	Configuration	Capacity (m^3/d)	Notes
[146], [304]	15	ETC+ORC+RO	1.8	Study carried out through the Agriculture University of Athens, Greece. Authors' design radiation was 1000 W/m^2. Based on location of Athens, GHI was 4.58 kWh/m^2/day.
[145]	9	ETC+ORC+RO	16	Study carried out through the Agriculture University of Athens, Greece. Authors' design radiation was 1000 W/m^2.
[146], [153]	12.5	ETC-ORC-RO	8	Study carried out through the Agriculture University of Athens, Greece. Authors' design radiation was 1000 W/m^2.
[145], [147], [154]	6.85	ETC-Cascade ORC-RO	24	Study carried out through the Agriculture University of Athens, Greece. Authors' design radiation was 1000 W/m^2.
[126]	10.4	PV-RO	0.4	PV panels working at solar irradiance half that of the test conditions (1000W/m^2) shown by the Agriculture University of Athens, Greece. Reported cost was €7.8/m^3 water, and PV capacity was 0.85kW.
[128]	6.95	PV-RO	12	PV capacity was 30.22 kW; design solar radiation was 1000 W/m2. With two wind turbines and 40% PV, this system has the lowest water production cost (€ 5.21/m3).
[128]	8.88	PV-RO	12	3096 cubic meters per year production with 100% PV driven; cost was €6.64/m^3 fresh water; design solar radiation was 1000 W/$m^{2;}$ and PV capacity was 13.2 kW.
[135]	0.94	FPC-ORC-RO	1,166	Design points were 850 W/m^2, based on the studied location; NASA GHI data was 5.69 kWh/m^2/day.
[135]	0.93	CPC-ORC-RO	1,166	Design points were 850 W/m^2. Based on the studied location the DNI was 7.01 kWh/m^2/day.

Appendix A. (Continued)

Ref.	Cost ($)	Configuration	Capacity (m^3/d)	Notes
[135]	0.90	PTC-ORC-RO	1,166	Design points were 850 W/m^2; Based on the studied location the DNI was 7.01 kWh/m^2/day.
[74], [236]	15	FPC-PV-MD	0.1	Location: Aqaba Port, Jordan; the GHI is 5.891 kWh/m^2/day.
[236]	18	Flat Collector-MD	0.4	Location: Aqaba Port, Jordan; the GHI is 5.891 kWh/m^2/day.
[73]	2.15-4.70	FPC-MED	0.2	Location: Jordan; the GHI is 4.571 kWh/m^2/day.
[108]	2.2-4.7	PTC-MED	72	Experimental. Convert to US dollar by using 192.21 Spain Pesetas per United States Dollar. Based on the studied location the DNI was 5.601 kWh/m^2/day.
[76]	4	FPC-MED	100	Experiments at Sydney; the GHI was 4.981 kWh/m^2/day.
[76]	5.1	ETC-MED	100	Experiments at Sydney; the GHI was 4.981 kWh/m^2/day.
[69], [76]	5-6.7	ETC-MED	500	Location: Abu Dhabi; the GHI was 5.611 kWh/m^2 day.
[69], [74]	8.3-9.3	ETC-MED	100	Location: Abu Dhabi; the GHI was 5.611 kWh/m^2 day.
[69], [74]	3.4-4.4	ETC-MED	1,000	Location: Abu Dhabi; the GHI was 5.611 kWh/m^2 day.
[75]	7-10	ETC-MED	80	Experiments at; Abu Dhabi, the GHI is 5.611 kWh/m^2 day.
[74], [109] [318]	2	PTC-MED	800	Based on studied location in Spain, the DNI was estimated as 5.601 kWh/m^2 day.
[109]	3.82-4.93	PTC-MED	72	Based on studied location in Spain, the DNI wa estimated as 5.601 kWh/m^2 day.
[72]	0.92	Collector-MED	10,000	Based on studied location: Eilat, Israel, the NASA data showed GHI was 5.65 kWh/m^2 day.
[131]	2	solar thermal collector - MED	5,000	Annual insulation was 2,000kWh/m^2; peak radiation was 1000W/m^2.
[44]	0.9	FPC-MSF	8.5	Experiments at Tamilnadu, India; the author mentioned 400-900 W/m^2.

Appendix A. (Continued)

Ref.	Cost ($)	Configuration	Capacity (m^3/d)	Notes
[39]	4.67	FPC-MSF	0.3	Based on studied location in Tianjin, China, which has an estimated DNI from the NASA database at 4.36kWh/m^2 day.
[39]	3.9	FPC-MSF	6	Based on studied location in Tianjin, China, which has an estimated DNI from the NASA database at 4.36kWh/m^2 day.
[40]	2.5 - 3.8	PTC-MSF	1800 - 3000	Studied location: SE Spain, which has an estimated DNI from the NASA database at 5.6kWh/m^2day.
[236]	2.84	Collector-MSF	1	Authors were in Kuwait which has GHI at about 5.40kWh/m^2 day.
[319]	3.3	HDH	10	
[319]	2.4	HDH	30	
[76], [320] [321]	29.46	HDH	2,000	Location: South Tunisia, which has GHI at about 5.24 kWh/m^2 day.
[322]	8.87	FPC-CAOW HDH	1	A demonstration system was installed and commissioned in Jeddah/Kingdom of Saudi-Arabia.
[322]	6.25	FPC - CAOW HDH	5	Assumed in Jeddah /Saudi Arabia.
[322]	5.71	FPC -CAOW HDH	10	Assumed in Jeddah /Saudi Arabia.
[210]	45	FPC-HDH	0.4	Location: Sfax in Tunisia. Based on NASA database, GHI was estimated at about 4.87 kWh/m^2 day.
[210]	80	FPC-HDH	0.5	Location: Sfax in Tunisia. Based on NASA database, GHI was estimated at about 4.87 kWh/m^2 day.
[320]	61.65-109.6	HDH	0.44 - 0.5	Location: Sfax in Tunisia. Based on NASA database, GHI was estimated at about 4.87 kWh/m^2 day.
[320]	39.25	FPC-CAOW HDH	10	Location: Tunisia, Solar radiation 510 W/m^2.

Appendix A. (Continued)

Ref.	Cost ($)	Configuration	Capacity (m^3/d)	Notes
[320]	59.6	FPC-CAOW HDH	10	Location: Tunisia, Solar radiation 510 W/m^2.
[320]	49.05	FPC-CAOW HDH	10	Location: Tunisia, Solar radiation 510 W/m^2.
[320]	46.31	FPC-CAOW HDH	10	Location: Tunisia, Solar radiation 510 W/m^2.
[108]	2.34	Hybrid-MED-HP	100	Model only; cost information calculated by converting 192.21 Spain Pesetas per United States Dollar. Based on studied location, using the NASA database GHI could be estimated at about 4.65 kWh/m^2 day.
[108]	1.82	Hybrid-MED-HP	500	Model only; cost information calculated by converting 192.21 Spain Pesetas per United States Dollar. Based on studied location, using the NASA database GHI could be estimated at about 4.65 kWh/m^2 day.
[108]	1.66	Hybrid-MED-HP	1,000	Model only; cost information calculated by converting 192.21 Spain Pesetas per United States Dollar. Based on studied location, using the NASA database GHI could be estimated at about 4.65 kWh/m^2 day.
[108]	1.25	Hybrid-MED-HP	5,000	Model only; cost information calculated by converting 192.21 Spain Pesetas per United States Dollar. Based on studied location, using the NASA database GHI could be estimated at about 4.65 kWh/m^2 day.
[72]	0.64	Hybrid-MED	100,000	Location: Zikim, Israel; Based on studied locations, readers could use NASA database and estimate GHI close to 5.57 kWh/m^2 day.
[62]	0.79	Hybrid-SP-MED/RO	20,000	Paper used 2000 kWh/m^2 annual solar insulation; authors' Location is Tel Aviv, Israel.
[62]	0.65	Hybrid-SP-MED/RO	200,000	Paper used 2000 kWh/m^2 annual solar insulation; authors location is Tel Aviv, Israel.

Appendix A. (Continued)

Ref.	Cost ($)	Configuration	Capacity (m^3/d)	Notes
[30], [76]	1.79	Hybrid-SP-MSF	1	Based on studied location, Safat in Kuwait, GHI could be estimated at about 5.4kWh/m^2 day from the NASA database.
[180]	1	PVD	0.013	Monthly average daily global solar radiation in Bahrain was 3000-7200 W/m^2/day. Location: Isatown, Bahrain.
[180]	0.702	PVD	0.1	Monthly average daily global solar radiation in Bahrain was 3000-7200 W/m^2/day. Location: Isatown, Bahrain.
[108]	3.9	PV-RO	100	Model only; cost information calculated by converting 192.21 Spain Pesetas per United States Dollar. Based on studied location, using the NASA database GHI could be estimated at about 4.65 kWh/m^2 day.
[108]	2.99	PV-RO	500	Model only; cost information calculated by converting 192.21 Spain Pesetas per United States Dollar. Based on studied location, using the NASA database GHI could be estimated at about 4.65 kWh/m^2 day.
[108]	2.76	PV-RO	1,000	Model only; cost information calculated by converting 192.21 Spain Pesetas per United States Dollar. Based on studied location, using the NASA database GHI could be estimated at about 4.65 kWh/m^2 day.
[108]	2.34	PV-RO	5,000	Model only; cost information calculated by converting 192.21 Spain Pesetas per United States Dollar. Based on studied location, using the NASA database GHI could be estimated at about 4.65 kWh/m^2 day.
[74], [138]	31	PV-RO	3.1	PV capacity was 4kW; study carried out by CRES, at Laviro in Greece; water production wais 130 l/h with an RO unit energy recovery system ; reported cost was €23/m^3 for water. Based on studied location, the NASA database could estimate GHI as 4.95 kWh/m^2 day.
[74]	9.75	PV-RO	40	
[323], [324]	9	PV-RO	4	Yearly solar insulation was 2000kW h/m^2.

Appendix A. (Continued)

Ref.	Cost ($)	Configuration	Capacity (m^3/d)	Notes
[325]	16	PV-RO	1	A small reverse osmosis (RO) plant supplied by a photovoltaic (PV) power supply was been installed at the island of Grand Canary, Canary Islands, Spain. Based on studied location, GHI could be estimated close to 5.67kWh/m^2 day.
[139]	13.16	PV-RO	10	PV capacity 4.8kW; location is ITC-DESSOL, Grand Canary, Canary Islands, Spain, based on studied location, GHI could be estimated from NASA data as 5.4 kWh/m^2/day.
[326]	38 - 42	PV-RO	3.1 - 4.6	Studied location was Tan Tan City, Morocco; solar insulation was 4624 Wh/m^2, and the desalination system operated 2434 hours per year. A lifetime of 20 years for the equipment is considered. The analysis was made assuming a 3% to 5% rate of return and a yearly water production of 1,350 m^3. A total fresh water cost of €29 /m^3 for a rate of return of 3% is calculated while a total water cost of around €32/m^3 is calculated for 5% annual rate of return.
[131]	2	PV-RO	5,000	Annual solar energy was 2,000kWh/m².
[137]	7.21	PV-RO	20	PV capacity was 11.25kW; the system wa a diesel-assisted system. Location was Abu Dhabi. Based on studied location, GHI could be estimated close to 5.61kWh/m^2/day.
[137]	7.3	PV-RO	44	PV capacity was 22.49 kW 100% driven by solar energy. Location was Abu Dhabi. Based on studied location, GHI could be estimated as close to 5.61kWh/m^2/day.
[74], [140] [141]	3	PV-RO	3	Location at Loughborough University, UK. PV system has solar tracking system. Location GHI could be estimated as 2.65kWh/m^2/day.
[142]	9.6	PV-RO	1.2	PV capacity 4.8 kW; location is CIEA-ITC, Canary Islands, Spain; Based on studied location, GHI could be estimated at close to 5.4kWh/m2/day based on NASA data.

Appendix A. (Continued)

Ref.	Cost ($)	Configuration	Capacity (m^3/d)	Notes
[144]	3	PV-RO	300	PV capacity 50kW; Location was GECOL at Ras Ejder, Libya. Based on studied location, solar radiation could be estimated as 5.24kWh/m^2/day.
[236]	2.7	PV-RO	500	Annual insulation as 2,000kWh/m², design radiation was 1000W/m^2.
[236]	12.05	PV-RO	1	Location: Safat in Kuwait; using the NASA database to estimate GHI 5.4kWh/m^2/day.
[76]	0.67 - 1.44	SP-MED	100,000	Annual solar insulation was 2400 kWh/m^2/y.
[62]	0.89	SP-MED	20,000	Authors used 2000kWh/m^2 annual insulation; authors location was Tel Aviv, Israel.
[62]	0.71	SP-MED	200,000	Authors used 2000kWh/m^2 annual insulation. Aauthors location was Tel Aviv, Israel.
[27]	0.621	SP-MED	2,348	30MW gas engine waste heat was discharged into a solar pond. Solar pond size was 7800m^2. If authors' location was used, the GHI could be estimated as 4.54kWh/m^2/day.
[27]	0.466	SP-MED	15,044	120MW gas engine waste heat was discharged into a solar pond. Solar pond size was 7800m^2. If authors' location was used, the GHI could be estimated as 4.54kWh/m^2/day.
[30]	2.84	SP-MSF	1	Paper reported 1.63 KD per cubic meter water cost, but the authors used 1KD=$3.4. Location: Safat, Kuwait where the NASA database showed GHI was 5.40kWh/m^2/day.
[30]	5.7	SP-RO	1	Paper reported 1.63 KD per cubic meter water cost, but the authors used 1KD=$3.4. Location: Safat, Kuwait where the NASA database showed GHI was 5.40kWh/m^2/day.
[25]	5.48	SP-MSF	15	Location: Tan Tan City, Morrocco where the NASA database showed GHI was 5.75kWh/m^2/day; Solar pond size was 2500 m^2.

Appendix A. (Continued)

Ref.	Cost ($)	Configuration	Capacity (m^3/d)	Notes
[25]	2.39	SP-MSF	300	Location: Tan Tan City, Morrocco where the NASA database showed GHI was 5.75kWh/m^2/day; Solar pond size was 36000 m^2.
[26]	2.85	SP-MSF	1,000	Pond size was 80000 m^2. Based on studied location, the NASA database and estimated DNI at 6 kWh/m^2/day.
[26]	1.84	SP-MSF	10,000	Pond size was 80000 m^2. Based on studied location, the NASA database and estimated DNI at 6 kWh/m^2/day.
[27]	0.916	SP-MSF	2,040	30MW gas engine waste heat was discharged into a 7800m^2 solar pond. If authors' location was used, the GHI could be estimated as 4.54 kWh/m^2/day.
[27]	0.827	SP-MSF	12,378	120MW gas engine waste heat was discharged into a solar pond. The solar pond size was 7800m^2; If authors' location was used, the GHI could be estimated as 4.54kWh/m^2/day.
[28]	1.8	SP-MSF	1,570	Pond size was 70000 $m^{2;}$ radiation was less than <350W/m^2.
[24]	3.71	SP-MSF	550	The author listed a location but chose data from Dakar due to lack of solar data; solar pond size was 65361 m^2; solar insulation was 246.3W/m^2.
[24]	3.42	SP-MSF	550	The author listed a location but chose data from Dakar due to lack of solar data; solar pond size was 49441 m^2; solar insulationwas 246.3W/m^2.
[327]	2.88	ST	70	
[76], [320]	4.11	ST	1-50	
[76], [328]	3	ST	10	
[76], [328]	6	ST	10	
[76], [328]	12	ST	10	
[76], [328]	3	ST	50	
[76], [328]	6	ST	50	
[76]	23.8	FPC-ST	0.004	
[76]	9.95	Multi-effect ST	0.012	

Appendix A. (Continued)

Ref.	Cost ($)	Configuration	Capacity (m^3/d)	Notes
[76]	9	Multi-effect ST	0.02	
[76], [320]	39.456	Multi-effect ST	10	
[76], [320]	11.99	ST	20	Location: Sydney where the NASA database showed GHI was 4.98kWh/m^2/day.
[30], [236]	12.5	ST	0.8	Location: Safat, Kuwait where the NASA database showed GHI was 5.4kWh/m^2/day.
[329]	25.2	Single-slope ST	0.00888	Design solar insulation 850 W/m^2. Based on studied location, the NASA database showed GHI was 5.35kWh/m^2/day.
[329]	14	Single-slope ST	0.00132	Design solar insulation 800 W/m^2. Based on studied location, the NASA database showed GHI was 5.05kWh/m^2/day.
[329]	39	ST with solar collector	0.00463	Design solar insulation 850 W/m^2. Based on studied location, the NASA database showed GHI was 3.35kWh/m^2/day.
[329]	13.8	ST with solar concentrator	0.0038	Design solar insulation 800 W/m^2. Based on studied location, the NASA database showed GHI was 5.35kWh/m^2/day.
[329]	22.6	ST using pyramid-shaped	0.009	Design solar insulation 800 W/m^2. Based on studied location, the NASA database showed GHI was 5.05kWh/m^2/day.

a) For capacity range, use low end, i.e. 7-10 m^3/day, choose 7 m^3/day
b) For cost range, pick middle cost, i.e. 7-10 \$/m^3, use low cost due to the technology development and solar products price drop
c) Convert all the currency into dollars based on Oct.14, 2011 currency rate
d) If hourly rate is given, convert to daily production using 8 hours, i.e. 3m^3/h, converted as 24m^3/day (except that the authors' directly mentioned operation hours and daily production).
e) For research given by L/year, convert to daily production by dividing 365.
f) FPC, ETC, CPC and PTC combined with desalination system is just generalized as collector+desalination (i.e. FPC+RO) and is called collector+RO in the cost figure.
g) Single-effect solar still, multi-effect solar still and collector/PV combined with solar still are all abbreviated as ST.
h) All kinds of power cycles are called engine in Figures (i.e. FPC with ORC-driven RO) used collector-engine-RO in the figure.
i) Different HDH processes are generalized and called HDH process (i.e. FPC+CAOW HDH) is represented as HDH only.

Appendix A. (Continued)

j) GHI: NASA 22-year monthly and annual average showed Insolation Incident on a horizontal surface, unit kWh/m^2 day. Data is estimated based on authors' studied location and the NASA database.

k) DNI: Based on the studied location, NASA 22-year monthly and annual average data showed direct normal radiation, unit is kWh/m^2/day. Data is estimated based on authors' studied location and theNASA database.

Appendix B. Error Analysis

In order to validate the property of the working fluids that were used in the investigation, a comparison between the data from NIST and EES was carried out in the following.

Table B.1 Error analysis

Data Source	R152a	
	T_c (K)	P_c (MPa)
NIST	386.41	4.5168
EES	386.40	4.5200

The standard deviation of T_c is $\sigma_{T_c} = \sqrt{\frac{\sum_k (T_{c_k} - \overline{T_c})^2}{N}}$ =0.005K

The standard deviation of P_c is $\sigma_{P_c} = \sqrt{\frac{\sum_k (P_{c_k} - \overline{P_c})^2}{N}}$ =0.0016MPa

Table B2 shows the differences of thermal power input at given conditions between the developed model and published data from the reference. The comparison shows the difference is within 2%, and the standard deviation of the difference is 0.77%. It indicates the developed model has good agreement with the referenced data, and the model is reasonably reliable for MED process predication.

Table B.2 Comparison of model predictions and data for MED unit*from reference [52]

Input Temp. (°C)	Performance Ratio	Recovery rate		Thermal power input (kW)		
		Reported	Model	Reported	Model	Difference, %
57	8.9	0.2375	0.2375	137	135.6	1.02%
60	9.1	0.275	0.275	153	153.5	-0.33%
63	9.3	0.3	0.3	166	163.9	1.27%
65	9	0.3375	0.3375	191	190.5	0.26%
68	10	0.3625	0.375	182	184.2	-1.21%
70	9.5	0.3625	0.3625	195	193.9	0.56%
72	9.4	0.375	0.375	203	202.7	0.15%
74	9.3	0.375	0.375	207	204.9	1.01%
				Standard deviation		0.77%

Appendix C. Selected Publications

Journal Papers

1. Chennan Li, D. Yogi Goswami, and Elias Stefanakos. “Solar-assisted Seawater Desalination: A review”, *Renewable and Sustainable Energy Review*, (Decision in Process).
2. Chennan Li, Saeb Besaratia, Yogi Goswami, Elias Stefanakos, Huijuan Chen, “Reverse Osmosis Desalination Driven By Low-temperature Supercritical Organic Rankine Cycle”, *Applied Energy*, (In Press).
3. Chennan Li, Yogi Goswami, Andrew Shapiro, Elias Stefanakos, “A New Combined Power and Desalination System Driven by Low-grade Heat for Concentrated Brine”, *Energy*, (Accepted with minor revision).
4. Chennan Li, George Kosmadakis, Elias Stefanakos, Yogi Goswami, “Parabolic Trough Solar Collector Driven Supercritical Cycle for Power-Desalination Cogeneration”, *Renewable Energy*, (Finished, to be submitted).
5. Saeb Besarati , Yogi Goswami, Elias Stefanakos, Chennan Li, “A Novel Combined Cycle using Supercritical CO_2 for Power Generation”, *Applied Energy*, (In Preparation) .
6. Chennan Li, Gongquan Sun, Suzhen Ren, “Casting Nafion–sulfonated Organic Silane Nano Composite Membranes Used in Direct Methanol Fuel Cells”, *Journal of Membrane Science,* vol. 15, pp. 50-57, 2006.
7. Li Chennan, Sun Gongquan, “Development of The Perfluorosulfonic Acid and Modified Composite Membranes Used in Fuel Cells”, *Chinese Science Bulletin*, vol.50, no 19, pp. 2049-2054, 2005.
8. Li Chennan, Sun Gongquan, Liang Zhenxing, “Recycling the waste Nafion membrane and the use of recast Nafion membrane in direct methanol fuel cell”, *Journal of Functional Materials* , vol.36, no.7, pp.1030-1033, 2005.
9. Suzhen Ren, Chennan Li, Xinsheng Zhao “Surface modification of sulfonated poly(ether ether ketone) membranes using Nafion solution for direct methanol fuel cells”, *Journal of Membrane Science* vol. 247, pp. 59–63, 2005.
10. Suzhen Ren, Gongquan Sun, Chennan Li , “Organic silica/Nafion composite membrane for direct methanol fuel cells”, *Journal of Membrane Science*, vol. 282, no. 1-2, pp. 450-455, 2006.
11. Suzhen Ren, Gongquan Sun, Chennan Li , “Sulfonated poly (ether ether ketone)/polyvinylidene fluoride polymer blends for direct methanol fuel cells”, *Materials Letters*, vol. 60, no.1, pp. 44-47, 2006.
12. Suzhen Ren, Gongquan Sun, Chennan Li . “Sulfated zirconia/Nafion compositemembranes for higher temperature DMFCs”. *Journal of Power Sources*, vol. 157, no. 2, pp. 724-726, 2006.
13. Ren Su-zhen, Sun Gong-quan, Wu Zhi-mou, Li Chen-nan ., “Blend membranes of sulfonated polyether ether ketone/polyvinylidene fluoride”, *Chinese Journal of Power Sources*, vol. 3, pp. 200-203, 2006.

Appendix C. (Continued)

14. Shuang Gu, Gaohong He, Xuemei Wu, Chennan Li . "Synthesis and characteristics of sulfonated poly(phthalazinone ether sulfone ketone) (SPPESK) for direct methanol fuel cell (DMFC)", *Journal of Membrane Science*, vol. 281, no. 1-2, pp. 121-129, 2006.

Conference Proceedings

1. Chennan Li, Sesha S. Srinivasan, Nikolai Kislov. "Photocatalytic activity by N-doping using the gas phase impregnation method", Mater. Res. Soc. Symp. Proc, Materials Research Society,vol 1217, pp 1217-Y03-35, 2010.
2. Chennan Li, Sesha S. Srinivasan, Nikolai Kislov., "Increasing the photocatalytic activity by mechano-chemically milling on Zn- doped TiO2", Mater. Res. Soc. Symp. Proc. Materials Research Society, vol.1217, pp. 1217-Y03-34, 2010.
3. Chennan Li, Zhenxing Liang, "Nafion–sulfonated organic silane proton conductive composite membranes with low methanol permeation", Processing and Fabrication of Advanced Materials XIII, vol.1, pp. 221-239, 2004.

Patents Disclosures

1. Chennan Li, D. Yogi Goswami, and Elias Stefanakos. "Method and systems for water and power cogeneration using organic Rankine Cycle-Ejector-Thermal Desalination for low- and mid-grade temperature sources", U.S. 11A070. (Prepared to file; disclosure issued)
2. Chennan Li, D. Yogi Goswami, and Elias Stefanakos. "Method and systems for water and power cogeneration using supercritical power cycles for low- and mid-grade temperature sources", U.S. 11A071. (Disclosure issued)

Book Chapter

1. Mohammad Abutayeh, D. Yogi Goswami, Chennan Li and Elias Stefanakos. "Desalination: Water From Water", *Chapter 11: Solar Desalination*, Scrivener/Wiley to be published.

Appendix D. Journal Reviewer

The author was invited to review papers submitted for the following journals for his expertise:

1. Journal of Membrane Sciences
2. Journal of Chemical Product and Process Modeling
3. Journal of Solar Energy Engineering
4. Energy Conversion and Management

Appendix E. List of Symbols

Nomenclature

e	Specific exergy (J)
E	Exergy (J)
$\dot{E}$	Rate of exergy (J/s)
h	Specific enthalpy (J/kg)
I	Irreversibility (J)
$\dot{I}$	Rate of irreversibility (J/s)
L	Latent heat (J)
$\dot{m}$	Flow rate (kg/s)
N_p	Power of the pump (J/s, W)
N_t	Power of the turbine (J/s, W)
P	Pressure (bar)
P_c	Critical pressure (MPa)
$\dot{q}$	Heat flow (J/s)
Q	Heat input (J)
q	Heat input per mass (J/kg)
R	Universal gas constant (J/ K–mol)
s	Salt concentration(%), entropy (J/K)
T	Temperature (K)
T_c	Critical temperature (K)
T_{rH}	Reduced evaporation temperature (K)
T_o	Temperature at dead state (K)
v_m	Mole volume (m^3/mol)
w	Work output (J)
z	Vertical coordinate (m)
ΔH	Enthalpy of vaporization (J)
ΔV	Volume change of the phase transition (m^3)
η	Efficiency
ξ	Ratio of entropy and temperature on a saturation curve (J/K^2)
ρ	Density (g/cm^3)

Appendix E. (Continued)

Subscripts

c	Condenser
cov	Energy conversion
ex	Exergy
f	Fluid
h	high-temperature, heating process
in	Input
l	Low-temperature
out	Output
p	pump
t	Turbine
th	Thermal
zeo	Zeotropic mixture

Superscripts

in	Input
out	Output

Common parameters used in MED system

T_n	Temperature of the effect n
Tf_n	Feed-in water temperature come out of the preheater of the effect n
Tv_n	Vapor temperature in effect n
$T^*{}_n$	Vapor generated at this temperature by brine flash in effect n
$\bar{T}_n$	Vapor flashed from condensed fresh water at the effect n
λ_n	Latent heat of vaporization at the vapor temperature Tv_n in effect n
$\lambda^*{}_n$	Latent heat related to the brine flash temperature $T^*{}_n$ in effect n
$\bar{\lambda}_n$	Latent heat related to the condensed fresh water $\bar{T}_n$ in effect n flash box
$Salt_n$	Salt concentration in the brine stream leaving effect n
$Salt_f$	Salt concentration in the feed stream
D_n	Vapor generated by evaporation within effect n
$d^*{}_n$	Vapor generated by brine flash in effect n
$\bar{d}_n$	Vapor generated by condensed fresh water in flash box of the effect n
M_d	Total distillate flow rate

Appendix E. (Continued)

BPE_n	Boiling point elevation of effect n caused by dissolved salt
Ue_n	The overall heat transfer coefficients in the evaporator for effect n
Uc_n	The overall heat transfer coefficients in the preheater for effect n
NEA^*_n	The nonequilibrium allowance of brine flash in effect n
$\overline{NEA}_n$	Nonequilibrium allowance of fresh water condensate flash in effect n
B_n	The concentrated brine mass come out of effect n
θ_n	The percentage of the vapor condensed in the preheater of effect n
$A_{e,n}$	The evaporator area in the effect n, all effects have the same area
$A_{p,n}$	The preheater area in the effect n, all effects have the same area
Cp_n	The mean specific heat of feed-in water happened in preheater
Cp^*_n	Mean specific heat of brine happened during brine flash process
$\overline{Cp}_n$	Mean specific heat of condensed fresh water during flash process
$LMTD_{p,n}$	The log mean temperature of the preheater in effect n

Appendix F. Figure Copyright Disclaimer

The author disclaims that Jutta Höflich at DESERTEC Foundation has all the rights to Figure 6.3, and acknowledges his permission of reference in this dissertation. Below is his email confirmation.

From: **pop.desertec.org** <request@desertec.org>
Date: Wed, Oct 26, 2011 at 2:04 AM
Subject: Re: E-Mail through DESERTEC.org Contact Form
To: cli3@mail.usf.edu

Dear Mr. Chennan,

You are welcome to use the picture as long as you note our copyright.

Kind regards,

Jutta Höflich

Office DESERTEC Foundation
Ferdinandstr. 28-30

D-20095 Hamburg

Phone: + 49 (0)40 32 507 795
E-mail: office@desertec.org

www.desertec.org
Clean Power from Deserts

ABOUT THE AUTHOR

Chennan Li, born in Dalian, China, completed his Bachelor degrees at Dalian University of Technology before completing his Master of Science degree at the Chinese Academy of Sciences in 2005. His Master's thesis is entitled "Organic/inorganic nano composite membranes for fuel cell applications."

In August 2005, he entered the Graduate School at Rice University to conduct his Master study in Environmental Engineering. After working in industry for several years, he started his part-time graduate study at the University of South Florida and worked on the development and modification of photo-catalysts. In August 2010 he returned to full-time graduate studies and began research on "Using Low-grade Heat for Desalination" as his Ph.D. study topic.